LILIAN ANNE KRUG

OCEAN SURFACE PROVINCES OFF SOUTHWEST IBERIA BASED ON SATELLITE REMOTE SENSING

UNIVERSIDADE DO ALGARVE

Faculdade de Ciências e Tecnologia

2017

LILIAN ANNE KRUG

OCEAN SURFACE PROVINCES OFF SOUTHWEST IBERIA BASED ON SATELLITE REMOTE SENSING

Doutoramento em Ciências do Mar, da Terra e do Ambiente (ramo Ciências do Mar, especialidade em Processos e Ecossistemas Marinhos)

Trabalho efetuado sob orientação de:
Prof Dra Ana Maria Branco Barbosa
Dra Shubha Sathyendranath

UNIVERSIDADE DO ALGARVE
Faculdade de Ciências e Tecnologia
2017

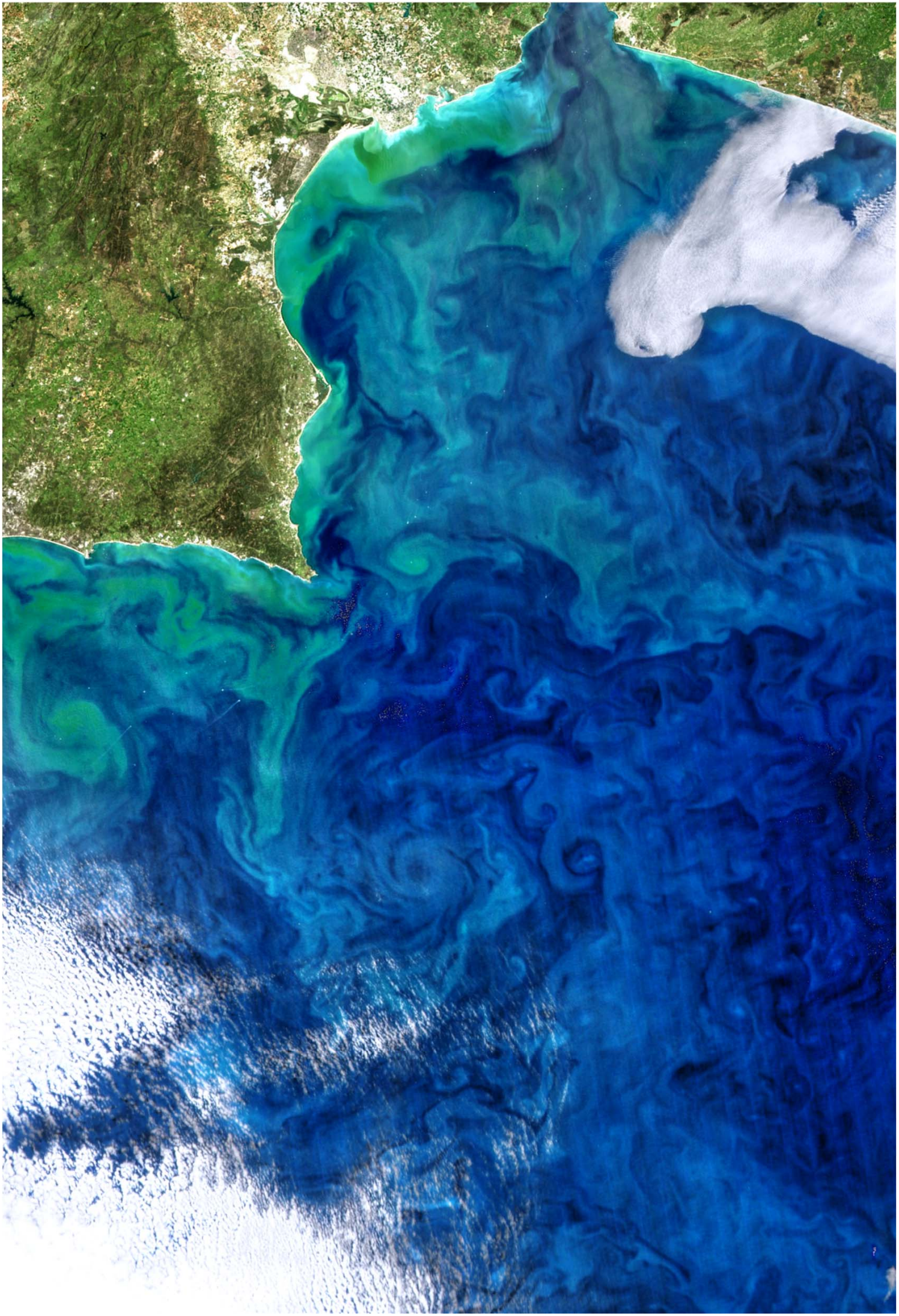

Image: MODIS-Aqua and VIIRS-Suomi NPP composite (March 8, 2017; Credits: Norman Kuring, NASA Earth Observatory)

THIS THESIS WAS SUPPORTED BY

Science without Borders Programme from the Brazilian National Council for Scientific and Technological Development (237998/2012-2)

The Foundation of Science and Technology through the project Remote Sensing of Phytoplankton variability off South-Western Iberia: A sentinel for climate change? – PHYTOCLIMA (PTDC/AAC-CLI/114512/2009)

"A century from now humanity will live in a managed - or mismanaged - global garden" (Steele et al., 1989). Presently, we worry about what to do about overfishing, ponder possible sub-lethal effect of oil or sewage discharge into the coastal oceans, and are scared by red and brown tides; we discuss the necessity to save some of the tropical forests; we are beginning to control emission of "greenhouse gases" into the atmosphere; and we struggle to calculate how fast and how much the climate will become warmer with and without such controls. A century from now these separate concerns will have been integrated into a single management system because of objective needs, but perhaps also because of broad intolerance of the mismanagement of nature. Obviously, the running of such a controlled system will require massive, continuous data-collecting or monitoring, which will presumably be largely automated. Our great-grandchildren, therefore, will live on a "wired earth" (Steele et al., 1989). Using the data so gathered, however, will demand massive improvements in scientific concepts, and this improvement is already the task for the present generation.

Banse (1995)

To my grandparents

ACKNOWLEDGMENTS

I would like to gratefully acknowledge…

… my supervisors Dr Ana Barbosa, Dr Shubha Sathyendranath and Dr Trevor Platt, for giving me constant encouragement and unabridged availability. They are, without a doubt, special people and exceptional mentors. These years were an emotional ride and their guidance was more than crucial. Trevor and Shubha were always supportive, kind and present, even with the physical distance. Ana is the best example I have ever met of a dedicated and ethical researcher, and I cannot think on words to express my gratitude for her.

… the Science without Borders Programme of the Brazilian National Council for Scientific and Technological Development (CsF-CNPq) and the Portuguese Foundation of Science and Technology (FCT), for the financial support. The CsF-CNPq was impeccable during the entire fellowship period and I deeply appreciate the opportunity given to me and to several other Brazilian young researchers.

… the Ocean Colour Climate Change Initiative (European Space Agency), OceanColor (USA's National Aeronautics and Space Administration), Copernicus Marine Environment Monitoring Service, Ocean Productivity (Oregon University) and every group that works hard to provide free and high quality products for a data-thirsty ocean science community.

… the Marine Microbiology laboratory, the Centre for Marine and Environmental Research and the Faculty of Sciences and Technology of the University of the Algarve, for the space and conditions. In special, I want to thank Paula Caboz from the FCT Secretariat, Dr Oscar Ferreira and Dr Pedro Andrade, former and current directors of the CMTA programme.

… the International Relations and Mobility Office of the University of the Algarve, in particular to Carla Mendes Ferro and Antonio Ramos.

… the International Oceanographic Data and Information Exchange (IODE), the European Space Agency (ESA), the Partnership for Observation of Global Ocean (POGO), the Scientific Committee on Oceanic Research (SCOR), the Surface Ocean - Lower Atmosphere Study (SOLAS) project, the NF-POGO Alumni Network for Oceans (NANO), the Gordon Research Conferences, the Portuguese Estrutura de Missão para a Extensão da Plataforma Continental (EMEPC) and other international organizations that provided me with resources to attend trainings and scientific events, allowing me to acquire and improve the techniques used in this thesis, as well as to present and discuss its partial results with my peers and renowned experienced researchers.

… the good-hearted people whose assistance was essential at some point along this thesis, including Mimoy, Paul, Dr Forough Fendereski, Dr Tom Jackson, Dr Tim Moore, Cátia L., Cátia G., Dr Rita Domingues, Dr Helena Galvão, Dr Joaquim Luis, Dr Paulo Relvas.

…. my Portuguese family (Cátia, Liliana, Sara, João, Paul, Giammi, Gui, Maria Rita, Camilla and Lucas), the ‘BBF’ Mari and my beloved goddaughter Nina, my suffering buddy ‘Frá’ (YES, we did it!), the ‘xu’ to my ‘xu’ Diego, MyLadies (Ellenzinha, Eurídice and Sara) and the rest of the gym gang, the NANO/POGO team (Sophie, Vikki, Laura and Olga), Dr Murray Brown, Dr Greg Reed, Rituxa, Ana Matias, Chiqui, Cat, Filipe, Carlos, Maria, Sandrinha, Sónia, Thi, Malão, Tati, Alex, Nathália, my lab hermano and coffee dealer Fran, Dna Maria do Carmo and Seu José, for the 24/7 emotional support system and guaranteed laughs.

…. my entire family, but in particular to my parents Osmar and Roseli, siblings Lian, Dan and Alethéa, sisters-in-law Denise and Ivy, nieces Ashley and Giuliana, nephew Enzo, aunt Wilma and my grandparents Alberto, Judith (*in memoriam*), Lino (*in memoriam*) and Margarida (*in memoriam*). Thank you for the unconditional love and for believing in me, supporting every single step in my professional and personal journeys even though it meant I gradually move farther and farther away from home and couldn’t visit for 3 long years or couldn’t properly say goodbye. *À toda a minha família, mas especialmente aos meus pais Osmar e Roseli, aos meus irmãos Lian, Dan e Alethéa, às minhas cunhadas Denise e Ivy, minhas sobrinhas Ashley e Giuliana, meu sobrinho Enzo, tia Wilma, meus avós Alberto, Judith (in memoriam), Lino (in memoriam) e Margarida (in memoriam). Muito obrigada pelo amor incondicional e por acreditarem em mim, apoiando cada passo da minha jornada profissional e pessoal, mesmo que isto significasse eu me mudar cada vez mais longe de casa, por três longos anos sem poder visitá-los, ou sem poder me despedir apropriadamente. Amo vocês.*

ABSTRACT

This thesis aimed to partition the complex surface marine domain off Southwest Iberia Peninsula (SWIP), using satellite remote sensing, and use it to assess phytoplankton variability patterns and underlying environmental drivers (1997 – 2015). Three unsupervised partition strategies, based on distinct input databases and temporal representations, detected a variable number of partition units (regions, provinces) of singular environmental and phytoplankton patterns within SWIP. An abiotic-based partition delineated 12 dynamic Environmental Provinces (EPs) that alternated coverage dominance along the annual cycle. EP patterns were in general related to phytoplankton biomass, indicated by satellite chlorophyll-a concentration (Chl-a), and productivity, thus supporting the biological relevance of this abiotic-based partition. A static partition, based on the main variability modes of Chl-a, derived 9 Chl-a regions. Moreover, a static partition strategy synthesised phytoplankton phenological patterns over SWIP into 5 phenoregions, with coherent patterns of timing, magnitude and duration of blooms. The spatial distribution of EPs, Chl-a regions and phenoregions shared similarities, which can be considered the main spatial patterns of SWIP ocean surface. In general, the spatial arrangement of the partition units showed a separation between coastal and open ocean, a latitudinal division (ca. 36.5^{o}N) over the open ocean and, over the coast and slope, the influence of coastal upwelling along the west Portuguese coast and Cape São Vicente, and of river discharge along the northeastern Gulf of Cadiz. The environmental drivers of phytoplankton varied across partition units. Water column stratification, riverine discharge and upwelling intensity were the most influential modulators, and large scale climate indices usually showed minor effects. Environmental variables, Chl-a and phenology showed significant seasonal variability patterns, varying across regions. Interannual patterns were more complex, and significant trends were mostly detected within the Gulf of Cadiz. Linkages between environmental variability and phytoplankton support their use as an indicator of ecosystem status and change.

Keywords: ocean surface partition, satellite remote sensing, unsupervised classification, environmental variability, phytoplankton variability, phytoplankton phenology

RESUMO ALARGADO

O oceano superficial é um domínio extremamente complexo e dinâmico, onde as interações com a atmosfera e o continente modulam a distribuição e atividade dos organismos marinhos e o clima da Terra. O fitoplâncton, principal produtor primário marinho, é fortemente influenciado pelos processos atuantes no oceano superficial, constituindo um importante indicador do estado e variabilidade dos ecossistemas marinhos. Assim, a organização espacial horizontal do oceano superficial, função da variabilidade das propriedades abióticas e comunidades biológicas (incluindo o fitoplâncton), apresenta uma série de unidades funcionais distintas (regiões ou províncias), com atributos e padrões de variabilidade específicos. A partição ou regionalização do oceano, com identificação e delimitação destas unidades funcionais, simplifica a complexidade do oceano superficial e representa uma ferramenta para avaliar e compreender o funcionamento do oceano superficial, apresentando diversas aplicações ao nível do estudo, gestão e conservação dos ecossistemas marinhos. A deteção remota por satélite constitui uma fonte valiosa de dados para a partição do oceano superficial, pois disponibiliza campos sinóticos de várias variáveis oceanográficas e atmosféricas, em escalas espacial e temporal pertinentes, abrangendo períodos de várias décadas.

A presente tese pretende particionar o complexo domínio marinho superficial do sudoeste da Península Ibérica (*Southwest Iberia Peninsula*, SWIP), com base em deteção remota por satélite, e avaliar a variabilidade do fitoplâncton e forçadores ambientais associados em regiões específicas (unidades funcionais) da área de estudo. Para atingir os objectivos principais foi inicialmente efetuada uma revisão do conhecimento científico sobre as estratégias de partição do oceano superficial baseadas em deteção remota por satélite (Capítulo 2) e, posteriormente, foram aplicadas diversas estratégias de partição não-supervisionadas à área de estudo (Capítulos 3 - 5). Tais estratégias permitiram particionar a área de estudo com base em diferentes caraterísticas do oceano superficial (propriedades abióticas, variação da concentração de clorofila-a e índices fenológicos do fitoplâncton) e diferentes abordagens metodológicas (métodos de partição e resolução temporal). As diferentes partições do SWIP foram utilizadas para avaliar os padrões de variabilidade da biomassa e fenologia do fitoplâncton e suas relações com diferentes forçantes ambientais. No contexto deste estudo, as variáveis ambientais avaliadas incluíram variáveis locais indicadoras do ambiente físico, químico e ótico, variáveis hidrológicas indicadoras de processos costeiros

(descarga dos rios e intensidade do afloramento costeiro) e indicadores climáticos de larga escala.

A revisão do estado do conhecimento na área da partição do oceano superficial em unidades funcionais (Capítulo 2) mostrou que a evolução das estratégias de partição acompanhou o desenvolvimento dos produtos de deteção remota da cor do oceano, os quais permitiram a definição de partições dirigidas à avaliação dos ecossistemas marinhos. Com base nesta revisão, as estratégias de partição do oceano superficial devem idealmente considerar os seguintes elementos: (i) objetivos e aplicações; (ii) critérios e dados de entrada; (iii) métodos de partição; e (iv) escalas espaciais e temporais. Para cada um dos elementos referidos, as abordagens utilizadas na literatura científica foram estruturadas e sumarizadas. A utilização do SWIP como um estudo de caso, com análise das partições prévias que contemplaram esta área, demonstrou que as estratégias que aplicaram uma resolução espacial de mesoescala e métodos de delineamento não supervisionados foram mais adequadas para discriminar os principais processos forçadores do fitoplâncton na área de estudo. Assim sendo, estas abordagens foram consideradas nas três estratégias de partição aplicadas na tese.

A partição dinâmica do SWIP, baseada na técnica não-supervisionada de Agrupamento Aglomerativo Hierárquico (*Hierarchical Agglomerative Clustering*, HAC), utilizou variáveis abióticas adquiridas a partir de deteção remota por satélite e modelos computacionais para o período de 2002 a 2011 (Capítulo 3). Inicialmente foram utilizadas 22 variáveis abióticas, representativas dos ambientes físico, químico e ótico do SWIP, com uma resolução temporal e espacial de 16-dias e 4 km, respetivamente. Esta estratégia de partição delineou doze Províncias Ambientais dinâmicas (*Environmental Provinces,* EP), sendo 2 predominantemente costeiras, 2 predominantemente localizadas sobre o talude continental e 8 predominantemente oceânicas. A distribuição espacio-temporal e as propriedades abióticas das EP, bem como sua relevância biológica, foram avaliadas. Durante o ciclo anual, foi detetada uma alternância na extensão e área de cobertura das EP, as quais foram agrupadas de acordo com o período de predominância: frio (outono-inverno) ou quente (primavera-verão). As EP predominantes durante o período frio apresentaram maior variabilidade, especialmente na área central oceânica do SWIP, enquanto as EP predominantes durante o período quente foram mais estáveis em termos de cobertura de área. As propriedades abióticas das EP refletiram os processos oceanográficos e costeiros predominantes dos domínios. Por exemplo, as EP de período quente dominante sobre o talude continental e costa oeste apresentaram

ventos meridionais fortes e intensificação do transporte de Ekman perpendicular à costa, ambos indicativos de aumento de intensidade de afloramento, típico neste período do ano. Adicionalmente, a avaliação da relevância biológica desta partição abiótica indicou diferenças significativas nas propriedades fitoplanctônicas das EP bem como similaridades entre os padrões espaciais desta partição e da partição baseada na abundância do fitoplâncton (resultante da estratégia aplicada no Capítulo 4). Tal resultado demonstrou que a classificação baseada exclusivamente em propriedades abióticas pode representar uma ferramenta valiosa para avaliar propriedades ambientais e estruturas ecológicas.

A segunda estratégia consistiu em uma partição estática do SWIP, baseada nos principais modos de variabilidade espacio-temporal da concentração de clorofila-a (Chl-a), indicadora da biomassa total de fitoplâncton (Capítulo 4). Esta partição utilizou a Chl-a derivada a partir de deteção remota por satélites, durante um período de 15 anos (1997-2012). Os modos dominantes de variabilidade da Chl-a foram extraídos através da análise das Funções Ortogonais Empíricas (*Empirical Orthogonal Functions*, EOF). Esta estratégia de partição identificou e delineou 9 regiões (*Chl-a regions)*, 4 costeiras, 2 sobre ao talude continental e 3 oceânicas. A aplicação de modelos aditivos generalizados a cada *Chl-a region* permitiu identificar os forçadores ambientais relevantes para a previsão da Chl-a em cada região, bem como os seus padrões de variabilidade intra-anuais e interanuais. O poder de previsão dos modelos regionais bem como as forçantes ambientais que os integram variaram marcadamente, apresentando melhor performance para o oceano aberto. As variáveis ambientais locais (ex.: temperatura da superfície do oceano, radiação fotossinteticamente ativa) emergiram como os preditores mais influentes em todas as *Chl-a regions*, enquanto os indicadores de padrões climáticos de larga escala apresentaram efeitos secundários mas ainda significativos. De modo geral, os modelos preditivos das *Chl-a regions* oceânicas indicaram a estratificação da camada superficial como principal fator relacionado ao aumento da disponibilidade de nutrientes. Para as regiões costeiras e sob o talude continental, as descargas fluviais e o afloramento costeiro representaram fontes adicionais de nutrientes. Padrões internanuais significativos, e opostos, foram detetados apenas nas regiões localizadas a sul de 37ºN, com um aumento de Chl-a na região oceânica e um declínio na zona costeira e talude continental. Estes padrões foram acompanhados por um aumento significativo na velocidade do vento e na profundidade da camada de mistura, nas mesmas *Chl-a regions*, os quais podem ter aumentado a disponibilidade de nutrientes e reduzido a intensidade média da luz na camada de mistura.

A terceira e última estratégia de partição aplicada (Capítulo 5) baseou-se nas propriedades fenológicas do fitoplâncton no SWIP, durante um período de 18 anos (1997-2015), e foi desenvolvida com base na aplicação da técnica não-supervisionada HAC. Os índices fenológicos foram derivados a partir de dados de Chl-a, obtidos por deteção remota por satélite, e incluíram o número de *blooms* por ano, a duração total de *blooms* por ano, duração média dos eventos, valor máximo de Chl-a, e datas do início, pico e término dos *blooms*. Esta estratégia de partição estática delineou 5 fenoregiões (*phenoregions*), 3 localizadas sobre a costa e talude continental e 2 oceânicas. No oceano, o fitoplâncton apresentou um único *bloom* por ano, com reduzida intensidade e longa duração, geralmente iniciado em Novembro. Este *bloom* iniciou maioritariamente durante o período de aumento da profundidade da camada de mistura, possivelmente devido ao aumento da disponibilidade de nutrientes. Pelo contrário, as fenoregiões costeiras apresentaram uma elevada variabilidade intra-anual, consequência da ocorrência de múltiplos *blooms* ao longo do ano, intensos e com duração e data de ocorrência variáveis. Nas regiões costeiras, as relações entre a fenologia do fitoplâncton e os forçadores ambientais foram mais complexas, especialmente na fenoregião *Upwelling-influenced*. Nesta, os *blooms* ocorreram maioritariamente em dois períodos, no final do inverno, início da primavera e durante a estação favorável ao afloramento costeiro (Maio-Setembro), reduzindo as associações significativas entre a intensidade do afloramento e os índices fenológicos. Nas restantes fenoregiões costeiras (*Coastal-slope* e *River-influenced*), a descarga do rio Guadalquivir representou um regulador significativo da frequência de *blooms* por ano, bem como da sua intensidade, duração e datas de início. Todas as fenoregiões, exceto uma (*Oceanic*), apresentaram padrões interanuais significativos, para pelo menos um dos índices fenológicos. Nas fenoregiões localizadas na área costeira e de talude continental, foi detetado um aumento linear na duração dos *blooms* de fitoplâncton e sua fase de desaceleração, enquanto a fenoregião *River-influenced* apresentou padrões significativos para as datas dos *blooms*. Adicionalmente, os índices climáticos de larga escala (AMO, NAO e WeMO) correlacionaram-se com os padrões fenológicos em todas as fenoregiões exceto na *Upwelling-influenced*.

De modo geral, a distribuição espacial das unidades de partição identificadas com base nas três estratégias de partição utilizadas na presente tese (EP, *Chl-a regions* e fenoregiões) apresentou similaridades, as quais podem ser consideradas os principais padrões espaciais do oceano superficial no SWIP. Apesar da identificação de um número variável de unidades de partição em função da estratégia aplicada, a organização espacial das mesmas destacou uma

separação gradual entre a costa, talude continental e oceano aberto, e uma divisão latitudinal (cerca de 36.5ºN) no último. Nas áreas sobre a costa e talude continental, as partições destacaram ainda as influências do afloramento costeiro, ao longo do setor oeste de Portugal e Cabo São Vicente, e da descarga fluvial, ao longo do setor nordeste do Golfo de Cadiz. A estratificação da coluna de água, a descarga dos rios Guadiana e Guadalquivir e a intensidade do afloramento costeiro na costa oeste de Portugal foram os fatores ambientais mais influentes nos padrões de variabilidade do ambiente abiótico e na biomassa e fenologia do fitoplâncton no SWIP. Todas as estratégias de partição detetaram uma variabilidade intra-anual significativa, a nível das variáveis abióticas e do fitoplâncton. Nas regiões oceânicas, a Chl-a apresentou um valor máximo anual no final do inverno/início da primavera, gerado pelo aumento da profundidade da camada de mistura e consequente aumento da concentração de nutrientes inorgânicos dissolvidos. Nas regiões costeiras, a variabilidade intra-anual da Chl-a foi mais complexa e apresentou um máximo secundário durante o verão em áreas sob a influência do afloramento costeiro. Em geral, a forte sazonalidade refletiu os efeitos da variabilidade de larga escala no forçamento atmosférico. Estas alteram a circulação do oceano superficial e os processos costeiros, afetando a disponibilidade de nutrientes e luz e, consequentemente, o crescimento líquido do fitoplâncton.

Em relação à variabilidade intra-anual, a variabilidade interanual da cobertura das EP e do fitoplâncton apresentou padrões mais complexos e as regiões com padrões significativos localizaram-se, principalmente, na área do Golfo de Cadiz. Nesta zona, entre o período entre 2002 e 2006, a percentagem da área de cobertura das EP localizadas sobre as áreas costeiras e de talude continental tendeu a diminuir, em simultâneo com o aumento da área das EP oceânicas, fato que pode associar-se à redução do caudal fluvial. A variabilidade interanual da Chl-a também apresentou tendências opostas nas zonas costeira e oceânica do Golfo de Cadiz, com um declínio nas *Chl-a regions* costeiras e de talude continental e um aumento na *Chl-a region* oceânica. Na fenoregião influenciada pela descarga dos rios, foi ainda detetado um atraso nas datas do início, pico e término dos *bloom*. A variabilidade ambiental não mostrou relações claras com os padrões fenológicos, embora a diminuição observada na descarga dos rios possa explicar o atraso nas datas dos *blooms*, devido à redução na disponibilidade de nutrientes. Dos índices de padrões climáticos de larga escala, AMO, NAO e WeMO destacaram-se como forçantes significativos de variações no fitoplâncton para o SWIP, com influências variáveis de acordo com a unidade de partição. De modo geral, AMO atuou mais significativamente sobre os domínios oceânico e do talude continental, a NAO apresentou

relações com o fitoplâncton sobre as regiões a sul de 36.5^{o}N e o WeMO relacionou-se significativamente com os padrões de fitoplâncton nas unidades de partição localizadas na zona de influência dos rios.

Considerando as relações entre o fitoplâncton e os forçadores ambientais identificadas na presente tese, é expectável que as alterações do clima previstas para o SWIP e região nordeste do Oceano Atlântico (ex.: redução da precipitação, aumento da frequência de ondas de calor, da temperatura da superfície do mar) afetem a variabilidade ambiental e o fitoplâncton de forma variável nas várias regiões identificadas no SWIP. A deteção de variações interanuais, bem como a diferenciação entre variações "naturais" e associadas à variabilidade climática, dependerá, contudo, da complexidade da região. De acordo com os resultados desta tese, estas alterações deverão ser mais facilmente detectadas nas regiões oceânicas do SWIP, domínio que apresentou relações menos complexas do SWIP. No entanto, a discriminação entre o efeito da variabilidade climática versus variabilidade natural requererá a análise de séries temporais mais extensas que as exploradas neste estudo. Globalmente, as estratégias de partição utilizadas na presente tese representam metodologias objetivas, reprodutíveis e de custo reduzido, que podem ser aplicadas em diversos ecossistemas marinhos. Adicionalmente, as partições do do oceano superficial podem ser aplicadas com objetivos distintos, incluindo o estudo de processos oceanográficos específicos ou a gestão e conservação de recursos e ecossistemas marinhos. No geral, este estudo evidenciou uma relação significativa entre o fitoplâncton e a variabilidade ambiental no SWIP, suportando a utilização do fitoplâncton como indicador do estado do ecossistema e como elemento-chave para avaliar as respostas dos ecossistemas à variabilidade e alterações climáticas.

Palavras-chave: partição do oceano superficial, deteção remota por satélites, classificação não-supervisionada, variabilidade ambiental, variabilidade do fitoplâncton, fenologia do fitoplâncton.

TABLE OF CONTENTS

LIST OF FIGURES

LIST OF TABLES

CHAPTER 1

GENERAL INTRODUCTION

1.1 Ocean surface partition

The global ocean covers more than 70% of the Earth's surface, with a total volume of *ca.* 1335 million km^3 and an average depth of 3688 m (Eakins and Sharman, 2010). Nevertheless, it is in its surface domain that marine life is most plentiful and where exchanges with atmosphere and land more strongly modulate Earth's climate and impact human wellbeing (Le Quéré and Saltzman, 2009). This uppermost sector of the ocean is a highly dynamic environment, comprising distinct ocean ecosystems, where physical and biogeochemical properties (Fig. 1.1) dictate the distribution, abundance and activity of marine organisms. Due to their complexity, the study and management of ocean surface systems is often facilitated by the reduction of its variability through a partition into homogeneous functional units (IMO, 2005; Longhurst, 2007; Spalding et al., 2012; Dunn et al., 2014).

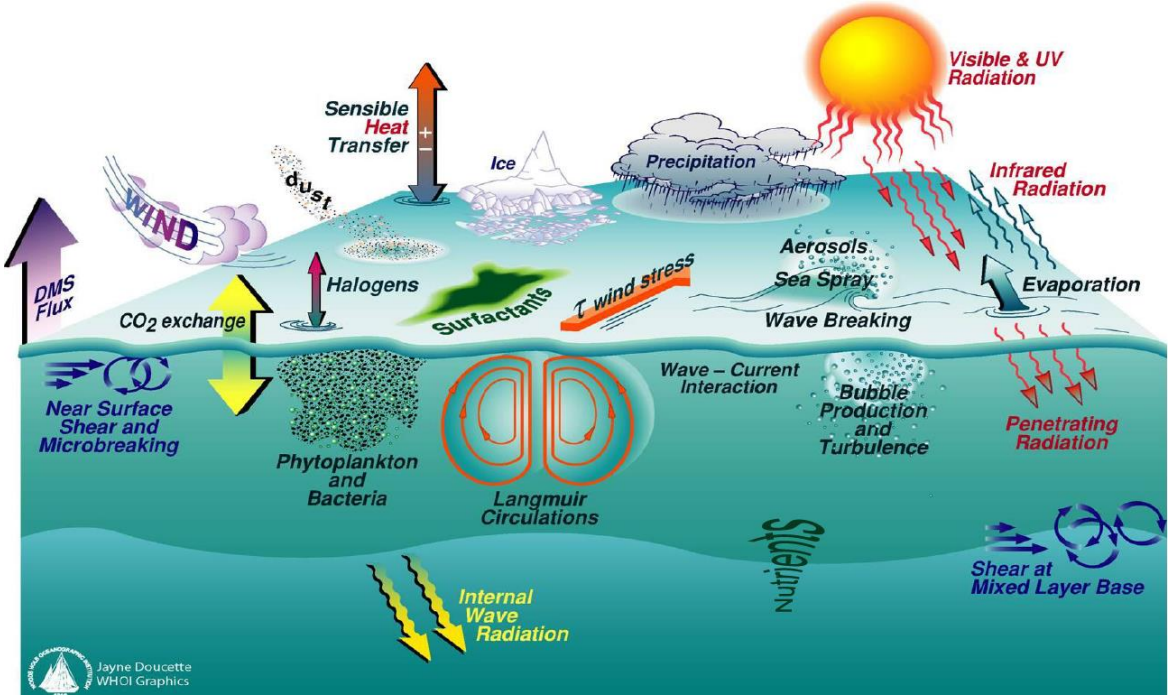

Figure 1.1 – Schematic representation of multiple processes occurring in the ocean surface, results of its interactions with adjacent deeper layer and atmosphere. Adapted from original image by Jayne Doucette (Woods Hole Oceanographic Institute).

Life in the surface ocean is dominated by the plankton, microscopic drifter organisms inhabiting mainly its euphotic (illuminated) zone. Phytoplankton, the autotrophic community within the plankton, are the dominant marine primary producers, responsible for 50% of the

oxygen production in the world (Field et al., 1998), and a fundamental element in the global carbon cycle. Phytoplankton are main actors in the biological pump, the uptake of carbon dioxide (CO_2), assimilated during photosynthesis, and export to the deep ocean (Turner, 2015). As the basis of the marine food web, phytoplankton direct and indirectly control all consumers in the ocean. For instance, phytoplankton phenology is tightly coupled to recruitment success of economically important fish and invertebrate resources (Platt et al., 2003; Fuentes-Yaco et al., 2007; Koeller et al., 2009; Malick et al., 2015). Due to their importance in the ocean system and susceptibility to environment conditions, phytoplankton are considered highly sensitive indicators of ecosystem condition and change (Platt and Sathyendranath, 2008; Barbosa et al., 2010, Racault et al., 2014a). Its variability in space and time, and the surface manifestation of underlying environmental drivers provide valuable aids to partitioning the ocean for enhancing the comprehensive understanding of its structure and functioning (e.g. Longhurst, 2007), as well as evaluation and prediction of ecosystem responses to climate change (e.g., Sarmiento et al., 2004; Henson et al., 2017).

Increasingly, intergovernmental actions incorporate the use of ocean surface partitions for identification and management of marine ecosystems and resources (e.g., IMO, 2005; UNESCO, 2009; Sayre et al., 2017). Concurrently, ocean surface partition has been the subject of intense research. The evolution of the number of indexed articles using simultaneously the terms “ocean surface” and “provinces or regions or partitions” and the number of citations of these articles, available at the Web of Science databases (WoS, Thomson Reuters), exemplify the recent research effort and interest on this topic (Fig. 1.2). A considerable increase is noted since 1995, the year of publication of the first global partition of the ocean surface based on variables that are considered drivers of phytoplankton activity (Longhurst, 1995, 1998, 2007). Alan Longhurst’s partition is widely recognized as an effective representation of the global ocean surface system in homogeneous functional units, designated biogeochemical provinces. An important element of Longhurst’s ocean surface partition is the inclusion, for the first time, of satellite-derived concentration of chlorophyll-a, a proxy for phytoplankton biomass, in the dataset used for the delineation of the biogeochemical provinces.

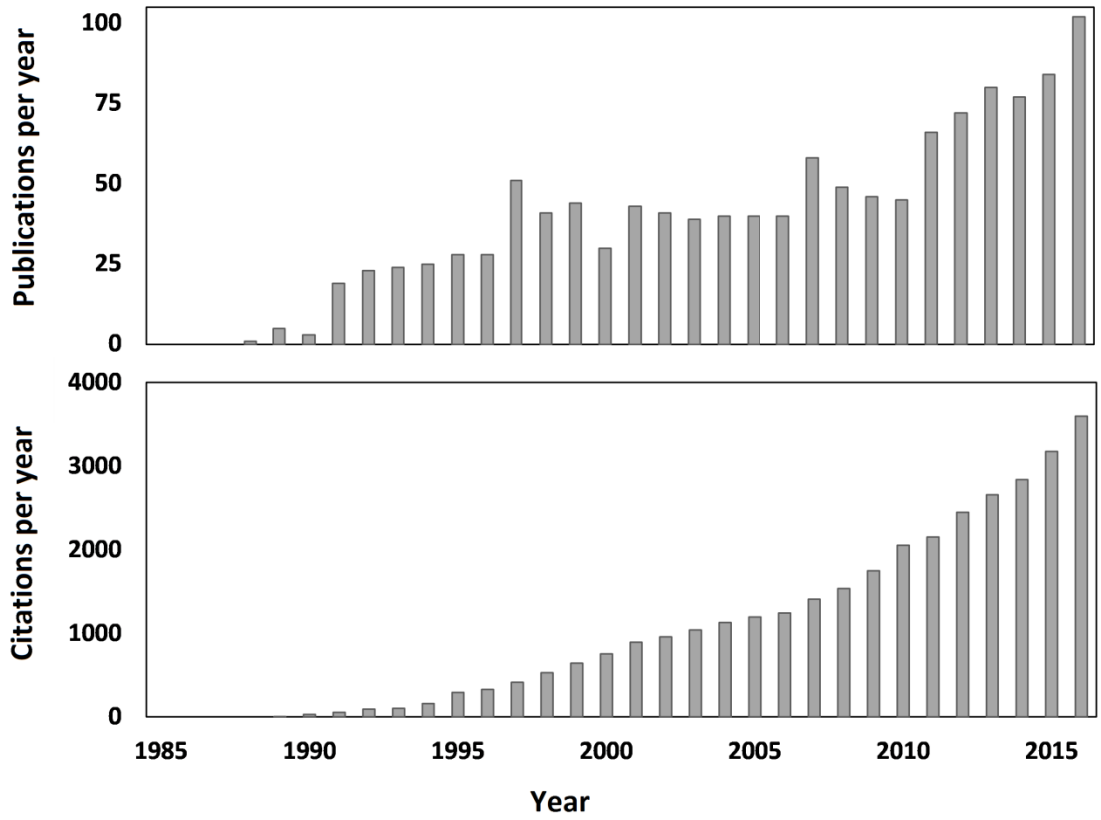

Figure 1.2 – Evolution of (top) the number of indexed articles using and the terms "ocean surface" and "provinces or regions or partitions" and (bottom) the number of citations of these articles, between 1980 and 2016, extracted from the Web of Science database, as in 16 August 2017.

1.2 Satellite remote sensing

Direct sampling and collection of ocean surface properties required for ocean partition are a challenging, complex and expensive task, given the difficult access to specific marine areas and the limitations associated with available funding. *In situ* sampling based on dedicated, "conventional" scientific cruises provides limited spatial and temporal coverage of the ocean surface, at high cost. The use of automated *in situ* sampling platforms (e.g., instrumented buoys, Argo floaters, gliders) has augmented the available *in situ* data, improving its coverage, but is still limited to a restricted set of variables. The World Ocean Database (WOD) provides the most complete quality-controlled database of *in situ* oceanographic data with nearly 19,000 datasets (Boyer et al., 2013). Nevertheless, available data in WOD emphasizes physical variables (e.g, temperature, salinity) in respect to chemical or biological data. The heterogeneous marine domain off southwest Iberian Peninsula (SWIP), NE Atlantic, represents an appropriate example of the limitations in the availability of *in situ* sampling of

ocean surface. According to the WOD database, between 1864 and 2013, surface (0-5 m depth) *in situ* data were sampled at *ca.* 30000 stations over the SWIP area (35-38^{o}N; 5.75-12^{o}W). While all stations included physical information (e.g., temperature), chemical (e.g., nitrate) and biological (e.g., chlorophyll-a) data were very restricted (Fig. 1.3). Moreover, most data were collected between 1950 and 2000, denoting problems associated with temporal coverage.

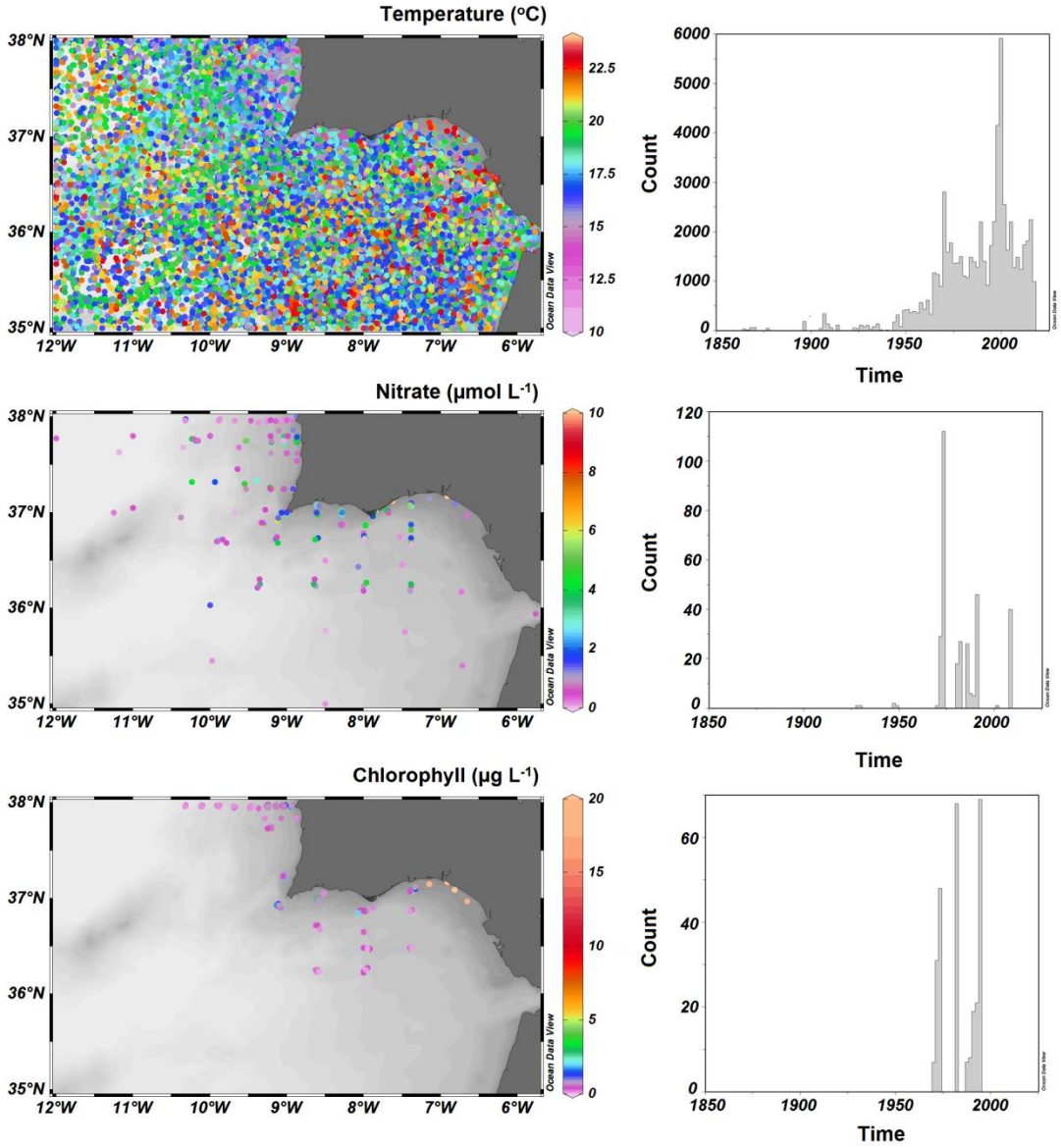

Figure 1.3 – Spatial (right) and temporal (left) distribution of *in situ* ocean surface (0 - 5 m depth) temperature, nitrate and chlorophyll-a data off the Southwest Iberian Peninsula (SWIP), sampled between 1864 and 2013 and available at the World Ocean Database (Boyer et al., 2013).

The ocean surface patterns exhibited in the third front page of this thesis, for instance, could not be captured, at this level of detail, using conventional *in situ* sampling methods. The limitation in temporal and spatial coverage of *in situ* sampling has been alleviated through the use of alternative sources including modelling (e.g. Griffies and Treguier, 2013) and satellite-based remote sensing (Robinson, 2010). Sensors onboard satellites are able to detect and measure the electromagnetic radiation streaming in their direction, assessing four primary properties of the surface ocean: colour, temperature, roughness and height. Any variable or phenomenon related to these properties can, therefore, be evaluated from space (Robinson, 2010). Many of the main oceanographic and atmospheric variables are currently being measured by or inferred from satellite data, on an operational basis, and are freely available from space agencies (Robinson, 2010).

Due to the intrinsic nature of the acquisition, satellite remote sensing data are subject to uncertainties (e.g., instrument noise and atmospheric, terrestrial and water constituents interferences, Robinson, 2010; Merchant et al., 2017). Moreover, an uninterrupted monitoring depends on long-term continuity of comparable missions. The Earth observation scientific community and space agencies are committed to minimize the uncertainties on their delivered products through rigorous data processing, masking and validation/calibration exercises, based on contemporaneous *in situ* data (e.g., Mélin et al., 2016; Jackson et al., *in press*). Likewise, efforts have been developed to merge information derived from different satellite sensors, in specific products, thereby enhancing the temporal and spatial resolution of satellite-retrieved products (e.g., Zhang et al., 2006; Sathyendranath et al., 2016). Despite these limitations, satellite remote sensing is currently the only method available that allows the observation and analysis of the surface marine biosphere, with synoptical coverage, multiple temporal and spatial scales, and near-real time data delivery. Satellite remote sensing is a powerful source of multiple ocean surface variables, relevant for ocean surface partitioning, ultimately supporting the evaluation of marine ecosystem structure and dynamics, and the impacts of environmental variability and change.

1.3 Thesis objectives

This thesis aims to partitioning the surface ocean of the complex marine domain of Southwest Iberia Peninsula (SWIP) based on satellite remote sensing and use it as a framework for assessing phytoplankton variability patterns and underlying environmental drivers. To accomplish the study aims, methods of ocean surface partitioning based on satellite remote sensing are reviewed, and different unsupervised strategies are then applied to the study area. The specific objectives of this thesis are: (1) to make a comprehensive review of ocean surface partitioning strategies using ocean colour remote sensing, its uses and benefits; (2) to use a dynamic strategy for partitioning the SWIP area based on abiotic variables, and assess its biological relevance; (3) to apply a static strategy for partitioning the SWIP area based on Chl-a, and use it to characterize phytoplankton variability patterns and region-specific environmental determinants; and (4) to apply a static strategy for partitioning the SWIP area based on phytoplankton phenological indices, and use it to evaluate phenological patterns and relationships with environmental drivers.

1.4 Thesis outline

The specific objectives are individually addressed and organized into seven chapters, including four main chapters, addressing the literature review (**Chapter 2**) and different SWIP partitioning strategies (**Chapters 3-5**), a general introductory chapter (**Chapter 1**, this section), a final concluding chapter (**Chapter 6**), and the references (**Chapter 7**). Supplemental materials, associated with the four main chapters (Chapters 2-5), are compiled at the end of the document (Appendices A-D, respectively). Each main chapter corresponds to an individual scientific article that has been either published (Chapters 2 and 4), submitted for publication (Chapter 3), or is being prepared for submission (Chapter 5) in indexed scientific journals (Science Citation Index, Thompson Reuters).

CHAPTER 2

OCEAN SURFACE PARTITIONING STRATEGIES USING OCEAN COLOUR REMOTE SENSING

Parts of this Chapter were published in:

Krug, L. A., Platt, T., Sathyendranath, S., Barbosa, A. B., 2017. Ocean surface partitioning strategies using Ocean Colour Remote Sensing: a review. Progress in Oceanography, Volume 155, Pages 41-53, DOI 10.1016/j.pocean.2017.05.013.

ABSTRACT

The ocean surface is organized into regions with distinct properties reflecting the complexity of interactions between environmental forcing and biological responses. The delineation of these functional units, each with unique, homogeneous properties and underlying ecosystem structure and dynamics, can be defined as ocean surface partitioning. The main purposes and applications of ocean partitioning include the evaluation of particular marine environments; generation of more accurate satellite ocean colour products; assimilation of data into biogeochemical and climate models; and establishment of ecosystem-based management practices. This paper reviews the diverse approaches implemented for ocean surface partition into functional units, using ocean colour remote sensing (OCRS) data, including their purposes, criteria, methods and scales. OCRS offers a synoptic, high spatial-temporal resolution, multi-decadal coverage of bio-optical properties, relevant to the applications and value of ocean surface partitioning. In combination with other biotic and/or abiotic data, OCRS-derived data (e.g., chlorophyll-a, optical properties) provide a broad and varied source of information that can be analysed using different delineation methods derived from subjective, expert-based to unsupervised learning approaches (e.g., cluster, fuzzy and empirical orthogonal function analyses). Partition schemes are applied at global to mesoscale spatial coverage, with static (time-invariant) or dynamic (time-varying) representations. A case study, the highly heterogeneous area off SW Iberian Peninsula (NE Atlantic), illustrates how the selection of spatial coverage and temporal representation affects the discrimination of distinct environmental drivers of phytoplankton variability. Advances in operational oceanography and in the subject area of satellite ocean colour, including development of new sensors, algorithms and products, are among the potential benefits from extended use, scope and applications of ocean surface partitioning using OCRS.

2.1 - Introduction

Phytoplankton are the dominant ocean primary producers, a key component of the carbon cycle, a useful indicator of ecosystem condition and a sentinel of change (Gregg et al., 2003; Smetacek and Cloern, 2008). Their distribution and variability reflect the interplay between bottom-up forces, acting directly on growth rates, and top-down forces related to phytoplankton loss (Platt et al., 1991; Cloern and Dufford, 2005). The availability of resources, namely light and inorganic nutrients, under strong physical forcing, is considered a key phytoplankton driver (Margalef, 1978; Longhurst, 1998; Cloern and Dufford, 2005). Phytoplankton, their resources and their consumers are subject to atmospheric and ocean circulation patterns, as well as atmosphere-ocean-land interactions. The physical forcing and associated biological responses determine at horizontal scale, directly or indirectly, a structure composed of units with distinctive ecological functions (Longhurst, 1995, 1998, 2007; Platt and Sathyendranath, 1999). Partitioning the ocean to reveal this complex spatial organization constitutes a tool to improve our understanding of processes regulating phytoplankton distribution, which in turn influences marine food web structure and dynamics (see review by Ducklow, 2003).

In general, partitioning ocean surface into discrete, functional units is valuable for representing environmental variability (e.g., maps); extrapolating local, usually limited, ship-based ocean observations over larger areas (e.g., Hooker et al., 2000); defining inclusive and balanced sampling strategies that avoid over- or under-sampling particular study regions; comparing results from different ocean science disciplines (Kahru et al., 2010; Estrada et al., 2016); and making weighted estimates of regional, basin and global scale biogeochemical fluxes (see Platt and Dowell, 2009; Fay and McKinley, 2014). Moreover, the delineation of surface ocean functional units can be used as template for data synthesis, and as an aid to interpret connections between biological processes (e.g., phytoplankton production) and environmental forcing, and testing ecological hypotheses across environmental gradients. Consequently, ocean partitioning can improve our understanding of global biogeochemical cycles, marine resources and even ecosystem trends under a climate change scenario (Ducklow, 2003; Sarmiento et al., 2004; Dutkiewicz et al., 2009; Morales et al., 2009; Fay and McKinley, 2014). Furthermore, classification of the surface marine environment is relevant for socio-political frameworks linked to sustainable environmental management,

each with specific criteria and approaches for ocean partitioning (see review by Gregr et al., 2012; Spalding et al., 2012; Hao et al., 2015).

The evolution of ocean surface partitioning is strongly linked to that of satellite oceanography, particularly, ocean colour remote sensing (OCRS). Satellite OCRS was initiated in 1978 with the launching of the NASA's Coastal Zone Colour Scanner (CZCS). After CZCS, other ocean colour sensors were developed by several space agencies and countries (see supplementary material, Table A.1). Data from these sensors were and still are extensively used and extremely valuable to biological oceanography. OCRS produces synoptic fields of several optically-active components in the first optical depth of the water column, including chlorophyll-a concentration (Chl-a). As a measure for phytoplankton abundance, Chl-a is one of the most important properties of marine ecosystems; it is commonly used to describe interactions between physical forcing and biological processes. Chl-a and other OCRS products are also used to generate plankton indicators to support ecosystem state assessment and management (Platt and Sathyendranath, 2008; Racault et al., 2014a; Cristina et al., 2015). In addition to OCRS, many of the principal oceanographic and atmospheric variables are currently being measured by satellites or inferred from satellite data, on an operational basis, and are freely available from space agencies (Robinson, 2010; IOCCG, 2012). Although limited to the top layers of the ocean, OCRS is the only method available that allows the analysis of the marine biosphere, at synoptic scales and in near real-time.

Against this background, this studies review the different strategies that have been implemented for partitioning the surface ocean by applying OCRS products, their uses and their benefits. For illustrative purposes and completeness, global key classification schemes that did not use OCRS data have also been reviewed. The paper includes a brief history of ocean surface partitioning using OCRS (Section 2.2) followed by a guide to the different elements to be considered in the partition of surface oceanic ecosystems, including: aims and uses (Section 2.3); variables or criteria (Section 2.4); methods (Section 2.5); and spatial coverage and temporal representation (Section 2.6). Each of these elements requires different approaches that are discussed and exemplified in the pertinent sections and summarized in corresponding tables. Oceanic and coastal areas off the SW Iberia Peninsula (NE Atlantic) are

then used as a case of study to exemplify the results of different classification schemes under complex environmental forcing (Section 2.7).

2.2 - Historical background of ocean surface partitioning using Ocean Colour Remote Sensing

Classification of the global surface ocean began with the navigation era. Gathering information on oceanic conditions (e.g., hydrographic and atmospheric regimes) relied mainly on ship observations and a deepening knowledge of global circulation patterns (see review by Priede, 2014). Surface ocean partition for ecological purposes dates back to the 1940s, and was mostly focused on the distribution of specific taxonomic groups, such as radiolarians, coccolithophorids and copepods (see Spalding et al., 2012 and references therein). During late 1980s, non-taxonomic spatial classification schemes, based mainly on environmental and biological productivity criteria, became more common (Spalding et al., 2012). The contemporaneous development of satellite remote sensing dedicated to ocean colour (Ocean Colour Remote Sensing - OCRS) was a fundamental stimulus for the popularization of these classification schemes.

Platt and Sathyendranath (1988) implemented a strategy to model, for the first time, ocean primary production at synoptic scales, using OCRS and season-specific geographical-dependent photosynthetic parameters. These parameters can be estimated by partitioning the ocean surface into functional units on the basis of their biogeochemical properties (Platt and Sathyendranath, 1988). Longhurst et al. (1995) and Longhurst (1995, 1998, 2007) extended this partition to the global ocean, establishing a set of biogeochemical provinces based on variables that are considered drivers of phytoplankton activity. Mixing and stratification of the water column, euphotic zone depth, wind, surface irradiance, nutrient concentrations and Chl-a were some of the variables used for partitioning. The global ocean was divided into four primary ecological biomes or domains (Polar, Westerly wind, Trade wind and Coastal), which were subsequently divided into 56 biogeochemical provinces. Longhurst provided, for the first time, a formal objective partition of the world ocean based on regional oceanography, introducing the utility of OCRS for this purpose (IOCCG, 2009). Longhurst's biogeochemical provinces are well-accepted and also used as a template in other ocean classification studies (e.g. Platt et al., 2005; Devred et al., 2007; Vichi et al., 2011; Reygondeau et al., 2013).

An important characteristic of Longhurst's provinces, however, is the rectilinear shape and static condition of the province boundaries, which were considered as an intermediate rather than final stage of a complete partition. The need to incorporate dynamism for the province boundaries, since they shift following temporal changes in environmental forcing, was emphasized by Platt and Sathyendranath (1988) and by Longhurst (1995) and later demonstrated by Devred et al. (2007, 2009) and Reygondeau et al. (2013). Moreover, Longhurst's partition overlooks the complexity of coastal domains and submesoscale processes, potential issues for the classification of specific areas of regional interest (e.g., Cloern and Jassby, 2008; Winder and Cloern, 2010). Nonetheless, his pioneering work laid the foundation for an invaluable and diverse application of OCRS to spatial classification, improving its uses for evaluation and management of marine ecosystems.

2.3 - Aims and uses of partitioning

In a dynamic environment, abiotic and biotic properties of the ocean surface are neither constant in time nor uniform in space. The classification of the surface ocean into spatial functional units aims to partition an area of interest into subareas, assumed internally-uniform in respect of environmental properties. The designation attributed to these functional units varies according to the aims and the set of environmental variables and/or criteria used for partition (Table 2.1). The Longhurst (1995, 1998, 2007) classification system, for instance, uses biomes (or domains) as primary units, and biogeochemical provinces are then defined based on biogeochemical properties. Province, along with region, is the most common term used to designate a spatial functional unit. A more specific designation is sometimes used, depending on the criteria used for classification (e.g., biophysical region, optical region, bio-physical-optical province; see Table 2.1).

Table 2.1 - Typical aims and uses of ocean surface partitioning studies, applying ocean colour remote sensing data, and specific designation of derived spatial units. *not including ocean colour remote sensing data.

Main aim/use of partition	Unit designation	References
Functional units		
Assessment/Classification of:		
Biogeochemical environment	biogeochemical province, zone, biome	Longhurst, 1995; Longhurst, 1998; Longhurst, 2007; Briceño and Boyer, 2010*; Kahru et al., 2010; Fay and McKinley, 2014

Biogeographic environment	ecological province, marine ecoregion, cluster, pelagic province, ecoregion, region	Spalding et al., 2007; Hardman-Mountford et al., 2008; D'Ortenzio and d'Alcalà, 2009; Taylor et al., 2011*; Spalding et al., 2012; Acevedo-Trejos et al., 2013; Baker and Hollowed, 2014*; Foukal and Thomas, 2014
Bio-physical-optical environment	region	Mueller and Lange, 1989*; Callejas-Jimenez et al., 2012
Bio-physical environment	eco-region, ecological province, biophysical region, region	Hoepffner and Dowell, 2005; Platt et al., 2005; Saraceno et al., 2006; Barale, 2010; Nieblas et al., 2014
Ecological environment	large marine ecosystem	Sherman, 1991*; Sherman, 1994*
Hydrographic environment	province	Hooker et al., 2000*
Optical environment	class of spectra, water type; water class, optical water type	Karabashev et al., 2002; Traykovsky and Sosik, 2003; Lubac and Loisel, 2007*; Vantrepotte et al., 2012; Mélin and Vantrepotte, 2015
Physical-geographic environment	marine region; ecoregion	Gregr and Botker, 2007; Fendereski et al., 2014
Physical-optical environment	water mass; biogeographic province	Oliver et al., 2004; Oliver and Irwin, 2008
Analysis of spatial-temporal variability patterns	zone, province, region, biogeochemical province, cluster, biome, bioregion	Brock et al., 1998; Navarro and Ruiz, 2006; Devred et al., 2007; Macías et al., 2007; Devred et al., 2009; Irwin and Oliver, 2009; Henson et al., 2010; Reygondeau et al., 2013; Waite and Mueter, 2013; Blondeau-Patissier et al., 2014b; Caballero et al., 2014; Fay and McKinley, 2014; Mayot et al., 2015
Application to ocean modelling	region, geographic province, biogeochemical province	Platt and Sathyendranath, 1988; Sathyendranath et al., 1991*; Sathyendranath et al., 1995; Longhurst et al., 1995; Watts et al., 1999; Hemmings et al., 2004; Sarmiento et al., 2004*
Ocean management and conservation	eco-region; biogeographic region	ICES, 2004*; Hao et al., 2015*; Muñoz et al., 2015
Water types		
Improvement of ocean colour remote sensing products	water class, water type	Moore et al., 1998; Moore et al., 2001; Feng et al., 2005*; D'Alimonte et al., 2007*; Moore et al., 2009; Shi et al., 2013

The main uses of ocean-surface partitioning into functional units include classification and/or assessment of environmental characteristics, analysis of ecosystem spatial-temporal patterns,

ecosystem modelling, and ocean management and conservation (Table 2.1). The use of functional units for the assessment of environmental variability within an area of interest is also a tool for evaluating ocean variability patterns, including global alterations in marine ecosystems. For instance, biome-specific areal coverage contraction and expansion rates were detected using a global classification of the surface open ocean (Fay and McKinley, 2014). An expansion in the area covered by extremely oligotrophic provinces, located in central-ocean areas, during a 10-year period (1998-2007) was observed by Irwin and Oliver (2009). Moreover, global shifts in the coverage of biogeochemical provinces during the period 1997-2007, under different phases of El Niño Southern Oscillation (ENSO), were reported by Reygondeau et al. (2013). The detection and understanding of temporal trends and connections between environmental forcing and biota, for example phytoplankton, are facilitated if the area of interest is partitioned into uniform functional units that share similar environment-biota interactions. In some heterogeneous areas, where distinct, sometimes opposing, phytoplankton temporal trends may occur in different functional units, the analysis of the study area as a whole precludes the detection and full understanding of phytoplankton variability patterns (Devred et al., 2009). Moreover, the use of ocean surface partitions can improve the discrimination of climate change-driven phytoplankton (Chl-a and primary production) trends from natural variability. For instance, more stable equatorial biomes require a shorter time series (ca. 20-30 years) compared with more variable mid-latitude biomes (Henson et al., 2010). Other applications of ocean partitioning for understanding phytoplankton responses to environmental forcing, were presented by Waite and Mueter (2013) and Blondeau-Patissier et al. (2014b) with static and dynamic functional units, respectively.

Ocean-surface partitioning has also been used as a framework for modelling purposes (e.g., Vichi et al., 2011). It was used by Platt and Sathyendranath (1988) as a framework for modelling phytoplankton primary production in the Atlantic Ocean; similar approaches were subsequently applied in regional (e.g., NW Indian Ocean, Watts et al., 1999) and global contexts (e.g., Longhurst et al., 1995). Other uses of ocean partitioning using OCRS data include the calibration of ecosystem models (Hemmings et al., 2004) and prediction of climate warming impacts on ocean ecosystems (Sarmiento et al., 2004; Dutkiewicz et al., 2009 and references therein; Britten and Primeau, 2016). According to Sarmiento et al. (2004), projected warming impacts include global shifts in the spatial distribution of nutrient

concentrations, physical attributes and phytoplankton, with resultant changes in province boundaries.

Ocean-surface classification schemes have also been used as structures for ocean management and conservation. Indeed, the global partitions of coastal areas into Large Marine Ecosystems (LME, Sherman, 1991, 1994) or Marine Ecoregions of the World (MEOW, Spalding et al., 2007), and oceanic areas into Pelagic Provinces of the World (PPOW, Spalding et al., 2012), were strongly motivated by partition benefits aimed at ecosystem monitoring, management and conservation. The LME partition delineates large areas (200,000 km²) with distinct hydrographic regimes, submarine topography, productivity and trophically-dependent populations (Sherman, 1991), whereas MEOWs and PPOWs consider biodiversity data (Spalding et al., 2007, 2012). At a more regional scale, classification studies, based on oceanographic variables, species richness and vulnerability, were also used to establish priority areas for conservation and prescribing appropriate management regulations (ICES, 2004; Hao et al., 2015; Muñoz et al., 2015; Table 2.1). As emphasized by Spalding et al. (2012), these environmental-based classifications of marine systems represent a much richer tool for management than existing geo-political administrative classifications (e.g., Exclusive Economic Zones). In effect, national and international directives move towards the use of ecosystem-based classification strategies to assess and mitigate risks to the marine environment (EU, 2008; FGDC, 2012). Although LME, PPOW or MEOW partitions did not use OCRS data explicitly, ocean-colour based approaches have an increasing role in such classifications schemes (e.g., Muñoz et al., 2015). Indeed, phytoplankton is an indicator listed explicitly in the Marine Framework Strategy Directive of the EU and, for example, Chla-based partitions can be used to evaluate eutrophication and marine environmental status (EU, 2008), and assess and predict environmental risk associated to harmful algal blooms (Anderson et al., 2016).

A special case of classification of surface ocean using OCRS data is the delineation of optical water types. Based on optical characteristics, water type classification has an important role in the improvement of ocean colour products at regional scales. In-water, *optically-active constituents,* water molecules, photosynthetic organisms, coloured dissolved organic matter (CDOM) and suspended materials interact differently with spectrally-resolved light. These differences are generally encapsulated in two basic water types: Case I and Case II (Morel and

Prieur, 1977; Morel, 1988). Case I waters, usually associated with open ocean environments, have optical properties predominantly affected by photosynthetic organisms (i.e., phytoplankton), associated biota (e.g., bacteria and virus) and related degradation products (e.g., detritus, dissolved organic matter). In Case II waters, typically located near the coast, particulate material (other than phytoplankton) and dissolved compounds significantly affect the behaviour of light in the water column. Furthermore, in Case II waters, we cannot assume any type of covariance between phytoplankton and other optically-active substances present in the water. Most standard algorithms for retrieval of ocean colour products have better performance in Case I waters, due to their lower optical complexity (Sathyendranath, 2000). Alternative algorithms dedicated to optically-complex Case II waters are not universally applicable due to differences in the relative composition of optically-active compounds between different coastal regions (Dowell et al., 2009; see review by Blondeau-Patissier et al., 2014a). Thus, the development of region-specific algorithms that incorporate variability in in-water optical properties is required to improve the accuracy of OCRS products in Case II waters (e.g., Sá et al., 2015; Cristina et al., 2016b).

The delineation of optical water types (hereafter designated water types) ultimately allows the development of regional algorithms that weight the contributions of specific water types (Table 2.1). Water types can also be used for estimation of uncertainties associated with OCRS products (Moore et al., 2009; Grant et al., 2016). Classification of water types is usually based on an input optical dataset derived from *in situ* observations. The input dataset is sorted into a number of types (classes or groups) according to their similarities, that is, similar elements of the dataset belong to same water type. The statistics are computed based on all observations in the dataset associated with each type, and then applied to OCRS images on a pixel-by-pixel basis, according to the memberships of the types in each pixel. Note that pixels are associated with one or multiple water types, according to the delineation method utilized (e.g. Moore et al., 2001; Shi et al., 2013).

2.4 - Partition variables and/or criteria (input dataset)

Any quantitative classification process implies grouping elements based on a set of specific variables and criteria, which are usually related to the main purpose of partition. For this review, ocean classification schemes using OCRS data were grouped according to the

variables used as input dataset in studies based exclusively on abiotic variables, based exclusively on biotic variables and on combinations of both. Studies using only abiotic optical variables were considered separately (Table 2.2). In this context, the biotic and abiotic variables derived from products of OCRS included: chlorophyll-a concentration (Chl-a), surface photosynthetically available radiation (PAR), euphotic zone depth (Z_{eu}), total organic carbon (TOC), total suspended matter (TSM), light attenuation coefficient ($K_{(\lambda)}$), absorption coefficients (a) of phytoplankton, particulate organic matter and coloured dissolved organic matter (CDOM), normalized water leaving radiance ($nLw_{(\lambda)}$) and remote sensing reflectance ($R_{rs(\lambda)}$), at specific wavelengths (see Robinson, 2010).

The exclusive use of optical variables represents a particular case of abiotic-based partition schemes (Table 2.2), which are usually used for water type classification. In such studies, the partition criteria use variables such as *in situ*-derived remote sensing reflectance, at specific wavelengths ($R_{rs(\lambda)}$, Lubac and Loisel, 2007; Mélin and Vantrepotte, 2015), and satellite-derived normalized water leaving radiance ($nLw_{(\lambda)}$, Karabashev et al., 2002; Santamaría-del-Angel et al., 2011; Callejas-Jimenez et al., 2012). Some studies used mixed datasets that combine optical and other abiotic variables (e.g., $R_{rs(\lambda)}$ and SST, Oliver et al., 2004; $nLw_{(\lambda)}$ and SST, Oliver and Irwin, 2008 and Irwin and Oliver, 2009).

Ocean classification schemes exclusively based on abiotic variables usually assume that there is a significant environmental control over the distribution and dynamics of biotic components (see Ducklow, 2003; Platt et al., 2005). Gregr and Botker (2007), for example, defined North Pacific marine regions using a set of abiotic environmental data (wind stress, surface current velocity, sea surface height, salinity and temperature), deliberately leaving biotic criteria out. Similarly, Fendereski et al. (2014) used abiotic data (sea surface salinity and temperature, total suspended matter, ice fraction and bathymetry) to classify the Caspian Sea into eco-regions, interpreting the partition as consequence of climate, circulation and riverine influence. Both studies demonstrate that bottom-up control of phytoplankton, a key biotic element, by physical drivers is reflected in purely abiotic-based ocean partitions. Indeed, satellite derived average Chl-a values were statistically dissimilar across functional units, for both studies. Furthermore, spatial distribution of higher trophic level species were also reflected in ocean partitions exclusively based on abiotic variables (e.g., Baker and Hallowed, 2014; Fendereski et al., 2014). The use of classification schemes predominantly based on

abiotic variables is particularly relevant for any marine domain where biological information is absent or sparse, such as submarine seamounts (Clark et al., 2011) and deep-sea floor (Watling et al., 2013).

Table 2.2 - Ocean surface classification studies applying ocean colour remote sensing (OCRS) data, organized according to the variables commonly used for partitioning. Legend: a = Absorption coefficients, Chl-a = Chlorophyll-a concentration, DO = Dissolved oxygen, $K_{(\lambda)}$ = Light attenuation coefficient at specific wavelengths, MLD = Mixed layer depth, nLw(λ) = Normalized water leaving radiance at specific wavelengths, PAR = Photosynthetically available radiation, PP = Primary productivity, $R_{(\lambda)}$ = reflectance at specific wavelengths, $R_{rs(\lambda)}$ = Remote sensing reflectance at specific wavelengths , S = Salinity vertical profile, SSH = Sea surface height, SSS = Sea surface salinity, SST = Sea surface temperature, T = Temperature vertical profile, TOC = Total organic carbon, TSM = Total suspended matter, Z =Depth, and Z_{eu} = Euphotic zone depth. * not including OCRS data. OCRS-derived variables are underlined.

Input dataset	**Variables**	**References**
Exclusively optic	$\underline{nLw_{(\lambda)}}$, $\underline{R_{(\lambda)}}$, $\underline{R_{rs(\lambda)}}$	Moore et al., 2001; Karabashev et al., 2002; Feng et al., 2005*; Lubac and Loisel, 2007*; Santamaría-Del-Ángel et al., 2011; Callejas-Jimenez et al., 2012; Vantrepotte et al., 2012; Shi et al., 2013; Mélin and Vantrepotte, 2015
Abiotic	currents, ice fraction, $\underline{K_{(\lambda)}}$, MLD, $\underline{nLw_{(\lambda)}}$, nutrients, picnocline, $\underline{R_{rs(\lambda)}}$, S, SSH, SSS, SST, T, <u>TSM</u>, wind, Z	Platt and Sathyendranath, 1988; Brock et al., 1998; Sathyendranath et al., 1991*; Hooker et al., 2000*; Oliver et al., 2004; Sarmiento et al., 2004*; Gregr and Botker, 2007; Oliver and Irwin, 2008; Irwin and Oliver, 2009; Henson et al., 2010; Fendereski et al., 2014; Hao et al., 2015*
Biotic	<u>Chl-a</u>, other specific photosynthetic pigments	Longhurst et al., 1995; Esaias et al., 2000; Navarro and Ruiz, 2006; Macías et al., 2007; Hardman-Mountford et al., 2008; D'Ortenzio and d'Alcalà, 2009; Taylor et al., 2011*; Waite and Mueter., 2013; Blondeau-Patissier et al., 2014b; Foukal and Thomas, 2014; Mayot et al., 2015
Mixed	<u>a</u>, <u>Chl-a</u>, density, DO, geographical coordinates, eddy activity, ice fraction, $\underline{K_{(\lambda)}}$, MLD, $\underline{nLw_{(\lambda)}}$, nutrients, <u>PAR</u>, $\underline{R_{rs(\lambda)}}$, S, Secchi depth, SSS, SST, T, <u>TOC</u>, <u>TSM</u>, <u>turbidity</u>, wind, $\underline{Z_{eu}}$, zooplankton abundance	Mueller and Lange, 1989*; Sherman, 1991*; Sherman, 1994*; Longhurst, 1995; Longhurst, 1998; Moore et al., 1998; Watts et al., 1999; Traykovski and Sosik, 2003; Hemmings et al., 2004; Hoepffner and Dowell, 2005; Platt et al., 2005; Saraceno et al., 2006; D'Alimonte et al., 2007*; Devred et al., 2007; Longhurst, 2007; Devred et al., 2009; Moore et al., 2009; Barale, 2010; Briceño and Boyer, 2010*; Kahru et al., 2010; Acevedo-Trejos et al., 2013; Reygondeau et al., 2013; Baker and Hallowed, 2014*; Caballero et al., 2014; Fay and McKinley, 2014; Nieblas et al., 2014; Muñoz et al., 2015

Ocean partitions based exclusively on biotic information, use *in situ* or satellite-derived Chl-a as an input variable, sometimes complemented by information on other phytoplankton photosynthetic pigments. Chl-a can be used directly, as a proxy for phytoplankton biomass, or indirectly in combination with other biotic and abiotic variables (Table 2.2). For instance, bloom phenology, derived from analysis of Chl-a time series data, was used to delineate bioregions in the Mediterranean (D'Ortenzio and d'Alcalà, 2009; Mayot et al., 2015), and ratios between specific photosynthetic pigments and surface Chl-a were used to delineate bio-optical provinces along a North-South Atlantic transect (Taylor et al., 2011). For the latter study, the distribution of station clusters closely followed Longhurst's biogeochemical provinces (see Fig. 1 in Taylor et al., 2011), which were based on a combination of abiotic and biotic variables.

In fact, variables and/or criteria for delineation of ocean surface functional units often combine biotic processes and abiotic driving forces (Table 2.2). The biotic variable(s) can be combined with single or multiple abiotic variables, or, as single compound variables, derived from statistical relationships between biotic and abiotic variables. For example, correlation patterns between satellite-derived Chl-a and global wind time series were used to classify the surface ocean objectively, providing a consistent view of the primary drivers of phytoplankton growth (nutrients or light, see Kahru et al., 2010). Although not used explicitly in the context of ocean partitioning, the application of correlation patterns between satellite-derived SST and phytoplankton primary production global time series (e.g., Behrenfeld et al., 2006) or correlations between Chl-a and absolute dynamic topography (Navarro et al., 2011) could also provide potential partition criteria. The use of a set of environmental variables with high biological relevance enables a more comprehensive evaluation of ocean biodiversity, biogeochemical processes and underlying controls (IOCCG, 2009; Acevedo-Trejos et al., 2013; Fay and McKinley, 2014). However whatever variables are used in the input dataset (abiotic and/or biotic), the ecological relevance of ocean partitions should be ideally inspected using independent comprehensive biological information, such as biomass, production and community composition of both pelagic and benthic communities (e.g., Gregr and Botker, 2007, Verfaillie et al., 2009, Fendenreski et al., 2014).

2.5 - Delineation methods

Until late 1990s, classification schemes for the surface ocean were based mostly on supervised learning strategies, relying on literature review and the use of expert judgment (Table 2.3). For instance, the Equatorial and North Atlantic (20^{o}S-50^{o}N) were partitioned using depth (shelf, slope, oceanic) and latitudinal zones (equatorial, subtropical and transitional, Platt and Sathyendranath, 1988). Oceanographic features, such as the California Current system and the North Pacific gyre, were used to delineate bio-optical provinces in the Northeast Pacific (Mueller and Lange, 1989). Expert judgment was also used subsequently in global classification of coastal areas (LMEs, Sherman, 1991, 1994; MEOWs, Spalding et al., 2007), epipelagic areas (PPOW, Spalding et al., 2012) and deep ecosystems (Clark et al., 2011; Watling et al., 2013), mostly aiming at the assessment of marine living resources and ecosystem management. Later, using less subjective approaches, Brock et al. (1998) and Watts et al. (1999) applied decision trees and Boolean logic for delineating surface provinces in the NW Indian Ocean. For instance, Watts et al. (1999) established a decision tree where stations were assigned first to provinces according to bathymetry; stations shallower than 2500 m were further classified according to SST (high or low), and stations deeper than 2500 m were categorized according to Chl-a (high or low).

The application of unsupervised learning methods for ocean surface classification was initiated in the early 2000s. This statistical approach recognizes inherent patterns through data exploration, without expert knowledge, being objective, easily reproduced, and appropriate to large datasets (Wilks, 2006). Clustering, or cluster analysis, is the most utilized unsupervised learning technique and became a popular method for delineation of ocean provinces (Table 2.3). This method identifies subsets (clusters) in the input dataset, based on similarity measured by distance metrics; closer elements belong to the same cluster and are separated by smaller distances relative to the distances between clusters (Wilks, 2006).

Table 2.3 - Main methods used for ocean surface classification, applying ocean colour remote sensing data. * not including ocean colour remote sensing data.

Method	References
Supervised	
Expert knowledge / literature review	Platt and Sathyendranath, 1988; Mueller and Lange, 1989*; Sherman, 1991*; Sherman, 1994*; Longhurst et al., 1995; Longhurst, 1995; Sathyendranath et al., 1995; Longhurst, 1998; ICES, 2004; Platt et al., 2005; Longhurst, 2007; Spalding et al., 2007; Henson et al., 2010; Spalding et al., 2012; Hao et al., 2015*
Boolean logic/ Decision tree	Sathyendranath et al., 1991*; Brock et al., 1998; Watts et al., 1999; Sarmiento et al., 2004*; Fay and McKinley, 2014
Unsupervised	
Clustering	
Hierarchical	Traykovski and Sosik, 2003; Oliver et al., 2004; Saraceno et al., 2006; Lubac and Loisel, 2007*; Oliver and Irwin, 2008; Irwin and Oliver, 2009; Briceño and Boyer, 2010*; Taylor et al., 2011*; Vantrepotte et al., 2012; Shi et al., 2013; Fendereski et al., 2014
Nonhierarchical	Moore et al., 1998; Karabashev et al., 2002; Oliver et al., 2004; Feng et al., 2005*; Devred et al., 2007; Oliver and Irwin, 2008; D'Ortenzio and d'Alcalà, 2009; Devred et al., 2009; Irwin and Oliver, 2009; Kahru et al., 2010; Acevedo-Trejos et al., 2013; Blondeau-Patissier et al., 2014b; Foukal and Thomas, 2014; Nieblas et al., 2014; Mayot et al., 2015; Mélin and Vantrepotte, 2015
Fuzzy	Moore et al., 2001; Hoepffner and Dowell, 2005; Lucieer and Lucieer, 2009*; Moore et al., 2009
Empirical Orthogonal Function	Navarro and Ruiz, 2006; Macías et al., 2007; Hardman-Mountford et al., 2008; Santamaría-Del-Ángel et al., 2011; Callejas-Jimenez et al., 2012; Caballero et al., 2014; Muñoz et al., 2015
Non-Parametric Probabilistic Ecological Niche Model	Reygondeau et al., 2013

Unsupervised clustering techniques include two basic approaches: hierarchical and nonhierarchical clustering (Table 2.3). Hierarchical Agglomerative Clustering (HAC) starts with single data elements as individual clusters and, at each step, pairs of elements that are closest in their n-dimensional space are merged into a new single cluster. The ideal final result is a division of the dataset that simultaneously minimizes differences between members of a given cluster, and maximizes differences between members of different clusters (Wilks, 2006). For surface ocean classification, the most commonly used functional metrics for

defining distance (how close two elements are) and linkage (how close two clusters are) are Euclidian distance and the Ward's linkage (Ward, 1963), respectively (e.g., Traykovski and Sosik, 2003; Oliver et al., 2004; Shi et al., 2013).

Nonhierarchical clustering, by contrast, starts with all data elements distributed into a predefined number of clusters and rearranges them, until the smallest distance ideal criterion (i.e., elements belong to the cluster with the closest centroid value) is satisfied. The most common nonhierarchical clustering approach for partitioning is the K-means method (e.g., Karabashev et al., 2002; Irwin and Oliver, 2009; Blondeau-Patissier et al., 2014b). In K-means, at each step, data elements are assigned to the cluster with the closest centroid value, which is then recalculated, until the smallest distance criterion is reached. A slightly modified version of K-means, the Iterative Self-Organizing Data Analysis Technique (ISODATA) was applied in Moore et al. (1998) and Mélin and Vantrepotte (2015) classification schemes.

All previously-mentioned clustering techniques divide data into 'crisp' or hard clusters, where each data element belongs to a single cluster. However, fuzzy analysis (FA), an alternative strategy, considers that a data element may be assigned to more than one cluster. Fuzzy partitioning has advantages over hard classifiers by allowing the quantification of uncertainty and the representation of transition zones between clusters (Lucieer and Lucieer, 2009). FA attributes degrees of membership to each specific data element with values between 0.0 (weak) and 1.0 (strong), which represent the strength of its association with a particular cluster. This approach is translated into smoother boundaries between provinces, highlighting a soft transition between neighbouring clusters, shifting from strong to weak association between data elements and a cluster (Moore et al., 2001). The most common fuzzy partitioning algorithm used for delineating ocean surface functional units and water types is the fuzzy C-means (FCM) (e.g., Moore et al., 2001; Oliver et al., 2004; Moore et al., 2009). Using Euclidean distance metrics, FCM derives fuzzy membership values based on the similarity between specific data elements and mean values of clusters located in a multivariate space (Bezdek et al., 1984). Other fuzzy techniques, such as Fuzzy Maximum Likelihood Estimation (FMLE), originally implemented for the classification of seabed sediments in SE Australia (Lucieer and Lucieer, 2009), could also represent a tool for the delineation of ocean surface functional units. According to these authors, the main advantage of FMLE is to accommodate a more realistic shape for the clusters in the multidimensional space.

In addition to cluster analysis, another unsupervised classification method often used for classifying surface ocean areas is the Empirical Orthogonal Function (EOF) analysis. Also known as Principal Component Analysis, the EOF can be useful for compressing the spatial-temporal variability in complex time series data, partitioning data variance into a set of dominant mathematically-orthogonal (independent) functions or modes (e.g., Yoder et al., 2002; Monahan et al., 2009). In the context of surface ocean classification using OCRS data, EOF analysis has usually been applied to remotely sensed Chl-a or $nLw_{(\lambda)}$ time series maps, whose pixels represent single vectors and are treated independently (e.g., Macías et al., 2007; Callejas-Jimenez et al., 2012). There are as many EOF modes as composite images, but most of the original variance is contained within the first few modes. The combination of dominant EOF spatial modes is subsequently used to delineate distinct coherent, co-varying units (e.g., Navarro and Ruiz, 2006).

2.6 - Spatial coverage and temporal representation

Ocean surface spatial classification studies can be grouped into three levels of spatial coverage, defined according to the extent of the area of interest (see Table 2.4): global, macroscale (> 1000 km) and mesoscale (10 - 1000 km). Global and macroscale ocean partitions have been used as a framework for ecosystem based management of marine living resources (Sherman, 1991; Sherman, 1994; ICES, 2004; Spalding et al., 2007, 2012), but also as structures for identifying large-scale ocean regions based on biogeochemical function, and interpreting or predicting biogeochemical processes (Longhurst et al., 1995, 1998, 2007; Fay and McKinley, 2014; Britten and Primeau, 2016; see Table 2.1). However, local phytoplankton productivity and associated food web dynamics are strongly affected by mesoscale (McGillicuddy Jr, 2016) and/or submesoscale (Mahadevan, 2016) natural (i.e., atmospheric and oceanic) and anthropogenic-related processes. Therefore, a comprehensive discrimination of the specificities in environmental-biological interactions, at regional or local scales, benefits from ocean partitioning at a finer spatial coverage: resolving the small scale helps to understand the larger-scale structure.

Table 2.4 - Typical spatial coverages and temporal representations used in surface ocean classification studies applying ocean colour remote sensing data. [C]*Coastal only;* [O]*Open ocean only.* * not including ocean colour remote sensing data.

Spatial coverage	**Temporal representation**	**References**
Global	Static	Sherman, 1991*[C]; Sherman, 1994*[C]; Longhurst et al., 1995; Longhurst, 1995; Longhurst, 1998; Longhurst, 2007; Spalding et al., 2007[C]; Hardman-Mountford et al., 2008; Henson et al., 2010; Kahru et al., 2010; Spalding et al., 2012[O]
	Dynamic	Esaias et al., 2000; Sarmiento et al., 2004*; Oliver and Irwin, 2008; Irwin and Oliver, 2009; Moore et al., 2009; Reygondeau et al., 2013; Fay and McKinley, 2014[O]; Mélin and Vantrepotte, 2015[C]
Macroscale *> 1000 km*	Static	Platt and Sathyendranath, 1988; Mueller and Lange, 1989*; Sathyendranath et al., 1995; Moore et al., 1998; Watts et al., 1999; Hooker et al., 2000*; Moore et al., 2001; ICES, 2004; Saraceno et al., 2006; Chassot et al., 2007; D'Ortenzio and d'Alcalà, 2009; Barale, 2010; Taylor et al., 2011*; Waite and Mueter, 2013; Hao et al., 2015*
	Dynamic	Brock et al., 1998; Hemmings et al., 2004; Hoepffner and Dowell, 2005; Platt et al., 2005; Devred et al., 2007; Gregr and Botker, 2007; Devred et al., 2009; Callejas-Jimenez et al., 2012; Baker and Hallowed, 2014*; Foukal and Thomas, 2014; Nieblas et al., 2014; Mayot et al., 2015
Mesoscale *10 - 1000 km*	Static	Sathyendranath et al., 1991*; Feng et al., 2005*; Navarro and Ruiz, 2006; D'Alimonte et al., 2007*; Lubac and Loisel, 2007*; Macías et al., 2007; Briceño and Boyer, 2010*; Blondeau-Patissier et al., 2014b; Caballero et al., 2014; Fendereski et al., 2014; Muñoz et al., 2015
	Dynamic	Karabashev et al., 2002; Traykovski and Sosik, 2003; Oliver et al., 2004; Santamaría-Del-Ángel et al., 2011; Vantrepotte et al., 2012; Shi et al., 2013

For example, the Mediterranean Sea constitutes a single unit in various global scale classification schemes: Longhurst's biogeochemical provinces (Longhurst, 2007), Large Marine Ecosystems (Sherman, 1994) and optical-based coastal water types (Mélin and Vantrepotte, 2015). At a macroscale level, the International Council for the Exploration of the Sea (ICES), whose classification of the European seas includes socio-political criteria,

classified the Mediterranean into three eco-regions delimited by geographical constraints (ICES, 2004). The Nieblas et al. (2014) combination of commonly-used variables (SST, Chl-a, bathymetry) with mesoscale circulation features (Chl-a and SST surface fronts, eddy kinetic energy, horizontal mixing and vorticity indices) assigned five dynamic subprovinces to the Mediterranean and Black Sea. Partition studies at the mesoscale spatial coverage level (10 to 1000 km), even illustrated singularities of specific sectors of the Mediterranean, including water type classification (Eastern Mediterranean, Karabashev et al., 2002; Northern Adriatic, D'Alimonte et al., 2007) and phytoplankton driving processes (Western Mediterranean, Macías et al., 2007). The mesoscale-level classification of the Alboran Sea (Western Mediterranean) depicted the strong connections between localized meso- and submesoscale features (coastal upwelling, Alboran Gyre) and phytoplankton variability (Macías et al., 2007), showing the overall benefits of smaller-scale coverage for ocean spatial classification.

With respect to temporal representation, two levels have been considered for ocean classification studies: static and dynamic (Table 2.4). Static representations of ocean surface spatial units (water types or functional units) are useful for many purposes (see section 2.2). However, these time-invariant ocean partitions do not capture an important aspect of real ocean systems, its temporal dynamism. Indeed, boundaries between ocean functional units move, as the environmental forcing varies over time, at intra-annual, interannual and longer-time scales. The use of time-varying dynamic partitions, with elastic boundaries and without pre-determined spatial units, enables the analysis of ocean processes at multiple, biologically-relevant temporal scales (e.g., El Niño, climate change; see review by IOCCG, 2009; Fay and McKinley, 2014). Computation of temporal and spatial stability of province boundaries provides visual and quantitative metrics for evaluating local impacts of mesoscale features (Nieblas et al., 2014). Likewise, core biome maps, which include only pixels that do not change partition assignment over time (Fay and McKinley, 2014), can be used to identify more stable and/or resilient regions. Furthermore, dynamic partitions provide valuable insights into the levels of environmental heterogeneity, an issue related to a phenotypic plasticity of biota and climate change (Boyd et al., 2016).

Benefits of the implementation of dynamic over static partitions are better inferred from the comparison of studies that applied the same partition criteria for the same area of interest. For instance, both D'Ortenzio and d'Alcalà (2009) and Mayot et al. (2015) used phytoplankton

phenology for the classification of the Mediterranean Sea, but the latter used a dynamic approach. This dynamic classification generated average annual maps (1999-2014), allowing the evaluation of inter-annual variability of multiple key environmental drivers (winter deep convection events, frontal instabilities, inflow of Atlantic and Black Sea waters and river runoff) on phytoplankton dynamics (Mayot et al., 2015).

In some cases, static classification schemes (Longhurst, 1998, 2007) can be used as a framework for implementing dynamic partitions (Platt et al., 2005; Devred et al., 2007, 2009). These studies implemented an objective dynamic classification scheme to delineate provinces in the NW Atlantic Ocean, using Longhurst's provinces as a template and a set of abiotic and biotic variables (satellite-derived SST, Chl-a, geographical coordinates and bathymetry). Derived time-varying season-specific, dynamic partitions demonstrated seasonal shifts in province boundaries, and afforded a better interpretation of *in situ* phytoplankton production patterns (Devred et al., 2007). The use of an unsupervised dynamic approach also introduced an additional partition over and above the original partitions of Longhurst, a slope transition province (Devred et al., 2007). This study clearly demonstrated how OCRS data may be used, in real time, to refine the conventional Longhurst's biogeochemical provinces, replacing rectilinear artificial province boundaries by realistic moving boundaries, which even reproduce the meandering structure of NW Atlantic currents (see Dowell et al., 2009). Devred et al. (2009) have subsequently analysed decadal changes in SST, Chl-a and diatom occurrence in the NW Atlantic Ocean. For some provinces, trends based on dynamically-assigned provinces, i.e., accounting for the movement of the boundaries, are significantly different from trends derived using province average positions (Devred et al., 2009), adding a new perspective to the detection and interpretation of long-term changes.

2.7 - Study case: partitioning areas off South West Iberian Peninsula

This case study presents the results of different ocean partition schemes in an area under highly complex environmental forcing, the SW Iberia Peninsula (SWIP). Located at the south-western most part of Europe (NE Atlantic, Fig. 2.1), the SWIP encompasses a wide variety of coastal and oceanographic regimes, and phytoplankton dynamics is impacted by processes such as coastal upwelling (Navarro and Ruiz, 2006; Cardeira et al., 2013; Goela et al., 2015), riverine inputs (Prieto et al., 2009; Caballero et al., 2014), submarine groundwater

discharge (Piló et al., *in prep*.), tidal currents (García-Lafuente and Ruiz, 2007), mesoscale circulation patterns (Reul et al., 2006), and stratification of water column (Navarro and Ruiz, 2006). Along the SWIP coast, the Ria Formosa coastal lagoon (Portugal) and the Marismas de Odiel, Guadalquivir Estuary and Doñana National Park (Spain) have considerable ecological and economic importance. These ecosystems and related drainage basins support a wide range of human uses (e.g., tourism, fisheries, aquaculture, agriculture), and are impacted by multiple anthropogenic disturbances (Newton et al., 2014; Ruiz et al., 2014). Furthermore, SWIP, along with Southern Europe, is classified as a region particularly vulnerable to climate change; projected alterations include decreased precipitation, increased frequency and intensity of heat-waves and decline in provision of ecosystem services (Kovats et al., 2014). Partitioning the SWIP area into functional units can be used as a tool to improve our understanding of the effects of natural and anthropogenic forces on the regional marine ecosystems, and to predict how projected climate change scenarios will specifically affect a very heterogeneous marine domain.

The SWIP area is usually poorly represented in global scale classification schemes with coarse spatial resolution. According to the Longhurst (2007) global classification, the SWIP is partitioned into two biogeochemical provinces (Fig. 2.1, see green line): an oceanic province (depth> 2500 m), the eastern North Atlantic Subtropical Gyre Province (NAST-E); and a coastal province (depth> 2500 m), the Canary Current Coastal Province (CNRY). NAST-E shows an annual stratification-destratification cycle, with a deep winter mixed layer depth (MLD), which promotes the advection of inorganic nutrients into the euphotic zone. Due to nutrient limitation, this pattern indirectly controls phytoplankton production leading to late winter-early spring blooms, tightly coupled to zooplankton (Longhurst, 2007). At CNRY province, in addition to late winter-spring blooms, the wind-driven vertical transport of nutrients, eddies and filaments associated with seasonal coastal upwelling are key determinants of phytoplankton variability (Longhurst, 2007). The SWIP area was also partitioned into two provinces in the global classification of the epipelagic areas (PPOW, Spalding et al., 2012): the North Atlantic Transitional, most of the SWIP offshore sector, and the Canary Current, which comprises the southern sector of the Gulf of Cadiz (Fig. 2.1, see dashed red line). According to the global dynamic classification of the open ocean of Fay and Mckinley (2014), the SWIP area was again integrated into two biomes: the subtropical, seasonally-stratified biome, and the subtropical permanently stratified biome, in the most

offshore southwestern sector. Interestingly, global classification schemes using OCRS data and unsupervised methods partitioned the SWIP area into a higher number (3 - 4 units) of spatial functional units (Hardman-Mountford et al., 2008; Oliver and Irwin, 2008; Reygondeau et al., 2013; Mélin and Vantrepotte, 2015), underlining its heterogeneity.

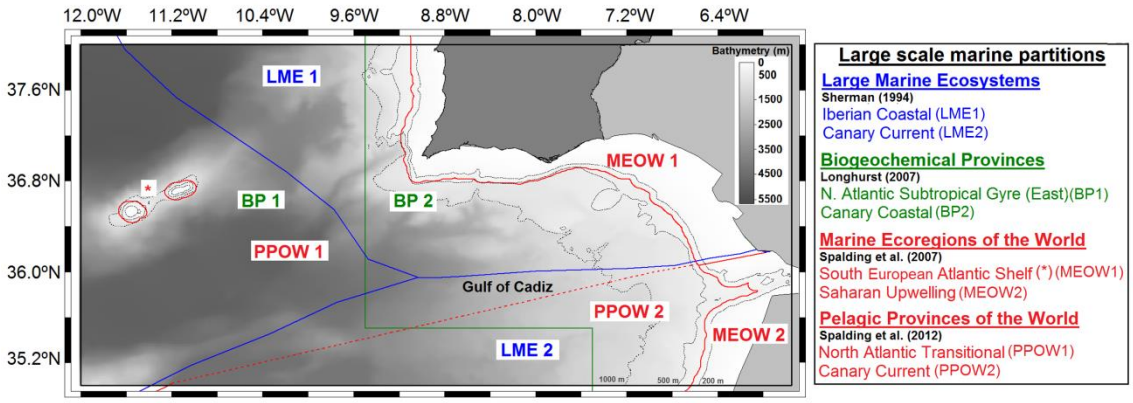

Figure 2.1 - Global ocean surface partitions for the domains off South West Iberian Peninsula (NE Atlantic) with overlaid bathymetry (General Bathymetric Chart of the Oceans, GEBCO_2014 Grid, version 20150318, http://www.gebco.net). Large Marine Ecosystems and Biogeochemical Provinces shapefiles downloaded from Claus et al. (2016). Marine Ecoregions and Pelagic Provinces of the World shapefiles provided by The Nature Conservancy (2012).

Considering global classification schemes of coastal and shelf areas, the SWIP area is also partitioned into two units (Fig. 2.1) for both the Large Marine Ecosystems (Sherman, 1991; Sherman, 1994) and Marine Ecoregions of the World (MEOW, Spalding et al., 2007). According to the LME classification, whose boundaries expand beyond the continental shelf, the SWIP is segmented into two ecosystems (Fig. 2.1, see blue lines), both under the influence of coastal upwelling processes: the Iberian Coastal, which covers the Atlantic coast of the Peninsula; and the Canary Current LME, that integrates the upwelling region off the coast of northwest Africa (see reviews by Aquarone et al., 2008 and Heileman and Tandstad, 2008). According to the MEOWs classification, the coastal SWIP, integrated in the Lusitanian Province, is partitioned into two ecoregions: South European Atlantic Shelf and Saharan Upwelling (Fig. 2.1, see continuous red line).

At the macroscale coverage level, the SWIP was included in the dynamic unsupervised fuzzy classification of the European Seas (Hoepffner and Dowell, 2005). This partition scheme, based on satellite retrieved Chl-a, SST and photosynthetic available radiation (PAR) data,

partitioned the European Seas into nine classes, generating monthly maps of dominant provinces for the 1999-2000 period (Hoepffner and Dowell, 2005). According to this study, the SWIP area is partitioned into three main provinces that vary on a seasonal basis: Province 1 (Oligotrophic Tropical), Province 2 (Temperate with shallow MLD), and Province 3 (Temperate with deep MLD), with very low to low Chl-a. These provinces expand and contract over the annual cycle, leaving usually two provinces during each specific season. Province 2 is present most of the year whereas the importance of provinces 1 and 3 increases during summer and winter, respectively. Apparently, a fourth province, with medium Chl-a, is occasionally present during spring, in the SWIP coastal area (see Fig. 4A-D in Hoepffner and Dowell, 2005). Hoepffner and Dowell (2005) introduced a valuable dynamism into this macroscale partition, allowing the detection of province shifts over the year. However, the temporal coverage (2 years) and level of detail for the SWIP area are still limited, particularly for the coastal domains.

The south sector of the SWIP area was later the focus of three mesoscale level classification studies, based on EOF analysis (Fig. 2.2). Not explicitly addressing ocean partitioning, Navarro and Ruiz (2006) used weekly Chl-a time series, covering a 5-year period (1998-2002), to evaluate region-specific physical-biological coupling in the Gulf of Cadiz (Fig. 2.2A). This study delineated five zones (four coastal and one offshore), showing distinct region-specific relationships between Chl-a and environmental forcing variables (mixed layer depth, nutricline depth, zonal winds, rainfall, riverine discharge). At a more local scale (Fig. 2.2B, see red rectangle), Caballero et al. (2014), using weekly composites of Chl-a and nLw_{555} over a 10-year period (2003-2013), showed the strong dynamism of the Guadalquivir turbidity plume region, with respect to both location and areal extent, with impacts on phytoplankton distribution.

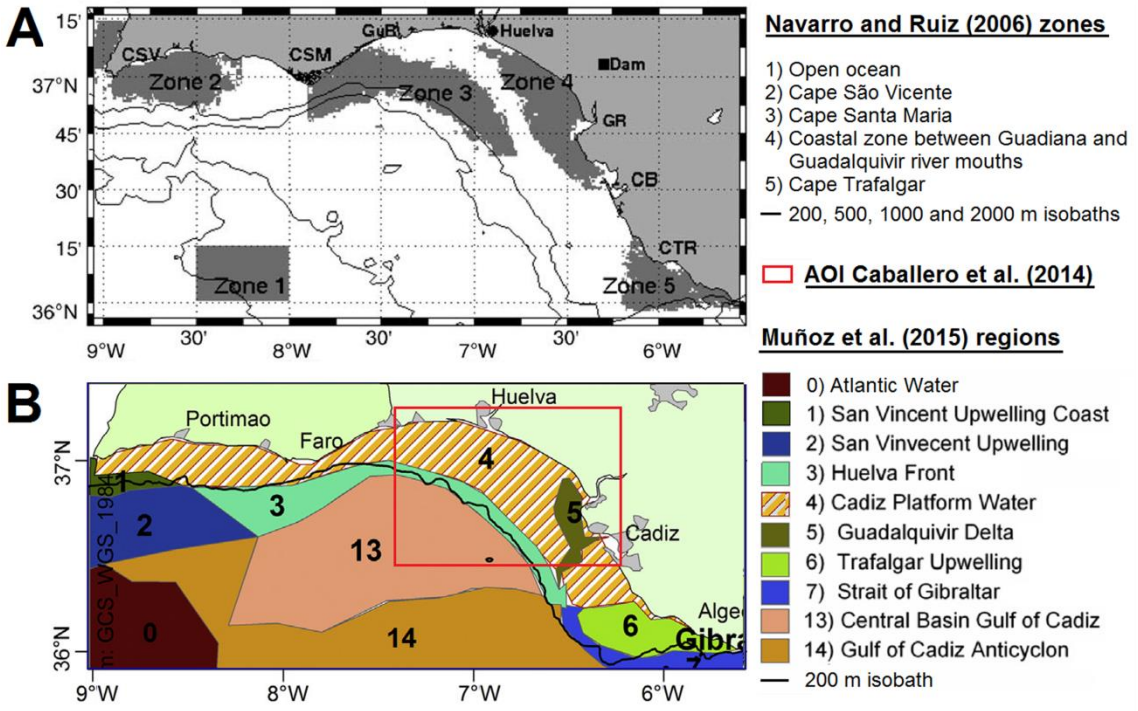

Figure 2.2 - Representation of spatial functional units in the Gulf of Cadiz (NE Atlantic) associated to mesoscale-level partition studies, based on spatial empirical orthogonal function analysis. (A) Zones of distinct phytoplankton variability patterns (left) and respective designations (right). Source: adapted from Navarro and Ruiz (2006). (B) Gulf of Cadiz section of the regionalization of marine waters of the South Iberia Peninsula (left) and designations (right). Source: adapted from Muñoz et al. (2015). The red rectangle represents the approximate area of interest (AOI) of Caballero et al. (2014). See the text for further details.

Also based on EOF analysis, Muñoz et al. (2015) used dynamics of geostrophic currents and 3-day composites of SST and Chl-a over a 5-year period (2005-2009) to regionalize (classify) the Gulf of Cadiz and the Alborán Sea (W Mediterranean). The Gulf of Cadiz was divided into 10 out of 24 regions (Fig. 2.2B), reflecting recognized mesoscale and local features including upwelling areas, fronts and riverine influence (Muñoz et al., 2015). This classification was used to discuss the need for marine spatial planning and coastal management strategies to facilitate the conservation and recovery of resources by reducing cumulative human impacts, especially in more vulnerable areas (e.g., productivity hot spots in coastal and enclosed areas; Muñoz et al., 2015).

These mesoscale-level classifications of the SWIP area present an appropriate level of spatial detail, and partition confirmed high levels of spatial-temporal variability, a consequence of the complexity of multiple natural and anthropogenic processes, operating at multiple

timescales, acting on phytoplankton across the land-sea interface (Cloern and Jassby, 2008, 2010; Cloern et al., 2016). However, the implementation of a dynamic time-varying classification would certainly facilitate the interpretation of this spatial-temporal variability and heterogeneity. Lastly, in the context of the SWIP area, these three mesoscale classification studies covered only the more enclosed Gulf of Cadiz, excluding the western coastal sectors and NE Atlantic open ocean waters. According to Relvas et al. (2007), western Iberian domains are also subject to intense mesoscale activity throughout the year, superimposed on larger scale variability, making use of a dynamic partition particularly suitable for the SWIP.

2.8 - Concluding remarks and future directions

As stated by Platt and Sathyendranath (1999), "*parameters controlling the ecophysiology of the ocean are distributed in a piecewise manner"* and the partition of surface ocean areas into functional units facilitates the interpretation of ocean processes. At that time, the challenge was to define methodologies capable of objectively assigning grid cells, at any given time, to specific units. We can state with confidence that this challenge was conquered mainly by developments in OCRS and statistical techniques for analyses of the data (IOCCG, 2009). The main advantages of OCRS as data source include: (i) a spatial coverage which allows global to submesoscale assessments (≤ 1 km) at low cost; (ii) a near real time, systematic high-frequency sampling (1 day) since 1997, providing multi-decadal time series; (iii) a set of relevant products (e.g., Chl-a, optical properties) used to derive various ecological indicators relevant for the characterization of climate, biogeochemical cycles and marine food web dynamics (Platt and Sathyendranath, 2008; Racault et al., 2014a); and (iv) a gridded geo-referenced format, which provides uniform distribution of data.

The full inclusion of time series of OCRS data, along with other variables, creates large datasets whose analyses require considerable computational and statistical power. The development of these technologies supported the transition of subjective classification methods towards unsupervised methods (e.g., clustering, EOF analyses; IOCCG, 2009). For the latter, objective metrics can be serially applied, providing a less biased delineation of ocean partitions with a more accurate representation of ocean surface dynamics. In addition,

the use of fuzzy classification schemes that admits membership to multiple partition units, permits smooth transitioning between unit boundaries (Moore et al., 2001).

Independently of the partition method, temporal representation of partition schemes can be static (time-invariant) or dynamic (time-varying). Static partition schemes provide multiple benefits for understanding environmental-biological interactions in the marine domain. However, dynamic approaches offer a more realistic depiction of surface ecosystems by adding to these benefits the increment of spatial-temporal environmental heterogeneity evaluation. Dynamic approaches allow the distinction between stable and unstable regions (Nieblas et al., 2014), the detection of shifts in environmental conditions and the discrimination of unit-specific trends sometimes undetectable when considering the entire area (Devred et al., 2007, 2009). As shown using the SW Iberian Peninsula case study, the selection of areal spatial coverage is fundamental for assessing linkages between environment forcing and biota for a highly-heterogeneous area (Navarro and Ruiz, 2006; Muñoz et al., 2015). Mesoscale partitions reflected the relevance of mesoscale and local processes for phytoplankton (a fundamental indicator of ecosystem status and dynamics), and were further discussed as a putative tool for marine spatial planning and management (Muñoz et al., 2015).

This review demonstrated that OCRS data integrated into different schemes of ocean partitioning support the interpretation of ocean processes and, specifically, phytoplankton dynamics. Current and future developments on OCRS and other remote sensing platforms may extend the power of ocean-surface partitioning applicability to investigate patterns and processes of the biodiversity-ecosystem functional relationship. OCRS-derived variables, namely global (Saba et al., 2011; Jacox et al., 2015) and class-specific phytoplankton primary production (Uitz et al., 2010), loss rate and growth rate (Platt and Sathyendranath, 2008), ocean carbon export (Siegel et al., 2014, 2016) and community structure (IOCCG, 2014) are still underexplored. The recent development of specific algorithms, that allow the evaluation of other biological properties, including planktonic dimethylsulfoniopropionate (Galí et al., 2015), specific types of algal blooms (Blondeau-Patissier et al., 2014a) and phytoplankton groups, including size classes or functional types (see IOCCG, 2014; Rousseaux and Gregg, 2015), could represent a promising approach for surface ocean partitioning. The continuation of OCRS satellite missions is assured by new dedicated sun-synchronous sensors (See Table A.1). Novel applications of geostationary satellite sensors for ocean colour additionally

improve the temporal resolution for specific regional domains, to several times a day, allowing the inclusion of short-term processes (e.g., tides, vertical migration, storms and internal waves; IOCCG, 2012). The development of other automated indirect ocean observing systems, including mooring stations, autonomous drifters (e.g., BIO-Argo floats, IOCCG, 2011) and gliders, represent valuable additional sources of biotic and abiotic data for ocean partitioning, also allowing the exploration of ocean vertical structure (Racault et al., 2014a).

In summary, all different strategies of ocean surface partition reviewed here offer valuable insights for assessing ocean ecological structure. The incorporation of OCRS data into objective methods for delineation of dynamic functional units, however, allows a more flexible and realistic representation. Partition of the surface ocean is still underexplored and, due to its benefits, this practice merits a more extensive implementation in ocean science. Direct applications comprise the definition of inclusive balanced field sampling strategies, assimilation into climate and biogeochemical models, and estimation of uncertainties for OCRS products. In fact, the latter are currently provided by ESA's Ocean Colour Climate Change Initiative (Moore et al., 2009; Grant et al., 2016). Partitioning ocean surface is also fundamental for science-based environmental management decisions. Indeed, intergovernmental actions concerning increased human-driven alterations of marine ecosystems are moving towards the use of integrated ecosystem-based management approaches (e.g., United Nations Environment Programme) and integrated governance on the high seas will benefit from the availability of an ocean partition as a template for action.

CHAPTER 3

DELINEATION OF OCEAN SURFACE PROVINCES OVER A COMPLEX MARINE DOMAIN (OFF SW IBERIA): AN OBJECTIVE ABIOTIC-BASED APPROACH

Parts of this Chapter were submitted to:

Krug, L.A., Platt,T., Barbosa, A.B. Delineation of ocean surface provinces over a complex marine domain (off SW Iberia): an objective abiotic-based approach. Submitted to Regional Studies in Marine Science journal in 6 September 2017.

ABSTRACT

The partition of complex marine domains into homogeneous units serves as a tool to assess their driving forces and patterns, but should ideally incorporate the dynamic nature of marine ecosystems. The area off South West Iberian Peninsula (SWIP, NE Atlantic) is located in a biogeographical transition zone between temperate and subtropical waters, including diverse oceanic and coastal domains. These domains are influenced by local and large scale oceanic and atmospheric circulation patterns, topographic irregularities, coastal upwelling and continental freshwater outflows. The main objective of this study was to delineate a dynamic abiotic-based partition of the heterogeneous surface SWIP area into environmental provinces (EPs). The specific objectives were to evaluate the spatial-temporal distribution and abiotic properties of the EPs, as well as the biological relevance of this abiotic partition. Hierarchical Agglomerative Clustering, an unsupervised classification technique, was used for establishing SWIP dynamic EPs, based on a nearly 10-year time series (2002 - 2011) of physical, chemical and optical variables, acquired from satellite remote sensing and model-derived data, at a 16-day, 4-km resolution. The biological relevance of this abiotic-based partition was assessed using province-specific phytoplankton properties and a comparative analysis with a previous, exclusively biotic-based static partition of the study area. SWIP abiotic environmental variability was incorporated into 12 dynamic spatially coherent EPs, two coastal, two slope and eight oceanic EPs, whose areas and location varied over the year. EPs predominant during the cold period (autumn-winter) presented higher variability, especially over the oceanic central SWIP area. During the warm period (spring-summer), the signature of coastal upwelling was evident, particularly over the western slope and coastal EPs. Riverine discharge was also a relevant local control of abiotic properties over coastal EPs. Overall, the spatial-temporal coverage patterns of EPs and abiotic and biotic properties showed a good agreement with previous remote sensing and in situ-based studies of the SWIP area, especially over the oceanic and slope sectors. Differences in phytoplankton metrics across EPs and similarities with a previous static biotic-based SWIP regionalization indicated the biological relevance of this dynamic abiotic partition. The combination of a broad dataset, derived from remote-sensing and modelling products which are available through operational oceanography programs, and objective unsupervised data compression and classification methods, represented a suitable strategy for characterizing SWIP ocean surface environment. Direct applications of this partition strategy include its use as support for designing sampling strategies, ocean modelling, assessing and interpreting environmental and biological patterns, and ecosystem-based management and conservation.

3.1 – Introduction

Ocean surface environmental properties vary in both time and space, under the control of circulation patterns, geographical constraints and atmosphere-ocean-land interactions. In addition, anthropogenic influences and climate change are also altering marine ecosystem properties and several aspects of their functions (Scheffers et al., 2016). An effective approach for assessing and understanding the patterns of ocean spatio-temporal variability is to partition ocean surface into units with similar properties, often (and hereafter) designated as provinces (Longhurst, 2007; IOCCG, 2009). The delineation of ocean provinces is a valuable strategy for evaluating environmental variability, modelling biogeochemical processes, the improvement of ocean-colour remote sensing product, marine spatial planning and ecosystem-based management and conservation strategies (see review in Chapter 2, also and hereafter Krug et al., 2017).

Ocean partition has also been used to detect and interpret connections between environmental forcing and biological responses, including phytoplankton biomass and productivity, fundamental indicators of ecosystem status and dynamics (e.g., Platt and Sathyendranath, 1988; Waite and Mueter, 2013; Blondeau-Patissier et al., 2014b; Mayot et al., 2015). These studies used partitions based on satellite-retrieved chlorophyll-a concentration (Chl-a), a proxy for phytoplankton biomass, either exclusively or in combination with abiotic environmental variables. However, in some studies, ocean partitioning was based exclusively on abiotic environmental properties, assuming that physical-chemical forcing has a strong control over the biotic components, a common premise in plankton (e.g., Gregr and Bodtker, 2007; see Fendereski et al., 2014 and references therein) and benthic ecology (Verfaille et al., 2009; Akoumianaki et al., 2013). Ecosystem partitions based on satellite-retrieved abiotic products offer a valuable alternative when biological information is absent or scarce, and can be used to delineate ecological zones ideally after a comparison with biological information (Verfaille et al., 2009; Gregr et al., 2012; Grilli and Shumchenia, 2015). Satellite remote sensing is frequently used as a data source due to its multiple advantages (Robinson, 2010), all of which greatly benefit ocean-partition exercises (IOCCG, 2009; see review by Krug et al., 2017). Moreover, many satellite-retrieved products (e.g., sea-surface temperature, chlorophyll-a concentration, wind speed and direction) are defined as Essential Climate

Variables (ECV), that is, they are relevant for climate characterization and are systematically measured at a global scale, on an operational basis (Bojinski et al., 2014).

The southwest area off the Iberian Peninsula (SWIP, NE Atlantic) constitutes a complex environment with offshore and coastal domains influenced by coastal upwelling, riverine and submarine groundwater discharges, mesoscale circulation features and the confluence of Mediterranean and Atlantic waters (García-Lafuente and Ruiz, 2007; Relvas et al., 2007). SWIP is located in a biogeographical transition zone, between temperate and subtropical waters, and is classified as being very vulnerable to climate change. Projected climate trends for the area include increased frequency and intensity of heatwaves and decline in precipitation and provision of ecosystem services (Kovats et al., 2014), and an intensification of coastal upwelling along the western Iberia coast (Sousa et al., 2017).

Previous global scale studies partitioned the SWIP area into two to four provinces (Sherman, 1994; Longhurst, 2007; Spalding et al., 2007, 2012; Fay and McKinley, 2014), whereas a macroscale study of the European Seas included three main provinces within SWIP (Hoepffner and Dowell, 2005). At the regional (mesoscale) scale, several partitioning studies addressed the SWIP area (see Chapter 4, also and hereafter Krug et al., *in press*) or the Gulf of Cadiz sub-area (Navarro and Ruiz, 2006; Muñoz et al., 2015). These studies, either solely based on Chl-a variability (Navarro and Ruiz, 2006; Krug et al., *in press*) or on its combination with abiotic variables (Muñoz et al., 2015), delineated up to 10 provinces within SWIP. However, except for Hoepffner and Dowell (2005), a macroscale dynamic partition based on a short temporal coverage (two-year), all SWIP partitions used a static delineation approach, yielding provinces whose fixed boundaries do not reproduce the natural dynamism of the ocean surface (see review by Krug et al., 2017).

In this context, our study aimed to characterize the abiotic environmental conditions and variability in surface SWIP area during a *ca.* 10-year period (February 2002 - December 2011), using a dynamic approach. A set of abiotic variables representative of physical, chemical and optical environments, and an unsupervised classification technique were used to delineate dynamic environmental provinces (EPs) within SWIP, a novel approach for the study area. Specific study objectives were: (1) to partition the highly heterogeneous surface SWIP area into dynamic EPs, based on abiotic variables; (2) to evaluate province-specific

spatial distribution and temporal patterns, at both seasonal and interannual time scales; (3) to characterize SWIP abiotic environmental provinces; and (4) to assess the biological relevance of this abiotic-based partition, using province-specific phytoplankton properties as proxies for biological responses. Based on previously reported phytoplankton environmental driving forces over the SWIP area (see Krug et al., *in press* and references therein), we hypothesized that EPs based solely on abiotic variables would have both physical-chemical and biological significance.

3.2 - Materials and Methods

3.2.1 Study area

SWIP integrates a deep oceanic area, interspersed by submarine seamounts and canyons, and a 5 to 35 km wide continental shelf (Fig. 3.1). Coastal orientation changes from meridional to zonal at Cape São Vicente (CSV), the northwest limit of Gulf of Cadiz (GoC), a basin that connects the Mediterranean Sea and the Atlantic Ocean. Main continental influences over SWIP include topographic irregularities, such as prominent capes (e.g., Cape Santa Maria, CSM; CSV) and the Strait of Gibraltar, which affect coastal circulation dynamics (García-Lafuente et al., 2006), and significant freshwater inputs, particularly within the GoC area (e.g., Guadiana and Guadalquivir rivers; Caballero et al., 2014; submarine groundwater discharges; e.g., Hugman et al., 2015). SWIP is located in the Iberian Canary Eastern Boundary Upwelling system. As such, it is affected by a strong seasonal upwelling, promoted by a combination of coastal orientation and intense, northerly and/or westerly winds (Relvas et al., 2007; Goela et al., 2016). The offshore circulation is affected by mesoscale and submesoscale features such as fronts, cyclonic and anti-cyclonic eddies, jets and upwelling filaments (García-Lafuente and Ruiz, 2007; Relvas et al., 2007). Processes acting over the SWIP area are under the influence of local forces and large-scale ocean circulation (e.g., Longhurst, 2007) and climate patterns, connected to basin-scale climate indices such as the Eastern Atlantic Pattern (EA), North Atlantic Oscillation (NAO) and Western Mediterranean Oscillation (WeMO) (see Krug et al., *in press* and references therein).

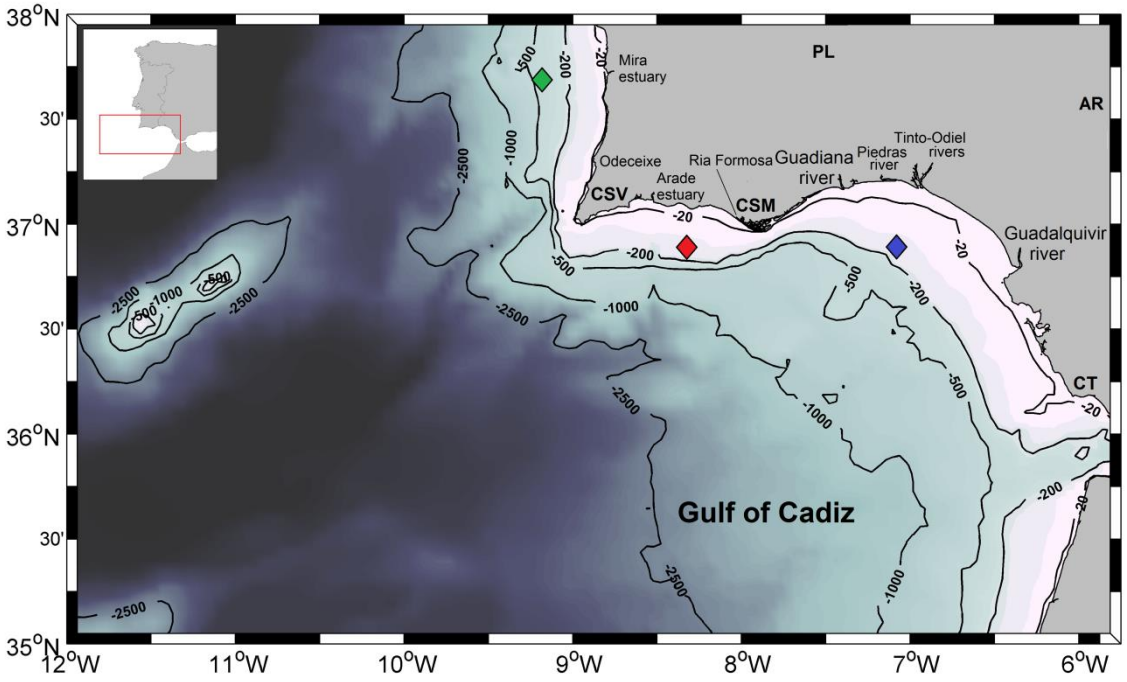

Figure 3.1 - The southwest area off the Iberian Peninsula (SWIP) bathymetry and main sources of freshwater discharges. CSV, CSM and CT depict the location of prominent topographic features, Cape São Vicente, Cape Santa Maria and Cape Trafalgar, respectively. PL and AR depict the location of Pulo do Lobo and Alcalá del Río hydrographic stations, respectively. Diamonds show the position of pixels used for the calculation of Cross Shore Ekman Transport for the West Coast (green), and west (red) and east Cape Santa Maria sectors (blue). Location of the outflow of major estuarine systems is also shown (see text for further details).

SWIP coastal and oceanic processes and their interaction with atmospheric forcing and continental inputs affect the physical, optical and chemical properties of the top layers of the water column, resonating with the biotic components, from plankton to fishes (e.g., see review by García-LaFuente and Ruiz, 2007). Indeed, wind forcing, coastal upwelling, mixing-stratification cycles, rainfall and riverine discharges, tidal currents and internal waves are known to promote increases in phytoplankton biomass within SWIP (e.g., Navarro and Ruiz, 2006; García-Lafuente and Ruiz, 2007; Prieto et al., 2009; Navarro et al., 2012; Bruno et al., 2013; Goela et al., 2013; Caballero et al., 2014; Krug et al., *in press*;).

3.2.2 Input datasets

A set of abiotic environmental variables, related to ocean and atmosphere circulation, and land-ocean-atmosphere interaction, representative of physical, chemical and optical

environments in the SWIP area, was acquired from satellite remote sensing and from models, at various temporal and spatial resolutions. For consistency, all data were regridded to spatial and temporal resolutions of 4-km and 16-days, respectively, covering a period when all variables were available. For each of the abiotic variables used, the time series (February 2002 - December 2011) comprised a total of 228 images with 10,800 pixels, each.

3.2.2.1 Physical environment

Daily 4-km satellite-derived sea surface temperature (SST) data were derived from a combination of: (a) Advanced Very-High Resolution Radiometer (2002-2009), from the Pathfinder (http://data.nodc.noaa.gov/pathfinder/Version5.0/); and (b) MODerate-resolution Imaging Spectroradiometer, MODIS-Aqua (2010-2011), from NASA's Oceancolor portal (http://oceancolor.gsfc.nasa.gov/). SST data were limited to night time passes, to avoid diurnal solar heating effects (Robinson, 2010), and high quality data (AVHRR quality flags 6 and 7, and MODIS-A quality flag 0).

Weekly mixed layer depth (MLD) composites were retrieved from the Ocean Productivity website (http://www.science.oregonstate.edu/ocean.productivity/mld.html), based on three data-assimilating models with spatial resolution varying from 0.25^{o} to 1^{o}: Simple Ocean Data Assimilation (SODA; 2002-2004); Thermal Ocean Prediction Model based on The Navy Coupled Ocean Data Assimilation system (NCODA/TOPS; January 2005 - May 2005); and Fleet Numerical Meteorology and Oceanography Center model (FNMOC; June 2005 to 2011). This combination of MLD data was selected in accordance with the preferred MLD sources used by the Ocean Productivity for their net primary production models. MLD data was further constrained to the bathymetry value (Z), obtained from the General Bathymetric Chart of the Oceans (GEBCO) gridded database (IOC, IHO and BODC, 2003) at *ca.* 1 km resolution.

Daily sea surface zonal (U) and meridional (V) wind fields, at 0.25^{o} spatial resolution, were obtained from the Blended Sea Winds dataset (BSW; http://www.ncdc.noaa.gov/oa/rsad/air-sea/seawinds.html). This product is based on a combination of several scatterometers, standardized across platforms, hence allowing a high quality and more complete temporal and

spatial coverage of ocean wind (Zhang et al., 2006). The third power of the resultant wind was used as an index of turbulent mixing (W^3) of the upper water column (Elsberry and Camp, 1978).

3.2.2.2 Optical environment

Daily 1-km surface photosynthetically available radiation (PAR), from Sea-viewing Wide Field of View Sensor (SeaWiFS) and MODIS-Aqua, was obtained from the NASA Oceancolor Group portal. Weekly 4-km composites of satellite-derived light attenuation coefficient at 490 nm (K_{490}), and absorption coefficient by detrital and coloured dissolved organic matter (a_{dg}) at six different wavelengths (412 nm, 443 nm, 490 nm, 510 nm, 555 nm and 670 nm), were accessed from Ocean Colour Climate Change Initiative Group (OC-CCI version 1; http://www.esa-oceancolour-cci.org). OC-CCI products use remote sensing reflectances from SeaWiFS, MODIS-Aqua and MEdium Resolution Imaging Spectrometer (*MERIS*) sensors, wavelength synchronized, bias corrected and merged (Sathyendranath et al., 2016, *in press*).

Light attenuation coefficient at 490 nm wavelength (K_{490}, m^{-1}) was converted to PAR vertical attenuation coefficient (K, m^{-1}) according to Rochford et al. (2001). Euphotic zone depth (Z_{eu}, m), defined as the depth at which the irradiance is 1% of incident surface PAR, was estimated according to the Lambert-Beer law, assuming a constant attenuation coefficient and optically homogeneous waters. Mean PAR intensity in the mixed layer (I_m, µmol photons m^{-2} s^{-1}) was calculated according to Kirk (1986).

3.2.2.3 Chemical environment

Subsurface (depth level, 0.5 - 1.5 m), model-derived chemical data for the Atlantic-Iberian Biscay Irish-Ocean area, at a ~9-km resolution, were retrieved from the Copernicus Marine Environment Monitoring Service (Products: IBI_REANALYSIS_PHYS_005_002 and IBI_REANALYSIS_BIO_005_003; http://marine.copernicus.eu/). Daily salinity data (Sal) were derived from the physical model reanalysis (Nucleus for European Modelling of the

Ocean, NEMO). Monthly mean concentrations of dissolved oxygen (DO), dissolved inorganic macronutrients (nitrate, NO_3; phosphate, PO_4) and micronutrients (iron, Fe), were based on a biogeochemical model reanalysis (Pelagic Interaction Scheme for Carbon and Ecosystem Studies – PISCES), coupled with NEMO.

3.2.2.4 Indicators of local and remote forcing

A wind-based upwelling index, the cross-shore Ekman transport, was used to estimate upwelling intensity over the west (UI_{WC}) and south (UI_{SC}). UI_{SC} was estimated as the average value for two locations on the south Portuguese coast, at western and eastern sectors of Cape Santa Maria (see Fig. 3.1). Negative UI values indicate offshore Ekman transport and upwelling-favourable conditions; conversely, positive values indicate onshore Ekman transport and downwelling-favourable conditions (see Krug et al., *in press* for further details).

Guadiana river discharge (Gdn), measured at the hydrometric station Pulo do Lobo (see Fig. 3.1), was obtained from the Portuguese Environmental Agency public database (http://snirh.apambiente.pt/). Guadalquivir river discharge (Gdq), measured at the Alcalá del Río station (see Fig. 3.1), was acquired from the Spanish Regional Water Management Agency (http://www.chguadalquivir.es/saih/).

Four large-scale climate indices were used as indicators of remote forcing over the study area: (i) the North Atlantic Oscillation (NAO) Index, a normalized pressure difference between the Azores and Iceland, representative of the north sector of the Atlantic Ocean (Hurrell, 1995); (ii) the Eastern Atlantic Pattern (EA), the second mode of sea-level pressure (SLP) variation in the North Atlantic (Hurrell et al., 2003); (iii) the Atlantic Multidecadal Oscillation (AMO), a SST-based index for the North Atlantic (Kaplan et al., 1998); and (iv) the Western Mediterranean Oscillation (WeMO) Index, a barometric ratio between Padua (north Italy), and San Fernando (southwest Spain), representative of the western Mediterranean basin (Martin-Vide and Lopez-Bustins, 2006).

AMO data were assessed from NOAA's Earth System Research Laboratory portal (https://www.esrl.noaa.gov/psd/data/climateindices/), EA data were acquired at NOAA's Climate Prediction Center website (http://www.cpc.ncep.noaa.gov/), NAO were retrieved from the (USA) National Center for Atmospheric Research website (https://climatedataguide.ucar.edu/climate-data), and WeMO data were retrieved from the University of Barcelona's Climatology Group website (http://www.ub.edu/gc/en/2016/06/08/wemo/).

3.2.3 Data analyses

The general strategy used for partitioning SWIP area consisted of the following four steps (Fig. 3.2). Briefly, in Step 1 (Pre-processing), a dissimilarity analysis was used to select the set of independent partitioning variables, from the complete dataset (24 uniformly gridded variables), hence eliminating redundant variables: In Step 2 (Data Reduction), an artificial neural network technique was used to reduce data and computational time. In Step 3 (Delineation of Provinces), an unsupervised classification technique was used to partition SWIP into EPs. Steps 1 to 3 were adapted from the computationally efficient strategy used by Fendereski et al. (2014). Step 4 (Analysis of Provinces), included the evaluation of province-specific area coverage, spatial-temporal variability, environmental properties and potential biological significance, using phytoplankton data.

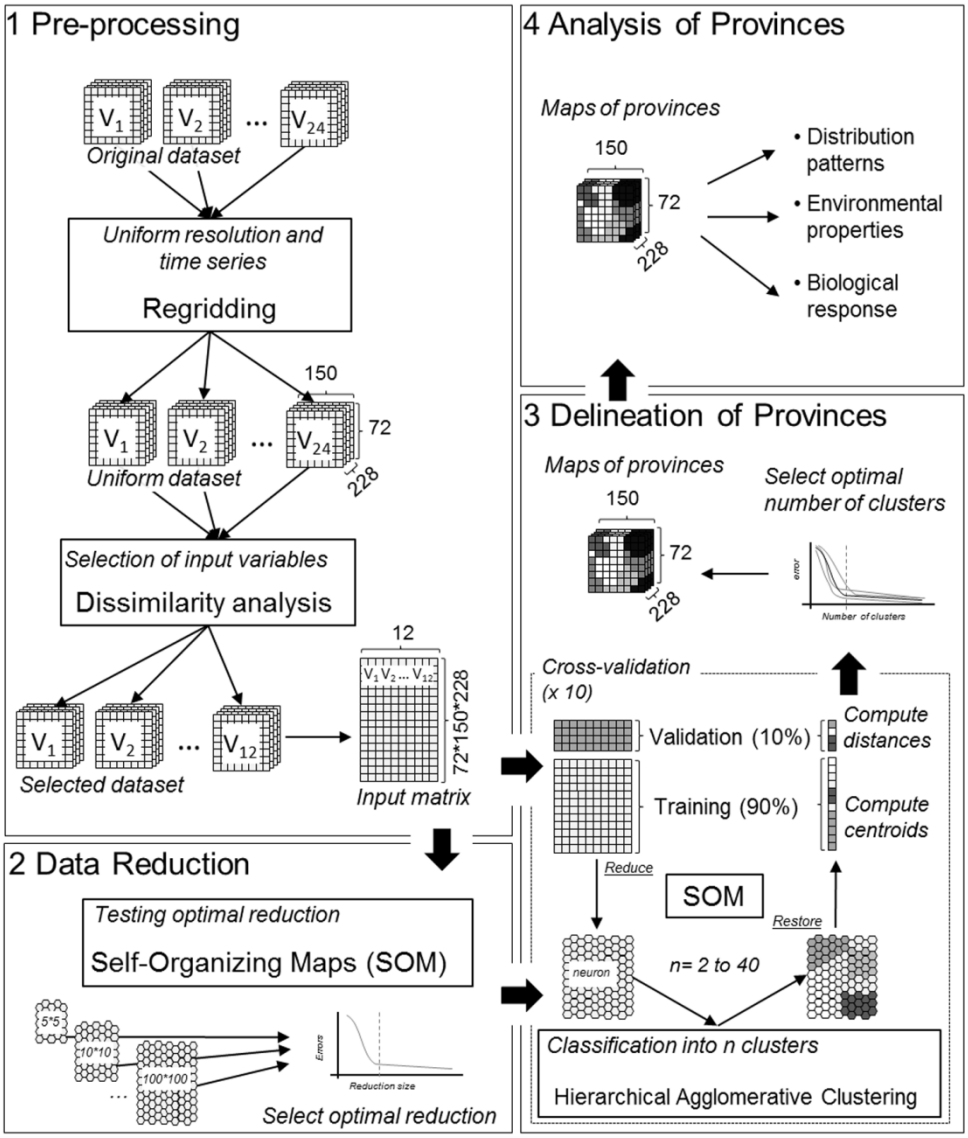

Figure 3.2 - Flow diagram representing the four steps associated to the delineation of environmental provinces in the area off South West Iberian Peninsula: 1 - Data pre-processing; 2 - Data reduction; 3 - Delineation of Provinces; and 4 - Analysis of Provinces. See text for further details.

3.2.3.1 Data pre-processing

Spearman rank correlation coefficient (r_S) was used to evaluate the strength of monotonic relationships between variables. Correlation values ($1-r_s$) between the 24 environmental variables (22 abiotic variables plus geographical coordinates) were used to build a dissimilarity hierarchical cluster tree. A dissimilarity value of 0.25 was used as a threshold to eliminate redundant, strongly correlated abiotic variables. For groups of redundant variables (dissimilarity below 0.25), a single variable was selected for the classification input dataset.

3.2.3.2 Data reduction

Self-Organizing Map (SOM) is an artificial neural network reduction technique that transforms a nonlinear projection of high-dimensional input data into a lower (usually two-) dimensional space (a neuron map) while preserving data relationships (Kohonen, 2001; Liu and Weisberg, 2011). A hexagonal map of neurons is structured based on their neighbourhood relationships, given by the similarities among neurons' weight vectors. The adjustment of the output neuron map to the original data is assessed using quantization and topographic errors; the former represent the average (Euclidian) distance between each data vector and their best match unit (BMU), and the latter give the percentage of data vectors for which two BMUs are not neighbouring map units (Vesanto et al., 2000). The SOM Toolbox for Matlab was used on a matrix composed by pixel-normalized values (zero mean and finite constant variance) for the selected set of abiotic environmental variables (see section 3.2.3.1). The toolbox's default settings for number of iterations and learning rates were applied to 25 different neuron map sizes (sizes varied between 2 and 100). Total error of each neuron map size, estimated as the sum of quantization and topographic errors, was used to determine the optimal size of the neuron map, defined as the first of three consecutive reductions in total error less than 5% (Vesanto et al., 2000; Fendereski et al., 2014).

3.2.3.3 Delineation of provinces

Hierarchical Agglomerative Clustering (HAC) analysis was used to classify SWIP into EPs. HAC associates objects that are closer in a n-dimensional space into the same cluster, using a division that simultaneously minimizes differences between objects of a given cluster and maximizes differences between objects of different clusters, based on Euclidian distance and Ward's linkage (Ward, 1963), respectively (Wilks, 2006). As the number of clusters must be defined in advance, HAC analysis was applied multiple times, using a cluster number that varied between 2 and 40. The original data were divided into a training (90%) and a validation (10%) dataset, used for cross-validation. At each round of the 10-fold cross-validation, HAC was applied on the neuron map derived from the training dataset (see section 3.2.3.2), and pixels from both training and validation datasets were assigned to a cluster based on the BMU. The cross-validation error was computed as the sum of the root mean square deviation between individual pixels of the validation dataset and their respective cluster mean

values (centroids). The final error, calculated as the average error of the cross-validations, was used to determine the optimal cluster number (i.e., number of EPs), defined as the first of three consecutive final error reductions below 1% after addition of an additional province (Oliver et al., 2004).

3.2.3.4 Analysis of province-specific spatial-temporal variability patterns and abiotic properties

The spatial distribution of the dynamic EPs over the SWIP area was evaluated for the whole study period (February 2002 - December 2011), using a 16-day temporal resolution (n=228 composite maps). This map time series was used to derive global modal maps and seasonal modal maps, and to evaluate temporal variability in province relative area coverage. Time series of province-specific maps were used to derive the pixel-based frequency of occurrence of each EP during particular seasons (winter, spring, summer and autumn). The assessment of regional consistency in provinces, in province-specific abiotic environmental properties and in their ecological relevance was based on seasonal core maps, which included only pixels that retained the same EP assignment for at least 40% of the analysed period (Fay and McKinley, 2014). Intra-annual (seasonal) and interannual variability patterns in province-specific area coverage were investigated with Generalized Additive Mixed Modelling (GAMM; Wood, 2006). Province-specific area coverage were modelled as a cyclic spline smoother function of time of the year (year-fortnight) and a cubic spline smoother function of time (year), using a first order autoregressive correlation structure to deal with temporal autocorrelation (serial dependency; for details see Krug et al., *in press*). GAMM analyses were conducted with the 'mgcv' library (version 1.8-11), in R statistical software, version 2.5.1 (R Core Team, 2016).

The strength of monotonic relationships between local and regional processes and the area covered by each EP were explored using the Spearman rank (r_S), with Bonferroni-corrected p-values (Wilks, 2006; Hauke and Kossowski, 2011). Province-specific physical, chemical and optical properties were characterized using the median values of MLD, SST, W^3, U, V, Sal, PAR, Z_{eu}, I_m, Fe, PO_4, NO_3 and DO, extracted from the areas covered by each EP in the core maps.

3.2.3.5 Assessment of the biological significance of the partition

Due to restrictions in the availability and/or spatial-temporal resolution of biological data for the study area, a preliminary assessment of the biological relevance of this abiotic-derived SWIP partition was based on province-specific phytoplankton properties as proxies for biological responses. Phytoplankton are a relevant indicator of ecosystem structure and functioning (Platt and Sathyendranath, 2008; Platt et al., 2010; Racault et al., 2014a). Moreover, Chl-a, a measure of phytoplankton concentration, and essential for computation of phytoplankton net primary production (PP) are available from synoptic and regular (daily) measurements derived from ocean-colour remote sensing. Chl-a weekly composites, at a 4-km resolution, were obtained from the OC-CCI portal (see Section 3.2.2.3). Weekly modelled PP, based on Eppley-Vertically Generalized Production Model, derived from SeaWiFS (February to July, 2002) and MODIS-Aqua (July 2002 to December 2011) data, were obtained from the Ocean Productivity site of the Oregon State University (http://www.science.oregonstate.edu/ocean.productivity/). Differences in Chl-a and PP across EPs were analysed using the Kruskal-Wallis test, a one-way analyses of variance on ranks, and pair-wise comparisons using the Dunn's test (Sokal and Rohlf, 1995).

Additionally, the comparison between a previous biotic-based partition of the SWIP area (Krug et al., *in press*) and our abiotic-based partition was also used to evaluate the biological relevance of the latter. The objective static partition established by Krug et al. *(in press*) was based on Empirical Orthogonal Function (EOF) analysis of a 15-year Chl-a time series (1997-2012), which used the sign (negative/positive) of the spatial components of dominant EOF modes, refined with non-biological criteria (geographic location and bathymetry), and identified nine regions within the SWIP area (see Fig. 4.6 in this thesis; Fig. 6 in Krug et al., *in press*), with distinct phytoplankton biomass, variability (intra- and interannual) patterns. In order to retain only biological criteria, we used the regions established by Krug et al. (*in press*) based only on the sign of the spatial components of dominant EOF modes (EOF1, EO2, EOF3), designated hereafter as Chl-a regions. However, in the case of the west and south Portuguese continental margins, due to the marked distinction in the values of the EOF spatial components between coastal and slope waters (Fig. 4.5A-C in this thesis; Fig. 5A-C in Krug et al., *in press*), these were considered distinct Chl-a regions. The comparison between

our abiotic-based EPs and the Chl-a regions was based on the percentage area of each EP covered by different Chl-a regions.

3.3 - Results

3.3.1 Delineation of environmental provinces off SW Iberia

3.3.1.1 Selection of input variables

The selection of relevant variables to be included in HAC analyses was based on a dissimilarity dendogram generated by the inversion of the correlation matrix of all 22 abiotic variables plus geographical coordinates (Fig. 3.3). Four groups of variables presented dissimilarity values below the defined threshold (0.25). Variables representing the optical environment (K_{490}, K_{PAR}, $a_{dg(\lambda)}$, Z_{eu}) showed the lowest dissimilarity values. Moreover, dissimilarities between SST, NO_3 and DO, between MLD and I_m, and between Z and longitude (Lon) were also below the defined threshold. Variables Z_{eu}, SST, MLD and Lon were selected as being representative of each of these four groups (Fig. 3.3). The input dataset, representative of the abiotic environment in the SWIP area, was therefore based on 10 variables (plus geographical coordinates): MLD, SST, PAR, Z_{eu}, Sal, W^3, U, V, PO_4 and Fe (Fig. B.1). The mean distribution of the selected environmental variables over the SWIP area between 2002 and 2011 showed, in general, strong spatial patterns including latitudinal (SST, PAR, Sal; Figs. B.1B, B.1C and B.1E), longitudinal (W^3, U, V; Fig. B.1F, B.1G and B.1H), and coastal-offshore gradients (Z_{eu}, Sal, PO_4, Fe; Figs. B.1D, B.1E, B.1I and B.1J). The signature of coastal upwelling activity was also evident (SST, Fig. B.1B).

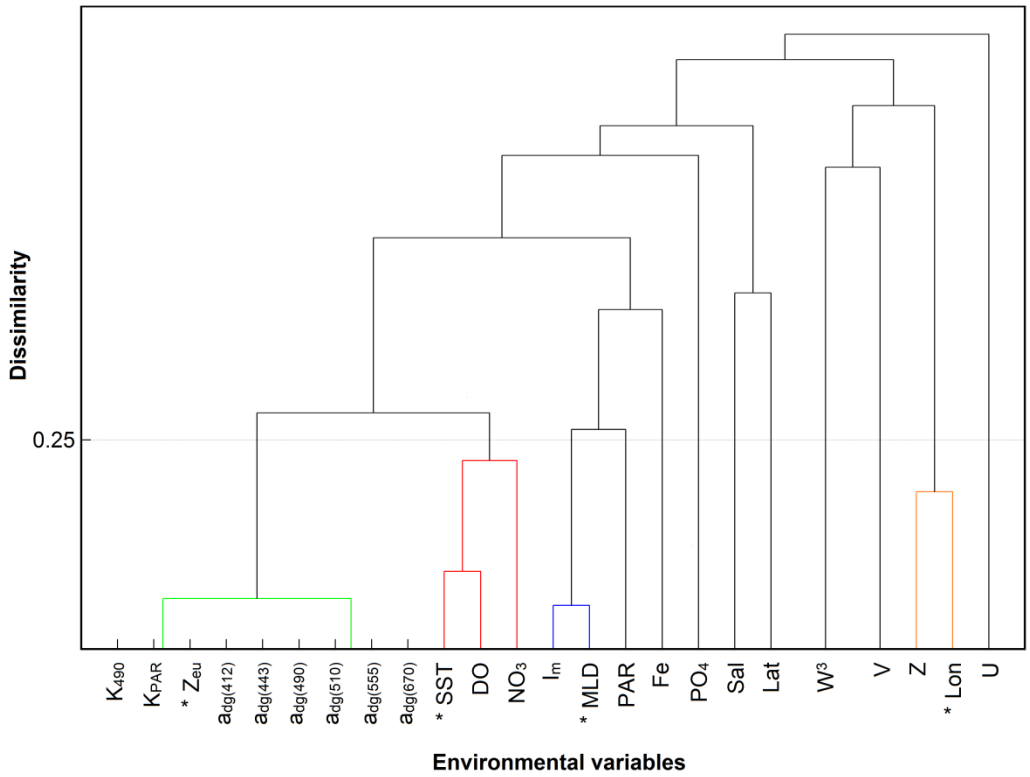

Figure 3.3 - Dissimilarity analysis based on variables representative of the abiotic environment off SW Iberia, during the 2002-2011 period. Coloured nodes indicate groups with dissimilarity values below the defined threshold (0.25), and * denotes the variables selected to represent each group. Variables include: K_{490} = Light attenuation at 490 nm coefficient, K_{PAR} = photosynthetically available radiation attenuation coefficient, Z_{eu}= euphotic depth, $a_{dg(\lambda)}$ = absorption by detrital and coloured dissolved organic matter coefficient at specific wavelengths, SST = sea surface temperature, DO = subsurface dissolved oxygen, NO_3 = subsurface nitrate concentration, MLD = mixed layer depth, Fe = subsurface iron concentration, PAR = photosynthetically available radiation, PO_4 = subsurface phosphate concentration, Sal = subsurface salinity, Lat = latitude, V = meridional component of wind, W^3 = turbulent mixing index, Z = bathymetry, Lon = longitude and U = zonal component of wind.

3.3.1.2 Data reduction and cluster analysis

When multiple runs of SOM were performed using neuron map sizes varying from 2 to 100 to define the optimal neuron map size required for data reduction, the total error decreased with increasing neuron map size and, a map size with 20 neurons was selected for HAC analyse, according to the criteria defined (Fig. B.2A). Cross-validation errors associated with HAC analyses, estimated using a number of clusters varying between 2 and 40, indicated that the abiotic variability over the SWIP area was optimally represented by 12 EPs (Fig. B.2B).

3.3.2 Environmental provinces off South Western Iberia

3.3.2.1 Spatial-temporal distribution patterns of environmental provinces

The relative area coverages of the 12 EPs, expressed as percentage of the SWIP area, presented a consistent seasonal pattern during the nearly 10-year study period (Fig. 3.4A). For each time step (16-day) of the series, the study area was usually delineated into six or seven EPs, including: one relatively large EP covering 20-40% of SWIP; one relatively small EP, encompassing less than 1% of SWIP; and four or five EPs, individually covering between 1% and 20% of SWIP (Fig. 3.4A, Video B.1). The average number of concurrent EPs was highest during autumn (October - December) and lowest during winter (January - March). For both seasons, the areas covered by dominant EPs tended to increase, in respect to spring (April-June) and summer (July-September) seasons (Fig. 3.4A and 3.4C).

The modal spatial distribution of the EPs for the whole 10-year period showed the predominance of six EPs (Fig. 3.4B). Most of the SWIP coastal domain (latitude >36^{o}N) was associated with EP9, except for small areas (*ca.* 20m isobath) near the Guadalquivir river mouth and the west coast, predominantly associated with EP3. Five EPs predominated over the oceanic domain (depth > 200m). The northern oceanic domain (latitude > *ca.* 36.5^{o}N) integrated the EP8 offshore the 2500 m isobath, while the areas between the 500 m and 2500 m isobaths were covered by EP11, following approximately the continental shelf and slope contours, south-eastwards to CSM. The southern open ocean domain integrated EP7, EP10 and EP12, from west to east, respectively. Most of the GoC, including its coastal areas south of 36^{o}N, was classified as EP12.

The analysis of season-specific EP modal spatial distribution revealed similarities between spring and summer (Fig. 3.4C), both seasons showing some resemblance with the time-series modal map (Fig. 3.4B). In contrast, marked changes were detected during autumn and winter (Fig. 3.4C). During autumn, relative increases in areal coverage were detected for EP3 (coastal areas), EP6 (slope), and EP5, EP1 and EP2 (oceanic areas). During winter, EPs spatial distribution changed profoundly, with the dominance of EP3 over coastal areas, EP6 over slope areas, and EP1, EP2 and EP4 over oceanic areas (Table 3.1, Fig. 3.4C).

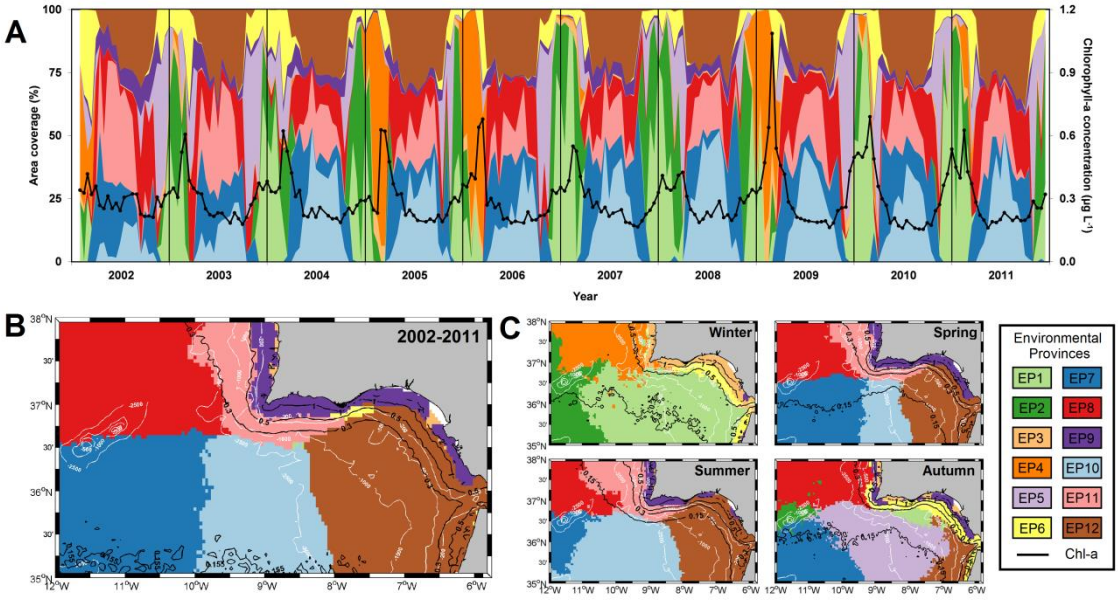

Figure 3.4 - Spatial and temporal dynamics of the 12 environmental provinces (EPs, see colours) delineated off the South West Iberian Peninsula, during the period February 2002 - December 2011. (A) Temporal variability of the relative area coverage of the EPs (as % of the study area). (B) Province modal maps for the whole time series, and (C) Season-specific province modal maps. Black lines represent average surface chlorophyll-a concentration (Chl-a, µg L^{-1}) for the study area (A, B) or period (C). White lines (B, C) are isobathymetric contours (200m, 500m, 1000m and 2500m).

Table 3.1 – Environmental provinces (EPs) delineated off the Southwest Iberia Peninsula (SWIP) with indication of its predominant season(s) and area of occurrence, and median and maximum area coverage values (as % SWIP area). During the study period (February 2002 - December 2011), all EPs showed minimum area coverage values of 0%. EPs are organized into four groups (I, II, III and IV), according to their predominant season(s) of occurrence (see text for details).

Group	Environmental Province	Predominant Season(s)	Predominant SWIP area	Coverage of SWIP area (%)	
				Median	Maximum
I	EP1	Winter	Gulf of Cadiz	12.9	92.8
I	EP2	Winter	W Off	16.4	94.8
I	EP3	Winter	Coast	0.9	17.5
I	EP4	Winter	N Off	0.9	88.7
II	EP5	Winter/Autumn	S Off	6.5	80.0
II	EP6	Winter/Autumn	Slope	2.7	44.0
III	EP7	Spring/Autumn	SW Off	13.8	58.6
III	EP8	Spring/Autumn	NW Off	12.4	44.8
III	EP9	Spring/Autumn	Coast	2.4	12.8
IV	EP10	Spring/Summer	S Off	15.7	52.2
IV	EP11	Spring/Summer	Slope	9.8	48.4
IV	EP12	Spring/Summer	Gulf of Cadiz	18.5	39.2

Season-specific province modal maps for the SWIP area (see Fig. 3.4C) and province-specific seasonal maps (Fig. 3.5) revealed strong intra-annual variability in abiotic properties over the SWIP area, with distinct retractions or expansions of province boundaries over the annual cycle. Most EPs were relevant (pixel-based occurrence frequency >40%) during one or two seasons, and absent or present in low frequency (pixel-based occurrence <20%) during the remaining seasons (Figs. 3.5 and B.3). Seasonal core maps, based on a frequency ≥40%, captured a higher province temporal stability and regional consistency during the 'warm' period (spring - summer) in comparison to the 'cold' period (winter - autumn). During the latter, a higher temporal variability was evident over a large area, mostly oceanic, where none of the EPs occurred for more than 40% of each season (see bottom panel, Fig. 3.5).

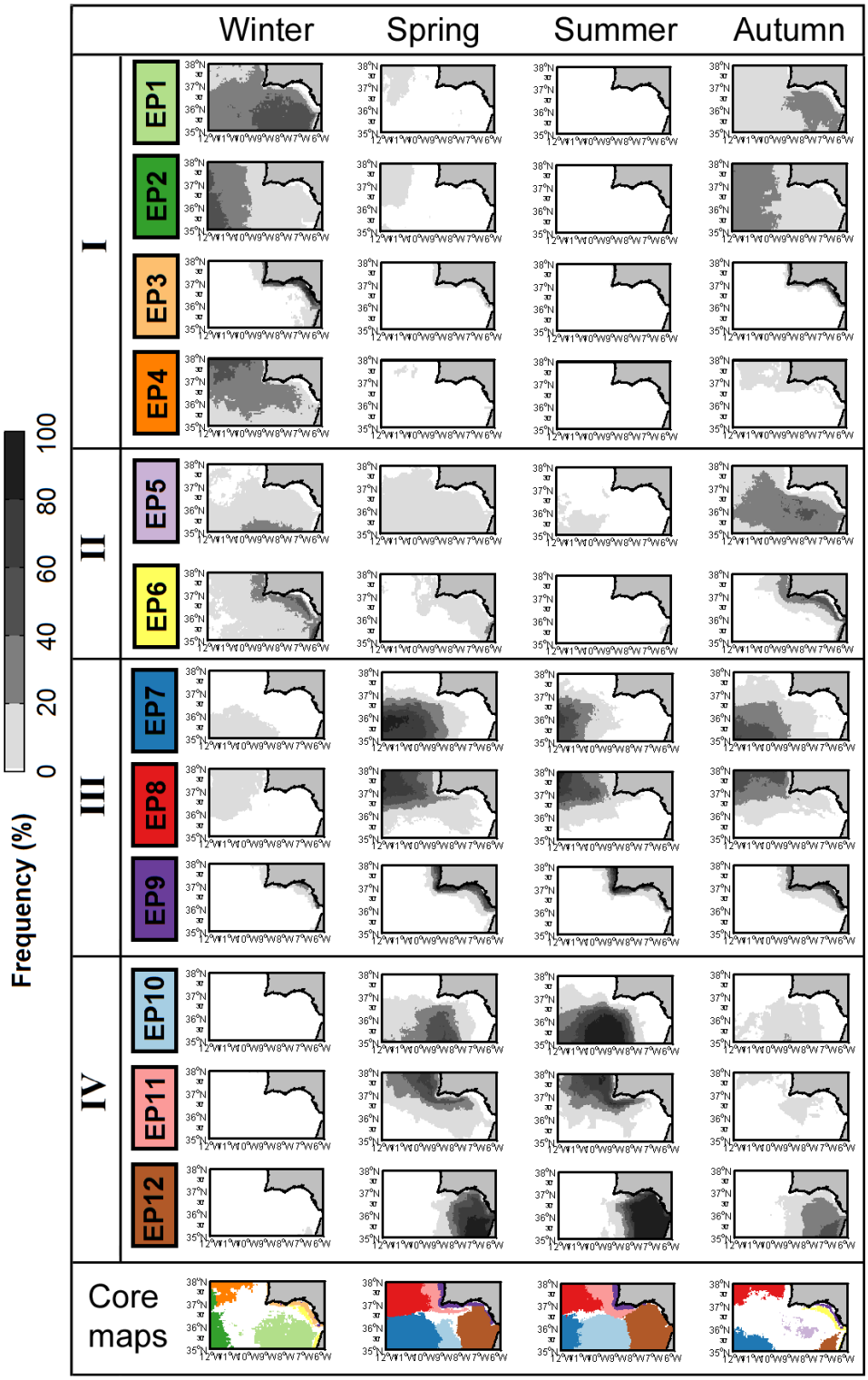

Figure 3.5 - Seasonal distribution of the occurrence (pixel-based frequency, as %) of the 12 environmental provinces (EPs) delineated off the South West Iberian Peninsula, during the period February 2002 - December 2011, organized into four groups (I, II, III, and IV), based on their prevailing season(s) of occurrence. Season-specific EP core maps, based on occurrence frequencies equal to, or higher than, 40%, are depicted at the bottom (white areas: EPs frequency < 40%).

During the study period, intra-annual (seasonal) variability patterns in province-specific area coverage (Fig. B.3) were non-linear and highly significant, for all EPs (GAMM, $p < 0.0001$; Fig. 3.6, Table B.1), allowing the establishment of four different groups of provinces based on their seasonal cycles. Group I (EP1, EP2, EP3 and EP4) showed a unimodal annual cycle, with maximum coverages during winter; Group II (EP5 and EP6) showed a bimodal annual cycle with maximum coverages during the winter and autumn; Group IIII (EP7, EP8 and EP9) also showed a bimodal annual cycle, but with maximum coverages during spring and autumn; and Group IV (EP10, EP11 and EP12) showed a unimodal annual cycle, with maximum coverages during spring and summer. Conversely, with respect to interannual variability (period 2002-2011), only the EP6, EP9 and EP11 showed significant patterns, with highly significant ($p < 0.0001$) non-linear interannual declining trends, stronger during the period 2002-2006 (Fig. 3.6). Moreover, EP4, predominant during the winter, covered large oceanic areas (>80% SWIP), only in the years 2005, 2006 and 2009 (Fig. B.3). These maximal coverages coincided with periods of high PO_4 and NO_3 concentration for the oceanic domain, especially in the north oceanic region (data not shown).

Correlation analyses revealed, for specific EPs, significant relationships between area coverage and different indicators of local and remote forcing during the *ca*. 10-year study period. The upwelling index over the west coast (UI_{WC}) was strongly positively correlated with the oceanic EP8 ($r_S = 0.30$; $p<0.01$) and negatively correlated with the slope EP11 ($r_S = -0.46$; $p<0.01$), and the upwelling index over the south coast (UI_{SC}) was negatively correlated with the coastal EP9 ($r_S = -0.25$; $p<0.05$). The Guadiana river discharge presented a positive correlation with the area coverage of the coastal EP3 ($r_S = 0.26$; $p<0.05$), and a negative correlation with the coastal EP9 and the mostly oceanic EP12 ($r_S = -0.35$ and -0.31, respectively; $p<0.01$). In the case of basin-scale climate indices, the only significant correlations detected were between AMO and the area coverages of the coastal EP3, and the oceanic EP4 and EP12 ($r_S = -0.34$, -0.35 and 0.35, respectively; $p<0.01$).

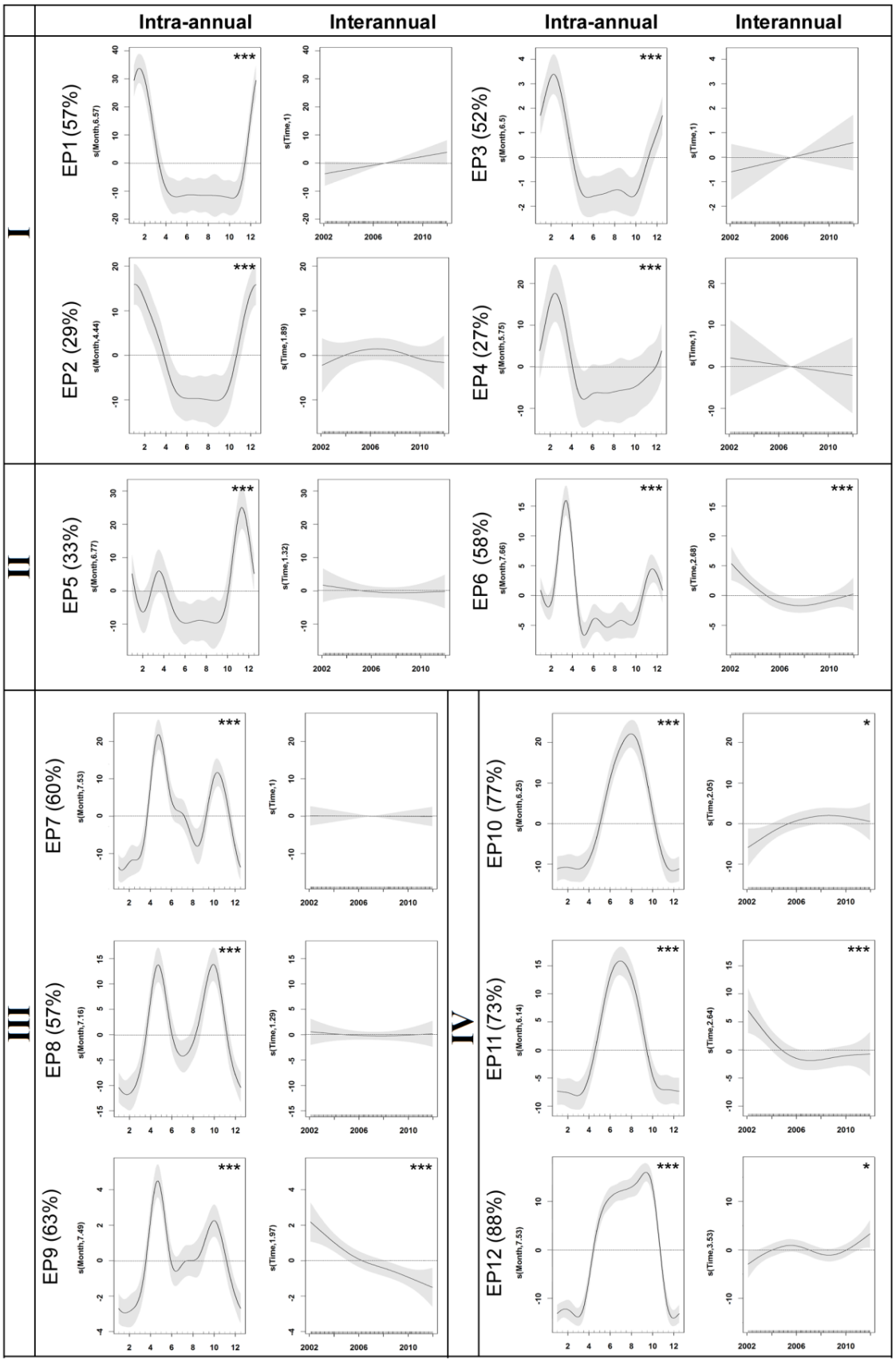

Figure 3.6 -Partial effects of intra-annual (expressed as month) and interannual variability

(expressed as year) on the area coverage of the 12 environmental provinces (EP) off Southwest Iberia Peninsula (period: 2002-2011), derived from generalized additive mixed models (GAMMs). EPs are organized into four groups (I, II, III, and IV), based on their prevailing season(s) of occurrence. Model explanatory power (as % explained variance) is shown next to each EP designation (in parenthesis), and the significance level (p-value) of each predictor (month, time) is denoted by asterisk symbols (top right), where *, **, *** indicate p-value <0.05, <0.01 and <0.001, respectively. For each plot, predictor values are represented on the x-axis, where short vertical lines indicate the exact predictor observations. Values on the y-axis represent the partial effects of the specific predictor, holding the other predictor constant. Numbers in parentheses on the y-axis represent the effective degrees of freedom (edf), indicative of the smoothness of each function; values of edf equal to 1 represent a linear effect of the predictor, and values higher than 1 indicate progressively stronger non-linear effects. Solid lines indicate the smoothed non-parametric trends, and gray shaded areas designate the point-wise 95% confidence intervals. Regions where the 95% CI bands enclose the x-axis line indicate no significant effects of the prediction. At each stage, the value of the EP areal coverage is given by the sum of the partial effects of both predictors plus a constant (see Table B.1 for detailed statistics).

3.3.2.2 Province-specific environmental properties

The characterization of province-specific properties (Figs. 3.7 and 3.8), extracted from province core maps (see bottom panel in Fig. 3.5), was based on physical (MLD, SST, U, V, W^3), optical (I_m, PAR, Z_{eu}) and chemical variables (Fe, PO_4, DO, NO_3). Basic statistical information for abiotic properties for each EP is provided in Table B.2. Significant across-province differences were detected for all abiotic variables, with at least one EP different from the others (Kruskall-Wallis test, p-value <0.001). For both physical and optical environments, a distinction in province-specific characteristics between predominantly cold (Groups I and II) and warm (Groups III and IV) periods was detected (Fig. 3.7). EPs dominant during the cold period generally presented higher MLD, and lower SST, V, PAR, I_m and Z_{eu}. Oceanic EPs dominant during winter (EP1, EP2 and EP4) were statistically similar, and distinct from the coastal winter EP3 only in terms of MLD and Z_{eu}. For the optical environment, province-specific I_m and PAR were similar within cold and warm periods, whereas Z_{eu} varied mostly between coastal (EP3 and EP9) and other EPs.

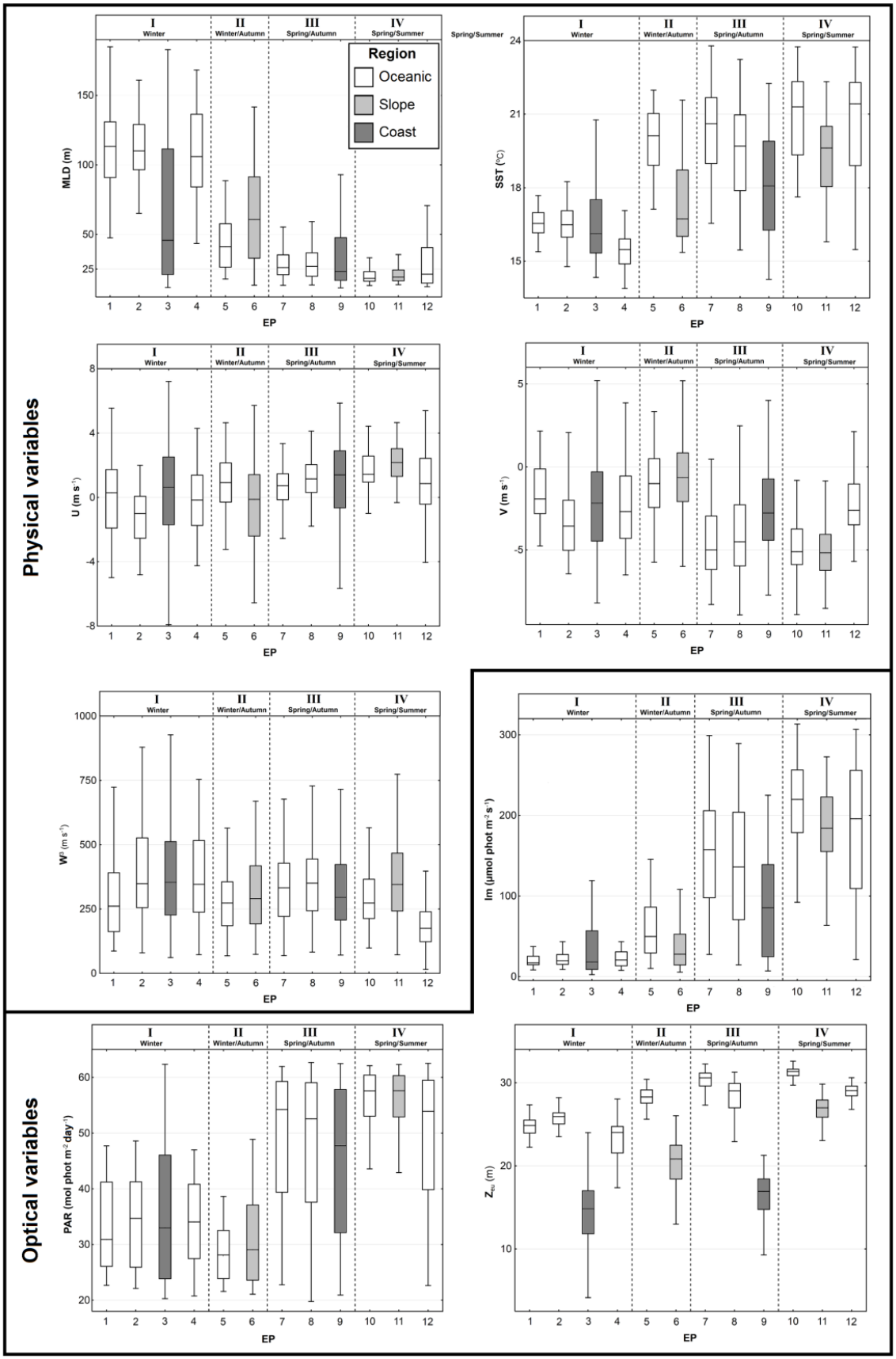

Figure 3.7 – Characterization of each of the 12 environmental provinces (EPs) delineated off the

SW Iberia study area based on variables representative of physical and optical environments, during the period 2002-2011. EPs are organized into four groups (I, II, III, and IV), based on their prevailing season(s) of occurrence (seasons of maximum coverage are indicated). Grayscale indicates the predominant region of occurrence of EPs. Physical variables: MLD – mixed layer depth, SST - sea surface temperature, W^3- turbulent mixing index; U - zonal and V - meridional wind components. Optical variables: PAR - photosynthetically available radiation, Z_{eu} - euphotic zone depth and I_m - mean PAR intensity in the mixed layer. Median values are represented by the lines within the boxes, 25^{th} to 75^{th} percentiles are denoted by box edges and non-outlier limits are denoted by whiskers.

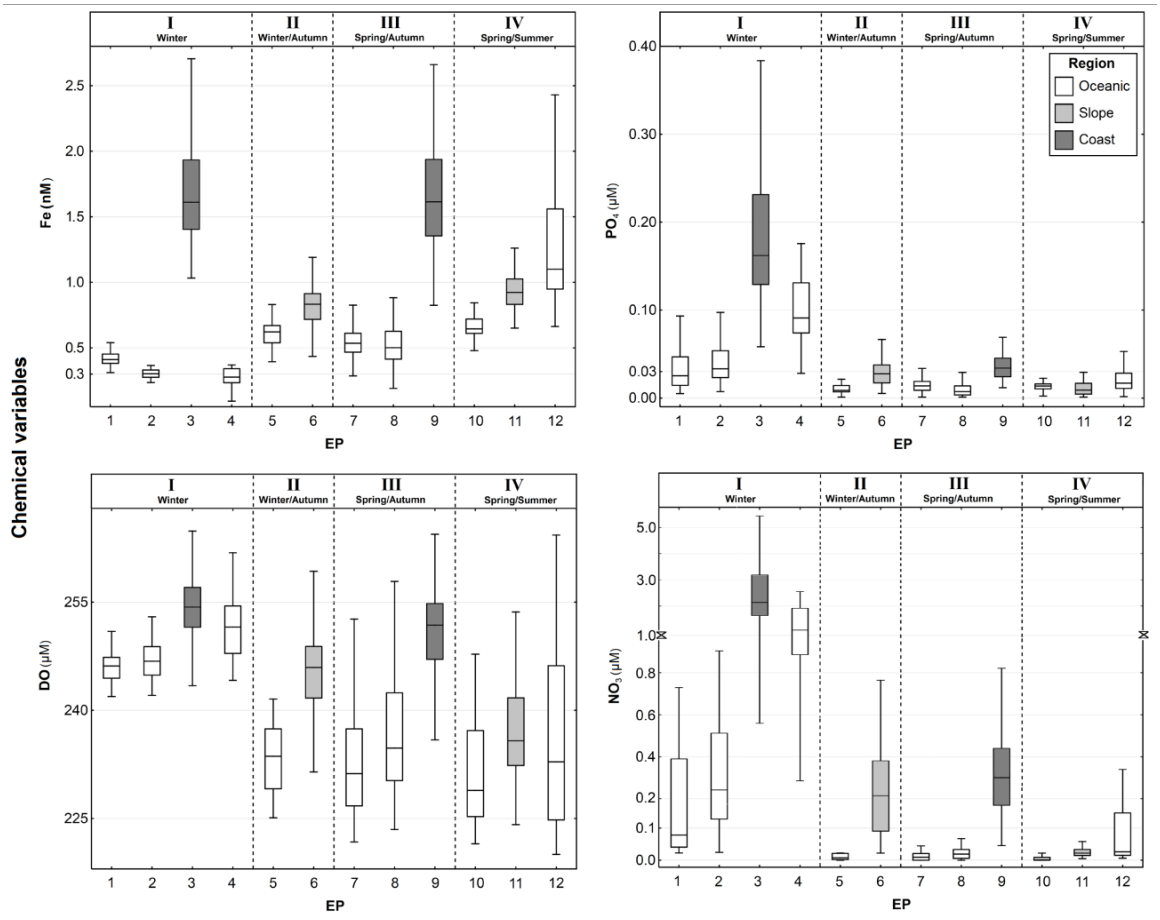

Figure 3.8 - Characterization of each of the 12 environmental provinces (EPs) delineated off the SW Iberia study area based on variables representative of chemical environment, during the period 2002-2011. EPs are organized into four groups (I, II, III, and IV), based on their prevailing season(s) of occurrence (seasons of maximum coverage are indicated), and grayscale indicates the predominant region of occurrence of EPs. Variables: Fe - iron, PO_4 - phosphate, DO - dissolved oxygen and NO_3 - nitrate subsurface concentrations. Median values are represented by the lines within the boxes, 25^{th} to 75^{th} percentiles are denoted by box edges and non-outlier limits are denoted by whiskers.

With respect to the chemical environment, a clear distinction was detected between Group I (winter EPs) and the other groups, with generally higher PO_4, DO and NO_3 and lower Fe

concentrations for Group I (Fig. 3.8, Table B.2). Moreover, the coastal EP3 and EP9 usually presented higher median concentrations of nutrients and DO than co-occuring oceanic EPs, with globally higher values for EP3 (winter) in respect to EP9 (spring/autumn). Among the oceanic EPs, the winter EP4, positioned over the northern SWIP area (see Fig. 3.4C), exhibited the highest median concentrations of PO_4 and NO_3, while EP12, dominating over the GoC, namely during the warm period (see Fig. 3.5C), presented significantly higher Fe concentrations (Fig. 3.8 and Table B.2).

3.3.3.3 Assessment of the biological relevance of the partition

Surface chlorophyll-a concentration (Chl-a) and phytoplankton net primary productivity (PP) during the study period were used to assess the potential biological relevance of our abiotic-based SWIP partition. Spatial distribution of Chl-a (0.04-16.84 µg L^{-1}) and PP (135-9550 mg C m^{-2} day^{-1}) over the SWIP area showed marked cross-shelf gradients, with higher values over coastal domains, and latitudinal gradients, with lowest values over the southern open-ocean SWIP areas (see Fig. 3.4B for Chl-a; PP data not shown). The spatial distribution of Chl-a isolines over the SWIP area, overlaid onto the province global maps (Fig. 3.4B) and season-specific modal maps (Fig. 3.4C), showed recurring spatial patterns. For example, EP11 was approximately delimited by the 0.3 and 0.5 µg L^{-1} Chl-a isolines, and the external limits of the coastal EP9 approximately followed the 0.5 or 1.0 µg L^{-1} Chl-a isolines (Fig. 3.4B). Moreover, the summer westward expansion of EP11 followed the 0.15 µg L^{-1} Chl-a isoline. With the exception of summer, the lowest Chl-a isoline (0.15 µg L^{-1} in spring and autumn, 0.30 µg L^{-1} during winter) delimited the southernmost oceanic region of SWIP (*ca.* 36.5°N), which included segments of the oceanic EP5, EP7, EP10 and EP12 (spring and autumn; Fig. 3.4C), and EP1 and EP2 (winter; Fig. 3.4C).

Province-specific Chl-a and PP variability during the study period ranged between 0.05-2.60 µg L^{-1} and 100-2700 mg C m^{-2} day^{-1}, respectively (Fig. 3.9). Analyses of variance of province-specific phytoplankton properties showed an overall offshoreward decrease in both Chl-a and PP (i.e., coast>slope>ocean; Fig. 3.9). The coastal EPs (EP3 and EP9) presented similar Chl-a and PP values but more variable and significantly higher than those of other EPs ($p<0.01$, Fig. B.4). Chl-a in the slope EP6 was statistically similar to EP1 and EP4, two winter oceanic EPs, while PP in EP6 was statistically similar to the summer slope EP11. Oceanic

EPs predominant during winter (Group I - EP1, EP2 and EP4) and over southern SWIP (EP5, EP7 and EP10) were statistically similar for both Chl-a and PP properties ($p > 0.05$, Fig. B.4).

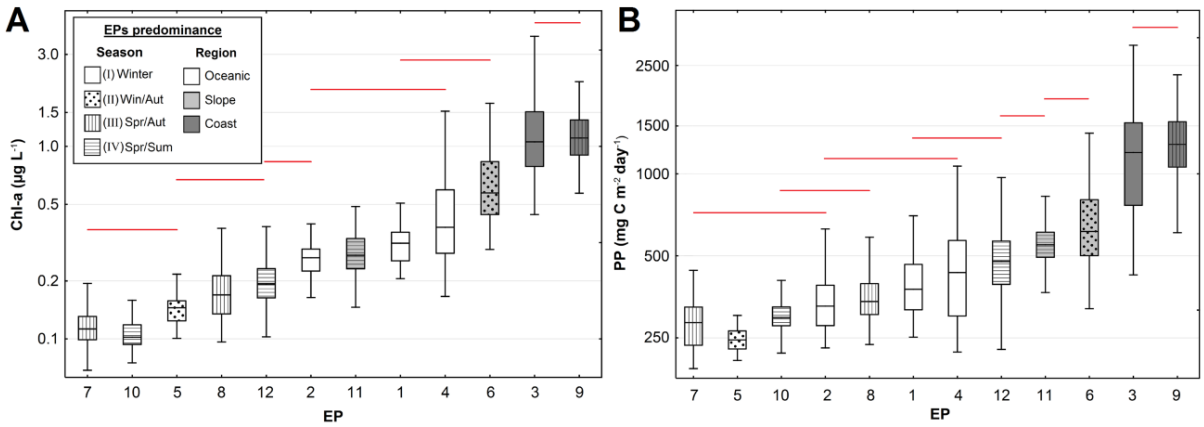

Figure 3.9 – (A) Surface chlorophyll-a concentration (Chl-a) and (B) phytoplankton net primary productivity for each of the 12 environmental provinces (EPs) delineated within the region off SW Iberia based on abiotic variables representative of physical, optical and chemical environments, during the period 2002-2011. EPs are organized into four groups (I, II, III, and IV), based on their prevailing season(s) of occurrence (seasons of maximum coverage are indicated), and coloured according to region of predominance (offshore, slope or coastal). Median values are represented by the lines within the boxes, 25th to 75th percentiles are denoted by box edges and non-outliers limits are denoted by whiskers. Horizontal red lines over the bars represent statistically similar EPs. For further information and p-values, see Fig. B.4.

The comparative analysis between the 12 EPs (Fig. 3.4B) and nine Chl-a regions derived from a previous SWIP partition showed a good agreement between abiotic provinces and biological regions (Fig. 3.10). Oceanic EPs (EP8, EP7 and EP10) areas were predominantly dominated by the Offshore (Off), North Offshore (NOff) and Gulf of Cadiz (GoC) (oceanic) Chl-a regions, with an increasing contribution of GoC in respect to Off region from northern (EP8) to southern oceanic EPs (EP7 and EP10). EP12, predominantly oceanic, was also mostly covered by the GoC Chl-a region (68% of EP12; Fig. 3.10), with small contributions of different (coastal and slope) Chl-a regions (1.5%-9% coverages; Fig. 3.10B) over its slope and coastal areas. The slope EP6, located within the GoC, was covered mostly by South Slope Chl-a region (SSlp; 82%), whereas the area of the slope EP11 was mostly covered by the West Slope (WSlp) and NOff Chl-a regions (36 and 30%, respectively). The coastal EP9, dominant over all the coastal SWIP domain (see inset in Fig. 3.10A), was mostly covered by West Coast (WC; 24%) and South Coast (SC; 23%) Chl-a coastal regions, while Guadiana (Gdn) and Guadalquivir (Gdq) Chl-a regions jointly represented a smaller contribution (15%).

The coastal EP3, limited to narrow areas over the west coast and in the vicinity of the Guadalquivir river mouth (Fig. 3.4B), was covered by the WC (31%) and Gdq (16%) Chl-a regions. Since the biotic-based regionalization was not applied to nearshore coastal waters (Z<20m), a large proportion of the coastal areas of EP3 and EP9, 49% and 20% respectively, was not associated to any Chl-a region.

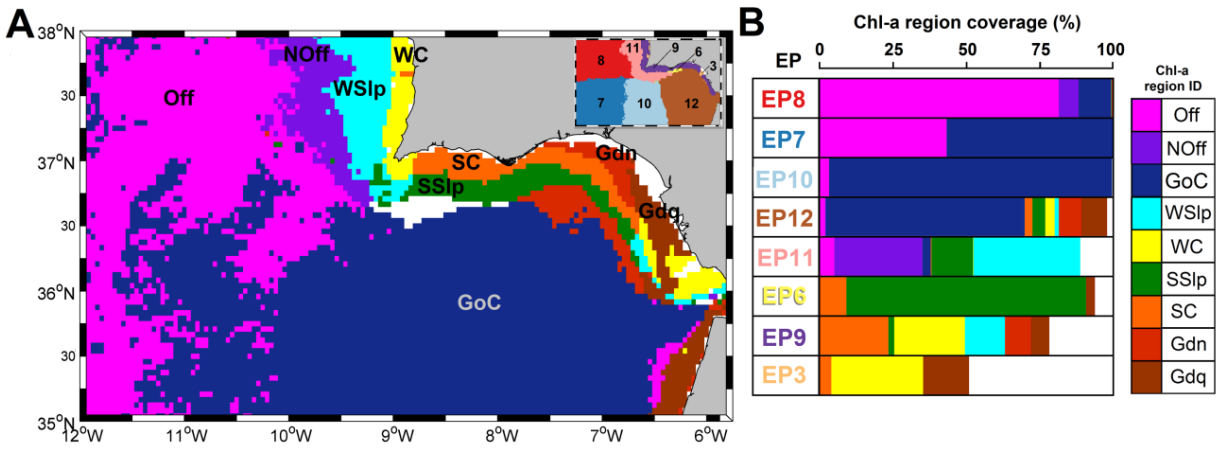

Figure 3.10 – Comparative analysis between a previous biotic-based and the present study's abiotic-based partition of the area off SW Iberia (SWIP). (A) Regionalization of the SWIP area based solely on dominant modes of chlorophyll-a (Chl-a) variability patterns, between 1997 and 2012 (adapted from Krug et al., *in press*). Chl-a regions: Offshore (Off); North offshore (NOff); Gulf of Cadiz (GoC); West Slope (WSlp); West Coast (WC); South Slope (SSlp); South Coast (SC); Guadiana (Gdn); and Guadalquivir (Gdq). The inset represents the modal map of the 12 abiotic-based environmental provinces (EP), derived from the present study, for comparison. (B) Percent area coverage of each of the 12 EPs by the nine Chl-a regions (panel A), based on EP modal distribution (inset, panel A). Non-classified areas are represented in white, for both A and B.

3.4 – Discussion

The combination of clustering techniques, and an input dataset at appropriate resolution, was recognized as a suitable strategy for the global partition (classification) of marine areas, and identification of ecologically and biologically significant areas of the ocean surface (Gregr et al., 2012). In the present study, the application of an unsupervised classification method (the HAC), over a 10-year dataset comprising variables representative of the physical, chemical and optical environments, allowed the objective delineation of 12 EPs over the complex SWIP area, with distinct ocean surface abiotic properties. From an original dataset including 24 variables, dissimilarity analysis and SOM permitted the selection of 12 independent partitioning variables, the input dataset, and the reduction of data and computational time. The

selected input dataset included a combination of 10 abiotic variables plus geolocation (latitude and longitude). These variables, of which some are Essential Climate Variables (Bojinski et al., 2014), are commonly used for ocean surface partition (see Table 2.2 in Chapter 2; Table 2 in Krug et al., 2017), and were revealed to be important determinants controlling phytoplankton over the SWIP area (Krug et al., *in press*). Although remote sensing and model-derived data, the sources of input variables, have inherent uncertainties (e.g., Boss and Maritorena, 2006; Sotillo et al., 2015), their use is particularly relevant in areas with sparse *in situ* sampling, such as SWIP. Moreover, specific advantages of the use of remote sensing include: (i) access to a wide variety of products, relevant for marine environmental studies; (ii) a spatial coverage that allows global to submesoscale assessments, at low cost for the user; (iii) systematic high-frequency sampling, providing multi-decadal time series; and (iv) a gridded geo-referenced format providing uniform distribution of data (see review by Krug et al., 2017).

The spatial-temporal dynamics and properties (both abiotic and biotic) of the EPs outlined by this study showed a good agreement between remote sensing and *in situ*-based data, including circulation patterns, reported in previous studies of the SWIP area, especially over the oceanic and slope sectors, supporting the suitability of our dataset (variables and sources) and delineation methods (unsupervised data reduction and classification), and the potential of this partition strategy for the assessment of environmental variability over a complex marine domain. This SWIP regionalization can also be used as a template for data synthesis, as a guide for defining inclusive and balanced sampling strategies over the area, as a support for interpreting connections between environmental forcing and biological patterns, predicting species distribution (e.g., Amorim et al., 2017), testing ecological hypotheses across environmental gradients, and as a basis for effective ecosystem conservation and management (see review by Krug et al., 2017).

3.4.1 Environmental provinces off SW Iberia and previous partitions of the study area

Overall, our unsupervised partition of ocean surface over the SWIP area showed clear distinctions between oceanic and coastal areas, and oceanic sectors north and south of *ca.* 36.5^{o}N, features that were also captured by previous supervised and unsupervised partitions of the study area. Global scale subjective partitions (Sherman, 1994; Longhurst, 2007; Spalding

et al., 2007, 2012), based on a coarse spatial resolution, delineated two partition units within SWIP area (see Fig. 2.1 in Chapter 2; Fig. 1 in Krug et al., 2017). These studies separated coastal and oceanic regions using the 200 nautical mile limit (Spalding et al., 2007, 2012) or an arbitrary rectilinear limit, offshore of the 1000 m isobath (Longhurst, 2007). Some studies used a latitudinal limit (*ca.* 36^{o}N), considering the southern regions to be within the Canary Current system (Sherman, 1994; Spalding et al., 2007, 2012). These coastal-offshore and latitudinal gradients were also visible in previous unsupervised partitions, including the macroscale dynamic classification of the European seas (Hoepffner and Dowell, 2005) and the static mesoscale SWIP partition (Krug et al., *in press*). Unsupervised static mesoscale partitions addressing a specific SWIP sector, the Gulf of Cadiz (GoC), also presented marked differences between coastal and oceanic regions (Navarro and Ruiz, 2006; Muñoz et al., 2015).

With respect to the number of regions, our abiotic-based partition identified a total of 12 dynamic EPs (8 oceanic, 2 slope and 2 coastal EPs) over the SWIP area, but only 8 EPs were retained in the modal map for the whole 10-year time series. Using EOF dominant modes of Chl-a variability, Krug et al. (*in press*) identified 9 regions over SWIP: two slope regions; three oceanic regions; and four coastal regions. Using an analogous strategy, Navarro and Ruiz (2006) reported a higher number of coastal regions (4) over the northern GoC, compared with the two coastal EPs in the present study. Likewise, Muñoz et al. (2015), using a partition based on Chl-a and SST, also presented 4 coastal regions over GoC, but a similar number of slope and oceanic regions as our study (GoC sector: 2 slope and 4 oceanic EPs). The use of Chl-a as a input variable was associated to an enhanced spatial resolution over the coastal SWIP domain (Navarro and Ruiz, 2006; Muñoz et al., 2015; Krug et al., *in press*).

Coastal areas are highly-heterogeneous transition zones, influenced by multiple natural (continental-oceanic) and anthropogenic forces. Moreover, the SWIP area is also strongly influenced by mesoscale circulation features, promoted by topographic irregularities (CSV, CSM, Strait of Gibraltar), including cyclonic and anticyclonic gyres, upwelling filaments, and riverine plumes, that globally create a high spatial heterogeneity (Garcia-Lafuente and Ruiz, 2007; Relvas et al., 2007; Criado-Aldeanueva et al., 2009). Model and remote sensing-derived data, and their original spatial resolution, probably did not accurately capture the individual abiotic properties over coastal areas. Hence, a more precise discrimination of coastal SWIP

sectors would require a dataset with high-resolution and high-accuracy, and a region-specific calibration/validation of remote-sensing and model-derived products. Additionally, the inclusion of other chemical variables (e.g., concentration of other dissolved inorganic macro- and micro nutrients, and dissolved organic carbon), physical variables as indicators of circulation and mesoscale ocean features (e.g., sea surface height, current speed and direction, stratification index, Ekman pumping, eddy kinetic energy; e.g., Gregr and Bodtker, 2007; Nieblas et al., 2014), and biological variables (see review by Krug et al., 2017) would probably increase the number of partitions that emerge from the classification of the SWIP area.

3.4.2 Spatial-temporal dynamics of environmental provinces

The spatial distribution of the 12 dynamic EPs identified over the study area was usually coherent during the 10-year time series, with each EP consistently associated with specific SWIP coastal (two EPs), slope (two EPs), or oceanic domains (eight EPs). Despite the high variability of most abiotic and biotic properties (Figs. 3.7 – 3.9) and the diversity reported for the coastal SWIP sector (circulation patterns: Relvas et al., 2007; Garel et al., 2016; abiotic properties and phytoplankton interannual patterns: Navarro and Ruiz, 2006; Krug et al., *in press*), the anticipated discrimination between coastal areas affected mostly by upwelling (western Portuguese coast) and those areas mostly influenced by riverine discharges (northeastern GoC), were not clearly resolved by our partition strategy. With respect to the slope domains, our abiotic-partition identified two EPs (EP6 and EP11), whose offshore extension indicated differences in cross-shore processes. EP11 (more relevant over the western margin), extended up to the 2500 m isobath, indicating the relevance of cross-shore processes, whereas EP6 (affecting mostly the northern GoC) extended only up to the 500 m isobath, reflecting a continental margin more strongly dominated by along-shore currents (Garcia-Lafuente et al., 2006; Relvas et al., 2007; Criado-Aldeanueva et al., 2009; Garel et al., 2016). With respect to spatial distribution patterns over oceanic SWIP domains, a decrease in the number of co-occurring EPs and spatial heterogeneity in abiotic properties were detected during winter, probably reflecting the increased homogenisation of the water column and its abiotic properties during this period (Criado-Aldeanueva et al., 2009).

Most EPs retracted or expanded seasonally, in some cases ranging from complete absence to dominance (see, for example, EP1 and EP5 in Figs. 3.4 and B.3), and their areal coverage showed significant unimodal or bimodal annual patterns (Fig. 3.6). This seasonal variability was also captured by the unsupervised dynamic classification of the European seas, based on a two-year time series of SST, PAR and Chl-a (Hoepffner and Dowell, 2005). Monthly maps of the distribution of European ecological provinces showed regular intrusions of a northern province with temperate characteristics ('medium SST and Chl-a') during the cold period (*ca.* October - February), and the progression of a southwestern province with tropical characteristics ('high SST, very low Chl-a') during the warm period of the year (*ca.* May - October). Over the year, the dynamic nature of the EPs denoted the occurrence of significant seasonal changes in the abiotic properties of SWIP surface waters, which are driven by large-scale seasonal variability in atmospheric forcing over the study area (air temperature, PAR, wind speed and direction; e.g., Criado-Aldeanueva et al., 2009; Martinez et al., 2009), leading to changes in SST, MLD, circulation and inorganic nutrients. Seasonal changes in phytoplankton biomass and activity over the study area (e.g., Krug et al., *in press*) are also relevant drivers of ocean surface abiotic properties, affecting water turbidity, Z_{eu} (i.e., optical properties) and concentration of oxygen and inorganic nutrients (e.g. IOCCG, 2000; Weber and Deutsch, 2010).

The pace of change in province boundaries and area coverage, a proxy for spatial-temporal environmental heterogeneity within the SWIP area, was variable over the year. During the warm period, the study area was almost entirely covered by the same six EPs, with slight shifts in province boundaries between seasons, whereas marked changes were detected during the cold period, especially in the central oceanic SWIP area, where none of the EPs dominated for more than 40% of each season (Figs. 3.4C and 3.5, bottom panel). The lowest variability during the warm period was probably linked to the higher stability in large-scale atmospheric forcing and ocean surface dynamics over the area (Hurrell and Dickson, 2004; Silva et al., 2015), which probably contributed to maintaining EPs (and their properties) more stable compared with the cold period. Moreover, the effects of specific local processes were also relevant to the seasonal variability of some EPs. In the case of coastal EPs, the expansion of EP3 and retraction of EP9 during winter, and the opposite during the warm period, were positively correlated with riverine discharge. In fact, both Guadiana and Guadalquivir rivers

are significant sources of inorganic nutrients during the cold period, also affecting water turbidity and Z_{eu} (Cravo et al., 2006; Prieto et al., 2009; Caballero et al., 2014).

Coastal upwelling was also a driver of abiotic conditions over the study area, affecting more markedly the Portuguese western margin, namely the area coverages of slope EP11 and the oceanic EP8. Upwelling intensity was negatively correlated with the areal extent of EP8 and positively correlated with that of EP11, which expanded during the spring-summer, upwelling-favourable, period (Relvas et al., 2007), affecting northern oceanic SWIP domains beyond the 2500 m isobath (summer, see Fig. 3.4C). Upwelling events are sources of inorganic nutrients over SWIP (Cravo et al., 2010) and indirect drivers of water turbidity, due to their stimulatory effects on phytoplankton (e.g. Goela et al., 2014). Over the west Portuguese coast, the extension of upwelling effects into open ocean domains, sometimes promoted by the offshore advection of upwelling filaments associated to topographic structures such as Cape Sines (north of the study area limit) and CSV (Peliz et al, 2004; Santos et al., 2007; Sánchez et al., 2008; Rossi et al., 2013), was recently captured by the biotic-partition of Krug. et al. (*in press*). Moreover, the spatial configuration of EP11 probably represented the effects of the eastward advection of cold, nutrient-rich, upwelled waters, north of CSV, along the shelf break and slope of northwestern GoC (Criado-Aldeanueva et al., 2006; Relvas et al., 2007). Over the northern GoC, the intensification of upwelling-favourable westerly winds during summer tends to decrease the westward progression of the recurrent warm coastal counter-current (Relvas et al., 2007; Garel et al., 2016). These conditions, reinforced by the presence of CSM, promotes the isolation of northwestern and northeastern GoC shelfs (Criado-Aldeanueva et al., 2006, 2009) and, probably, the expansion of the oceanic EP12 into the latter.

In addition to intra-annual variability, the areas covered by some EPs also showed significant interannual patterns. EP6, EP11 (slope) and EP9 (coastal) showed highly significant non-linear declining trends, steeper between 2002 and *ca.* 2006, whereas the adjoining oceanic EP10 and EP12 displayed increasing trends for the same period (Fig. 3.6). Although a weakening in upwelling intensity and an increase in riverine discharge could, explain these interannual trends in the case of EP11 and EP9, respectively, no significant interannual trends in these processes were detected during the study period (data not shown). In fact, a clear decrease in riverine discharge was observed during the period 2002-2006, a significant linear

intensification of upwelling off the west coast was observed by Krug et al. (*in press*), and confirmed recent projection (Sousa et al., 2017). Although most studies report a decline in coastal upwelling over NW Iberia (e.g., Barton et al., 2013), interannual trends for the Canary Upwelling system are inconclusive, varying according to region, season, length of the time series and statistical analysis (Goela et al., 2016; Santos et al., 2011b; see review by Varela et al., 2015).

3.4.3 Abiotic properties of environmental provinces

SWIP area represents a complex marine domain, affected by multiple local and large-scale processes, and is also classified as being very vulnerable to climate change (Kovats et al., 2014). Effective ecosystem management and conservation of this area, and the study of potential climate-change impacts, strongly rely on the availability of oceanic environmental data (e.g., Amorim et al., 2017; Henson et al., 2017). However, information on ocean abiotic environmental data for the area are fragmentary, and mostly limited to specific areas within the continental margin of the GoC sector (e.g., Arístegui et al., 2009; García-Lafuente and Ruiz, 2007; Relvas et al., 2007). Based on a 10-year time series, we assembled and structured the spatial and temporal variability in abiotic properties over the whole surface SWIP area into 12 distinct EPs, thus contributing to a comprehensive knowledge of SWIP physical, chemical and optical characteristics and underlying variability.

Due to their spatial coherency and temporal consistency, the abiotic characteristics of EPs were interpreted as being characteristic of their specific areas and/or seasons of predominant occurrence (Figs. 3.7 and 3.8). With respect to spatial variability of optical properties, marked offshoreward increases in water transparency and Z_{eu} were detected, especially over the more oligotrophic southern EPs (EP7 and EP10). This pattern has been reported for parts of the SWIP area (CSV, Goela et al., 2014; Guadalquivir river plume, Caballero et al., 2014), and is probably related to the reduction in both suspended particulate matter and phytoplankton biomass (Krug et al., *in press*; Longhurst, 2007).

With respect to chemical properties, a coastal-offshore decline in the concentration of macronutrients (NO_3 and PO_4) was detected over the SWIP area, and intensified over the western margin during the warm period. This pattern, previously reported for the GoC, was probably associated with higher nutrient inputs over the coastal areas, from continental

freshwater sources (e.g., Cravo et al., 2006; García-Lafuente and Ruiz, 2007; Prieto et al., 2009) and coastal upwelling (e.g., Cardeira et al., 2013; Cravo et al., 2013). In the case of Fe, coastal EPs (EP3 and EP9) presented high concentrations, probably a result of upwelling activity and riverine discharges (Jickells et al., 2005). However, high Fe was also detected over the warm periods in oceanic EP12, located in the eastern GoC, probably indicative of Saharan desert as an iron source over the study area (Escudero et al., 2005). Indeed, strong events of Saharan desert dust deposition over southern Europe are more frequent during this season (Escudero et al., 2005).

With respect to seasonal variability, EPs predominant during the cold period (EP1-EP6) usually presented deeper MLD, lower SST, PAR and I_m, and higher PO_4 and NO_3 concentrations, reflecting the seasonality in atmospheric forcing, the importance of deep water masses as primary nutrient sources, which are brought into surface waters of SWIP during periods of increased MLD (Moita, 2001; Navarro and Ruiz, 2006; Navarro et al., 2012), and atmospheric wet deposition (e.g., Thompson et al., 2015). Over the coast, the higher nutrient concentrations detected in EP3 (cold period), compared with EP9 (warm period), probably reflects the signature of additional nutrient inputs, associated with riverine (e.g., Cravo et al., 2006; Reul et al., 2006) and submarine groundwater discharges (e.g., Hugman et al., 2015).

EPs predominantly associated with the warm period overall revealed stronger northerly (V) and westerly (U) winds typically associated with upwelling intensification over the west and south Portuguese coasts, respectively (Relvas et al., 2007; Krug et al., *in press*). Indeed, the coastal EP9 and slope EP11 presented significantly lower SST and higher nutrient concentrations in comparison with other concurrent EPs, a signature of intensified upwelling activity (Cravo et al., 2010, 2013; Relvas et al., 2007), as well as increased phytoplankton biomass and production.

3.4.4 Biotic relevance of the abiotic-based environmental provinces

The objective partition of SWIP ocean surface based solely on abiotic properties, a novel strategy for this study area, allowed the characterization of SWIP environmental variability, including its spatial and temporal dynamics. Assuming that physical-chemical forcing has a strong control over the biotic components, a common premise in marine ecology (e.g., Gregr and Bodtker, 2007; Fendereski et al., 2014 and references therein), this study hypothesized

that the EPs delineated solely on the basis of abiotic variables would have biological significance. Therefore, significant differences in Chl-a and PP, used as indicators of biological processes, were anticipated across EPs.

The analysis of variance showed significant differences on phytoplankton properties (Chl-a and PP) between EPs (Fig. 3.9). There was a relatively stronger influence of spatial over temporal (interannual) variability, more evident for PP but also valid for Chl-a, with overall distinctions between coastal, slope and oceanic EPs. EPs predominantly located over eutrophic coastal areas (EP3 and EP9) and over the southern oligotrophic oceanic SWIP sector (EP5, EP7 and EP10) were, for both variables, statistically similar among themselves, even with distinct predominant season(s) of occurrence. This marked coastal-oceanic distinction was also identified as the dominant variability mode underlying Chl-a spatio-temporal variability over the SWIP, based on EOF analysis (Krug et al., *in press;* Navarro and Ruiz, 2006; Reboreda et al., 2014a).

The comparison between the biotic-based partition of Krug et al. (*in press*), which identified nine Chl-a regions, and the modal spatial distribution of our abiotic-based EPs, was also used for assessing the biological relevance of the latter. Despite differences in the relative discrimination of coastal *versus* oceanic regions between these two partitions (lower number of coastal and higher number of oceanic EPs in respect to Chl-a regions; see section 3.4.1), the overall agreement in the geographic location of the boundaries of both partition units (EPs and Chl-a regions), generally supported our working hypothesis. Previous studies have also demonstrated the biological relevance of regions delineated using only abiotic variables (Gregr and Bodtker, 2007; Verfaille et al., 2009; Fendereski et al., 2014).

A remarkable similarity was detected over the SWIP domain more strongly affected by the upwelling off the west Portuguese coast, where the boundaries of slope EP11 included most of the NOff, WSlp and SSlp Chl-a regions (see Fig. 3.10A). Over these areas, coastal upwelling, intensified during summer, induces alterations in the abiotic properties (Fig. B.1B, B.1I; Sánchez and Relvas, 2003; Relvas et al., 2007), also affecting phytoplankton biomass temporal variability (Krug et al., *in press*). The stimulatory effect of upwelling on phytoplankton was noted for WSlp and NOff Chl-a regions, with summer secondary maximum and occasional positive anomalies, respectively (Krug et al., *in press*). The latter

has been associated with the offshore advection of chlorophyll-rich mesoscale filaments (e.g., Sánchez et al., 2008; Rossi et al., 2013).

Although a more profound evaluation of the biological/ecological relevance of this abiotic-driven SWIP partition would require the inclusion of other biological information (e.g., biomass, production, composition and diversity of both pelagic and benthic communities; Gregr and Bodtker, 2007; Verfaille et al., 2009; Fendereski et al., 2014), phytoplankton metrics are usually considered important ecosystem indicators. It is relevant to emphasize that Chl-a regions derived from Krug et al. (*in press*) represent SWIP areas with distinct phytoplankton spatio-temporal variability patterns. These phytoplankton features are considered valuable indicators of marine ecosystem status, structure and functioning, affecting upper trophic levels and multiple biological processes (e.g., fish larvae survival, efficiency of ocean's biological carbon pump; Platt et al., 2010, Racault et al., 2014a), hence representing a valuable framework for evaluating the biological and ecological relevance of our abiotic-based partition.

3.5 - Conclusions

This study provided a mesoscale classification of the abiotic environment of the complex SWIP area, based on a *ca.* 10-year time series of a set of optical, physical and chemical variables, at a relatively fine spatial (4 km) and temporal (16 day) resolution. Twelve spatially-coherent dynamic EPs were delineated over SWIP, two coastal, two slope and eight oceanic EPs, whose boundaries recurrently expanded and retracted over the year. EPs were more stable during the warm period (spring-summer), in particular over the central oceanic SWIP domain. The signature of coastal upwelling was evident throughout spring and summer, particularly over the slope and west Portuguese coast, and the effects of riverine discharge were captured over the coastal EPs. Significant interannual declining trends were detected in the areas covered by the two slope and one coastal EPs, despite the apparent lack of relationship between these coastal processes. A more precise discrimination of the heterogeneous coastal SWIP sectors would probably require a dataset with high-resolution and high-accuracy, and a region-specific calibration/validation of remote sensing and model-derived products. Overall, the spatial-temporal dynamics and abiotic properties of the EPs were congruent with remote sensing and *in situ*-based data, including circulation patterns

reported for the SWIP area, especially over the oceanic and slope sectors. Significant differences in phytoplankton biomass and production between EPs, in tandem with the general agreement between the geographical location and boundaries of our EPs and those associated to an exclusively biotic-based SWIP partition, confirmed the biological and ecological relevance hypothesized for our abiotic-based partition strategy. Hence, this purely abiotic-based classification can be a valuable tool for assessing surface ocean environment properties and ecological structure in regions where *in situ* information is absent or scarce.

Although our analysis dealt, necessarily, with a specific location (SWIP) by way of example, the same approach could be applied to elucidate the dominant drivers of pelagic dynamics in other complex regimes around the global ocean. This regionalization strategy can be used as a template for data synthesis and sampling design as well as a basis for interpreting environmental and biological patterns, and supporting the effective management of marine complex domains such as SWIP.

CHAPTER 4

UNRAVELLING REGION-SPECIFIC ENVIRONMENTAL DRIVERS OF PHYTOPLANKTON ACROSS A COMPLEX MARINE DOMAIN (OFF SW IBERIA)

Parts of this Chapter were published in:

Krug, L. A., Platt, T., Sathyendranath, S., Barbosa, A. B., *in press*. Unravelling region-specific environmental drivers of phytoplankton across a complex marine domain (off SW Iberia), Remote Sensing of Environment, DOI 10.1016/j.rse.2017.05.029.

ABSTRACT

Phytoplankton, the dominant marine primary producers, are considered to be highly sensitive indicators of ecosystem condition and change. The southwest area off the Iberian Peninsula (SWIP, NE Atlantic) is located in a biogeographical transition zone between temperate and subtropical waters, and classified as being very vulnerable to climate change. SWIP includes a variety of oceanic and coastal domains, under the influence of topographic irregularities, coastal upwelling and continental freshwater outflows, that collectively challenge the understanding of phytoplankton dynamics and controls. This study aimed to evaluate patterns in seasonal and interannual variability in phytoplankton and underlying environmental determinants within specific regions of SWIP, during a 15-year period (1997 - 2012), and to assess whether climate variability affects the regions in different ways. Empirical Orthogonal Function (EOF) analysis of satellite-retrieved sea surface chlorophyll-a concentration (Chl-a), acquired from the Ocean Colour Climate Change Initiative (OC-CCI), 4-km, 16-day resolution, was used to regionalize the study area. Region-specific Chl-a variability patterns and their linkages with environmental determinants were explored using Generalized Additive Mixed Models (GAMM). A set of local physical-chemical variables, derived from satellite and model data, and large-scale climate indices, were used as environmental variables. EOF analysis of Chl-a variability over the heterogeneous SWIP area identified nine coherent regions, with distinctive variability patterns (4 coastal, 2 slope and 3 open-ocean regions). Region-specific GAMM models explained between 32% and 82% of Chl-a variance, with higher explanatory power (>61%) for open ocean regions and coastal regions under increased riverine influence. Chl-a model predictors, as well as their effects, varied markedly among SWIP regions. However, climate-sensitive local environmental variables (sea surface temperature – SST and photosynthetically available radiation) emerged as the most influential general predictors overall, and large-scale climate indices showed significant but minor effects. Over oceanic SWIP regions, Chl-a (0.08-1.50 µg L^{-1}) showed a uni-modal annual cycle, with increases during the mixed-layer deepening and late-winter maxima, reflecting seasonal changes in SST and ocean stratification, and probably related to increased nutrient availability and/or decreased mortality. Over coastal regions south of 37^{o}N, Chl-a (0.23-10 µg L^{-1}) also benefited from riverine discharges, mostly during winter, and upwelling induced by zonal westerly winds, stronger during summer. Over the Portuguese west coast region, Chl-a (0.26-2.20 µg L^{-1}) showed a uni-modal annual cycle, with summer maxima, associated with the stimulatory effects of meridional northerly winds and coastal upwelling that partially extended into slope waters. Chl-a interannual variability showed zonal differences within SWIP, with significant interannual patterns only for regions south of 37^{o}N. Nonetheless, contrasting trends were detected in coastal (decline) and oceanic (increase) regions, possibly a consequence of between-region differences in the relative roles of nutrient and light limitation, corresponding to significant interannual increases in wind speed and mixed layer depth. Our study used a biologically-relevant objective regionalization of a heterogeneous area, to elucidate phytoplankton dynamics and controls. The region-specific associations observed between phytoplankton and multiple climate-sensitive environmental drivers over the SWIP area reinforce the role of phytoplankton as a strategic element for evaluating ecosystem responses to climate variability and change.

4.1 - Introduction

Phytoplankton are the dominant primary producers of marine ecosystems, responsible for ca. 50% of global primary production (Field, 1998), and are key contributors to carbon dioxide uptake by the ocean (Gregg et al., 2003; Smetacek and Cloern, 2008). The distribution and variability patterns of phytoplankton reflect the interplay between bottom-up forces, directly regulating growth rates, and top-down forces related to phytoplankton losses (e.g., grazing, sinking, lysis) processes. Both forces are, in turn, controlled by atmosphere and ocean circulation patterns and atmosphere-land-ocean interactions (Cloern and Dufford, 2005; Longhurst, 2007). Indeed, not only phytoplankton resources (e.g., light, inorganic nutrients), but also their dominant grazers, are controlled by atmosphere and ocean physical-forcing, being strongly affected by climate variability and change (Behrenfeld, 2014; Chavez et al., 2011; Cloern et al., 2016). The increasing concerns on the effects of anthropogenic and global climate changes, linked to the pivotal role of phytoplankton and their value as highly sensitive ecological indicators, make the study of phytoplankton regulation a key approach to evaluating ecosystem status and change, and to forecasting ecosystem responses under environmental change (Cloern et al., 2016; Platt and Sathyendranath, 2008; Racault et al., 2014a; Smetacek and Cloern, 2008).

Temporal and spatial phytoplankton variability patterns in the ocean can be assessed using satellite-retrieved surface chlorophyll-a concentration (Chl-a), a proxy for phytoplankton biomass, derived from ocean colour remote sensing (OCRS). Although limited to the top layers of the ocean, OCRS offers a unique synoptic, high spatial-temporal resolution, multi-decadal coverage of surface marine bio-optical environment. OCRS products are considered to belong to the Essential Climate Variables (ECV), a suite of environmental properties comprising physical, chemical and biological variables critical to the characterization of climate, and also measured systematically, direct or indirectly, at a global scale on an operational basis (Bojinski et al., 2014). Likewise, several biologically-relevant oceanographic and atmospheric variables are routinely measured or inferred from satellite remote sensing (Robinson, 2010) and coupled climate, hydrodynamic-biogeochemical models (Siedler et al., 2013). The integrated analysis of time series of Chl-a and concurrent environmental variables supports the identification of dominant drivers of phytoplankton variability, allowing the discrimination between local anthropogenic influences and climate-

driven changes or the relative importance of physical forcing versus biological interactions (Cloern et al., 2016; Smetacek and Cloern, 2008). Accumulating evidence shows that climate variability is impacting marine phytoplankton but its effects are variable depending on period of analysis, phytoplankton controls and ecosystem properties (Boyd et al., 2016; Cloern and Jassby, 2010; Devred et al., 2009; Henson et al., 2016; Martinez et al., 2016). Comparative analysis, across different ecosystems, will then allow an increased perception of how phytoplankton controls and ecosystem-specific attributes may modulate phytoplankton responses to climate change. Ultimately, this information may be used to identify more climate-susceptible ecosystems, and to improve our ability to forecast marine ecosystem alterations under projected climate change scenarios.

The southwest area off the Iberian Peninsula (SWIP; NE Atlantic) constitutes a complex environment with distinct offshore and coastal domains, with meridional and zonal orientation (Fig. 4.1). SWIP south sector includes the Gulf of Cadiz, a basin that receives waters from the Mediterranean Sea. This heterogeneous area, located in a biogeographical transition zone between temperate and subtropical waters, is influenced by Atlantic and Mediterranean circulation patterns, coastline and topographic irregularities, coastal upwelling events, intense mesoscale activity and continental freshwater discharges (Arístegui et al., 2009; García-Lafuente and Ruiz, 2007; Muñoz et al., 2015; Relvas et al., 2007). Furthermore, SWIP, along with Southern Europe and Mediterranean, is classified as a region particularly vulnerable to climate change. Alterations projected for this region by the Intergovernmental Panel on Climate Change (IPCC) include decreased precipitation, increased frequency and intensity of heatwaves and decline in provision of ecosystem services (Kovats et al., 2014). Indeed, several climate-driven alterations over recent decades were already reported for the area including an enhancement in the frequency of heatwaves, a decrease in storm frequency and intensity (Trigo, 2006), sea surface warming (Belkin, 2009; Lima and Wethey, 2012; Goela et al., 2016), changes in upwelling intensity and patterns (Lemos and Pires, 2004; Lemos and Sansó, 2006; Relvas et al., 2009; review by Varela et al., 2015), fluctuations in the abundance of small pelagic fishes and fish landings (see Arístegui et al., 2009; Catalán et al., 2006; Gamito et al., 2016; Ruiz et al., 2009), and species range shifts with a northern expansion of subtropical species (Horta e Costa et al., 2014; Lourenço et al., 2012; Nicastro et al., 2013).

Phytoplankton studies in the SWIP area included *in situ* and remote-sensing-based observational approaches. *In situ*-based studies (Moita, 2001), usually involving irregular low frequency sampling and a limited time coverage, mostly addressed specific coastal zones located in the Gulf of Cadiz's northwestern (Cravo et al., 2010; Goela et al., 2014; Loureiro et al., 2005, 2011) and north-northeastern sectors (Cardeira et al., 2013; Echevarría et al., 2009; Huertas et al., 2005, 2006; Macías et al., 2008; Navarro et al., 2006; Reul et al., 2006). Observational studies based on OCRS products allowed a regular high-frequency sampling, covering most SWIP areas (Navarro et al., 2007, 2012, 2013; Peliz and Fiúza, 1999; Sousa and Bricaud, 1992) or specific regions within the north margin of the Gulf of Cadiz (Caballero et al., 2014; Cravo et al., 2013; Cristina et al., 2016a, 2016b; Goela et al., 2015; Navarro and Ruiz, 2006; Prieto et al., 2009; Ramírez-Romero et al., 2012; Vázquez et al., 2009). Other study strategies have also included model-based inferences (Macías et al., 2014; Marta-Almeida et al., 2012; Reboreda et al., 2014a, 2014b) and dedicated experiments (Loureiro et al., 2008; Weissbach et al., 2011). Overall, these studies have contributed to our understanding of phytoplankton variability and regulation in some, mostly coastal, domains of the SWIP area. Additionally, these studies indicated that the influence of specific environmental drivers, including climate-related variables (e.g., wind forcing, coastal upwelling and mixing-stratification cycles; rainfall and riverine discharges; tidal currents and internal waves), depends on location and study period (e.g., Caballero et al., 2014; García-Lafuente and Ruiz, 2007; Navarro and Ruiz, 2006; Navarro et al., 2012; Peliz and Fiúza, 1999; Prieto et al., 2009). Indeed, 5-year Chl-a time series, retrieved from OCRS, were decomposed into dominant modes and used to regionalize the Gulf of Cadiz basin (Muñoz et al., 2015; Navarro and Ruiz, 2006). Despite the connectivity across-domains, recent studies mostly addressed the zonal and meridional Iberian margins separately, often overlooking the open ocean domain, so an integrated comprehensive view of phytoplankton dynamics and controls over the heterogeneous SWIP area is still lacking.

In this context, the objectives of our study are: (i) to evaluate phytoplankton seasonal and interannual variability patterns in the SWIP area, over a 15-year period (1997 - 2012); (ii) to identify region-specific phytoplankton environmental determinants within this heterogeneous study area; and (iii) to investigate whether climate variability affects specific SWIP regions in particular ways. To accomplish this goal, SWIP was partitioned into regions with similar phytoplankton variability, using satellite-retrieved Chl-a and Empirical Orthogonal Function

analysis, and region-specific linkages between environmental drivers and phytoplankton were later explored using Generalized Additive Mixed Models. Phenology of phytoplankton blooms will be addressed specifically in a dedicated article.

4.2 - Materials and Methods

4.2.1 Study area

SWIP area is currently partitioned into distinct spatial functional units, depending on the global ocean classification scheme used (see Chapter 2, also and hereafter Krug et al., 2017): eastern North Atlantic Subtropical Gyre Province and Canary Current Coastal Province (Longhurst, 2007); and North Atlantic Transitional and Canary Current epipelagic areas (Spalding et al., 2012). Coastal SWIP domains are further integrated into two large marine ecosystems (Iberian Coastal, and Canary Current; Sherman, 1994) and two marine ecoregions (South European Atlantic Shelf, and Saharan Upwelling; Spalding et al., 2007). Concurrently, mesoscale approaches delineated a higher number of regions over SWIP (e.g., Muñoz et al., 2015; Navarro and Ruiz, 2006), underlying its heterogeneity.

The SWIP area (Fig. 4.1) includes deep ocean domains, interspaced with submarine seamounts and canyons, and a 5-35 km wide continental shelf that changes orientation markedly, from meridional to zonal, at Cape São Vicente (CSV). Open ocean SWIP domains show an annual stratification-destratification cycle, with a deep winter mixed layer, which promotes the advection of inorganic nutrients into the euphotic zone (e.g., Longhurst, 2007). The SWIP south sector includes a semi-sheltered basin, the Gulf of Cadiz (GoC), that receives waters from the Mediterranean Sea, through the Strait of Gibraltar, as well as significant continental freshwater inputs from rivers (e.g., Guadiana, Piedras, Tinto-Odiel and Guadalquivir rivers; Caballero et al., 2014) and submarine groundwater discharges (e.g., Hugman et al., 2015). Other small estuarine systems, associated with mediterranean rivers and streams (mean annual river flow: 1-10 $m^3 s^{-1}$) with intermittent torrential flow, predominantly restricted to the winter period, drain directly into the Portuguese south (Arade estuary, Alvor and Ria Formosa coastal lagoons) and southwest coasts (Mira estuary, Odeceixe, Aljezur and Bordeira streams; Cabral et al., 2012; Cardoso et al., 2012; see Fig. 4.1).

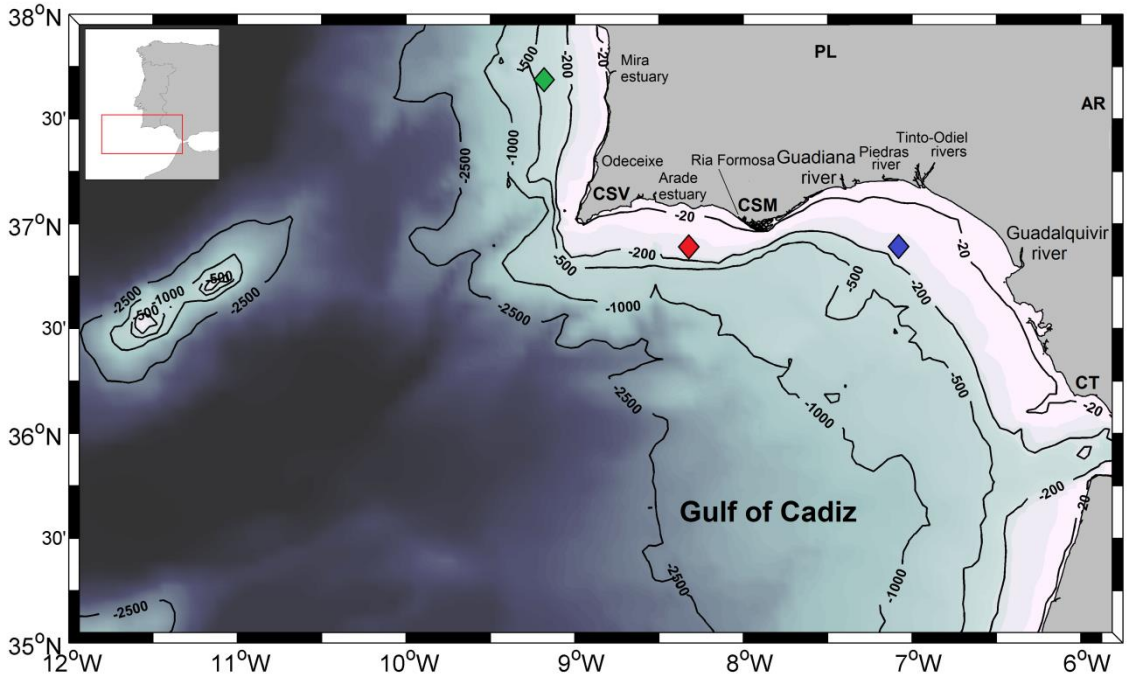

Figure 4.1 - The southwest area off the Iberian Peninsula (SWIP) bathymetry and main sources of freshwater discharges. CSV, CSM and CT depict the location of prominent topographic features, Cape São Vicente, Cape Santa Maria and Cape Trafalgar, respectively. PL and AR depict the location of Pulo do Lobo and Alcalá del Río hydrographic stations, respectively. Diamonds show the position of pixels used for the calculation of Cross Shore Ekman Transport for the West Coast (green), and west (red) and east Cape Santa Maria sectors (blue). Location of the outflow of major estuarine systems is also shown (see text for further details).

SWIP is located in the Iberian Canary Eastern Boundary Upwelling system (EBUS), one of the most biologically productive systems in global oceans (Carr and Kearns, 2003). More favourable light and temperature conditions, high iron inputs, a wide continental shelf, long nearshore water residence times (low eddy activity) and shallow mixed layer globally support higher phytoplankton production at the Iberian Canary EBUS in respect to other EBUS (Lachkar and Gruber, 2011, 2012). However, over SWIP area, decreased offshore Ekman transport, a narrower continental shelf and lower water column stability inhibit upwelling effects in comparison to other sections of this EBUS (e.g., NW Africa; Patti et al., 2008; Arístegui et al., 2009; Pardo et al., 2011). Nonetheless, upwelling over SWIP affects significantly phytoplankton biomass, community structure and production, promoting diatom-based communities (Goela et al., 2014; Moita, 2001; Reul et al., 2006; Silva et al., 2009). Its stimulatory effects are crucial for local marine food webs and fisheries (Malta et al., 2016; Stratoudakis et al., 2003; Santos et al., 2001; 2007). Upwelling activity depicts a strong

seasonality, occurring predominantly between April and October, due to the zonal displacement of atmospheric pressure systems (Arístegui et al., 2009; Fiúza et al., 1982; García-Lafuente and Ruiz, 2007; Relvas et al., 2007, 2009). Along the meridional coast, summer northerly winds are associated with stronger and more persistent upwelling conditions. Westerly winds are associated with upwelling along the zonal northern coast of GoC, and upwelling relaxation is usually associated with the development of a warm near-shore coastal countercurrent moving westwards (Garel et al., 2016; Relvas et al., 2007). Multi-decadal changes in upwelling intensity have been reported for the Iberian Canary EBUS, including SWIP area, but trends are controversial, depending on region and length of the time series (see reviews by Barton et al., 2013; Varela et al., 2015). Mesoscale and sub-mesoscale patterns (e.g., upwelling filaments, fronts, cyclonic and anticyclonic eddies, jets) are characteristic of the SWIP continental margins, sometimes associated with prominent topographic features (CSV, Cape Santa Maria, Cape Trafalgar and Strait of Gibraltar; see reviews by García-Lafuente and Ruiz, 2007; García-Lafuente et al., 2006; Peliz et al., 2014; Relvas et al., 2007).

4.2.2 Phytoplankton data

Surface chlorophyll-a concentration was used to evaluate phytoplankton variability patterns in the SWIP area during the period 1997-2012. Level 3, 8-day composites of satellite-derived Chl-a, at 4 km spatial resolution, were accessed from the European Space Agency (ESA)'s Ocean Colour Climate Change Initiative Group (OC-CCI; http://www.esa-oceancolour-cci.org). The OC-CCI Chl-a product (Couto et al., 2016; Storm et al., 2013) uses remote sensing reflectances (R_{RS}), derived from Sea-viewing Wide Field of View Sensor (SeaWiFS), MODerate-resolution Imaging Spectroradiometer (MODIS-Aqua) and MEdium Resolution Imaging Spectrometer (*MERIS*) sensors, which are wavelength synchronized to account for sensor specific centre bands, bias corrected and merged, allowing a greater spatial-temporal resolution with respect to the use of single sensors. Chl-a values are computed using merged R_{RS} and version 6 of Ocean-Colour-4 algorithm (OC4v6), an updated version of a four-band blue-green reflectance ratio empirical algorithm developed for SeaWiFS (O'Reilly et al., 2000). Since OC-CCI Chl-a product is primarily designed for application in Case I waters, to minimize problems associated with Case II (coastal optically-complex) waters, Chl-a was retrieved only for areas outside the 20 m isobath, located at a minimum distance of

approximately 4 km from the coastline. All Chl-a values were retained since unusually high Chl-a values for the study area (> 20 µg L^{-1}; Caballero et al., 2014; Moita, 2001; Navarro and Ruiz, 2006) represented only less than 0.002% of valid data. To minimize the effects of missing data, usually associated with cloud cover, Chl-a 8-day composite time-series were re-gridded to fortnight (16-day) composites by averaging two consecutive 8-day composites (final n=342). Data analyses and visualization maps were generated using MATLAB software. Accuracy of satellite-derived Chl-a for the study region and adjacent Atlantic areas was previously assessed during calibration-validation exercises dedicated to different (standard and alternative) bio-optical algorithms and sensors, including SeaWiFS (Navarro and Ruiz, 2006), MERIS (Cristina et al., 2014, 2015, 2016a, 2016b; Nechad et al., 2015), MODIS-Aqua (Caballero et al., 2014; Sá et al., 2015) and OC-CCI products (Sá et al., 2015). Overall, these studies show that satellite radiometry provides reasonable estimates of *in situ* Chl-a, but usually larger than contemporaneous *in situ* estimates. Higher uncertainty is reported for coastal Chl-a retrievals, with systematic overestimation in nearshore Case II waters.

4.2.3 Environmental data

A set of potential environmental drivers of phytoplankton variability, including ocean physical (sea surface temperature, mixed layer depth, light intensity) and chemical variables (nutrient concentrations), upwelling intensity and meteorological variables, was acquired from remote sensing and model-derived products for the study area and period (1997-2012), at variable temporal and spatial resolutions. All mapped variables were re-gridded to the same resolution of Chl-a (4-km, 16-day). Data analyses and visualization maps were generated using MATLAB software.

4.2.3.1 Ocean physical and chemical variables

Daily satellite-derived sea surface temperature (SST) data were retrieved from two databases: Advanced Very-High Resolution Radiometer (AVHRR) SST (1997-2009, 4 km resolution), extracted from the Pathfinder database (http://data.nodc.noaa.gov/pathfinder/Version5.0/); and MODIS-Aqua SST (2010-2012, 1 km spatial resolution), obtained from the NASA's Oceancolor portal (http://oceancolor.gsfc.nasa.gov/). SST data were limited to night time passes, to avoid diurnal solar heating effects (Robinson, 2010), and high quality data

(AVHRR quality flags 6 and 7, and MODIS-A quality flag 0). Relationships between daily satellite retrieved SST and *in situ* daily mean SST data measured by an instrumented buoy moored off the coast of Faro (36.9°N, 7.9°W; maintained by the Portuguese Instituto Hidrográfico da Marinha, http://www.hidrografico.pt/), for the period 2000-2012, were highly significant (R^2=0.94, n=2323, p<0.001, data not shown).

Daily level-2 mean surface photosynthetically available radiation (PAR) at 1 km spatial resolution, were obtained from NASA's Oceancolor Group for the study period (1997-2012). Data from SeaWiFS (1997-2003) and MODIS-Aqua (2002-2012) sensors were merged over the study period. Standard Level-2 flags were applied for quality control; land and quality-failed pixels were automatically masked and considered invalid. Light attenuation coefficient at 490 nm wavelength (K_{490}, m^{-1}), obtained from OC-CCI with Chl-a, was converted to PAR light attenuation coefficient (K_{PAR}, m^{-1}) using equation 4.1, according Rochford et al. (2001). K_{PAR} was used to estimate the euphotic zone depth (Z_{eu}, m), depth at which the irradiance has decreased to 1% of PAR, was estimated as $4.61/K_{PAR}$, using the Lambert-Beer law and assuming a constant attenuation coefficient and optically homogeneous waters. Mean PAR intensity in the mixed layer (I_m, µmol photons m^{-2} s^{-1}) was calculated using equation 4.2, according to Kirk (1986), where PAR represents PAR intensity at the surface (µmol photons m^{-2} s^{-1}), K_{PAR} is PAR light attenuation coefficient (m^{-1}), and MLD represents the mixed layer depth (m).

$$K_{PAR} = 0.085 + 1.6243K_{490} \qquad \text{Eq. 4.1}$$

$$I_m = \mathrm{PAR}\,\frac{(1-\mathrm{e}^{-K_{PAR}\,MLD})}{K_{PAR}\,MLD} \qquad \text{Eq. 4.2}$$

Mixed Layer Depth (MLD) 8-day-composites were retrieved from the Ocean Productivity group of the Oregon State University (http://www.science.oregonstate.edu/ocean.productivity/index.php), based on three data-assimilating models: Simple Ocean Data Assimilation (SODA), at a 0.5° spatial resolution (1997-2004); Thermal Ocean Prediction Model based on The Navy Coupled Ocean Data Assimilation system (NCODA/TOPS), at a 1° spatial resolution (January 2005 - May 2005); and Fleet Numerical Meteorology and Oceanography Center model (FNMOC – June 2005 to

July 2012), at a 0.25^{o} spatial resolution. This combination of MLD data was selected in accordance with the preferred MLD sources used by the Ocean Productivity for their net primary production models. MLD data was adjusted to GEBCO bathymetry (IOC, IHO and BODC, 2003), and maximum MLD values were limited to bathymetry values.

Due to the limited availability of *in situ* oceanographic chemical data for the study area, monthly subsurface (1 m depth) nitrate concentration (NO_3, µM), a key indicator of the availability of dissolved inorganic macronutrients, was obtained from the biogeochemical model reanalysis data provided by the Copernicus Marine Environment Monitoring Service for the Atlantic-Iberian Biscay Irish-Ocean area for the period February 2002 - December 2011 (Product: IBI_REANALYSIS_BIO_005_003; http://marine.copernicus.eu/). The biogeochemical model PISCES (Pelagic Interaction Scheme for Carbon and Ecosystem Studies) is coupled with ocean physics NEMO (Nucleus for European Modelling of the Ocean), providing 3D data, at a 0.08^{o} spatial resolution and monthly temporal resolution.

4.2.3.2 Upwelling intensity

A wind-based upwelling index, the cross-shore Ekman transport (CSET), was used to infer upwelling intensity and patterns during the study period (1997-2012). Daily sea surface wind (WIN) and its zonal (U) and meridional (V) component fields, at 0.25^{o} spatial resolution, were obtained from the Blended Sea Winds dataset (National Climatic Data Center - National Oceanic and Atmospheric Administration, NCFC-NOAA, http://www.ncdc.noaa.gov/oa/rsad/air-sea/seawinds.html). Blended Sea Winds dataset are based on a combination of several scatterometers, standardized across platforms, thus allowing a high quality and more complete temporal and spatial coverage of ocean wind vectors (Zhang et al., 2006). According to Sánchez et al. (2007), along the south Portuguese coast (characterized by intense mesoscale variability), satellite-derived wind retrievals provide more robust estimates of ocean winds than *in situ* wind measurements obtained at coastal locations. Due to the coarse spatial resolution of wind data, CSET (16 day-composites) were estimated for only three locations, positioned at ca. 75 km from the coastline (see Fig. 4.1): one location on the west Portuguese coast ($CSET_{WC}$) and two locations on the south Portuguese coast, at western and eastern sectors of Cape Santa Maria

($CSET_{wCSM}$ and $CSET_{eCSM}$, respectively). For each location, CSET values represent the average of a 0.75^o x 0.75^o box centred at the target location.

Macroscopically, the south Portuguese coastline is zonally (west-east) oriented and the west coast is meridionally oriented (Fig. 4.1). Thus, the meridional component of the Ekman transport, $CSET_y$, induced by the zonal component of wind-stress (τ_x), was used as an upwelling index over the south coast ($CSET_{wCSM}$ and $CSET_{eCSM}$). Conversely, the zonal component of the Ekman transport, $CSET_x$, induced by the meridional component of wind-stress (τ_y), was used as an upwelling index over the west coast ($CSET_{WC}$). $CSET_y$ and $CSET_x$ (m^3 s^{-1} km^{-1} coastline) were calculated according to equations 4.3 and 4.4 (Alvarez et al., 2011; Bakun, 1973):

$$CSET_y = - \frac{1000\ \tau_x}{\rho_w f} = - \frac{\rho_a\ c_d}{\rho_w f}\ (W_x^2+W_y^2)^{1/2}\ 1000\ W_x \qquad \text{Eq. 4.3}$$

$$CSET_x = \frac{1000\ \tau_y}{\rho_w f} = \frac{\rho_a\ c_d}{\rho_w f}\ (W_x^2+W_y^2)^{1/2}\ 1000\ W_y \qquad \text{Eq. 4.4}$$

where W represents wind magnitude (m s^{-1}), ρ_w is seawater density (1025 kg m^{-3}), ρ_a is air density (1.22 kg m^{-3}), C_d is the drag coefficient ($1.4x10^{-3}$) and *f* is the Coriolis parameter, estimated as 2 Ω sin(θ) where Ω and θ represent the vertical component of the Earth's angular velocity and local latitude, respectively. Subscripts *x* and *y* correspond to zonal and meridional components, respectively.

Negative $CSET_y$ and $CSET_y$ values indicate offshore Ekman transport and upwelling-favourable periods; conversely, positive values indicate onshore Ekman transport and downwelling-favourable periods. No significant differences were detected between $CSET_{wCSM}$ and $CSET_{eCSM}$ values ($p<0.01$); as consequence, average values were used as indices of cross-shore Ekman transport for the south coast ($CSET_{SC}$).

4.2.3.3 Hydrographic and meteorological variables

Guadiana river discharge during the study period (1997-2012), measured at the hydrometric station Pulo do Lobo at daily resolution, was accessed from the Portuguese Environmental Agency public database (http://snirh.apambiente.pt/). Daily Guadalquivir river discharge,

measured at the Alcalá del Río station, was acquired from the Spanish Regional Water Management Agency (http://www.chguadalquivir.es/saih/).

Five large-scale climate indices were used as indicators of remote forcing over the study area: (i) the Multivariate El Niño Southern Oscillation (ENSO) Index (MEI), which monitors ENSO patterns based on six ocean-atmosphere variables over the tropical Pacific (Wolter and Timlin, 2011); (ii) the North Atlantic Oscillation (NAO) index, a normalized pressure difference between the Azores and Iceland (Hurrell, 1995); (iii) the Atlantic Multidecadal Oscillation (AMO) index, a SST-based monitoring of the north Atlantic (Enfield et al., 2001); (iv) the East Atlantic pattern (EA) index, derived from the second mode of sea-level pressure (SLP) variation in the North Atlantic (Hurrell et al., 2003), particularly relevant for southern Europe sector (see Iglesias et al., 2014); and (v) the Western Mediterranean Oscillation (WeMO) Index, a barometric ratio between Padua (north Italy), and San Fernando (southwest Spain), representative of the western Mediterranean basin (Martin-Vide and Lopez-Bustins, 2006). MEI and AMO data were available at NOAA's Earth System Research Laboratory portal (https://www.esrl.noaa.gov/psd/data/climateindices/), EA data were acquired at NOAA's Climate Prediction Center website (http://www.cpc.ncep.noaa.gov/), NAO were retrieved from the (USA) National Center for Atmospheric Research website (https://climatedataguide.ucar.edu/climate-data) and WeMO data were retrieved from the University of Barcelona's Climatology Group website (http://www.ub.edu/gc/en/2016/06/08/wemo/).

4.2.4 Data analyses

The strength of monotonic relationships between variables was assessed using Spearman rank correlation coefficient (r_S; Hauke and Kossowski, 2011; Wilks, 2006). Empirical Orthogonal Function (EOF) analysis was used to partition the study area into regions with similar Chl-a variability patterns. Generalized Additive Modelling (GAM) techniques were used to decompose region-specific temporal variability of both abiotic variables and Chl-a, and explore linkages between phytoplankton and environmental determinants. All statistical hypotheses were tested at an $\alpha = 0.05$ level.

4.2.4.1 Empirical Orthogonal Function analysis and study area regionalization

EOF analysis was used to evaluate spatial-temporal variability patterns of Chl-a over the 15-year time-series, and to delineate coherent, co-varying regions in the SWIP study area. EOF analysis requires complete matrices so missing data pixels were filled using a three-step linear interpolation procedure, based on Racault et al. (2014b). The output resulted in a few missing values (<0.05% of no-land pixels), which were replaced by the average value for the adjacent 3x3 pixels. Prior to EOF analysis, the image time series was de-meaned, by subtracting the 15-year temporal mean of each pixel, for reducing the effects of dominant seasonal signals, and spatially normalized, for reducing the effects of extreme areas of high variability relative those with low variability (Eastman, 1992; Santamaría-del-Angel et al., 2011; Wilks, 2006; Yoder et al., 2002).

EOF is an objective powerful tool for compressing the spatial and temporal variability of complex time series data, partitioning data variance into a set of dominant, mathematically-orthogonal (independent) spatial functions or modes and associated time-varying amplitudes (Monahan et al., 2009; Yoder et al., 2002). Singular value decomposition of the Chl-a time series was used to calculate the EOF spatial components, associated eigenvalues (percent of explained variance) and time-varying amplitudes. The spatial components of each mode are global maps depicting the modal spatial patterns, with both positive and negative deviations with respect to the 15-year temporal mean. The modal temporal patterns (time-varying amplitude coefficients) show how each modal spatial pattern evolved during the study period (Yoder and Kenelly, 2003). The integration of both the modal spatial and temporal patterns can be obtained multiplying the spatial coefficient by the temporal amplitudes. There are as many EOFs as input images, however most of the variance is contained within the first few modes. The sampling error of each EOF mode ($\Delta\lambda$) was evaluated according to North et al. (1982), using equation 4.5:

$$\Delta\lambda \approx \lambda\sqrt{\frac{2}{n}} \qquad \text{Eq. 4.5}$$

where λ is mode eigenvalue and n is the number of images used in the EOF analyses (342 images of 16-day composites). An EOF mode was considered statistically significant if its Δλ was smaller than the difference between its eigenvalue and its closest neighbour eigenvalue.

EOF analysis is particularly effective in reducing phytoplankton variability patterns when only a few modes explain most of the variability, spatial patterns are relatively simple and coherent over large study area domains, and the amplitude time series exhibit a smooth periodic signal (see Yoder and Kenelly, 2003). EOF modal spatial and temporal Chl-a patterns were interpreted in relation to environmental processes, to elucidate their underlying driving forces. Relationships between time-varying amplitude coefficients for dominant EOF modes and environmental variables were explored using GAM analyses (see Section 4.2.4.2). However, statistical EOF modes may not necessarily capture real oceanic bio-physical patterns and should be interpreted cautiously (see Thomas et al., 2012).

The spatial components of the dominant EOF modes were used to delineate regions with coherent, co-varying Chl-a variability patterns (e.g., Caballero et al., 2014; Macías et al., 2007; Muñoz et al., 2015; Navarro and Ruiz, 2006; Waite and Mueter, 2013; Xu et al., 2011), within SWIP. For some regions, subsequent partitioning was applied using geographic location and bathymetry (± 200 m depth).

4.2.4.2 Region-specific phytoplankton temporal variability patterns and environmental drivers

GAM techniques (Wood, 2006) were used to evaluate region-specific phytoplankton temporal variability patterns and underlying environmental determinants. GAMs are a flexible class of statistical models that accommodate complex non-linear relationships between a dependent or response variable and multiple predictors or covariates. GAMs do not require *a priori* specification of the functional relationships between response variables and predictors, and offer a data-driven empirical optimal approach, able to handle multicollinearity between variables and minimize the effects of extreme observations (Llope et al., 2009; Wood, 2006; Zarauz et al., 2008).

The basic GAM model structure is represented by equation 4.6:

$$Y = \propto + \sum_{j=1}^{n} s_j \left(X_j\right) + \varepsilon \qquad \text{Eq. 4.6}$$

where $\propto$ is the intercept, s_j are nonparametric smoothing functions specifying the partial additive effect of each predictor (X_j), and ε represents a random error term assumed to be normally distributed with zero mean and finite constant variance.

Underlying statistical assumptions (residuals normality, homoscedasticity) of the GAMs were tested using graphical residual diagnostics. Model residues were tested for temporal autocorrelation (serial dependency) using an autocorrelation function. Since residuals showed temporal autocorrelation (lag 1 or lag 2), GAMs were extended to Generalized Additive Mixed Models (GAMM) by including a first or second order autoregressive correlation structure in the models (e.g., Otto et al., 2014; Thackeray et al., 2008). GAM and GAMM analyses were conducted using the "mgcv" library (version 1.8-11), in R statistical software (R Development Core Team, 2016).

Intra-annual (seasonal) and inter-annual trends in climate indices, EOF temporal coefficients and region-specific environmental variables and Chl-a during the study period (1997 - 2012) were investigated using GAMM analyses. Environmental data and log-transformed Chl-a (Y) were modelled as a cyclic spline smoother function (t) of time of the year (year-fortnight) and a cubic spline smoother function (s) of time (year), according to equation 4.7 (Wood, 2006),

$$Y = \propto + t\,(time\ of\ year) + s\,(time) + \varepsilon \qquad \text{Eq. 4.7}$$

where $\propto$ represents the intercept, and ε represents a random error term which includes an autoregressive correlation structure (Wood, 2006).

GAMM were also used to identify linkages between environmental forcing and phytoplankton variability for the specific regions previously identified by EOF analysis. Predictor variables (X_i) included atmospheric and oceanographic variables, representative of the local study area or its regions, and global to regional climate indices, with both current and past (one-month lagged) values (see section 4.2.3). Response variables (Y), region-specific Chl-a and time-varying amplitude coefficients for the dominant EOF modes, were $\log_{10}$-transformed to reduce over-dispersion and the influence of outliers, and cubic regression

splines (*t*) were used as smoother functions (see equation 4.6). Prior to the analysis, colinearity among covariates was tested using Spearman rank correlation coefficients (r_S), and variables significantly correlated at $|r_S|>0.70$ were not used as covariates for the same model run (Dormann et al., 2013). The majority of predictor variables were, at most, moderately correlated ($|r_S|< 0.50$). However, correlation values ($|r_S|$) between SST, MLD and NO_3 were systematically >0.7; as consequence these variables were not used simultaneously as predictors for any model run. Since NO_3 data were available only for a shorter period (2002-2011), this variable was not further explored. For each specific region, GAMMs were run using all possible combinations of environmental predictor variables rather than a standard stepwise procedure (see Doyle et al., 2009). Analysis of variance (ANOVA) and an F-test were used to compare different GAM models. Criteria used to select the best-performing models included: minimizing the generalized cross-validation (GCV) score, a measure of the predictive error of the model and its complexity related to Akaike's Information Criterion (AIC); maximizing the level of deviance explained; and the confidence envelopes for the smoothing which should not include zero throughout the covariate range (Llope et al., 2009; Wood, 2006; Zarauz et al., 2007).

4.3 - Results

4.3.1 Large-scale environmental setting off SW Iberia

Mean spatial distribution of selected environmental variables in the SWIP area during the study period showed clear latitudinal patterns in case of SST (Fig. 4.2A) and PAR (Fig. 4.2B), with higher values for southern domains, and strong coastal-offshore gradients, with higher NO_3 (Fig. 4.2I) and K_{PAR} values (see supplementary material, Fig. C.1) and lower Z_{eu} values (Fig. 4.2G) for coastal domains. MLD (Fig. 4.2C) and WIN (Fig. 4.2D) were generally lower in the semi-sheltered GoC basin, and wind components showed a predominance of northerlies ($V < 0$ m s^{-1}) and westerlies ($U > 0$ m s^{-1}) for the west exposed SWIP sector and GoC, respectively (Fig. 4.2E-F). The latter area also presented the highest I_m mean values (Fig. 4.2H), a consequence of shallow MLD and high mean PAR values.

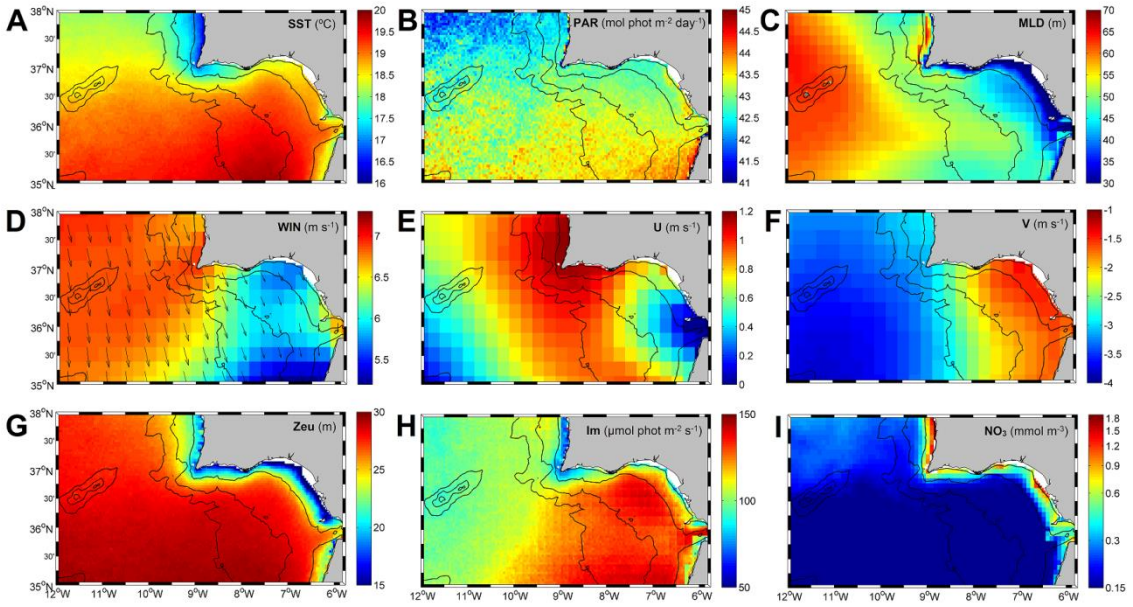

Figure 4.2 - Distribution of mean values of A) sea surface temperature (SST), B) surface photosynthetically active radiation (PAR), C) mixed layer depth (MLD), D) wind intensity (WIN; coloured) and direction (black arrows), E) zonal (U) and F) meridional (V) wind speed, G) euphotic depth (Zeu), H) average PAR intensity in the MLD (Im) and I) subsurface nitrate concentration (NO_3), in the southwest area off the Iberian Peninsula, during the period between September 1997 and July 2012. Black lines represent 20m, 200m, 1000m and 2500m isobathimetric contours.

The presence of cold, high-nitrate water masses over the west and southwest Portuguese continental shelf, extending to the shelf-edge off the west coast, represented the wind-driven coastal upwelling signature (Figs. 4.2A, 4.2I). Temporal variability of cross-shore Ekman transport ($CSET_{WC}$ and $CSET_{SC}$) showed a more-extended and significantly stronger upwelling intensity for the west coast compared with that of the south coast ($CSET_{WC}$=-342.6±23.5 *versus* $CSET_{SC}$=-97.4±19.62 $m^3\ s^{-1}\ km^{-1}$ coastline, Mann-Whitney U test, $p<0.01$), and a significant seasonal pattern (GAMM, $p<0.01$, data not shown), with upwelling-favourable conditions during the spring-summer period peaking in June and July on the south and west Portuguese coasts, respectively (see red line, Fig. 4.3A-B). Interannual CSET patterns showed particularly strong upwelling events during summer (WC: 2002, 2011; SC: 2002) and autumn-winter periods (WC: 2004-2005, 2008-2009); SC: 2000-2001, 2008-2009; 2009-2010; Fig. 4.3A-B). GAMM decomposition of $CSET_{WC}$ and $CSET_{SC}$ revealed a linear interannual increasing trend in upwelling intensity over the west coast (i.e., decline in $CSET_{WC}$; GAMM, $p<0.05$, data not shown), and no significant trend for the south coast. Upwelling intensity off the west coast was positively correlated with NAO index (r_s=0.18,

n=342, p<0.001). Conversely, upwelling intensity off the south coast was negatively correlated with NAO (r_s=-0.28, n=342, p<0.0001), and positively correlated with WeMO (r_s=0.19, n=342, p<0.01) and MEI (r_s=0.14, n=342, p<0.001) indices.

During the study period, Guadiana (Gdn) and Guadalquivir (Gdq) river discharges averaged 63.2±9.8 and 90.8±13.7 m^3 s^{-1}, respectively, and major flood events were detected during 1997-1998, 2000-2001 and 2009-2010 autumn-winter periods (Fig. 4.3C-D), coinciding with strongly negative NAO phases (Fig. C.2B). Gdq river discharge was negatively correlated to NAO (r_s=-0.30, n=296, p<0.01), while Gdn river discharge showed a negative correlation with WeMO (r_s=-0.28, n=304, p<0.01). In terms of temporal variability, while both presented significant seasonal patterns, Gdq also showed significant non-linear interannual trend (GAMM, p<0.001, data not shown). Among climate indices (Fig. C.2), MEI presented a highly significant non-linear interannual trend (GAMM, p<0.001, data not shown), whereas WeMO presented a weakly significant linear interannual declining trend (GAMM, p<0.05, data not shown).

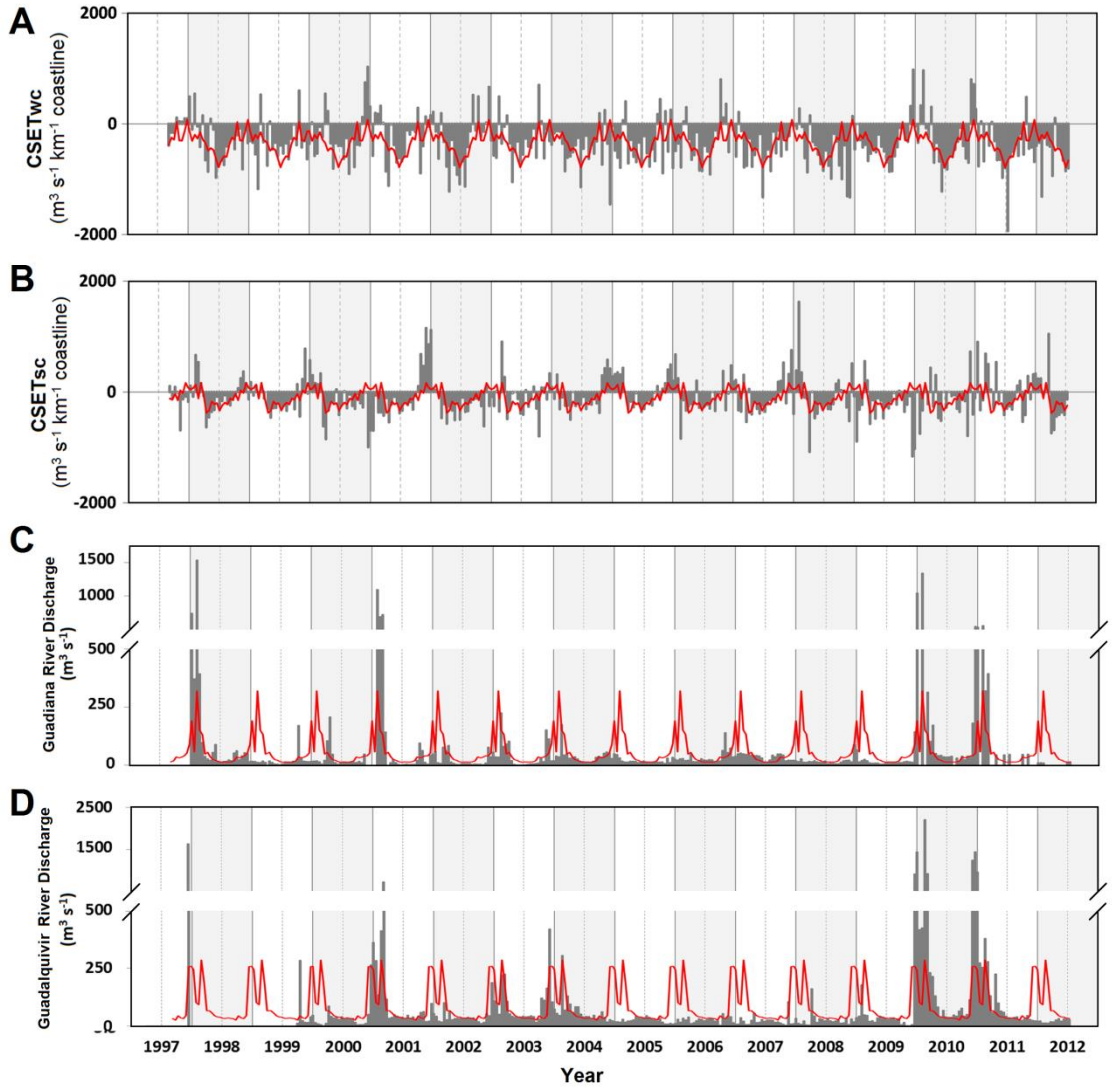

Figure 4.3 - Temporal variability of upwelling intensity and river discharge over the southwest area off the Iberian Peninsula (SWIP), during the period 1997 to 2012. (A-B) Cross-shore Ekman transport, a wind-based upwelling index, for the west ($CSET_{WC}$) and south ($CSET_{SC}$) Portuguese coasts; negative (positive) values indicate upwelling-favorable (upwelling-unfavorable) conditions. (C-D) Guadiana and Guadalquivir river discharge. Red lines represent fortnightly-based climatologies for the study period.

4.3.2 Large-scale phytoplankton variability patterns off SW Iberia

Chl-a over the study period showed an intense cross-shelf gradient with higher values over inner shelf waters, mostly close to the 20 m isobath, and lower values over slope and oceanic waters (Fig. 4.4). Global seasonal mean Chl-a values ranged between 0.05-0.5 µg L^{-1} and 0.5-3.5 µg L^{-1} for offshore and shelf waters, respectively, showing an offshore latitudinal gradient, with higher Chl-a values north of ca. 37°N. Chl-a values above 0.5 µg L^{-1} were

usually located shoreward of the 1000 m isobath for the west Portuguese coast, but were confined to shelf waters (< 200 m) over the GoC basin. Climatological seasonal composites showed clear winter maxima and summer minima for offshore waters, and less pronounced seasonal variability for coastal domains. Generally, a winter expansion of the coastal band of Chl-a enriched waters was detected between east of CSM and CT coasts, areas impacted by the freshwater outflow of Guadiana and Guadalquivir rivers. A summer extension of Chl-a enriched waters was observed for the west and southwest Portuguese coastal domains, areas under significantly stronger upwelling intensities (see Fig. 4.3A-B and 4.4).

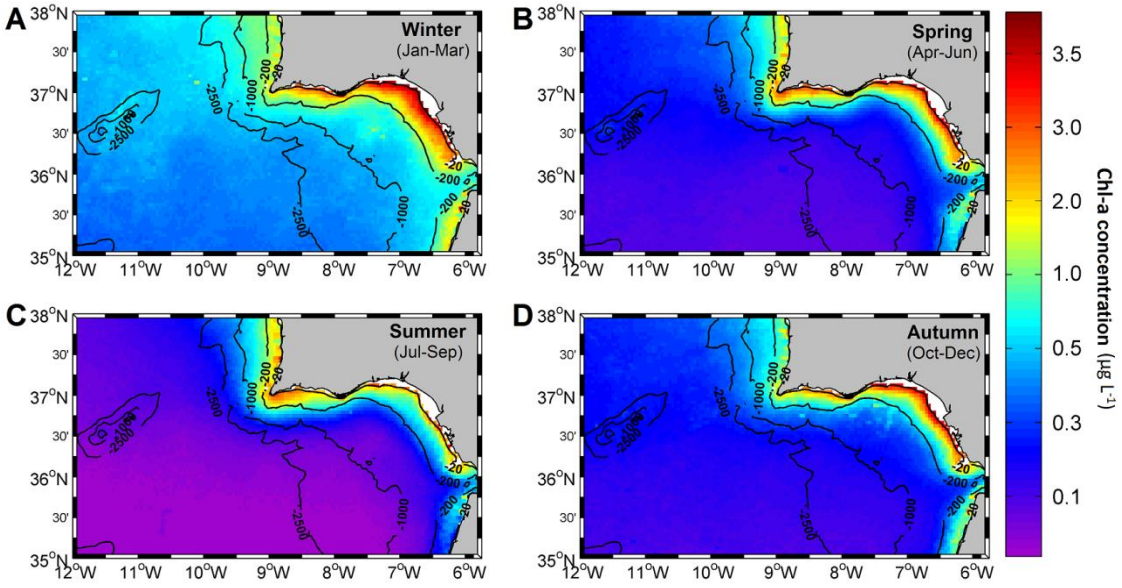

Figure 4.4 - Large-scale seasonal climatologies (September 1997-July 2012) for chlorophyll-a concentration (µg L^{-1}) off SW Iberia during: (A) Winter, (B) Spring, (C) Summer, and (D) Autumn. Black lines represent 20m, 200m, 1000m and 2500m isobathymetric contours.

4.3.3 Dominant modes of chlorophyll-a variability off SW Iberia

EOF analysis reduced the whole Chl-a data set to three significant dominant modes (spatial components; Fig. 4.5A, 4.5C, 4.5E) and associated temporal coefficients (Fig. 4.5B, 4.5D, 4.5F), which overall accounted for 47% of Chl-a temporal-spatial variability. The first EOF mode (EOF1) explained 27% of Chl-a variability; its spatial component primarily separated two large-scale coherent regions within the study area (Fig. 4.5A), fluctuating out of phase, the continental shelf and slope waters (negative spatial coefficients) and oceanic waters (positive coefficients). As also observed for Chl-a distribution (see Fig. 4.4), for latitudes

north of 37°N (off west coast) negative spatial coefficients extended offshore the 1000 m isobath. Higher negative spatial coefficients were associated with coastal areas near the 20 m isobath. Very low (positive) spatial coefficients were detected over oceanic waters, indicating its higher Chl-a temporal stability in respect to coastal and slope regions (see Fig. 4.5A). Decomposition of EOF1 temporal component (Fig. 4.5B) using GAMM revealed a highly significant intra-annual pattern (Fig. C.3A-B; Table C.1), presenting minima during winter-early spring and maxima during summer associated to Chl-a positive deviations and negative deviations, respectively, for shelf/slope waters. Extended periods of negative temporal coefficients, including minimum temporal coefficients, were observed during years of high riverine discharge. Best-performing GAMM model of EOF1 temporal coefficients, based on a set of eight predictors (MLD, Gdq, WeMO, U, PAR, WIN, AMO, NAO-1, where -1 denotes one-month lag), explained 62% of its variance, with MLD, Gdq and U as the most relevant variables (Fig. C.4A, Table C.2).

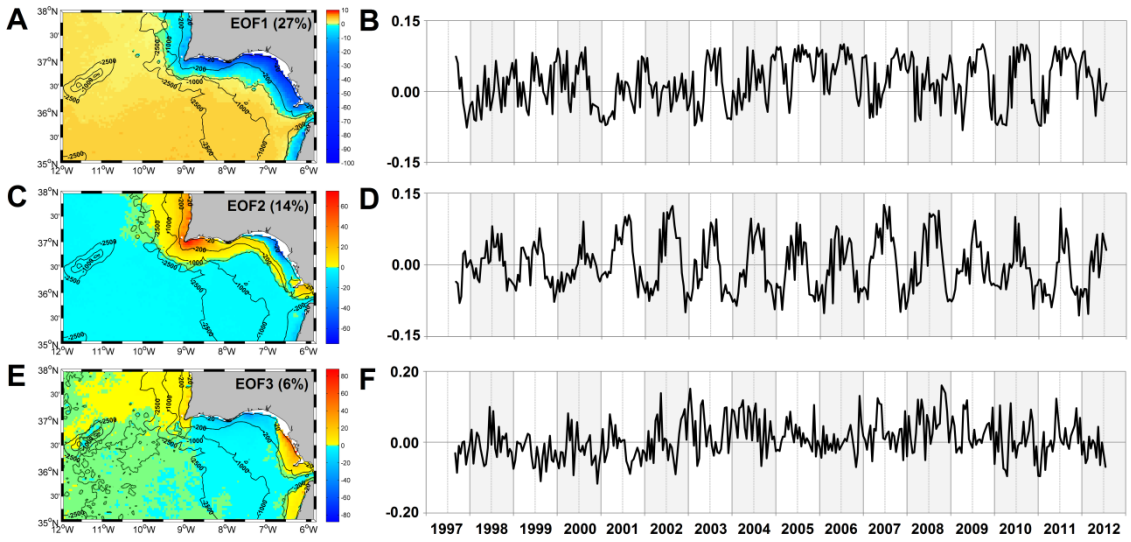

Figure 4.5 - Empirical orthogonal function (EOF) analyses of surface chlorophyll-a concentration off SW Iberia, during 1997-2012. Spatial components (A, C, E) and time-varying amplitude coefficients (B, D, F) for the first (EOF1), second (EOF2) and third (EOF3) EOF mode, respectively. Solid black lines shown on the maps represent 20 m, 200 m, 1000 m and 2500 m isobathymetric contours, and dashed lines depict spatial coefficient zero contour.

The second EOF mode (EOF2) explained 14% of Chl-a variability, and its spatial function differentiated two SWIP regions (Fig. 4.5C). Most of the study area (ocean domain) presented low negative EOF2 spatial coefficients, and highest negative values were associated with a

coastal fringe area, between the Guadiana and Guadalquivir rivers mouths. Positive EOF2 spatial coefficients were restricted to the continental shelf and slope waters of the west and south-west Portuguese coasts, extending further offshore (ca. 2500 m isobath) off the west coast, and following the shelf-edge region from CSM eastwards, up to Strait of Gibraltar and Cape Trafalgar (Fig. 4.5C). EOF2 temporal coefficients showed a recurrent harmonic seasonal cycle, with winter minima and summer maxima (Fig. 4.5D), confirmed by GAMM analyses which revealed significant intra-annual patterns and no interannual trends (Fig. C.3C-D; Table C.1). GAMM models, based on a set of five predictors (PAR, SST, V, WeMO-1 and NAO-1), explained 56% of the variance in EOF2 temporal coefficients (Fig. C.4B; Table C.2). Interestingly, V showed significant positive partial effects for increasing northerly winds, indicative of upwelling off the west coast. In respect to EOF1, EOF2 captured additional Chl-a increases over the west and south-west Portuguese coasts during summer, under increased upwelling generated by northerly winds (Fig. 4.3A).

The third EOF mode (EOF3), explained 6% of Chl-a variability, and its spatial component differentiated three regions: (i) a southern open oceanic area, with very low spatial coefficients (<|0.5|; see green area in Fig. 4.5E); (ii) a region within the GoC basin, with negative coefficients; and (iii) the oceanic area north of 37^{o}N, and two coastal areas north and south off the Strait of Gibraltar, with positive coefficients (Fig. 4.5E). EOF3 temporal coefficients exhibited a complex variability over the study period (Fig. 4.5F), showing both significant intra-annual and interannual patterns (Figs. 4.5F, C.3C; Table C.1). Seasonal bi-modal patterns exhibited peaks during late-spring and autumn, and interannnual patterns showed predominantly positive values between ca. 2003 and 2009, associated to relative increases in Chl-a over areas with positive spatial coefficients, and mostly negative values for previous and subsequent periods, associated to relative Chl-a increases over most of the GoC basin. Best GAMM model, based on a set of seven predictors (V, NAO, EA, MLD, Gdq, U, AMO), explained 20% of the variance in EOF3 temporal coefficients, with V as the most relevant (Fig. C.4C; Table C.2).

4.3.4 Region-specific phytoplankton temporal variability patterns

Phytoplankton variability patterns were specifically investigated in selected regions within the study area, with similar Chl-a variability patterns. Based on spatial components of dominant

variability modes (Fig. 4.5A, 4.5C and 4.5E), geographical location and bathymetry, nine spatially-coherent regions were delineated, excluding pixels associated with transitional areas (Fig. 4.6). GAMM analysis, used to decompose temporal variability in region-specific abiotic variables, revealed significant seasonal patterns for SST, PAR, MLD, WIN, V and U over the nine SWIP regions ($p<0.001$, see selected examples in Fig. C.5, Table C.3). Highly significant ($p<0.01$) interannual patterns included a non-linear increase in WIN over all regions (except Off, see selected examples in Fig. C.5, Table C.3), stronger during 1997-2002, and a linear increase in MLD for all regions (except Off and NOff, see selected examples in Fig. C.5, Table C.3). A weakly significant increase in V was also detected over WSlp and WC regions (GAMM, $p<0.05$, data not shown).

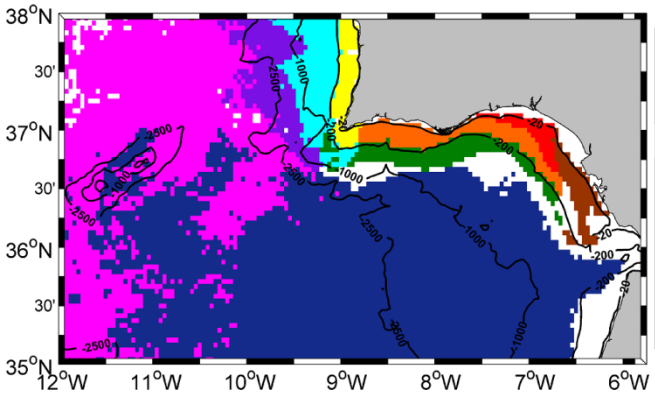

ID	Region	EOF1	EOF2	EOF3	Z(m)	Coord
	Off	+	-	+	------	>9ºW
	NOff	+	+	+	------	>9ºW
	GoC	+	-	-	------	<37ºN
	WSlp	-	+	+	>200	>8ºW
	WC	-	+	+	<200	>8ºW
	SSlp	-	+	-	>200	<37.2ºN 6.5ºW<x<9.5ºW
	SC	-	+	-	<200	<37.2ºN 6.5ºW<x<9.5ºW
	Gdn	-	-	-	<200	>36ºN
	Gdq	-	-	+	------	>36ºN

Figure 4.6 - Regions with coherent, co-varying chlorophyll-a variability patterns off SW Iberia (period: 1997-2012), established using the signal (positive (+) or negative (-)) of the spatial coefficient of dominant modes of Chl-a variability (EOF1, EOF2, EOF3), geographical limits (in degrees) and bathymetry (in meters): Offshore (Off), North offshore (NOff), Gulf of Cadiz (GoC), West slope (WSlp), South slope (SSlp), West coast (WC), South Coast (SC), Guadiana (Gdn), and Guadalquivir (Gdq). Black lines depict the 20m, 200m, 1000m and 2500m isobaths.

Region-specific Chl-a mean values over the 15-year period ranged between 0.18±0.11 µg L^{-1} and 1.47±1.09 µg L^{-1} for GoC and Gdn regions, respectively. Region-specific Chl-a intra-annual variability patterns, and Chl-a time series for the 15-year period are depicted in Fig. 4.7 and Fig. 4.8, respectively. In general, oceanic regions (Off, NOff and GoC) showed uni-modal annual cycles, with late-winter (March) maxima (Fig. 4.7A) and Chl-a increasing trends during the MLD deepening period (see selected examples in Fig. C.5, Table C.3). Slope regions (WSlp, SSlp) displayed additional summer increases (Fig. 4.7B-4.7C), and coastal regions under upwelling influence (WC, SC) exhibited bi-modal annual cycles, with late-winter and summer maxima (Fig. 4.7B-4.7C); at WC, more intensively affected by

upwelling, summer Chl-a maxima surpassed late-winter maxima. Conversely, coastal regions closer to river mouths (Gdn, Gdq) showed higher Chl-a, and a uni-modal annual cycle, with maxima during February and April for Gdn and Gdq, respectively (Fig. 4.7D). Indeed, GAMM analyses revealed a highly significant seasonal Chl-a variability pattern ($p<0.001$) for all SWIP regions (Fig. C.6, Table C.4). Moreover, significant Chl-a interannual trends were also detected for SWIP regions south of 37°N, with exception of SSlp: linear increasing trends for oceanic GoC region ($p<0.01$), and linear (Gdq, $p<0.05$) and non-linear (Gdn and SC, $p<0.05$) declining trends for coastal regions, stronger between 1997 and ca. 2006 for the later regions (Fig. C.6, Table C.4).

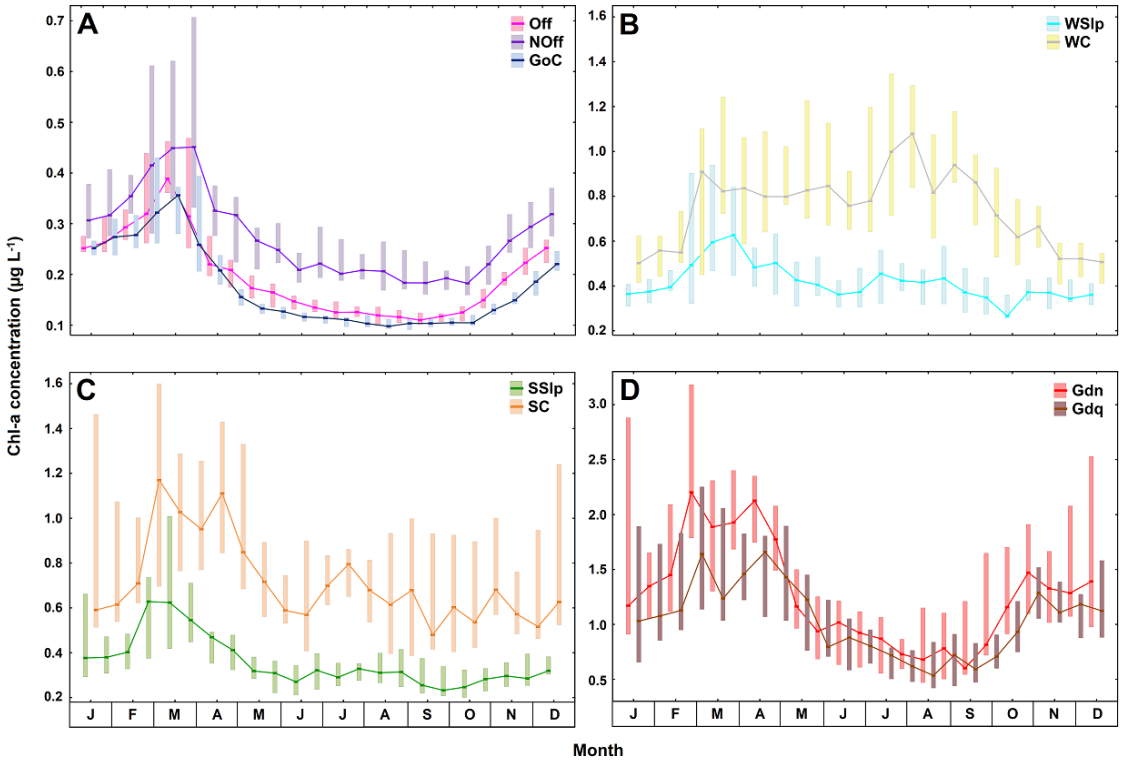

Figure 4.7 – Intra-annual variability of surface chlorophyll-a concentration during 1997-2012 for specific regions off SW Iberia, with co-varying variability patterns. Regions were grouped according to location as (A) open ocean; slope and coastal regions (B) north and (C-D) south of 37°N (see Fig. 4.6 for region location and abbreviations). Median values are represented by the lines within the boxes, and 25th to 75th percentiles are denoted by box edges.

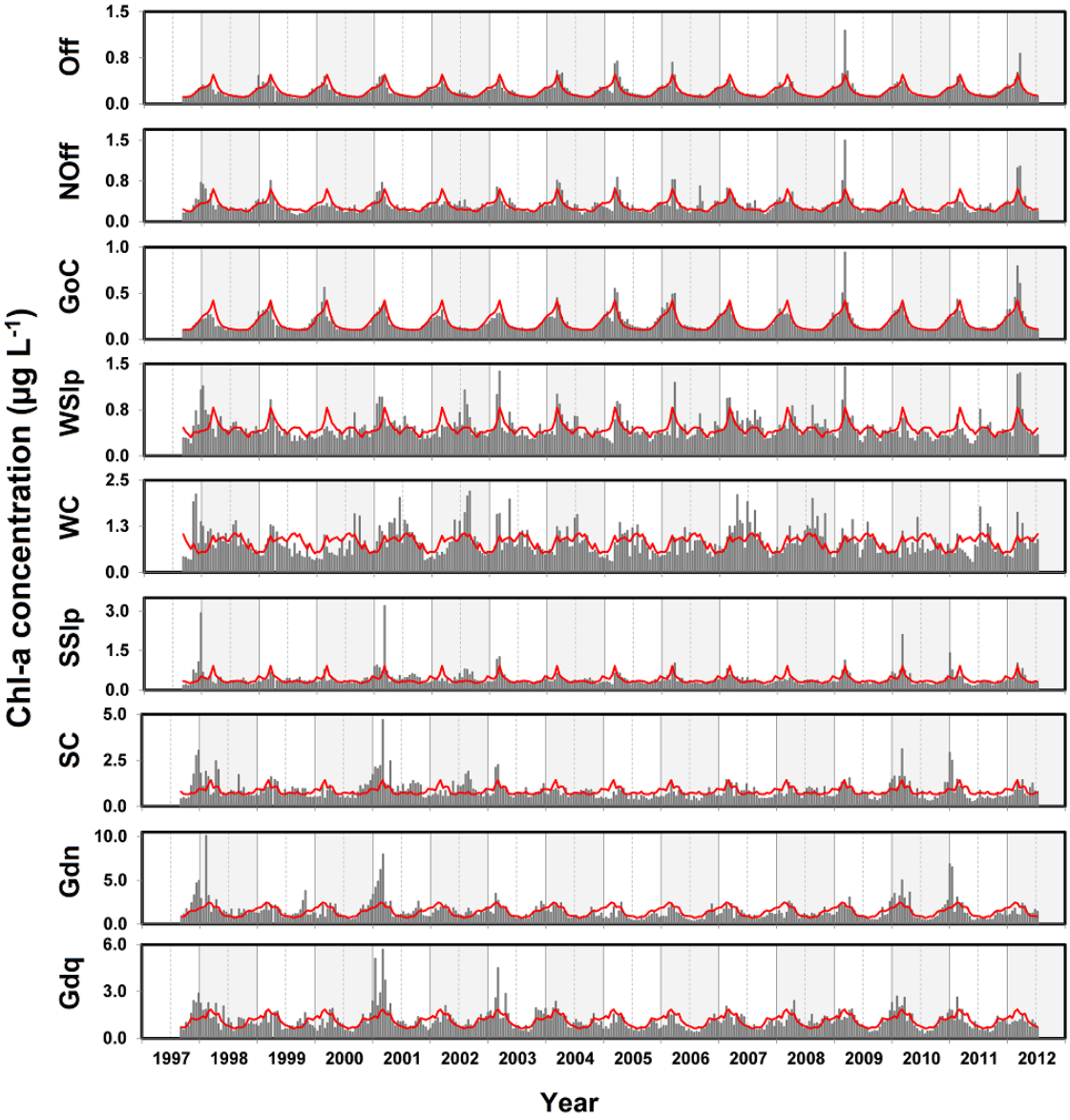

Figure 4.8 - Temporal variability of mean surface chlorophyll-a concentration (Chl-a) for specific regions off SW Iberia, with co-varying variability patterns (gray columns), and associated fortnightly-based climatologies (red lines), during the period 1997 to 2012 (See Fig. 4.6 for region location and abbreviations).

Chl-a time series for oceanic regions (Off, NOff, GoC) were less variable, showing smaller departures with respect to the annual mean values, comparing with the slope and coastal regions (Fig. 4.8). Positive Chl-a anomalies were detected, in all oceanic regions, during late-winter periods of 2005, 2006, 2009 and 2012, mostly coincident with extreme positive anomalies in both MLD and subsurface NO_3 concentration (data not shown). Positive Chl-a anomalies in WC, the coastal region under major upwelling influence, mostly occurred during

summer periods (2001, 2002, 2007), usually coinciding with strongly-favourable upwelling conditions (Fig. 4.3A) and negative SST anomalies (data not shown). Conversely, coastal areas under minor upwelling and stronger riverine influence (SC, Gdq, Gdn) commonly presented Chl-a positive anomalies between late-autumn and winter periods of 1998, 2001, 2003, 2010 and 2011, coincident with high Guadiana and Guadalquivir river discharges and negative NAO phases (Figs. 4.3C-D, C.2B). Summer positive anomalies were also observed in SC during summer 2002 and 2008, coinciding with strongly-favourable upwelling conditions (Figs. 4.3B) and negative SST anomalies (data not shown).

4.3.5 Region-specific phytoplankton environmental drivers

GAMM analysis was used to explore region-specific linkages between environmental variables and Chl-a variability. Since correlations ($|r_S|$) between SST, MLD and NO_3 were systematically >0.7, these variables were not used simultaneously as predictors for any model run. SST-based models showed the highest explanatory power (data not shown), for all SWIP regions, and were therefore selected as best-performing models. In general, the explanatory power of SST-based region-specific models, represented as percentage of Chl-a variance explained; Table 4.1), was higher for open ocean regions (Off, NOff, GoC; 55-82%) and riverine-influenced coastal domains (Gdq, Gdn; 61-70%), and lower for the remaining coastal and slope regions (WSlp, WC, SSlp, SC; 32-55%). In addition to SST, other abiotic variables (PAR, WIN, U, V and Gdn and Gdq river discharges) and climate indices (AMO, EA, MEI, NAO and WeMO) were significant predictors of region-specific Chl-a. However, the significance and partial effects of each predictor varied across SWIP regions (Table 4.1). Partial effects of individual environmental covariates (predictors) on region-specific Chl-a anomaly, derived from the best performing (SST-based) models, are shown in Figs. 4.9-4.11, and model statistics data are detailed in Table C.5.

Table 4.1 – Summary of best performing generalized additive mixed models (GAMMs) used to predict surface chlorophyll-a concentration (Chl-a) for specific regions off SW Iberia (SWIP), during the period 1997-2012, with indication of model explanatory power (MEP, as % Chl-a variance explained) and environmental predictors, shown in descending order of relevance. Symbols *, **, *** indicate p-value <0.05, <0.01 and <0.001, respectively. See Fig. 4.6 for region abbreviations and location, Figs. 4.2, 4.3 and C.2 for predictor abbreviations, Figs. 4.9-4.11 for partial effects of individual predictors and Table C.5 for detailed statistics.

Region	MEP	Predictors
Off	76%	SST***, PAR***, AMO-1**, U*
NOff	55%	SST***, PAR***, AMO**, U*, EA*, MEI*
GoC	82%	SST***,PAR***, U**, NAO**
WSlp	32%	SST***, PAR***, EA**, AMO*, V*
WC	33%	PAR***, V***, SST***, EA*, MEI-1*
SSlp	55%	SST***, Gdq***, PAR***, MEI-1***, AMO**, NAO*, Gdn*, WIN*
SC	51%	SST***, Gdq***, NAO-1**, PAR**, EA-1*, MEI-1*,U$^{'}$
Gdn	70%	SST***, Gdq***, U**, WeMO**, EA-1**, AMO-1**, NAO-1**, PAR**
Gdq	61%	SST***, U***, Gdq***, WIN***, V**, WeMO*

In oceanic regions (Off, NOff, GoC; Fig. 4.9; Tables 4.1 and C.5), SST was the predictor with the highest partial effect over Chl-a, showing negative linear or non-linear influences, with positive Chl-a anomalies for SST below ca. 18 ^{o}C. Partial effects of PAR, the second most influential covariate, were non-linear, with a positive influence for PAR below ca. 40-45 mol phot m^{-2} day^{-1} and a negative influence for higher PAR values. Zonal easterly winds (U < 0 m s^{-1}) showed partial positive effects in Chl-a for all oceanic regions, while different climate indices were associated to distinct oceanic regions. High positive and negative NAO values (|NAO|> 2) were associated to Chl-a positive anomalies in GoC; negative (one-month lagged) AMO values (AMO-1 < 0) were associated to Chl-a positive anomalies for Off; and both AMO below 0.2, and positive EA and MEI values were associated to positive Chl-a anomalies in NOff region.

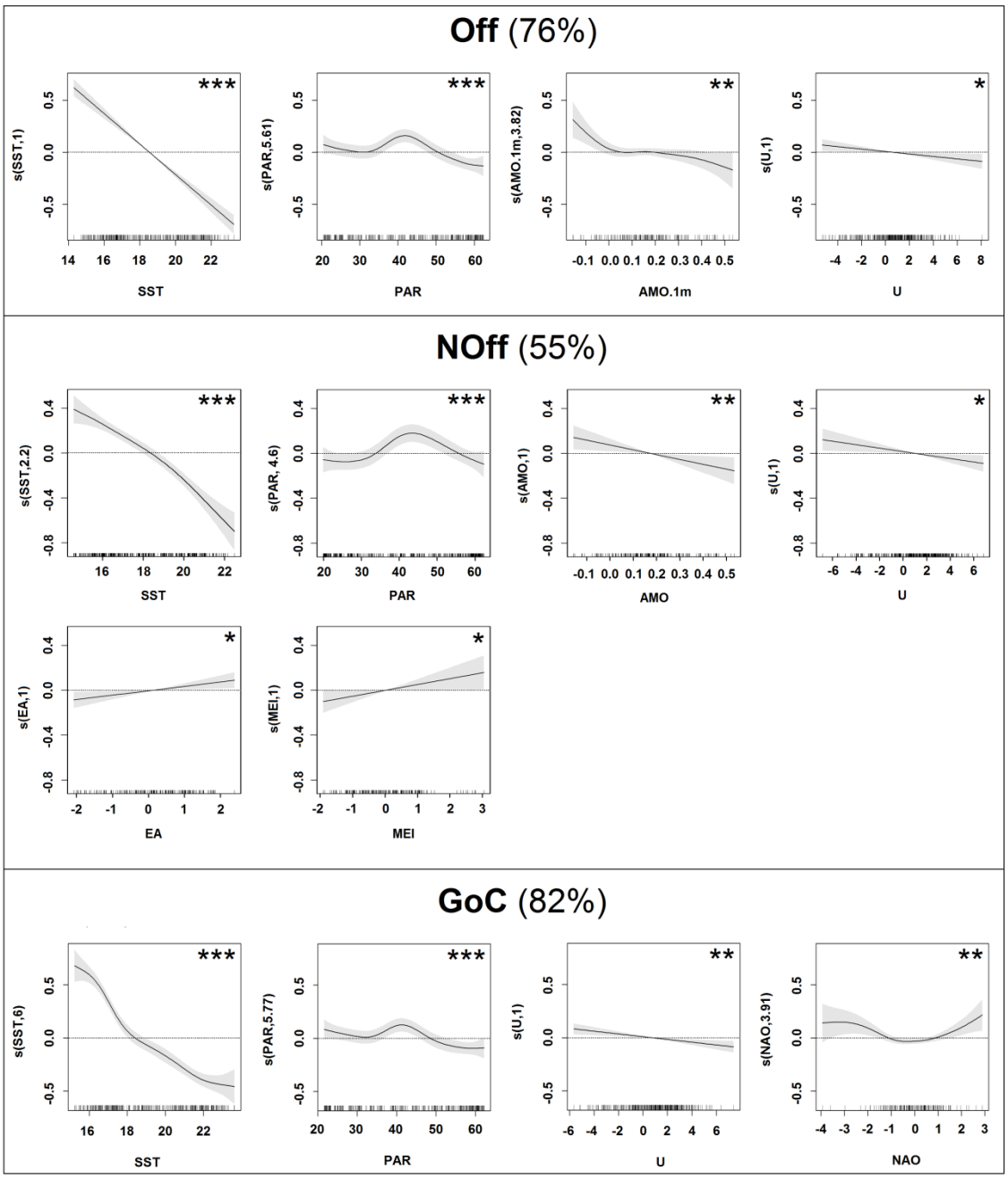

Figure 4.9 – Partial effects of individual environmental predictors on chlorophyll-a concentration (Chl-a), for SWIP oceanic regions (Off, NOff and GoC), derived from the best performing generalized additive mixed model (GAMM). For each region (model), the model explanatory power (as % of Chl-a variance explained) is shown in brackets (top center, after region abbreviation); individual predictor plots are organized in descending order of their explanatory power, and the significance level (p-value) of each predictor is denoted by asterisk symbols (top right), where *, **, *** indicate p-value <0.05, <0.01 and <0.001, respectively. For each plot, predictor values are represented on the x-axis, where short vertical lines indicate the exact predictor observations. Values on the y-axis represent the partial effects that the specific predictor has on Chl-a anomaly, holding the remaining predictor constant. On y-axis, numbers in parentheses represent the effective degrees of freedom (edf), indicative of the smoothness of each function. Values of edf equal to 1 represent a linear effect of the predictor on Chl-a anomaly, and values higher than 1 indicate progressively stronger non-linear effects.

Solid lines indicate the smoothed non-parametric trends, and gray shaded areas designate the point-wise 95% confidence intervals. Regions where the 95% CI bands enclose the x-axis line indicate no significant effects of the predictor. At each stage, the value of Chl-a is given by the sum of the partial effects of all predictors plus a constant. (See Fig. 4.6 for region location and abbreviations, Figs. 4.2, 4.3 and C.2 for predictor abbreviations and Table C.5 for detailed statistics).

Over slope and coastal regions north of 37^{o}N (WSlp and WC; Fig. 4.10, Tables 4.1 and C.5), SST and PAR were also significant non-linear predictors of Chl-a. SST showed a partial negative influence over ca. 19 ^{o}C, and PAR showed a positive influence below ca. 50 mol phot m^{-2} day^{-1}. In contrast to oceanic regions, meridional northerly, upwelling favourable, winds ($V < 0$ m s^{-1}) showed partial positive effects in Chl-a for both WSlp and WC, more significant over the latter. Over the WC region, positive effects of meridional winds on Chl-a were clearly intensified under strong northerly winds ($V < -5$ m s^{-1}), and non-significant for weaker northerly or southerly winds. As referred for NOff, positive EA values were associated to positive Chl-a anomalies in both WSlp and WC. Moreover, (one-month lagged) MEI and AMO were less relevant linear predictors of Chl-a ($p<0.05$), with positive Chl-a anomalies for positive MEI-1 values in WSlp and negative AMO values in WC.

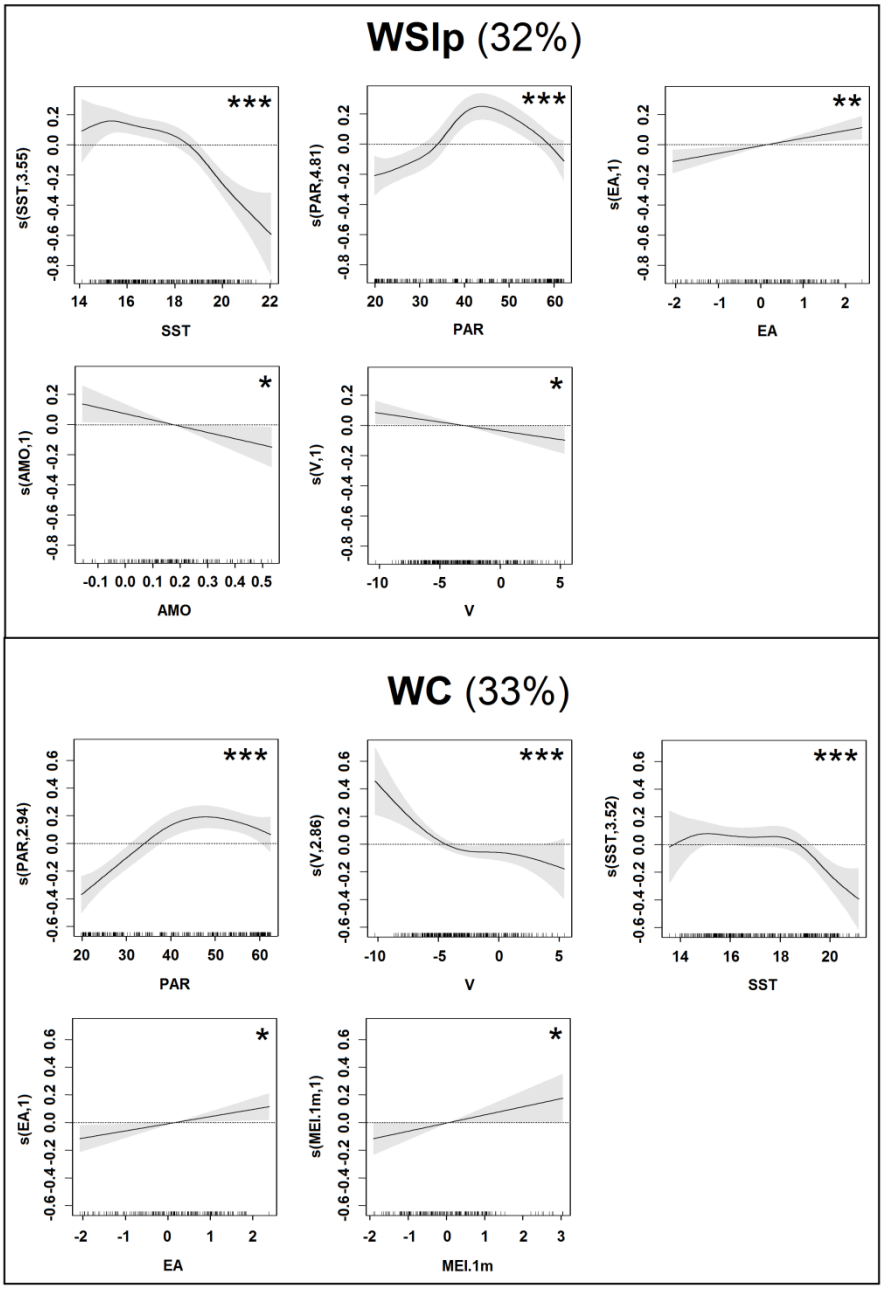

Figure 4.10 – Same as Fig. 4.9 for slope and coastal regions north of 37°N (WSlp and WC).

GAMM models for coastal and slope regions south of 37°N (SSlp, SC, Gdn and Gdq; Fig. 4.11, Tables 4.1 and C.5) were more complex, including six to eight predictors. SST was the most relevant predictor, showing mostly non-linear negative effects on Chl-a, stronger for SST > 19-20 °C. Guadalquivir river discharge appeared as a highly influential covariate for all regions, showing positive non-linear effects on Chl-a, stronger for river discharge below ca. 800-1000 m^3 s^{-1}. The significance and partial effects of WIN and its components U and V

varied across regions. U was a relevant Chl-a predictor for all coastal regions south of 37^{o}N (SC, Gdn, Gdq). In contrast to SWIP oceanic regions (promoted by easterly winds), positive Chl-a anomalies were associated to westerly winds (U > 0 m s^{-1}), probably related to favourable upwelling conditions over SC and Gdn regions. As also referred for the (meridional oriented) WC, meridional northerly winds (V < 0 m s^{-1}) showed a positive influence over Chl-a in Gdq region, likely related to upwelling favourable conditions as well. For the latter region, WIN was also a highly influential Chl-a predictor, showing linear positive effects (Fig. 4.11, Tables 4.1 and C.5).

The significance and partial effects of climate indices (non-lagged or one-month lagged) varied across regions. WeMO index was a significant Chl-a predictor only for GoC northeastern coastal regions, under strong riverine influence (Gdn, Gdq), showing linear positive influences on Chl-a anomalies (Fig. 4.11). NAO was a significant Chl-a predictor for all regions south of 37^{o}N, except Gdq, but its relevance and partial effects ranged across regions. Extreme (positive and negative) NAO values showed positive effects over GoC (Fig. 4.9), whereas NAO negative values were associated to positive Chl-a anomalies for SC and Gdn regions (Fig. 4.11). AMO was an influential predictor for Gdn, slope regions (WSlp, SSlp) and most ocean regions (except GoC). AMO consistently showed negative influences, linear (NOff, WSlp, SSlp) or non-linear (Off, Gdn), with higher positive Chl-a anomalies consistently associated to minimum (negative) AMO values (Figs. 4.9-4.11). EA and MEI were significant Chl-a predictors mostly for coastal and slope regions, showing no influence over open ocean areas (Off, GoC). Both EA and MEI significant partial effects were consistently linear and positive, with maximum EA values (NOff, WSlp, WC, SC, Gdn) and MEI (NOff, WC, SSlp, SC) values associated to higher positive Chl-a anomalies (Figs. 4.9-4.11).

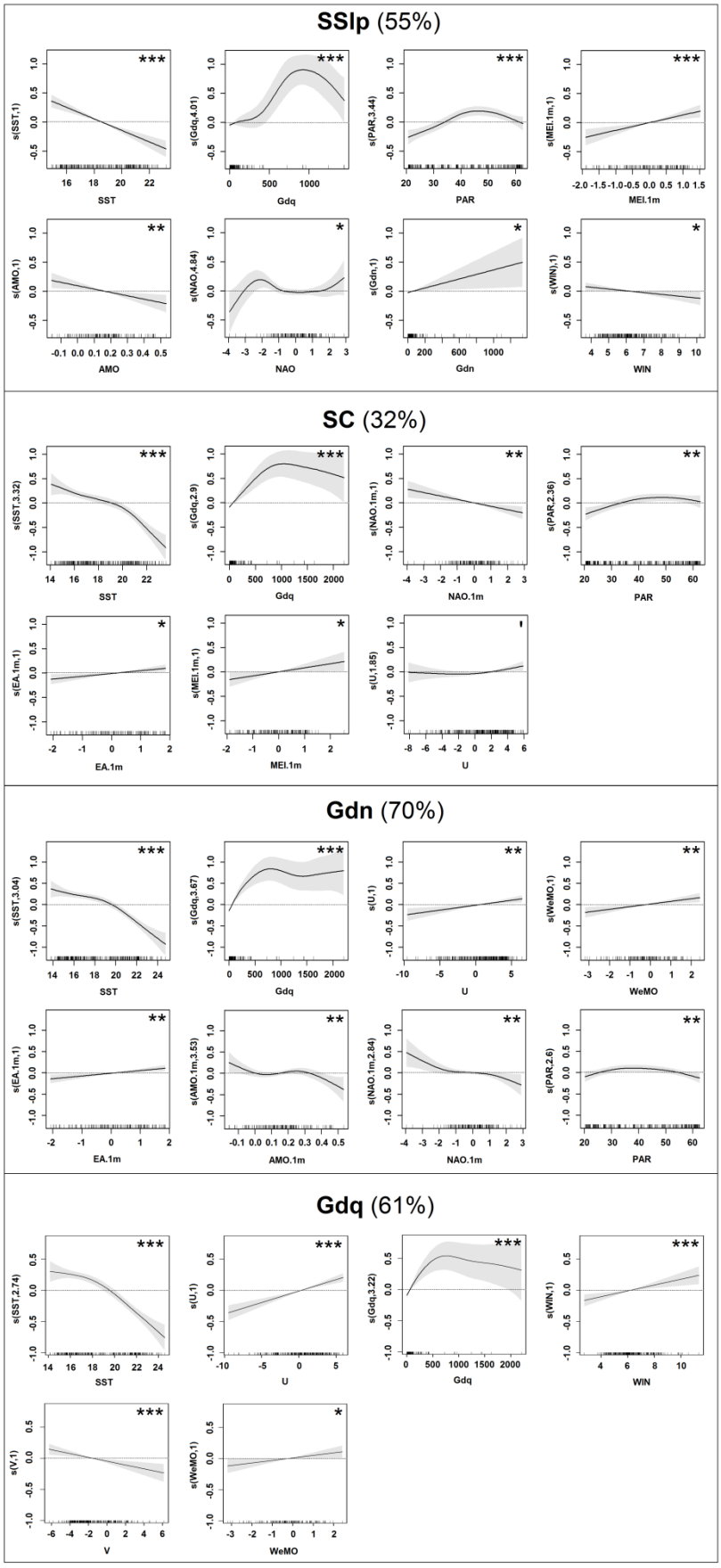
SSlp (55%)
s(SST,1)
SST
s(Gdq,4.01)
Gdq
s(PAR,3.44)
PAR
s(MEI.1m,1)
MEI.1m
s(AMO,1)
AMO
s(NAO,4.84)
NAO
s(Gdn,1)
Gdn
s(WIN),1)
WIN
SC (32%)
s(SST,3.32)
SST
s(Gdq,2.9)
Gdq
s(NAO.1m,1)
NAO.1m
s(PAR,2.36)
PAR
s(EA.1m,1)
EA.1m
s(MEI.1m,1)
MEI.1m
s(U,1.85)
U
Gdn (70%)
s(SST,3.04)
SST
s(Gdq,3.67)
Gdq
s(U,1)
U
s(WeMO,1)
WeMO
s(EA.1m,1)
EA.1m
s(AMO.1m,3.53)
AMO.1m
s(NAO.1m,2.84)
NAO.1m
s(PAR,2.6)
PAR
Gdq (61%)
s(SST,2.74)
SST
s(U,1)
U
s(Gdq,3.22)
Gdq
s(WIN,1)
WIN
s(V,1)
V
s(WeMO,1)
WeMO

Figure 4.11 – Same as Fig. 4.9 for slope and coastal regions below 37°N (SSlp, SC, Gdn and Gdq).

4.4 - Discussion

EOF analysis was used as a tool to compress the spatial-temporal phytoplankton variability over the highly heterogeneous SWIP area, during a 15-year period, and to regionalize the study area. Phytoplankton variability patterns were reduced to three significant variability modes (EOF1, EOF2 and EOF3; Fig. 4.5), which overall explained 47% of Ch-a variability and differentiated large-scale coherent regions within the study area. The spatial and temporal components of EOF1 and EOF2 showed similarities to dominant EOF modes previously reported for domains of the study area (Muñoz et al., 2015; Navarro and Ruiz, 2006; Picado et al., 2014; Reboreda et al., 2014a). EOF1 captured a strong coastal-oceanic difference in phytoplankton concentration (Chl-a) and variability patterns, most probably a response of phytoplankton to increased nutrient concentration over coastal areas (Fig. 4.2I), due to natural (e.g., upwelling, riverine inputs) and anthropogenic influences (e.g., Cardeira et al., 2013; Navarro et al., 2006). The strong positive influences of MLD, U and Gdq on EOF1 temporal variability possibly reflect the role of water column mixing and freshwater discharges as nutrient sources and drivers of phytoplankton seasonality (Navarro et al., 2012; Reboreda et al., 2014a; Picado et al., 2015). EOF2 captured the influence of meridional northerly winds and coastal upwelling, enhanced during summer mostly over the western Portuguese coast, but extending along the northern GoC slope region, an advection-based process previously reported for the area (Relvas et al., 2007). EOF3 spatial function captured an oceanic latitudinal distinction (north and south of ca. 37°N) and additional contrasts between meridionally and zonally-oriented coastal areas.

EOF3 was the only mode showing a significant (non-linear) interannual pattern, with a predominantly positive phase between 2003 and 2009, a period of higher wind intensity over all SWIP regions (Fig. C.3, C.5). The highly positive influence of northerly meridional winds on EOF3 temporal coefficients possibly reflects a contribution of upwelling-enhanced Chl-a over meridionally-oriented coastal areas. However, EOF3 positive periods were more frequent during spring and autumn (not summer, as for EOF2). Indeed, although more intense and regular during summer, upwelling events were observed during other seasons (see Fig.

4.3A) and already reported for NW Iberia (see Alvarez et al., 2008; Goela et al., 2016; Picado et al., 2014, 2015; Reboreda et al., 2014a). In some years, upwelling effects can amplify spring phytoplankton blooms. Winter upwelling events are apparently less efficient due to a lower nutrient content of upwelled waters (subtropical Eastern North Atlantic Central Water; Picado et al., 2015), and/or a lower light availability and higher surface nutrient concentration typical of the season.

EOF dominant modes were used to delineate nine specific regions within SWIP area, and GAMM analysis were used to (i) decompose region-specific Chl-a time-series into seasonal and interannual components, and (ii) to explore underlying region-specific environmental drivers (predictors). In general, the explanatory power of models was higher for open ocean and coastal regions under increased riverine influence (61-82%) than for slope and coastal regions strongly impacted by upwelling (32-55%). The higher complexity of coastal in respect to ocean regions has been previously reported for the study area (Cristina et al., 2016a) and other ecosystems (e.g., NW Iberia, Bode et al., 2011), probably reflecting the complexity of phytoplankton patterns and drivers at the land-sea interface (see review Cloern and Jassby, 2008, 2010; Cloern et al., 2016). The inclusion of additional phytoplankton drivers, namely phytoplankton top-down controls (e.g., grazing, viral lyses, apoptosis), not available for the study area and period, would probably enhance the prediction of phytoplankton over the SWIP area (e.g., Behrenfeld, 2014; Martinez et al., 2016). Overall, the main predictors of region-specific Chl-a included climate-susceptible environmental variables under strong atmospheric forcing (SST, PAR, zonal and meridional wind and river discharge). Additionally, significant effects of different climate indices on Chl-a were detected over all regions, capturing residual effects not included in the local variables. However, linkages between Chl-a and environmental variables varied across regions, therefore requiring a region-oriented exploration, at both intra-annual (seasonal) and interannual time scales.

4.4.1 Phytoplankton seasonal variability patterns and underlying environmental drivers

Phytoplankton in all SWIP regions presented a significant seasonal pattern, showing a marked increase during late winter-early spring period (Fig. 4.7). SWIP oceanic regions (Off, NOff, GoC) presented low Chl-a values, consistent with the oligotrophic nature of the eastern North Atlantic Subtropical Gyre province (Longhurst, 2007; Teira et al., 2005), and a unimodal

annual cycle with a late-winter bloom. Contrary to spring blooms, classically driven by increased PAR availability during the MLD shoaling period (critical depth hypothesis; Sverdrup, 1953), these oceanic blooms consistently developed during the MLD deepening period, starting usually around October, increasing steadily until March (Fig. 4.7A). This pattern probably reflects a stringent phytoplankton nutrient limitation, alleviated by the input of new nutrients provided by increased vertical mixing, and was also reported for our study area (Navarro and Ruiz, 2006; Navarro et al., 2012), further north (up to ca. 40^{o}N; Reboreda et al., 2014a), eastern Atlantic (Azores region; Amorim et al., 2017) and for other subtropical regions (Follows and Dutkiewicz, 2002; D'Ortenzio et al., 2012; Martinez et al., 2011). SST was the main predictor of Chl-a over ocean regions, but its negative influence probably reflected an indirect effect of concurrent changes in MLD, and the critical role of seasonal vertical mixing as a nutrient source. In addition to seasonal stratification-destratification cycles, other sources of inorganic nutrients for phytoplankton include biological remineralization processes, episodic storm effects (e.g., Painter et al., 2016) and Saharan dust intrusions (Cusack et al., 2012), not evaluated in this study. Interestingly, as also pointed out by Navarro et al. (2012), late-winter, early-spring blooms also support the recent disturbance-recovery hypothesis, which predicts a net increase in Chl-a during the MLD deepening period, due to a decline in phytoplankton grazing pressure induced by phytoplankton dilution (Behrenfeld, 2010; Behrenfeld and Boss, 2014). A secondary autumn bloom, common for some temperate oceanic regions (Bode et al., 2011; D'Ortenzio et al., 2012; Martinez et al., 2011), was not observed in the SWIP oceanic regions.

Over oceanic and slope regions, cross-shore processes, mostly associated with filaments originating in coastal upwelling regions, are relevant sources of nutrients (Cravo et al., 2010; Lévy, 2008; Nagai et al., 2015). The formation of filaments over SWIP (up to 400 km; Peliz et al., 2004) is associated with topographic features (e.g., CSV) and occurs mainly during the peak of the upwelling season (July-September), when up to six filaments can be developed in a single season (Haynes et al., 1993). Indeed, over NOff region, located beyond the 1000 m isobath (~70 km from the coast), occasional positive Chl-a anomalies were detected during summer (e.g., 2002, 2006; Fig. 4.8), probably reflecting the offshore advection associated with Chl-rich mesoscale filaments (Haynes et al., 1993; Peliz et al., 2004; Rossi et al., 2013; Sánchez et al., 2008; Souza and Bricaud, 1992).

The slope region over the western coast (WSlp) presented an intermediate Chl-a seasonal pattern in comparison with the adjacent oceanic region (NOff) and its coastal counterpart (WC). For WSlp and WC regions, a secondary Chl-a maximum occurred during summer, the upwelling favourable period, being even stronger than the winter bloom at WC (Fig. 4.7). The occurrence of upwelling-driven phytoplankton maxima during summer has been previously reported for the western coast of Iberia (e.g., Bode et al., 2011, 2015; Loureiro et al., 2011; Moita, 2001; Peliz and Fiúza, 1999; Picado et al., 2014; Reboreda et al., 2014a; Silva et al., 2009) and other upwelling coastal areas (e.g., Carr and Kearns, 2003). In contrast to the more nutrient-limited oceanic regions, PAR and V (not SST) were the most relevant environmental predictors of Chl-a over WC, suggesting that light could represent a more limiting resource for phytoplankton over this nutrient richer, upwelling-affected region. As expected due to coastline orientation, meridional northerly winds ($V < 0$ m s^{-1}) showed highly significant effects on Chl-a over WC and WSlp regions (Fig. 4.10). It was noteworthy that both WSlp and WC regions contour CSV, incorporating the westernmost-sector areas of the south Portuguese coast. This fact reinforces the effects of frequent anticlockwise advection of west-coast upwelled waters, driven by northerly winds around CSV, affecting the north-western sector of GoC, mostly the SSlp region. These eastward advected water masses can be retained within the SC and SSlp regions, into a cyclonic eddy delimited by the CSM or, depending on wind regime, may flow eastwards joining the Huelva front (east of CSM, see Criado-Aldeanueva et al., 2009; García-Lafuente et al., 2006; Sánchez and Relvas, 2003).

SSlp and SC regions also presented a secondary Chl-a maximum during summer but, in contrast to WC region, this was commonly lower than late-winter, early-spring bloom. Summer Chl-a maxima are usually associated to local upwelling driven by westerly winds (e.g., Cristina et al., 2016b; Goela et al., 2014, 2015; Loureiro et al., 2011; Moita, 2001; Navarro and Ruiz, 2006), significantly lower in comparison with the West coast. According to GAMM analysis, the effects on Chl-a associated with zonal westerly winds were less beneficial than those associated with the Gdq (SSlp, SC) and Gdn (SSlp) river discharges, which were higher during the autumn-winter period. Due to the physical proximity of the eastern domains of SSlp and SC regions and the areas directly affected by riverine plumes (Caballero et al., 2014), depending on circulation patterns and wind regimes, riverine effects may be spatially extended to adjacent coastal areas (Relvas and Barton, 2002), hence affecting SSlp and SC Chl-a values. In addition to water column convective mixing and riverine fluxes,

other nutrient sources supporting the relatively high late-winter Chl-a maxima over SC, in respect to WC region, probably include the large number of low-flow streams, lagoons and small estuaries in this region and the indirect effects of local submarine groundwater discharges (SGD; Hugman et al., 2015) and atmospheric wet deposition (Thompson et al., 2015; Zou et al., 2000). These processes have been reported as phytoplankton drivers in coastal systems (Lecher et al., 2015; Thompson et al., 2015), and positive effects of SGD on coastal benthic communities over the SC region have been reported (Encarnação et al., 2013; Leitão et al., 2015). Moreover, other sources of inorganic nutrients for phytoplankton in coastal and slope regions include oscillations of internal waves associated with south-coast submarine canyons (Bruno et al., 2006), a process referred for the Nazaré canyon (west coast of Iberia; Muacho et al., 2013), and episodic storm effects (e.g., Painter et al., 2016).

As expected, Gdq river discharge was an influential predictor of Chl-a over Gdn and Gdq regions, where the highest mean Chl-a values were detected. Chl-a seasonal patterns over these regions presented a unimodal annual cycle, with a winter maximum, concomitant with maximum riverine discharges, as reported by others for the study area (Caballero et al., 2014; Navarro and Ruiz, 2006; Prieto et al., 2009) and NW Iberia (Peliz and Fiúza, 1999; Picado et al., 2014). Indeed, these satellite-derived Chl-a values could represent an overestimate, common for turbid and Coloured Dissolved Organic Matter (CDOM)-rich Case-II water masses (e.g., Caballero et al., 2014; IOCCG, 2000; Picado et al., 2014), and the overestimate may be aggravated during high-discharge periods. Nonetheless, studies based on *in situ* sampling also reported the stimulatory influence of river discharges (Gdq, Gdn) on phytoplankton blooms over northeastern GoC (Prieto et al., 2009; Huertas et al., 2006). Mechanisms underlying positive effects of Gdq and Gdn river discharges on phytoplankton include its relevance as a nutrient source (Cravo et al., 2006; Reul et al., 2006), increased due to restricted water circulation in the northeastern GoC (Prieto et al., 2009), but also its role as a buoyancy source. In fact, despite high turbidity associated with riverine plumes (Caballero et al., 2014), mean light intensity in the mixed layer could increase due to haline stratification and shallowing of the MLD (Barbosa and Chícharo, 2011). Although less intense and temporally more restricted than for other coastal regions, the positive effects of zonal westerly winds (Gdn region) and meridional northerly winds (Gdq region) on Chl-a indicate that coastal upwelling may also affect the riverine-impacted GoC coastal areas, even influencing associated lower estuarine regions (e.g., Chícharo et al., 2006). Over Gdq region, WIN also

showed a positive linear effect on Chl-a, probably indicating effect of increased turbulence due to tide-topography interactions in the vicinity of the Strait of Gibraltar (Bruno et al., 2013; Ramirez-Romero et al., 2012; Vargas et al., 2003). Mesoscale eddies driven by gap winds (Peliz et al., 2009) and internal waves (Vázquez et al., 2009) were identified as main fertilizing mechanisms for primary production in the area (García-Lafuente and Ruiz, 2007; Navarro and Ruiz, 2006), under stronger wind speeds.

4.4.2 Phytoplankton interannual variability patterns and linkages to climate variability

The analyses of phytoplankton variability patterns and concurrent local environmental variables and large-scale climate indices, during this 15-year period, revealed across-region differences in phytoplankton drivers and climate linkages, also at the interannual time-scale. Yet, the use of long-term trends in Chl-a as a proxy for interannual variability in phytoplankton biomass should be approached cautiously, since concurrent physiological changes and photoacclimation may affect carbon to chlorophyll ratio (Behrenfeld et al., 2016; Boyd et al., 2016; Geider et al., 1987).

Abiotic (climate-sensitive) variables, which emerged as relevant phytoplankton drivers over the heterogenous SWIP area, showed significant interannual patterns. Despite several reports of significant warming trends over coastal and oceanic domains off Iberia and adjacent NE Atlantic (Belkin, 2009; Goela et al., 2016; Lima and Wethey, 2012; Nicastro et al., 2013; Santos et al., 2011a), no significant warming trends were detected using our 15-year time series. Several significant Chl-a predictors showed similar interannual patterns over a large number of SWIP regions; notably, highly significant ($p<0.01$) non-linear increases in WIN were detected over all regions (except Off), and linear increases in MLD were detected over GoC and all coastal and slope regions (Fig. C.5). To the best of our knowledge, these trends were not reported previously for the study area. Significant interannual patterns were also detected in river discharge (Gdq), with a low discharge period during 2005-2009, inversely correlated with NAO, as previously reported for the region (Hurrell and Dickson, 2004), and directly correlated with WeMO, a reflex of increased precipitation over western Mediterranean (Martin-Vide and Lopez-Bustins, 2006). In the case of upwelling, our results showed a weakly significant linear increase with time in the northerly meridional wind and upwelling intensity over the west coast, which has been shown to be positively correlated

with NAO for NW Iberia (Cropper et al., 2014; Pardo et al., 2011; Pérez et al., 2010). Although most studies report a decline in coastal upwelling over NW Iberia, interannual trends for this EBUS are not conclusive (see review by Varela et al., 2015), varying according to time-series length, statistical analysis (Santos et al., 2011b), region and season (Alvaréz et al., 2008; Goela et al., 2016; Gago et al., 2011; Pardo et al., 2011; Relvas et al., 2009). At the south coast, upwelling generated by westerly zonal winds, which were favoured by negative NAO (Hurrel and Dickson, 2004) and positive EA values, showed no significant interannual patterns.

Despite similarities in the interannual trends of some abiotic variables across regions, significant interannual trends in Chl-a were detected only for regions south of 37^{o}N, with opposing trends for the oceanic GoC region and coastal regions (Fig. C.6). The significant linear increase in Chl-a over GoC ($p<0.01$) contrasts with declines commonly reported for Chl-a and primary production over the North Atlantic basin (Behrenfeld et al., 2006; Demarcq, 2009; Gregg and Rousseaux, 2014 and references therein), sometimes associated with warming trends. However, it is noteworthy that GoC was the only oceanic region showing significant interannual increases in both WIN and MLD ($p<0.001$ and $p<0.01$, respectively; Fig. C.5). Then, the linear Chl-a increase over GoC, the most subtropical SWIP region (i.e., higher incident PAR and lower nutrient concentrations, Fig. 4.2B, 4.2I), could be explained by the entrainment of new nutrients into the euphotic zone due to increased vertical water mixing. In fact, positive relationships between wind speed and Chl-a have been identified in tropical and subtropical areas (i.e., deeper MLD and higher PAR) of most ocean basins, indicating the relevance of nutrient availability as a bottom-up factor controlling phytoplankton dynamics in these regions (Kahru et al., 2010).

In contrast to GoC, Chl-a over all coastal regions south of 37^{o}N (SC, Gdn and Gdq) exhibited significant interannually-decreasing trends, with the decrease being stronger between 1997 and 2005/2006 in the case of SC and Gdn (Fig. C.6). Demarcq (2009) also reported a declining tendency over the northern GoC coast, and no significant changes over the SWIP west coast. However, increasing (Demarcq, 2009), decreasing (Pérez et al., 2010), and no significant interannual trends (Bode et al., 2011) have been reported for NW Iberian areas. The declining Chl-a trends over the southern coastal regions could be related to the significant increases in WIN and MLD that, under higher nutrient conditions (Fig. 4.2I) and higher water

turbidity (Fig. C.1), could limit average light availability over the mixed layer and hence phytoplankton growth. Furthermore, decreases in river discharge, aggravated during 2002-2009, might have further limited nutrient availability (see previous section). For the WC region, with no significant effects of riverine discharges, potential negative effects of increased WIN and MLD might be masked by the stimulatory effects of increase in upwelling intensity. In fact, phytoplankton in coastal EBUS are adapted to frequent short-term disturbances and may be inherently more resilient (less sensitive) to changes in climate than more stable communities with shorter productive periods (Bode et al., 2015; García-Reyes et al., 2015). Nevertheless, high-frequency variation in coastal ecosystems can also mask climate change signals (Chavez et al., 2011).

In addition to climate-sensitive local environmental variables, large-scale climate indices were also significant predictors of Chl-a for all SWIP regions. However, the latter were not the most influential predictors and their linkages with Chl-a varied across regions. Climate indices reduce complex spatial-temporal variability in atmospheric (and oceanic) phenomena, showing variable typical scales of variance (from < 10 years for MEI and NAO to ca. 60-80 years to AMO; see review by Stenseth et al., 2003). Climate indices can affect, directly and indirectly, multiple phytoplankton drivers. However, their effects on specific drivers typically depend on season, geographic location and its local atmospheric circulation, and may be non-stationary. Off Iberia, for example, the effects of NAO, EA and AMO on upwelling intensity and SST (Cropper et al., 2014; deCastro et al., 2008; Pardo et al., 2011; Pérez et al., 2010; Santos et al., 2011a), EA and NAO on riverine discharge (deCastro et al., 2006), and AMO on precipitation patterns (Sutton and Dong, 2012) depend on period, season and location. Moreover, the effects of different climate indices can interact (e.g., Kumar et al., 2016; Marshall et al., 2001), and different indices may regulate distinct phytoplankton drivers (e.g., bottom-up under NAO, and top-down under AMO control; see Martinez et al., 2016), thus hindering the detection and interpretation of linkages between climate and phytoplankton. Moreover, significant associations between climate and phytoplankton may not represent causation, and should be interpreted with caution, even when plausible mechanistic relationships are proposed.

WeMO, a regional climate index representative of the western Mediterranean basin (Martin-Vide and Lopez-Bustins, 2006), showed a limited positive influence on Chl-a only over

northeastern GoC coastal regions (Gdn, Gdq). WeMO was significantly correlated to riverine discharge, an important nutrient source over these regions (see previous section). Previous studies indicate a strong link between WeMO and precipitation over eastern Iberian Peninsula (e.g. Hidalgo-Muñoz et al., 2011; Martin-Vide and Lopez-Bustins, 2006), closer to the Guadiana and Guadalquivir rivers sources. Precipitation over the south-western sector of Iberia, however, was better correlated with NAO (Martin-Vide and Lopez-Bustins, 2006).

NAO is considered the dominant mode of climate variability in the North Atlantic, influencing a wide set of variables (Marshall et al., 2001). Off Iberia, NAO index is positively correlated to SST (Marshall et al., 2001; Kumar et al., 2016), and to upwelling intensity over west Iberia (Cropper et al., 2014; Pardo et al., 2011; Pérez et al., 2010), and negatively related to precipitation (deCastro et al., 2006), zonal westerly winds, wave height and velocity (Kumar et al., 2016) and storminess (Plomaritis et al., 2015). Furthermore, Saharan dust-deposition events, which enhance phytoplankton over adjacent western Mediterranean, are also positively related to NAO index (Cusack et al., 2012). These potential multiple impacts could explain the region-specific linkages between NAO and Chl-a over SWIP regions, south of 37^{o}N. For example, its negative influence over SC and Gdn regions could represent an indirect effect, mediated by changes in river discharge (higher during negative NAO) and nutrient availability. Yet, over GoC, extreme (both negative and positive) NAO values favoured increase in Chl-a; this could represent the integrative effects of increased northerly winds or Saharan dust deposition (NAO-positive), and increased wave climate, storminess and atmospheric wet deposition (NAO-negative). Most studies linking phytoplankton responses to climate patterns over the eastern Atlantic Ocean were based on NAO index. For NW Iberia, negative relationships between NAO and phytoplankton were associated with a reduction in upwelling intensity (Pérez et al., 2010); but positive and no significant relationships have also been reported (Bode et al., 2011, 2015). NAO was associated with bloom phenology and species abundance over the North Atlantic subtropical region, but its influence varied according to region, suggesting the relevance of regional differences in phytoplankton regulation (Drinkwater et al., 2003; Ueyama and Monger, 2005; Friedland et al., 2016).

AMO, a quasi-periodic cycle representing SST variability over North Atlantic, is related to the thermohaline circulation (Stenseth et al., 2003). Off Iberia, AMO is significantly

correlated to precipitation patterns (Sutton and Dong, 2012) and SST, although this relationship decreases rapidly over coastal areas due to the effects of local mechanisms (Santos et al., 2011a). Contrary to NAO, the significant influences of AMO on Chl-a, detected over the slope (WSlp and SSlp) and over most oceanic regions (Off, NOff) located mainly north of 37^{o}N, were negative for all regions. This negative influence could partially represent a consequence of decreased nutrient inputs due to enhanced stratification (high AMO). However, our time series is clearly short in comparison with the typical AMO periods (ca. 60-80 years). AMO was identified as a relevant driver of basin-scale decadal variability of phytoplankton (Martinez et al., 2009), but no influence of AMO was reported for NW Iberia (Bode et al., 2011).

Over the west and south Portuguese coast and slope, regions under upwelling influence, both global-scale MEI and regional-scale EA indices were significant Chl-a predictors. EA represents the second prominent mode of inter-annual variability over the North Atlantic/Europe and is particularly important for southern Europe (see Iglesias et al., 2014). Considering that EA is positively correlated with SST and upwelling intensity off west Iberia (Pardo et al., 2011; Santos et al., 2011a), its weak positive linkages with Chl-a over the west and south Portuguese coastal and slope regions, could partially represent the stimulatory effects of upwelling. ENSO patterns are more relevant over tropical regions but some extra-tropical areas are influenced as well. Impacts of ENSO on eastern North Atlantic climate, and on air temperature and precipitation patterns over the Euro-Mediterranean sector (see review by Hertig et al., 2015), and global SST interannual changes (Chavez et al., 2011) have been already reported. Negative influences of MEI on interannual Chl-a patterns and/or net primary production have been reported for the Pacific Ocean (e.g., Chavez et al., 2011; Thomas et al., 2012) and global oceanic areas (between ~40^{o}N and 40^{o}S, Behrenfeld et al., 2006). Relative decreases in Chl-a during positive, warmer MEI phases are seen as result of increased stratification, which results in a diminished supply of nutrients to surface waters (Chavez et al., 2011; see Tilstone et al., 2015). By contrast, over SWIP, MEI usually showed weakly positive effects on Chl-a ($p<0.05$) on coastal and slope stations; however, the lack of information on ENSO effects over ocean properties off Iberia and the reduced significance of these relationships, limit further discussion.

Overall, GAMM analysis showed the relevance of climate-sensitive variables and, to a lower degree, of large-scale climate indices, as predictors of Chl-a over different SWIP regions, at both seasonal and inter-annual time scales (the latter more evident over southern SWIP regions). However, the explanatory power of the statistical model decreased and model complexity (i.e., number of predictors) increased towards WC and SC coastal regions, reflecting the intricate interplay of atmosphere-ocean-land interactions acting on phytoplankton (Cloern and Jassby, 2008).

Considering current climate predictions for the study area in particular, and for NE Atlantic in general (e.g., reduction in rainfall, increase in heat waves, sea surface warming; Goela et al., 2016; Henson et al., 2017; Kovats et al., 2014), climate-driven changes are expected to affect phytoplankton variability, but their impacts will probably vary across SWIP regions, depending on the dominant phytoplankton driving forces on a regional basis. The complexity of SWIP coastal regions may limit our capacity to identify and detect the impacts of environmental variability and climate change (Chavez et al., 2011; Bode et al., 2015). Hence, climate change signals will probably emerge earlier over the less complex, deep oceanic regions over SWIP. Moreover, the discrimination between climate-driven changes and natural phytoplankton variability requires time series longer than the 15-year period utilized in our study, given the decadal and even long cycles of variability to which the oceans are subject (see also Henson et al., 2016; 2017). In fact, phytoplankton integrate, directly and indirectly, bottom-up controls such as changes in light, temperature and nutrients as well as top-down controls; hence its response to climate change will be likely slower than the more stable abiotic variables (Henson et al., 2017). From a broad perspective, this supports the requirement of systematic and continuous observation for OCRS and other ECV variables, to allow the mobilisation of longer time series of observed data and clearer cut estimates of impacts.

4.5 - Conclusions

EOF analysis of Chl-a variability over the heterogeneous SWIP area, during a 15-year period, identified nine coherent regions with similar patterns of variability (4 coastal, 2 slope and 3 open-ocean regions). GAMM analysis of each region allowed the decomposition of temporal variability into seasonal and interannual modes, and an integrated evaluation of complex

linear and non-linear relationships between Chl-a and multiple environmental drivers. Generally, climate-sensitive local environmental variables (SST, PAR, WIN, U, V, and river discharge) emerged as the most influential Chl-a predictors, and large-scale climate indices (NAO, EA, AMO, WeMO and MEI) showed significant but minor effects. The set of relevant predictors, as well as their effects, were usually detectable at both seasonal and interannual scales, and varied markedly among regions.

Oceanic regions showed a uni-modal Chl-a annual cycle, with increases during the MLD deepening and late-winter maxima, reflecting seasonal changes in SST and ocean stratification, probably related to bottom-up and/or top-down controls. Chl-a over west and south coastal regions was more variable, leading to more complex models, with lower explanatory power. The stimulatory effects of meridional northerly winds and coastal upwelling lead to relative increases in Chl-a over WC during summer, partially extended into slope waters. Over the northern GoC, all coastal and slope regions (SC, Gdn, Gdq, SSlp) revealed the positive influences of riverine discharges, during winter. Significant interannual patterns in Chl-a were detected for all SWIP regions (except SSlp) south of 37^{o}N, but contrasting tendencies were exhibited over oceanic (increase) and coastal regions (decrease), probably reflecting relative differences in the role of nutrient and light availability, under significant interannual increase of wind speed and mixed layer depth. The strategy used in the present study promoted a biologically-relevant regionalization of the study area, improving our comprehensive understanding of phytoplankton driving forces over this highly heterogeneous area. Region-specific linkages between phytoplankton and multiple climate-sensitive environmental drivers over SWIP reinforce the potential role of phytoplankton as a key element for evaluating ecosystem responses to climate variability and change.

CHAPTER 5

PHYTOPLANKTON PHENOLOGY PATTERNS OFF SW IBERIA (NE ATLANTIC): A STRATEGY FOR OBJECTIVE PARTITIONING OF A COMPLEX MARINE DOMAIN

This Chapter is in preparation to be submitted:

Krug, L. A., Platt, T., Sathyendranath, S., Barbosa, A. B., *in preparation*. Phytoplankton phenology patterns off SW Iberia (NE Atlantic): a strategy for objective partitioning of a complex marine domain.

ABSTRACT

Phytoplankton phenology patterns, tightly linked to the dynamics of the ocean surface layer and atmospheric forcing, have major impacts on ecosystem functioning and are valuable indicators of ecosystem response to climate variability and change. Phytoplankton phenology and its underlying drivers are spatially variable, and the investigation of its patterns, particularly over heterogeneous regions, is benefited with a delineation of regions with specific phenological properties, or phenoregions. The area southwest of the Iberian Peninsula (SWIP, NE Atlantic) is a highly complex marine domain, located in a biogeographical transition zone between temperate and subtropical waters. SWIP includes a variety of oceanic and coastal domains, under the influence of topographic irregularities, coastal upwelling and continental freshwater outflows, that collectively challenge the understanding of phytoplankton phenology and related forcing mechanisms. This study aims to evaluate phytoplankton phenology patterns over the SWIP area, during an 18-year period (September 1997 - August 2015), using an objective, unsupervised partition based on phenological indices derived from satellite ocean colour data. The partition is then used to describe region-specific phytoplankton phenological patterns related to bloom magnitude, duration and timing as well as their interannual variability. Moreover, region-specific phytoplankton phenology relationship with environmental determinants, including local ocean physical-chemical variables, hydrodynamic variables and large scale climate indices, is evaluated. Phenology patterns as well as their environmental drivers, varied markedly among five phenoregions (two open ocean and three coastal). Over the open ocean, a low magnitude and long duration single bloom event per year had little intra-annual variability, whereas coastal phenoregions presented higher magnitude and intra-annual variability with three to four short period bloom events occurring during an year. Comparative analyses with mixed-layer deepening and shoaling onset timings and the association of phenological indices with physical, optical and chemical conditions preceding the events suggest that mechanisms triggering bloom initiation are likely enhanced by nutrient and light availability over open ocean and coastal phenoregions, respectively. Coastal phenoregions presented more complex linkages with environmental drivers, particularly over the Upwelling-influenced phenoregion. Over this phenoregion, blooms occurred during both periods, late winter-early spring and upwelling-favourable season (May-September), likely precluding significant associations of upwelling intensity with phenological indices. Over the Coastal-slope and River-influenced phenoregions, the Guadalquivir river discharge affected the number of blooms per year, as well as bloom magnitude, duration and timing of initiation. Large-scale climate indices (AMO, NAO and WeMO) were associated to phytoplankton phenology over all, except the Upwelling-influenced phenoregion. Overall, our phenology-based unsupervised approach promoted a biologically-relevant SWIP partition, enabling a better evaluation of the complexity of interactions between phytoplankton and multiple environmental forcing, particularly over coastal areas.

5.1 - Introduction

Phytoplankton are the dominant primary producers of marine ecosystems, responsible for ca. 50% of global primary production (Field et al., 1998), and a key component of the biological carbon pump (Gregg et al., 2003; Cermeño et al., 2008). Phytoplankton growth is mostly controlled by light and nutrient availability and, therefore, tightly linked to the dynamics of the ocean surface mixed layer (Longhurst, 2007; Cloern and Dufford, 2005) and regulated by atmospheric forcing and large scale climate variability patterns (Martinez et al., 2009, 2011, 2016; Boyce et al., 2010; Racault et al., 2012, 2017; Zhai et al., 2013). Over coastal zones, terrestrial nutrient inputs and topographic irregularities increase the complexity of phytoplankton patterns and driving forces (Carstensen et al., 2015; Cloern et al., 2016). Together with top-down controls, these environmental determinants modulate phytoplankton phenology, i.e., their periodically-recurring variability patterns, including the timing and intensity of phytoplankton blooms, short-term events that can represent a substantial fraction of the annual primary production in marine ecosystems (Behrenfeld, 2014; Sallée et al., 2015; Martinez et al., 2016). Phytoplankton phenology patterns, and alterations therein, have large impacts on ecosystem functioning (see review by Ji et al. 2010), affecting the efficiency of carbon transfer to higher trophic levels (Edwards and Richardson, 2004; Barth et al., 2007; Friedland et al., 2016), the recruitment success of economically important fish and invertebrate resources (Platt et al., 2003; Fuentes-Yaco et al., 2007; Koeller et al., 2009; Malick et al., 2015), benthic-pelagic coupling (Nixon et al., 2009), the carbon export efficiency and depth of remineralization (Lutz et al., 2007). Through such mechanisms, phytoplankton provide a critical connection between environmental changes and ecosystem dynamics and productivity.

Phytoplankton phenology has been the subject of intense research in the last decade, mostly stimulated by the availability of satellite-retrieved surface chlorophyll-a concentration (Chl-a) and the anticipated climate-induced changes in marine ecosystems (e.g., Platt and Sathyendranath, 2008; Platt et al., 2010; Racault et al., 2012, 2014a). As an integrative environmental science (Schwartz, 2003), phenological study has evaluated phytoplankton periodic events as well as their interactions with environmental conditions and climatic forcing (e.g., Henson et al., 2006; Demarcq et al., 2012; Racault et al., 2012; Sapiano et al., 2012; Cabré et al., 2016; Kostadinov et al., 2017). Phytoplankton phenology has usually been

synthesized into a set of ecologically relevant indices: the timing, duration and magnitude of bloom events (Platt and Sathyendranath, 2008; Platt et al., 2009, 2010; Racault et al., 2014a). These indices are currently considered key indicators of ecosystem functioning and its response to climate variability and change, at multiple scales (see Platt and Sathyendranath, 2008; Winder and Cloern, 2010; Racault et al., 2014a; Scheffers et al., 2016).

Global (Demarcq et al., 2012; D'Ortenzio et al., 2012; Racault et al., 2012, 2017; Sapiano et al., 2012) and regional phenological studies, based on satellite-remote sensing and *in situ* sampling, have reported significant interannual changes in phytoplankton phenology for a wide diversity of marine ecosystems including epipelagic, neritic (e.g., North Atlantic - Harrison et al., 2013; Henson et al., 2010; Land et al., 2014; Martinez et al., 2011; González Taboada and Anadón, 2014; Mediterranean - Lavigne et al., 2013; North Sea - Edwards and Richardson, 2004; North Pacific – Yoo et al., 2008; California Current – Foukal and Thomas, 2014; Arctic and Southern Ocean – Kahru et al., 2010; Ardyna et al., 2014; Soppa et al., 2016; Oziel et al., 2017) and confined/estuarine ecosystems (Wiltshire et al., 2008; Nixon et al., 2009; Kromkamp and van Engeland, 2010; Groetsch et al., 2016; Kahru et al., 2015). However, most interannual changes in phytoplankton phenology and their underlying drivers are spatially variable, even over particular ocean basins (e.g., Yoo et al., 2008; Henson et al., 2010; Kahru et al., 2010; Martinez et al., 2011; Sasaoka et al., 2011; Friedland et al., 2016) or domains (e.g., Song et al., 2010; Lavigne et al., 2013; Zhao et al., 2013; Foukal and Thomas, 2014), depending on region-specific properties and factors controlling the initiation, collapse and magnitude of phytoplankton blooms. These results indicate that a proper geographic partitioning of marine ecosystems should be implemented for the investigation of phytoplankton phenology (e.g., Zhao et al., 2013).

In fact, due to their ecological relevance, the shape of phytoplankton climatological seasonal cycles, extracted from Chl-a time series, has been used for objectively partitioning the complex spatial organization of ocean surface into biologically meaningful regions (bioregions, trophic regimes or bloom phenology regimes), at the global (D'Ortenzio et al., 2012) or regional scale (D'Ortenzio and Ribera d'Alcalà, 2009; Sasaoka et al., 2011; Foukal and Thomas, 2014; Lacour et al., 2015; Mayot et al., 2015; Ardyna et al., 2017; Eliasen et al., 2017; Chapter 4, also and hereafter Krug et al., *in press*). In some cases, phytoplankton phenology indices were used directly as input variables for delineating ocean surface

"phenological provinces" or (pheno)regions (see Sasaoka et al., 2011; Xu et al., 2013; Land et al., 2014). Ocean partition represents a relevant strategy to simplify ocean complexity and disentangle the interactions between phytoplankton and multiple environmental determinants, particularly relevant for heterogeneous marine domains, providing a framework for assessing marine ecosystem status and trends, as well as its resilience and vulnerability to climate change (see reviews IOCCG, 2009; and Chapter 2, also and hereafter Krug et al., 2017).

The southwest area off the Iberian Peninsula (SWIP; NE Atlantic), located at a transition zone between temperate and subtropical waters, constitutes a highly heterogeneous domain, particularly vulnerable to climate change (Kovats et al., 2014). A wide diversity of processes, including local and large scale oceanic and atmospheric circulation patterns, topographic irregularities, coastal upwelling and continental freshwater outflows, impacts phytoplankton spatial and temporal dynamics (e.g., Navarro and Ruiz, 2006; García-Lafuente and Ruiz, 2007; Prieto et al., 2009; Navarro et al., 2012; Bruno et al., 2013; Goela et al., 2013; Caballero et al., 2014), promoting the occurrence of distinct regions where phytoplankton are driven, differently, by specific combinations of physical and climatic environmental drivers (see Krug et al., *in press*). Due to its geographical location (eastern boundary of the North Atlantic basin), SWIP and its complex coastal areas are often overlooked (Follows and Dutkiewicz, 2002; Vargas et al., 2009; Racault et al., 2012; Ferreira et al., 2014) or sparsely resolved (e.g., Siegel et al., 2002; Ueyama and Monger, 2005; Henson et al., 2009; Kahru et al., 2010; Martinez et al., 2011; Demarcq et al., 2012; D'Ortenzio et al., 2012; Sapiano et al., 2012; Land et al., 2014; Racault et al., 2014b, 2017; González Taboada and Anadón, 2014; Cole et al., 2015; Cabré et al., 2016; Friedland et al., 2016; Zhang et al., 2017) in global or basin-scale phenological analysis. The analysis of phytoplankton phenology over SWIP at a finer, regional-scale resolution, however, has been restricted to the central Gulf of Cadiz area (Navarro et al., 2012). Thus, knowledge on phytoplankton phenology over the SWIP area, its interannual variability and underlying environmental drivers, is still limited.

In this context, our study aims to evaluate phytoplankton phenology patterns over the SWIP area, during an 18-year period (September 1997 - August 2015), using satellite ocean colour data, and to investigate the relevance of underlying environmental determinants. Our specific objectives are: (i) to evaluate the distribution of phytoplankton phenological indices over the study area and period, on a pixel-by-pixel basis; (ii) to partition the highly heterogeneous

surface SWIP area into phenoregions using an objective, unsupervised partition based on phenological indices; (iii) to describe region-specific phytoplankton phenological indices and their interannual variability patterns; and (iv) to evaluate region-specific environmental determinants of phytoplankton phenology, including local ocean physical-chemical variables (mixed layer depth, photosynthetically available radiation and dissolved inorganic nutrients), hydrodynamic variables (riverine discharges and coastal upwelling intensity), and large scale climate indices. The analysis of phytoplankton phenological indices over this heterogeneous climate-susceptible marine domain will improve our current knowledge of phytoplankton variability patterns and controls, potentially supporting the detection of eventual ongoing environmental changes, as well as the prediction of future environmental changes.

5.2 – Materials and methods

5.2.1 Study area

SWIP comprises a variety of oceanic and coastal domains. Open ocean domains are interspersed with submarine seamounts and canyons and, over the coast, a 5-35 km wide continental shelf shifts orientation, from meridional to zonal, at Cape São Vicente (CSV). CSV is the northwest limit of the Gulf of Cadiz (GoC), a basin that connects the Mediterranean Sea and the Atlantic Ocean. The main continental influences over SWIP include topographic irregularities, such as prominent capes as CSV, Cape Santa Maria (CSM) and Cape Trafalgar (CT), and the Strait of Gibraltar, which affect coastal circulation dynamics (García-Lafuente et al., 2006). Freshwater inputs, particularly into the GoC area (e.g., Guadiana and Guadalquivir rivers discharge; Caballero et al., 2014; submarine groundwater discharges; e.g., Hugman et al., 2015), are relevant local drivers of abiotic conditions and phytoplankton dynamics (Krug et al., *in press*). SWIP, embedded in the Iberian Canary Eastern Boundary Upwelling system, is strongly affected by a seasonal upwelling, promoted by northerly and westerly winds for western and southern coastal areas, respectively (Relvas et al., 2007; Goela et al., 2016). Offshore circulation over SWIP is affected by mesoscale and submesoscale features including fronts, cyclonic and anti-cyclonic eddies, jets and upwelling filaments (García-Lafuente and Ruiz, 2007; Relvas et al., 2007). SWIP coastal and oceanic processes and their interaction with atmospheric forcing and continental inputs affect the physical, optical and chemical properties of the top layers of the water column, affecting its

biotic components, from plankton to fishes (e.g., see review by García-LaFuente and Ruiz, 2007; Krug et al., *in press* and references therein; Chapter 3, also and hereafter Krug et al., *submitted* and references therein).

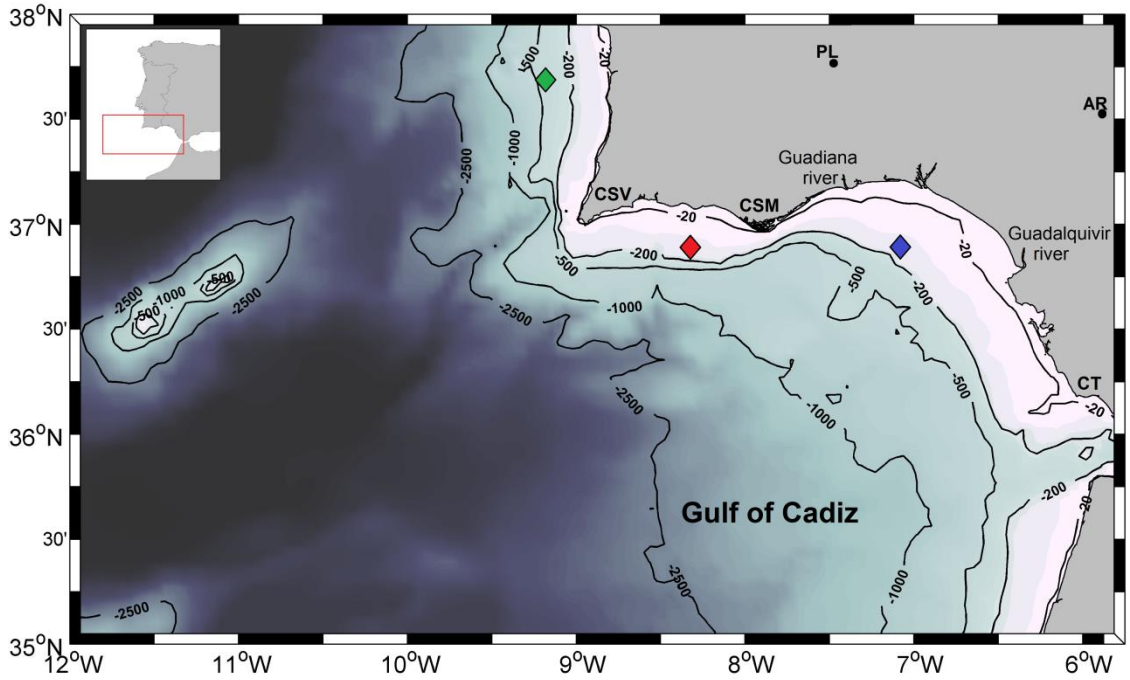

Figure 5.1 - The southwest area off the Iberian Peninsula (SWIP): bathymetry and main sources of freshwater discharges, the Guadiana and Guadalquivir rivers. CSV, CSM and CT depict the location of prominent topographic features, Cape São Vicente, Cape Santa Maria and Cape Trafalgar, respectively. PL and AR depict the location of Pulo do Lobo and Alcalá del Río hydrographic stations, respectively. Diamonds show the position of pixels used for the calculation of Cross Shore Ekman Transport, a wind-based upwelling index, for the West Coast (green), and west (red) and east Cape Santa Maria sectors (blue).

SWIP, along with Southern Europe and Mediterranean, is classified as a region particularly vulnerable to climate change, under effects of decreased precipitation, increased frequency and intensity of heatwaves and decline in provision of ecosystem services (Kovats et al., 2014). In fact, recent decadal climate-driven alterations were already reported for SWIP (e.g., increase in frequency of heatwaves: Trigo, 2006; sea surface warming: Goela et al., 2016; changes in upwelling intensity and patterns: see review by Varela et al., 2015; changes in abundance and fish landings: Gamito et al., 2016; and species range shifts with a northern expansion of subtropical species: Horta e Costa et al., 2014).

5.2.2 Phytoplankton chlorophyll-a concentration

Satellite-derived surface Chl-a from the European Space Agency's Ocean Colour Climate Change Initiative (OC-CCI), at 4 km and 8-day resolution, available at http://www.esa-oceancolour-cci.org/, was used to derive phytoplankton phenological indices over the SWIP area between September 1997 and August 2015 and subsequently used to derive phytoplankton phenological indices. The OC-CCI Chl-a version 3 product uses remote sensing reflectances (R_{RS}) derived from multiple sensors, Sea-viewing Wide Field of View Sensor (SeaWiFS), MODerate-resolution Imaging Spectroradiometer (MODIS-Aqua), MEdium Resolution Imaging Spectrometer (*MERIS*) and Visible Infrared Imaging Radiometer Suite(VIIRS), which are wavelength synchronized to account for sensor specific centre bands, bias corrected and merged, allowing an enhanced spatial-temporal resolution with respect to the use of single sensors. Moreover, Chl-a values are computed using the merged R_{RS} and estimated using a blended combination of best-performing algorithms in order to improve performance in case II waters (Sathyendranath et al., 2016, *in press*). Although this OC-CCI product is provided at daily resolution, the 8-day resolution (hereafter weekly) was selected to limit the data gaps and increase the accuracy and precision in the calculation of the phenological indices (Cole et al., 2012; Ferreira et al., 2014; Land et al., 2014; Racault et al., 2014b).

The accuracy of satellite-derived Chl-a for the study region and adjacent Atlantic areas was previously assessed during calibration-validation exercises dedicated to different (standard and alternative) bio-optical algorithms and sensors, including SeaWiFS (Navarro and Ruiz, 2006), MERIS (Cristina et al., 2014, 2015, 2016a, 2016b; Nechad et al., 2015), MODIS-Aqua (Caballero et al., 2014; Sá et al., 2015) and OC-CCI version 1 products (Sá et al., 2015). Overall, these studies indicated that satellite radiometry provides realistic estimates of *in situ* Chl-a, but usually larger than contemporaneous *in situ* estimates. Higher uncertainty and a systematic overestimation was found for nearshore optically-complex Case II waters. To minimize problems associated with Case II coastal waters, Chl-a was retrieved only for areas outside the 20 m isobath, located at a minimum distance of approximately 4 km from the coastline. All Chl-a values were retained, since unusually high Chl-a values for the study area (> 20 µg L^{-1}; Navarro and Ruiz, 2006; Moita, 2001; Caballero et al., 2014) represented only less than 0.0001% of valid data. Our strategy has not accounted for sub-surface phytoplankton

dynamics (e.g., subsurface chlorophyll maxima; Moita, 2001; García-Lafuente and Ruiz, 2007).

5.2.3 Optical variables

Weekly level-3 mapped mean surface photosynthetically available radiation (PAR) data, at 9 km spatial resolution, were obtained from SeaWiFS (1997-2002) and MODIS-Aqua (2002-2015) products, available at the NASA's Oceancolor Group website (https://oceandata.sci.gsfc.nasa.gov/). Weekly level-3 composites of satellite-derived light attenuation coefficient at 490 nm wavelength (K_{490}), at 4 km spatial resolution, were accessed from ESA's OC-CCI (see section 2.2). Mean PAR intensity in the mixed layer (I_m) was calculated according to Kirk (1986), using PAR vertical attenuation coefficient (K_{PAR}) and euphotic zone depth (Z_{eu}) estimates. K_{PAR} was derived from K_{490} according to Rochford et al. (2001), and Z_{eu}, was defined as the depth at which the irradiance is 1% of incident surface PAR, according to the Lambert-Beer law, assuming a constant attenuation coefficient and optically homogeneous waters (see Krug et al., *in press* for further details).

5.2.4 Physical and chemical variables

Due to the limited availability of *in situ* oceanographic data for the study area, physical and chemical variables were derived from model-based predictions. Mixed Layer Depth (MLD) weekly composites were retrieved from the Ocean Productivity group of the Oregon State University (http://www.science.oregonstate.edu/ocean.productivity/index.php), based on three data-assimilating models: Simple Ocean Data Assimilation (SODA), at a 0.5^o spatial resolution (1997-2004); Thermal Ocean Prediction Model based on The Navy Coupled Ocean Data Assimilation system (NCODA/TOPS), at a 1^o spatial resolution (January - May 2005); and Fleet Numerical Meteorology and Oceanography Center model (FNMOC – June 2005 to August 2015), at a 0.25^o spatial resolution. This combination of MLD data was selected in accordance with the preferred MLD sources used in net primary production models of the Ocean Productivity group. MLD data were adjusted to GEBCO bathymetry (IOC, IHO and BODC, 2003), and maximum MLD values were limited to bathymetry values.

The ratio of the mixed layer depth to the euphotic depth (MLD:Z_{eu}), usually used as an indicator of light limitation (e.g., Grobbelaar, 1985; Alpine and Cloern, 1988) and a predictor

of phytoplankton composition (Brown et al., 1995), and the timings of MLD shoaling and deepening (e.g., Lavigne et al., 2013; Shiozaki et al., 2014) were also explored as potential environmental determinants of phytoplankton phenology. For each annual cycle, the timing of MLD shoaling was considered as the week of the year coincident with the MLD maximum. The timing of MLD deepening was considered the week of the year when MLD started to increase significantly; it was defined as the time when 10% of the amplitude of the normalized MLD data (minima and maxima on a 0 -1 range), was reached.

Concentrations of dissolved inorganic macronutrients (nitrate, NO_3; phosphate, PO_4; silicate, Si) and micronutrients (iron, Fe) were obtained from the biogeochemical model reanalysis data provided by the Copernicus Marine Environment Monitoring Service for the Atlantic-Iberian Biscay Irish-Ocean area, for the period February 2002 - December 2014 (Product: IBI_REANALYSIS_BIO_005_003; http://marine.copernicus.eu/). This product, derived from the biogeochemical model PISCES (Pelagic Interaction Scheme for Carbon and Ecosystem Studies), coupled with ocean physics NEMO (Nucleus for European Modelling of the Ocean), is available at a 0.08^o spatial resolution and monthly temporal resolution, for 50 depth levels (0.50 m to 5500 m). To obtain a more robust estimate of nutrient availability (based on a higher number of data points), in comparison with subsurface level, relevant for phytoplankton, average nutrient concentrations were computed within the first layer, considered as the shallowest depth between MLD and Z_{eu}, for each pixel and time step.

5.2.5 Upwelling intensity and hydrographic variables

A wind-based upwelling index, the cross-shore Ekman transport (CSET), was used to infer upwelling intensity and patterns during the study period. Daily sea surface wind fields, at 0.25^o spatial resolution, were obtained from the Blended Sea Winds dataset (National Climatic Data Center - National Oceanic and Atmospheric Administration, NCFC-NOAA, (http://www.ncdc.noaa.gov/oa/rsad/air-sea/seawinds.html). Weekly CSET was estimated for three locations on the west and south Portuguese coasts, positioned at ca. 75 km from the coastline (see Fig. 5.1). CSET values represent the average of a 0.75^o x 0.75^o box centred at the target locations and was based on the zonal and meridional components of the Ekman transport, for the west and south coast, respectively. Negative CSET values indicate offshore Ekman transport and upwelling-favourable periods; conversely, positive values indicate

onshore Ekman transport and downwelling-favourable periods (Alvarez et al., 2011; Bakun, 1973; see Krug et al., *in press* for further details).

Freshwater discharge over the study area is strongly associated with Guadiana and Guadalquivir rivers. Daily Guadiana river discharge (Gdn), measured at the hydrometric station Pulo do Lobo (see Fig. 5.1), was accessed from the Portuguese Environmental Agency public database (http://snirh.apambiente.pt/). Daily Guadalquivir river discharge (Gdq), measured at the Alcalá del Río station (see Fig. 5.1), was acquired from the Spanish Regional Water Management Agency (http://www.chguadalquivir.es/saih/).

All environmental variables were re-gridded to the same spatial-temporal resolution of Chl-a data (4-km, 8-day). Data analyses and visualization maps were generated using MATLAB software.

5.2.6 Large scale climate indices

Six large-scale climate indices were used as indicators of remote forcing over the study area: (i) the Multivariate El Niño Southern Oscillation (ENSO) Index (MEI), a global scale index which monitors ENSO patterns based on six ocean-atmosphere variables over the tropical Pacific (Wolter and Timlin, 2011); (ii) the North Atlantic Oscillation (NAO) Index, a normalized pressure difference between the Azores and Iceland, representative of the dominant mode of climate variability in the north sector of the Atlantic Ocean (Hurrel, 1995); (iii) the Atlantic Multidecadal Oscillation (AMO), an SST-based index related to low frequency variability in SST and themohaline circulation in the North Atlantic (Kaplan et al., 1998); (iv) the Eastern Atlantic Pattern (EA), the second mode of sea-level pressure (SLP) variation in the North Atlantic (Hurrell et al., 2003); (v) the Western Mediterranean Oscillation (WeMO) Index, a barometric ratio between Padua (north Italy), and San Fernando (southwest Spain), representative of low frequency variability patterns of atmospheric circulation over the western Mediterranean basin (Martin-Vide and Lopez-Bustins, 2006); and (vi) the West Europe Pressure Anomaly (WEPA), based on winter (December – March) SLP, which is strongly related to winter wave height variability over the coast of western Europe (Castelle et al., 2017).

Monthly values of the large-scale climate indices were retrieved from diverse sources. MEI, NAO, and AMO indices were accessed at NOAA's Earth System Research Laboratory portal (https://www.esrl.noaa.gov/psd/data/climateindices/list/), EA was acquired at NOAA's Climate Prediction Center website (http://www.cpc.ncep.noaa.gov/data/teledoc/ea.shtml), WeMO was retrieved from the University of Barcelona's Climatology Group website (http://www.ub.edu/gc/en/2016/06/08/wemo/), and WEPA was extracted from supplementary material provided by Castelle et al. (2017). Significant connections between NAO, AMO, EA, MEI and WeMO and phytoplankton variability over SWIP were previously reported by Krug et al. (*in press*).

5.2.7 Data analyses

The general strategy used for partitioning the SWIP area, based on phytoplankton phenology, is summarized in Fig. 5.2. Chl-a time series, available for each study area pixel (n=8570 pixels), covered an 18-year period (n= 828 Chl-a 8-day composites). First, pixel-specific Chl-a time series were organized considering the start point of the annual cycle as the first week of September (week 1; year t) and the end point as the last week of August (week 46; year t+1), i.e., spanning two calendar years. This 12-month delineation period was chosen to follow phytoplankton seasonal variability patterns (see Krug et al., *in press*). Six phenological indices were then computed, for each pixel. A dissimilarity analysis was used to select the set of independent phenological indices that were subsequently used as partitioning variables. An unsupervised classification technique was then used to partition SWIP into regions sharing similar phytoplankton phenology (phenoregions). This phenology-based SWIP partition was later used as a framework to investigate region-specific phenological indices, their interannual variability during the study period, and the underlying environmental determinants of phytoplankton phenology.

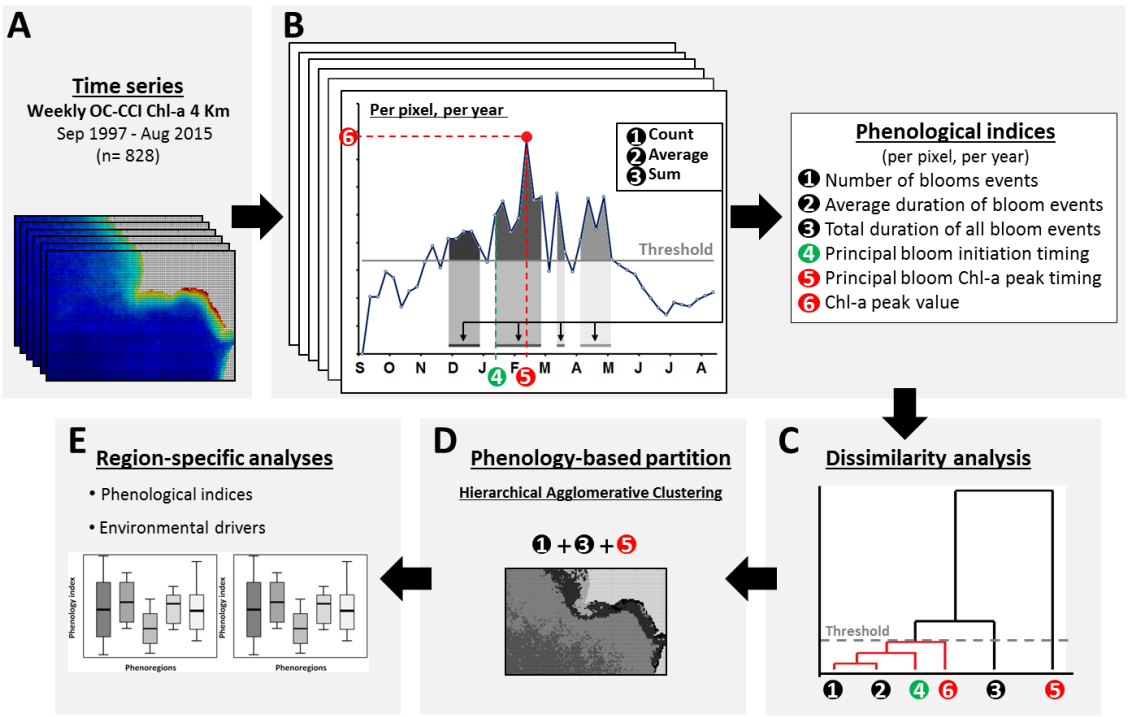

Figure 5.2 – Flow diagram representing the different steps (A – D) involved in the partition of the area off South West Iberian Peninsula (SWIP) based on phytoplankton phenology during a 18-year period (1997 – 2015). Workflow included: (A) Extraction of the Chl-a time series for SWIP, on a pixel-by-pixel basis; (B) calculation of six phenological indices, on a pixel-by-pixel basis; (C) selection of specific non-redundant phenological indices to be used as partitioning variables; and (D) delineation of phenology-based coherent regions (phenoregions) using an unsupervised objective classification technique (Hierarchical Agglomerative Clustering). Step E represents the analyses of region-specific phenological indices and environmental driving forces for different bloom stages. See text for further details.

5.2.7.1 Phytoplankton phenological indices

Several phenological indices have been applied to synthesize phytoplankton phenology patterns (see Platt and Sathyendranath, 2008; Platt et al., 2009, 2010), and multiple strategies have also been used to derive specific metrics (see Brody et al. 2013; Ferreira et al., 2014 and references therein; Land et al., 2014). Ideally, "a phenology metric should be accurate, precise, and simultaneously sensitive to the underlying environmental processes" (Ferreira et al., 2014). However, several observation-related and analysis-related issues (e.g., missing data, observational noise, temporal resolution, preprocessing, bloom amplitude, phenology metric), introduce errors in the estimates of phytoplankton phenology (Ferreira et al., 2014). These errors or uncertainties associated with phenology metrics usually exhibit a spatial

pattern, with smaller values for the latitudes over the study area (Cole et al., 2012; Ferreira et al., 2014; Racault et al., 2014b).

In this study, bloom events were defined as occurrences when Chl-a surpassed the threshold criterion of 5% above the annual local median value (Siegel et al., 2002), at least during two consecutive weeks (Cole et al., 2012; Brody et al., 2013). This biomass-based threshold approach is considered a robust and precise strategy (Ferreira et al., 2014), widely applied in studies of phytoplankton phenology (e.g., Henson et al., 2009; Racault et al., 2012, 2017; Sapiano et al., 2012; Lavigne et al., 2013). The following phenological indices were estimated on a pixel-by-pixel basis and for each phenoregion, using all detected bloom events (principal and secondary), for each annual cycle, (i) number of bloom events; (ii) total duration of all bloom events per year; (iii) average duration of the bloom events; and (iv) Chl-a peak value. Taking into consideration the principal annual bloom for each pixel or phenoregion (i.e., the events associated with Chl-a maxima for each year), the following phenological indices were also estimated: (v) timing of bloom initiation (first week when Chl-a surpassed the threshold criteria); (vi) bloom peak timing (week of Chl-a peak value within each bloom event); (vii) timing of bloom termination (last week of Chl-a above the threshold criteria); and (viii) bloom duration (time elapsed between bloom initiation and termination) (see Fig. 5.2). In addition to these eight indices, two other phenological metrics were also derived for each delineated SWIP phenoregion, considering the principal bloom during each year: (ix) duration of the bloom accumulation phase, i.e., time elapsed between bloom initiation and bloom peak; and (x) duration of the bloom deceleration phase, i.e., time elapsed between bloom peak and termination.

5.2.7.2 Delineation of phenology-based regions off SW Iberia

The climatological average values (18-year period) of six relevant phenological indices, derived for each year on a pixel-by-pixel basis, were tested as potential SWIP partitioning variables: number of bloom events per year, average duration of the bloom events, total yearly duration of the bloom events, timing of the initiation of the main bloom, bloom peak timing, and Chl-a peak value. The value of each index was normalized by subtracting its mean value (18-year) and dividing by its standard deviation. Spearman rank correlation coefficient (r_S) was used to evaluate the strength of monotonic relationships between these phytoplankton

phenological metrics (Hauke and Kossowski, 2011), and correlation values ($1-r_s$) were used to build a dissimilarity hierarchical cluster tree (Wilks, 2006). A dissimilarity value of 0.10 was used as a threshold to eliminate strongly correlated, redundant phenological indices. For groups of redundant indices (similarity above 0.90), a single index was selected as a SWIP partitioning variable.

Different delineation methods, based on OCRS, can be applied for ocean surface partition. However, unsupervised learning approaches provide a less biased delineation and more accurate representation of phytoplankton variability (see review by Krug et al., 2017). In this study, Hierarchical Agglomerative Clustering (HAC) analysis was used to classify SWIP into regions with similar phenological properties (phenoregions). HAC associates objects that are close to each other in an n-dimensional space into the same cluster, using a division that simultaneously minimizes differences between objects of a given cluster and maximizes differences between objects of different clusters, based on Euclidian distance and Ward's linkage (Ward, 1963), respectively (Wilks, 2006). As the number of clusters (i.e., phenoregions) must be defined in advance, HAC analysis was applied multiple times, using a cluster number that varied between 2 and 20. The original data were divided into a training (90%) and a validation (10%) dataset, and used for cross-validation. At each round of the 10-fold cross-validation, HAC was applied to the training dataset and pixels from both training and validation datasets were assigned to a cluster based on the lowest distance from the centroid values. The cross-validation error was computed as the sum of the root mean square deviation between individual pixels of the validation dataset and their respective cluster mean values (centroids). The final cluster number error, calculated as the average error of the 10 cross-validations, was used to determine the optimal number of clusters (phenoregions), defined as the first of three consecutive final error reductions below < 5%, after addition of a further cluster (Fendereski et al., 2014; Oliver et al., 2004).

5.2.7.3 Region-specific phenological properties, interannual variability patterns and environmental determinants

Phytoplankton phenological metrics for each delineated SWIP phenoregion, and their interannual variability patterns, were investigated during the 18-year study period (1997 - 2015). Region-specific Chl-a time series, based on average Chl-a values and annual Chl-a

threshold criteria (5% above the yearly median; Siegel et al., 2002) for each phenoregion, were used to compute the regional phenological metrics (see section 5.2.7.1). Differences in phenological indices across SWIP phenoregions were tested using the non-parametric Kruskal-Wallis test, a one-way analyses of variance on ranks, and pair-wise comparisons using the Dunn's test (Statistica software, version 10.0). Spearman correlation coefficients (r_S) were used to evaluate relationships between phenological indices over each phenoregion.

Interannual trends in the phenological indices over each phenoregion were investigated using Generalized Additive Mixed Modelling (GAMM), a flexible class of statistical models that accommodates linear as well as complex non-linear relationships (Wood, 2006). Phenological indices were modelled as a cubic spline smoother function of time (year), using a first order autoregressive correlation structure to deal with temporal autocorrelation (for further details see Krug et al., *in press*). GAMM analyses were conducted with the "mgcv" library (version 1.8-11), in R statistical software, version 2.5.1 (R Core Team, 2016). Due to the relatively short time series (18-year), trends significant at the p-level < 0.10 were also considered. GAMM analysis was also used to decompose the seasonal and interannual components of Chl-a and environmental variable time series, for each delineated phenoregion, during the 18-year study period (for details see Krug et al., *in press*).

To investigate the environmental drivers underlying phytoplankton phenology and their interannual variability patterns over each SWIP phenoregion, phenological indices were compared with a set of environmental variables. These included ocean optical variables (PAR, I_m), ocean physical variables and related indicators (MLD, MDL:Z_{eu}, timing of MLD shoaling and deepening onsets), ocean chemical variables (NO_3, PO_4, Si and Fe), local hydrodynamic variables (CSET, Gdn and Gdq) and large-scale climate indices (MEI, NAO, EA, AMO, WeMO and WEPA). The strength of monotonic relationships between phytoplankton phenological indices and environmental variables, for each phenoregion, was evaluated using correlation analysis (r_S). This analysis was undertaken using values of the environmental variables acquired during the conditions preceding the time of bloom initiation (pre-bloom stage) or averaged during specific periods (e.g., winter: December to March; upwelling-favourable period: May to September) or the whole annual cycle (September to August). All tests were considered at a 0.05 significance level. However, the analysis of interannual variability in region-specific phenological indices and underlying environmental drivers,

namely climate-related variables, should be interpreted with caution due the uncertainties associated with the estimates of phenological indices (see Cole et al., 2012; Ferreira et al., 2014) and the relatively short time series (e.g., typical AMO period: 60-80 years; see Henson et al., 2010, 2016, 2017).

5.3 – Results

5.3.1 Phytoplankton phenology off SW Iberia: a pixel-based assessment

Basic statistical information on selected phytoplankton phenological indices over SWIP, extracted on a pixel-by-pixel basis for an 18-year period (1997 - 2015), is summarized in Table 5.1. Mean spatial distribution of the phenological indices exhibited a substantial spatial variability over the SWIP area, with remarkable cross-shelf gradients, organised with a strong spatial coherency (see Fig. 5.3). For most indices, maximum variability areas followed approximately the 500 m isobath within most of the GoC area, spreading towards the 1000 m isobath in the vicinity of CSM, and towards the 2500 m isobath near CSV and over the west Portuguese coast (Fig. 5.3A-E). However, in case of bloom peak timing, cross-shelf gradients were less pronounced over most of the GoC margin (Fig. 5.3F). For most phenological indices (Fig. 5.3A, 5.3B, 5.3D, 5.3E), latitudinal gradients were also detected over the oceanic SWIP domains, with a latitudinal discontinuity located at *ca*. 36.5^{o}N (Fig. 5.3).

The number of bloom events per year varied from one to two in most of the oceanic SWIP domain, and increased up to six over the Portuguese west coast, CSM and CT area (Fig. 5.3A). The average duration of phytoplankton blooms showed an opposite pattern, with more prolonged events over the oceanic domain, average duration varying from eight to 20 weeks, and an increasingly greater bloom duration from northern to southern open ocean areas. Over slope and coastal areas, bloom events lasted, on average, two to six weeks (Fig. 5.3B). The distribution of the total duration of all bloom events during each annual cycle (Fig. 5.3C) revealed a distinct intermediate area, located along the shelf edge to upper slope (ca. 200 m – 500 m isobaths), with lower values (15 to 16 weeks.year^{-1}), compared with coastal and oceanic SWIP (> 18 weeks.year^{-1}). Chl-a peak values varied, on average, between 0.33 µg L^{-1} and 8.86 µg L^{-1}, with highest values over the continental shelf, especially for the northeastern GoC areas impacted by the freshwater outflow of Guadiana and Guadalquivir estuaries (Fig. 5.3D). Over the oceanic SWIP area, a latitudinal gradient was also observed, with higher Chl-

a peak values north of ca. 36.5°N. The timing of the principal bloom initiation, represented in Week of the Year (WOY), generally showed a northward progression, namely for the open ocean domain (Fig. 5.3E). Principal blooms initiated earlier, between November and January (WOY: 9 - 17), for most of the oceanic domain and a narrow coastal fringe area, over the northeastern and southeastern GoC (Fig. 5.3E). Over most of the shelf and slope areas within GoC, and spreading towards the 2500 m isobath over the Portuguese west coast, the main phytoplankton blooms started, in general, later, between February and March (WOY: 21 - 25). The area over the west coast and shelf-edge around CSV presented a relatively delayed bloom initiation, usually occurring between April and May (WOY: 29 - 36). Chl-a peak timing over SWIP showed a more homogeneous spatial distribution, occurring during February-March (WOY: 21 - 27) for most of SWIP oceanic and coastal domains (Fig. 5.3F). However, a narrow coastal sector along northeastern and southeastern GoC displayed an anticipated bloom peak (January-February, WOY 16-22), whereas the western Portuguese margin, including the CSV area, displayed a delayed bloom peak (April-May, WOY 28-35; Fig. 5.3F).

Table 5.1 – Descriptive statistics of phytoplankton phenological indices over the southwest area off the Iberian Peninsula, estimated for each annual cycle, on a pixel-by-pixel basis, during the period September 1997 - August 2015 (n = 18 years x 8,570 pixels = 154,260). Information includes minimum (Min), maximum (Max) and mean values and standard deviation (SD). *refers to primary blooms for each year.

Phenological index	Min - Max	Mean ± SD
Number of bloom events per year (bloom events.year^{-1})	1 - 9	2.48 ±0.07
Total duration of all bloom events per year (weeks.year^{-1})	5 - 23	18.93 ±0.10
Average duration of bloom events (weeks.bloom^{-1})	2 - 23	11.21 ±0.20
Chlorophyll-a peak value (µg L^{-1})	0.19 - 18.48	0.86 ±0.23
Timing of the bloom initiation* (week of the year)	1 - 45	16.33 ±0.54
Chl-a peak timing* (week of the year)	1 - 46	24.27 ±0.57
Timing of the bloom termination* (week of the year)	2 - 46	29.25 ±0.55

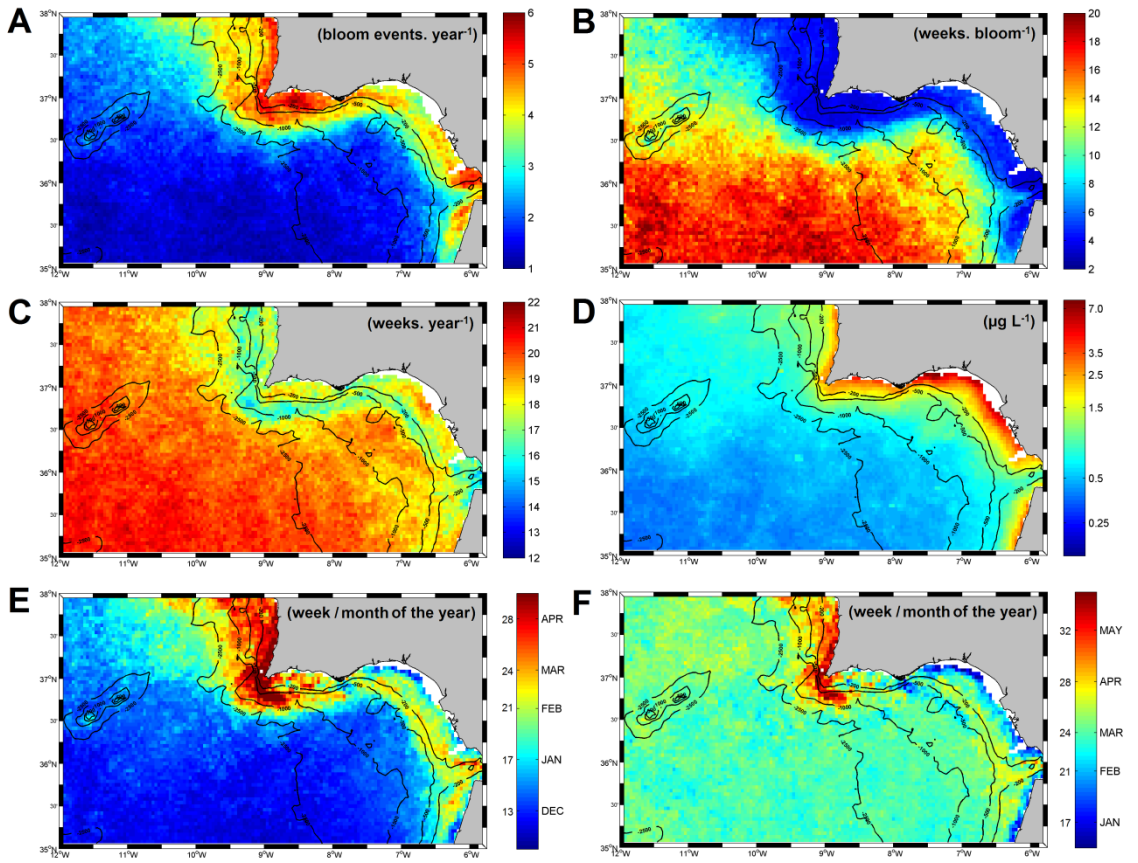

Figure 5.3 – Distribution of annual mean values of selected phytoplankton phenological indices over the southwest area off the Iberian Peninsula, estimated for each annual cycle, on a pixel-by-pixel basis, during a 18-year period (September 1997 - August 2015): (A) Number of bloom events per year; (B) Average duration of the bloom events; (C) Total duration of all bloom events per year; (D) Chlorophyll-a peak value; (E) Timing of the initiation of the primary bloom; and (F) Chlorophyll-a peak timing. Black lines represent the 200m, 500m 1000m and 2500m isobathymetric contours.

5.3.2 Phenology-based partition off SW Iberia

The selection of relevant partition variables to be included in HAC analyses was based on a dissimilarity dendogram, generated by the inversion of the correlation matrix of the six normalized phenological indices (see section 5.2.7.2). The indices Chl-a peak timing and total duration of all bloom events per annual cycle presented dissimilarity values above the defined threshold (0.10), whereas the remaining phenological indices showed dissimilarity values below this threshold. As consequence, a single index representative of this group of redundant variables was selected as a partition variable (Fig. D.1A). HAC analysis was run several times, each including one of these highly correlated redundant indices, in tandem with the two

dissimilar indices. Based on a higher spatial coherence of the resulting SWIP classifications (data not shown), the index number of bloom events per annual cycle was selected. The input dataset, representative of phytoplankton phenology over the SWIP area was, therefore, based on three phenological indices: Chl-a peak timing, total duration of all bloom events per year, and number of bloom events per year. Cross-validation errors associated with HAC analyses, estimated using a number of clusters (i.e, phenoregions) varying between 2 and 20, indicated that phytoplankton phenology over the SWIP area was optimally represented by five distinct phenoregions, with similar phytoplankton phenology patterns (Fig. D.1B).

The five delineated phenoregions over SWIP were organized coherently over the study area (Fig. 5.4A). The open ocean SWIP domain was predominantly associated with two regions: the SW Oceanic phenoregion, located over the southwestern SWIP oceanic domain, and the Oceanic phenoregion, covering most of the open ocean area over the GoC (depth > 500m) and the northwestern SWIP area (depth > 2500m). A single region was delineated over the SWIP continental margin, the Coastal-Slope phenoregion, which covered most of the coastal and slope areas. Notable exceptions were the west Portuguese coast and CSV area, covered by the Upwelling-influenced phenoregion, and the nearshore areas over the northeastern and southeastern GoC, covered by the River-influenced phenoregion (Fig. 5.4A).

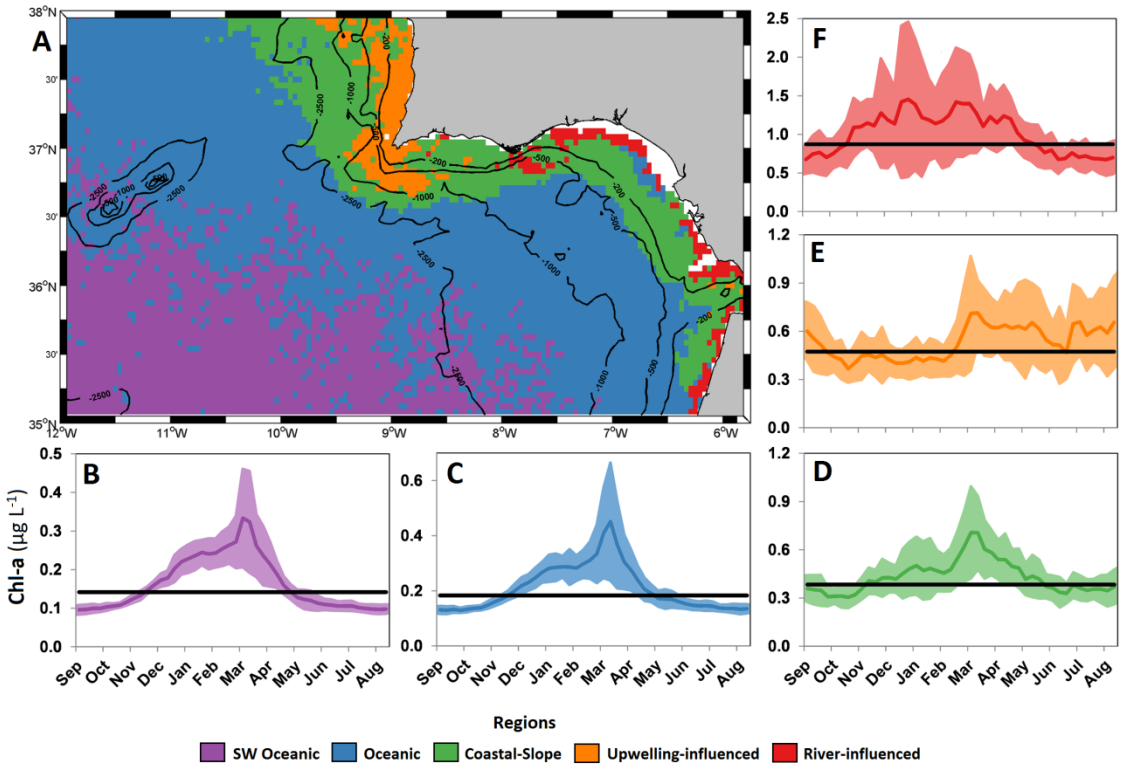

Figure 5.4 – Partition of the southwest area off the Iberian Peninsula (SWIP) into phenoregions based on phytoplankton phenological indices (number of bloom events per year, Chl-a peak timing and total duration of all bloom events per year), for the period between September 1997 and August 2015. (A) Spatial distribution of the five SWIP phenoregions. (B-F) Weekly-based phytoplankton climatological seasonal cycles, with mean chlorophyll-a (Chl-a) values (coloured lines) ± 1 standard deviation (shaded coloured areas) for each phenoregion: (B) SW Oceanic, (C) Oceanic, (D) Coastal-Slope, (E) Upwelling-influenced and (F) River-influenced regions. Black thick horizontal lines (B-F) represent the average annual Chl-a threshold criteria (5% above the yearly median) used to define a phytoplankton bloom for each phenoregion. Note different y-scales used for panels B to F.

5.3.3 Phytoplankton phenology off SW Iberia: a phenoregion-based assessment

Chl-a variability patterns during the 18-year study period (see complete Chl-a time series for each phenoregion in Figs. D.2-D.3) and weekly-based annual climatologies (Fig. 5.4B-F) varied across SWIP phenoregions. Both the SW Oceanic and Oceanic phenoregions presented low amplitude unimodal annual cycles. Phytoplankton bloom period occurred between November and May, for both oceanic phenoregions, with Chl-a maxima (0.34 - 0.41 µg L^{-1}) during February-March (Fig. 5.4B-C). The three coastal phenoregions presented higher Chl-a variability, longer periods with Chl-a above the threshold criteria, and blooms occurred during different periods of the year (Figs. 5.4D-F, D.2-D.3). The Coastal-slope phenoregion (Fig.

5.4D) showed a unimodal annual cycle, with Chl-a above the threshold between November and June, and Chl-a peak values (0.71 µg L^{-1}) during March. The Upwelling-influenced phenoregion presented a *quasi* bimodal annual cycle, with two distinct periods of Chl-a above the threshold criteria, February-June and June-September (Fig. 5.4E), and Chl-a peak values occurred during March (0.71 µg L^{-1}) and July (0.65 µg L^{-1}). The River-influenced phenoregion (Fig. 5.4F) presented a unimodal annual cycle, with Chl-a above the threshold between October-May, and Chl-a peak values between December and February (ca. 1.45 µg L^{-1}). At the interannual scale, Chl-a showed significant patterns only over the open ocean phenoregions, with strong linear increasing tendencies for both SW Oceanic and Oceanic regions ($p<0.001$; data not shown).

A total of 245 phytoplankton bloom events were identified over the five SWIP phenoregions during the 18-year study period, including 90 principal blooms and 155 secondary blooms mostly detected over the coastal phenoregions (Fig. 5.5A; see complete Chl-a time series, with identification of each bloom event, in Fig. D.3). Secondary blooms represented between 70% and 77% of the bloom events detected over the River- and Upwelling-influenced regions, respectively. In respect of phytoplankton phenology, a significant distinction between open ocean (SW Oceanic and Oceanic) and coastal (Coastal-slope, Upwelling- and River-influenced) phenoregions was detected for all phenological indicators (Fig. 5.5), except the total duration of all bloom events per year (20-24 weeks; Fig. 5.5B) and timing of bloom termination (Figs. 5.5I, 5.5L). SW Oceanic and Oceanic phenoregions usually showed a single prolonged (20-21 weeks) bloom event per year (Figs. 5.5A and 5.5D). Over the coastal phenoregions, bloom frequency was higher but highly variable, with from one up to seven events per year (Figs. 5.5A), and principal bloom duration varied from four to 25 weeks (Fig. 5.5D). Additionally, the duration of bloom accumulation phase (Figs. 5.5E) was significantly longer over the open ocean (*ca*. 15 weeks) in comparison with coastal phenoregions (*ca*. four to eight weeks). However, the duration of the bloom deceleration phase was similar among all phenoregions (*ca*. 5 to 8 weeks), except for the Upwelling-influenced region, which exhibited a shorter duration (*ca*. 2-3 weeks; Fig. 5.5F). Interestingly, the principal bloom event over open ocean phenoregions showed an accumulation phase significantly longer than the deceleration phase ($p<0.01$), whereas over coastal phenoregions the durations of these bloom phases were similar (Fig. 5.5E-F).

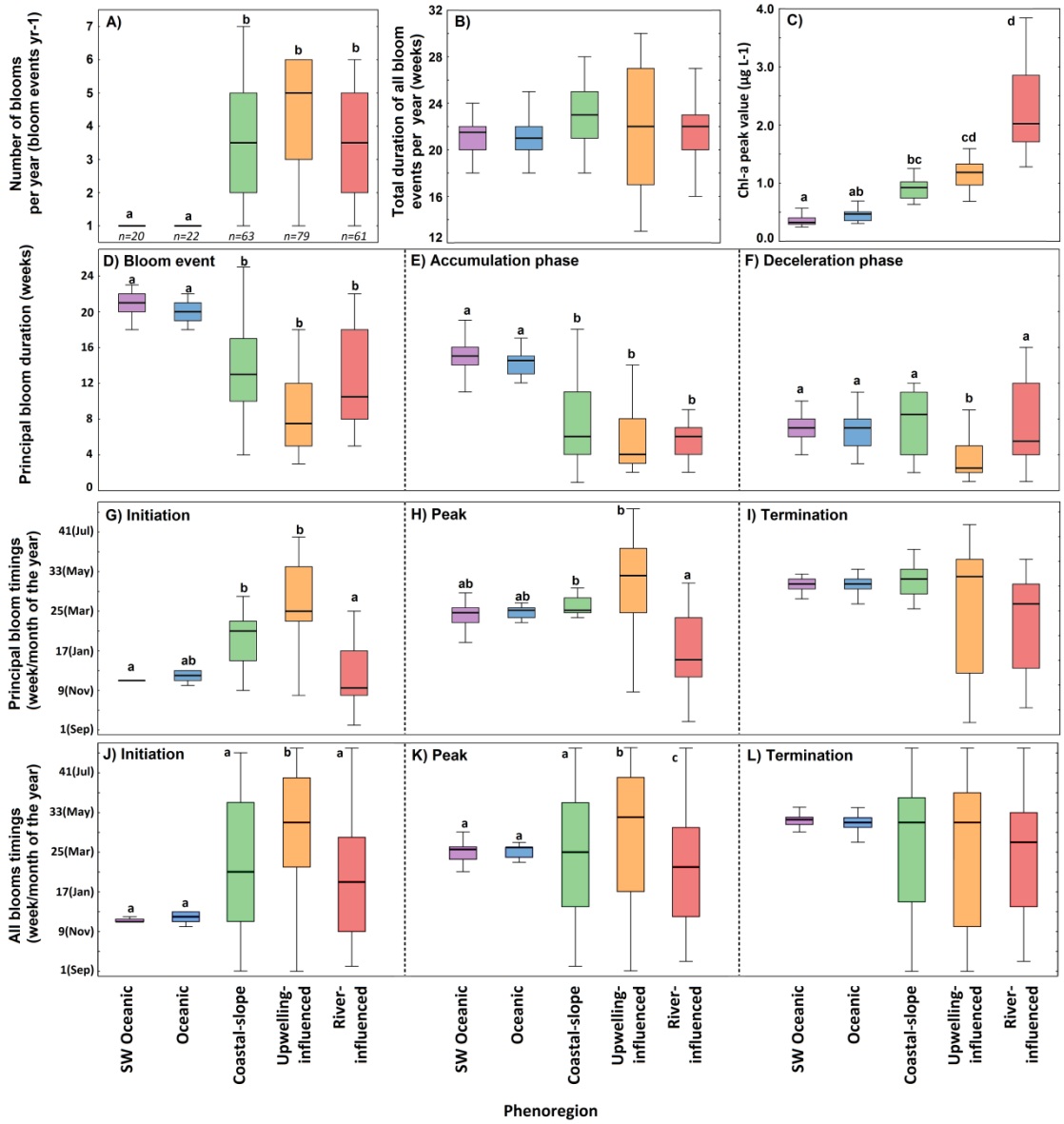

Figure 5.5 – Phytoplankton phenological metrics for the five phenoregions delineated off SW Iberia, estimated for each annual cycle during the period 1997 to 2015 (See Fig. 5.4 for region location and colour code). (A) Number of bloom events per year; (B) Total duration of all bloom events per year; and (C) Chlorophyll-a peak value. Considering only the principal blooms: (D) Duration of the bloom event, (E) duration of the bloom accumulation phase, (F) duration of the bloom deceleration phase, (G) Timing of bloom initiation; (H) Chl-a peak timing; and (I) Timing of bloom termination. Considering the average values for all bloom events (principal and secondary): (J) timing of bloom initiation; (K) Chl-a peak timing; and (L) timing of bloom termination. Median values are represented by the lines within the boxes, 25th to 75th percentiles are denoted by box edges and non-outlier limits are denoted by whiskers. For each phenological index, different lowercase letters over the bars represent significant differences across phenoregions ($p<0.05$). The number of blooms events identified during the study period for each phenoregion (n) is shown, in italics, in panel A.

The timings of initiation, peak and termination of the principal bloom over the open ocean and Coastal-Slope phenoregions were less variable than over the Upwelling- and River-influenced phenoregions (Figs. 5.5G-I). For SW Oceanic and Oceanic phenoregions, the principal bloom initiated around November (WOY: 10-11), during the MLD deepening phase (4.2±3.2 weeks after the onset of MLD deepening), peaked during March (WOY 25), 2.8±3.2 weeks after the onset of MLD shoaling, and terminated during April (WOY 29). Only a minor proportion of the principal oceanic blooms, 11 to 17% for SW Oceanic and Oceanic regions, respectively, effectively terminated during the MLD deepening stage. In comparison with open ocean, over the River-influenced phenoregion the timings of principal bloom initiation, termination and peak were similar, but highly variable (September to March, WOY 12-25). In fact, 17% of the principal bloom events (1998, 1999, 2001) initiated before the onset of MLD deepening, and 17% of the events initiated during the MLD shoaling phase (2005, 2008, 2013). With respect to this region, for Coastal-slope and Upwelling-influenced phenoregions, principal blooms initiated (on average in February, WOY 24; 15.6±9.4 weeks after the onset of MLD deepening) and peaked (on average in April, WOY 28; 6.9±9.1 weeks after the onset of MLD shoaling) significantly later, but no significant differences were detected in termination timing across phenoregions. Over the Coastal-Slope phenoregion, 38.9% of the principal bloom events initiated during the MLD shoaling, mostly before April, except for a single event (5.6%, year 2002) initiated afterwards. Conversely, over the Upweling-influenced region, a higher proportion of principal bloom events were initiated during the MLD shoaling stage (72.2%) and, from these events, a higher proportion (six events, 33.3%) initiated during the upwelling favourable period (May – September).

The phenological indices derived using all phytoplankton bloom events occurring each year, including principal and secondary blooms, also revealed a higher variability over the coastal phenoregions in respect to open ocean regions (Figs. 5.5J-L; see full Chl-a time series and bloom events in Fig. D.3). Bloom initiation consistently occurred earlier, between November and December (WOY: 11-12), for SW Oceanic and Oceanic phenoregions, whereas an extremely variable but usually delayed bloom initiation was detected over coastal phenoregions, significantly higher only for the Upwelling-influenced region; Fig. 5.5J). Over the latter phenoregion, 68.9% of the secondary bloom events (42 events) were initiated during the upwelling-favourable period (May-September), whereas this value was significantly lower for the Coastal-Slope region (46.7%, 21 events). However, for the Upwelling-influenced

phenoregion, no relation was found between the number of events within an year and the number of events initiated during favourable or unfavourable upwelling periods. Chl-a peak timing was consistently detected during March (WOY 25) for open ocean phenoregions, and was highly variable for coastal regions. For open ocean regions, significantly anticipated bloom peaks were observed over the River-influenced phenoregion (February, WOY 21), and delayed bloom peaks (April, WOY 28) were detected for the Upwelling-influenced region (Fig. 5.5K). No significant differences in the timing of bloom termination (March-April, WOY: 24-31) were detected across phenoregions (Fig. 5.5L). Chl-a peak values increased along the ocean-coastal gradient (Fig. 5.5C), with mean values ranging between 0.35 and 2.00 $\mu g\ L^{-1}$ for the SW Oceanic and River-influenced phenoregions, respectively.

Spearman correlation coefficients among all derived phenological indices, for each phenoregion, are presented in Table D.1. Strong negative correlations were detected between the number of bloom events per year and their annual average duration, for all phenoregions ($p<0.05$). Considering only the phenological indices associated with the principal bloom events for each year, bloom duration was positively correlated with the duration of both accumulation and deceleration phases over the three coastal phenoregions ($p< 0.01$), and with the duration of the accumulation phase over the SW Oceanic phenoregion ($p<0.05$). Moreover, the durations of the bloom accumulation and deceleration phases were inversely correlated for the two open ocean phenoregions ($p<0.01$). For indices related with timing of the principal bloom, the timing of bloom initiation was negatively correlated with bloom duration (i.e., early bloom initiation associated with longer blooms) over the Coastal-slope phenoregion ($p<0.01$), and negatively related with the duration of the bloom accumulation phase over the Oceanic and Coastal-slope phenoregions ($p<0.01$). Chl-a peak timing was positively correlated with the duration of the bloom accumulation phase over the open ocean (SW Oceanic, $p<0.01$; Oceanic, $p<0.05$) and River-influenced ($p<0.05$) phenoregions, and with the timing of bloom initiation over the River- and Upwelling-influenced phenoregions ($p<0.01$). The timing of bloom termination was positively correlated with bloom duration over the open ocean (SW Oceanic, $p<0.01$; Oceanic, $p<0.05$) and River-influenced phenoregions ($p<0.01$), with timing of bloom initiation over Oceanic and River-influenced phenoregions ($p<0.01$), and with Chl-a peak timing over the later ($p<0.01$). Chl-a peak value was negatively correlated with the timing of bloom initiation over the Coastal-slope phenoregion ($p<0.05$).

Interannual variability of the phytoplankton phenological indices during the 18-year study period was inspected, for each SWIP phenoregion, using GAMM analysis. Marginally significant ($p<0.10$) and significant ($p<0.05$) linear and non-linear interannual trends were detected for all SWIP phenoregions, with the exception of the Oceanic region (Fig. D.4; Table D.1). Over SW Oceanic phenoregion, the duration of the principal bloom ($p<0.10$) and its accumulation phase ($p<0.001$), and the Chl-a peak timing ($p<0.001$) showed significant non-linear trends; two periods of increasingly prolonged bloom accumulation and delayed bloom peaks were detected, before 2003 and after 2007. For the Coastal-slope phenoregion, both the total duration of all bloom events per year and the duration of the principal bloom displayed weak linear increasing trends ($p<0.10$). Over the Upwelling-influenced phenoregion, the duration of the bloom deceleration phase showed a strongly significant linear increase during the study period. For the River-influenced phenoregion, the total duration of all bloom events per year displayed a marginally significant non-linear trend ($p<0.10$), increasing linearly after *ca.* 2007. Moreover, the timings of the principal bloom initiation and termination exhibited a marginally significant linear increasing delay during the study period ($p<0.10$), whereas Chl-a peak timing showed a significant non-linear increase ($p<0.05$), with a generalized increasing delay until *ca.* 2007, and a subsequent stabilization (see Fig. D.4, Table D.1).

5.3.4 Region-specific drivers of bloom phenology off SW Iberia

The study period was characterised by a high variability in large-scale climate and local hydrodynamic forcings (see complete time series in Figs. D.5-D.6). Some environmental variables exhibited significant interannual linear trends (CSETwc: declining trend, i.e. upwelling intensification, $p<0.05$), whereas others showed non-linear monotonic (WeMO: declining trend, $p<0.05$) or complex trends (Gdq, $p<0.0001$; data not shown) during the study period. For physical, optical and chemical ocean variables, all variables showed significant seasonal patterns over all phenoregions ($p<0.001$). For interannual variability, linear increasing trends were detected in MLD over Coastal-slope ($p<0.001$) and Upwelling-influenced regions ($p<0.01$), and in NO_3 for all phenoregions ($p<0.01$), except the Upwelling- and River influenced region. In case of Fe, a linear increasing trend was detected over the River-influenced phenoregion ($p<0.01$), but a declining trend was observed for the open ocean phenoregions ($p<0.001$). PAR exhibited non-linear monotonic increasing trends for all phenoregions ($p<0.01$), and I_m interannual patterns ranged from a significant linear decline

over the Coastal-Slope ($p<0.01$) and Upwelling-influenced regions ($p<0.001$), to non-linear increases (SW Oceanic, $p<0.05$) or declines (River-influenced region, $p<0.001$). Moreover, significant interannual linear increasing delays in the onset timing of MLD deepening (SW Oceanic region, $p<0.05$; Oceanic region, $p<0.001$) and MLD shoaling (Upwelling-influenced region, $p<0.05$; River-influenced and Coastal-Slope regions, $p<0.01$; Oceanic region, $p<0.001$) were also observed (data not shown).

The physical conditions detected at the time of the principal bloom initiation, specifically MLD and I_m, were less variable over the open ocean regions. Mean (± 1SD) MLD values at the week of the principal bloom initiation ranged between 31.1±16.0 and 77.5±45.1 m, for River-influenced and Coastal-slope phenoregions, respectively, and was significantly lower for the former region (data not shown; $p<0.05$). Mean I_m values at the week of the principal bloom initiation fluctuated between 27.0±8.1 and 69.1±72.2 µmol photons m^{-2} s^{-1}, over the Oceanic and the Upwelling-influenced phenoregions, respectively, and no differences were detected across phenoregions. Conversely, the concentrations of dissolved inorganic nutrients (NO_3, PO_4, Si, and Fe) at the time of the principal bloom initiation showed significant differences across phenoregions, with higher values detected over coastal compared with open ocean phenoregions ($p<0.05$, data not shown). Mean concentrations of NO_3, PO_4, Si, and Fe ranged between 0.027±0.024 - 1.069±0.872 µM, 0.014±0.005 – 0.087±0.056 µM, 0.718±0.092 – 1.582±0.499 µM, and 0.449±0.050 – 1.419±0.151 nM, respectively, detected over the SW Oceanic and the River-influenced phenoregions.

The correlation coefficients between phytoplankton phenological indices and environmental abiotic variables, including large scale climate indices, local hydrodynamic processes and ocean physical, optical and chemical variables, for each SWIP phenoregion, are presented in Table 5.2. Over the SW Oceanic phenoregion, most significant correlations were related to large-scale climate indices. For this phenoregion, the number of blooms per year was positively correlated with winter AMO ($p<0.05$), and the Chl-a peak value was negatively associated with winter EA and positively correlated with maximum annual MLD and NO_3 during the pre-bloom stage ($p<0.05$). The duration of the primary bloom was negatively associated with annual AMO and positively correlated with annual WeMO ($p<0.01$). Interestingly, pre-bloom average Si was positively related to the duration of bloom accumulation phase but negatively correlated with the duration of the deceleration phase.

Moreover, Chl-a peak timing was positively correlated with NAO and Si ($p<0.05$), and bloom termination timing was negatively correlated with annual AMO and positively correlated with annual WeMO ($p<0.01$) and WEPA ($p<0.05$).

For the Oceanic region, physical-chemical conditions preceding the bloom initiation were more strongly related to all phenological indices than the large- and local-scale indices (Table 5.2). The number of blooms per year over this phenoregion was strongly positively correlated with PAR, and PO_4 ($p<0.01$), and weakly related with AMO and MEI ($p<0.05$). The total duration of all blooms per year was also directly related to PAR and PO_4 and Si, while Chl-a peak value was positively associated with NO_3 ($p<0.05$). Regarding the principal bloom, the duration of bloom accumulation phase was negatively correlated with NAO, MLD and MLD:Zeu ($p<0.05$), and positively correlated with PAR, Fe ($p<0.05$) and I_m ($p<0.01$). Contrarily, the duration of deceleration phase was negatively associated with I_m, Fe and EA ($p<0.05$). Moreover, the timing of bloom initiation was positively correlated with NAO, MLD, MLD:Zeu and NO_3, but negatively correlated with PAR, I_m ($p<0.01$) and Fe ($p<0.05$). The timing of bloom termination was negatively correlated with I_m ($p<0.01$) and positively correlated with Si ($p<0.05$).

Over the Coastal-slope phenoregion, the phenology indices were mainly correlated with NAO and Gdq, more strongly with the latter, with opposing effects (Table 5.2). The number of blooms per year and the timing of the bloom initiation were positively (negatively) associated with NAO (Gdq), while the duration of primary bloom and its deceleration phase were negatively (positively) associated with NAO (Gdq). Further, the duration of bloom accumulation phase was also directly related to Gdq and the timing of MLD shoaling onset ($p<0.05$), and inversely related to Fe ($p<0.01$). Chl-a peak value was negatively associated with NAO ($p<0.05$), and Chl-a peak timing was positively related to winter WeMO ($p<0.05$).

As for the previous phenoregion, phenological indices over the River-influenced region were also strongly related to both NAO and Gdq, and the relevance of WeMO was apparently stronger (Table 5.2). The number of bloom events per year was positively related to NAO, WeMO ($p<0.01$), Gdn ($p<0.05$), maximum annual MLD, and timing of MLD deepening onset ($p<0.05$). The total duration of all blooms per year was positively related to Gdn ($p<0.05$). Chl-a peak values were negatively related to NAO, I_m ($p<0.05$) and PAR ($p<0.01$), and

positively related to Gdq ($p<0.01$). Bloom duration, as well as its deceleration phase, were also negatively related to NAO, and positively related to Gdq ($p<0.01$). The timings of bloom initiation, peak and termination were indirectly related to annual WeMO ($p<0.05$), whereas the last two indices were also negatively correlated with NAO. In case of Chl-a peak timing, a weak positive relationship with Fe ($p<0.05$) was also detected.

In contrast to previous phenoregions, over the Upwelling-influenced region large-scale climate indices were not correlated with the phenological indices, and MLD values and deepening onset timing were apparently more relevant environmental determinants (Table 5.2). The total duration of all bloom events per year and winter mean MLD were negatively related ($p<0.05$). Moreover, the number of blooms per year was negatively correlated with annual MLD, MLD values preceding the bloom initiation, and MLD deepening onset timing, and positively related to Gdq and $CSET_{WC}$ conditions preceding bloom initiation ($p<0.05$). Chl-a peak values were positively associated with the aforementioned variables related to MLD (see Table 5.2) and Si ($p<0.05$), and inversely related to Gdq ($p<0.05$). Also, the duration of bloom accumulation phase was negatively related to NO_3 ($p<0.05$), and timing of bloom termination was strongly positively correlated with WeMO ($p<0.01$). Moreover, considering only the bloom events initiated during the upwelling-favourable period, significant negative correlations were detected between Chl-a peak value and timing with $CSET_{WC}$ conditions preceding the bloom events ($p<0.05$). No significant correlations were detected between the phenological indices and $CSET_{WC}$, considering the annual or the upwelling-favourable period.

Table 5.2 – Significant Spearman rank correlation values (r_S) between phytoplankton phenological indices and environmental determinants for the five phenoregions delineated off SW Iberia, estimated for each annual cycle during the period 1997 to 2015. Environmental variables include large-scale climate indices (NAO – North Atlantic Oscillation; AMO – Atlantic Multidecadal Oscillation; EA – Eastern Atlantic Pattern; MEI – Multivariate ENSO Index; WeMO – Western Mediterranean Oscillation; WEPA – West Europe Pressure Anomaly), local hydrodynamic variables (Gdn – Guadiana river discharge; Gdq – Guadalquivir river discharge), MLD values and MLD deepening and shoaling onset timings, and average environmental conditions preceding the initiation of the principal bloom. MLD – mixed layer depth; MLD:Zeu – Mixed Layer and Euphotic depths ratio; PAR – surface photosynthetically available radiation; I_m - mean PAR intensity in the mixed layer; NO_3 – nitrate, PO_4 – phosphate, Si – silicate, and Fe - iron concentrations, averaged within the first layer; $CSET_{WC}$ - cross shore Ekman transport off the western Portuguese coast. Underlined r_S indicate significant values at $p<0.01$.

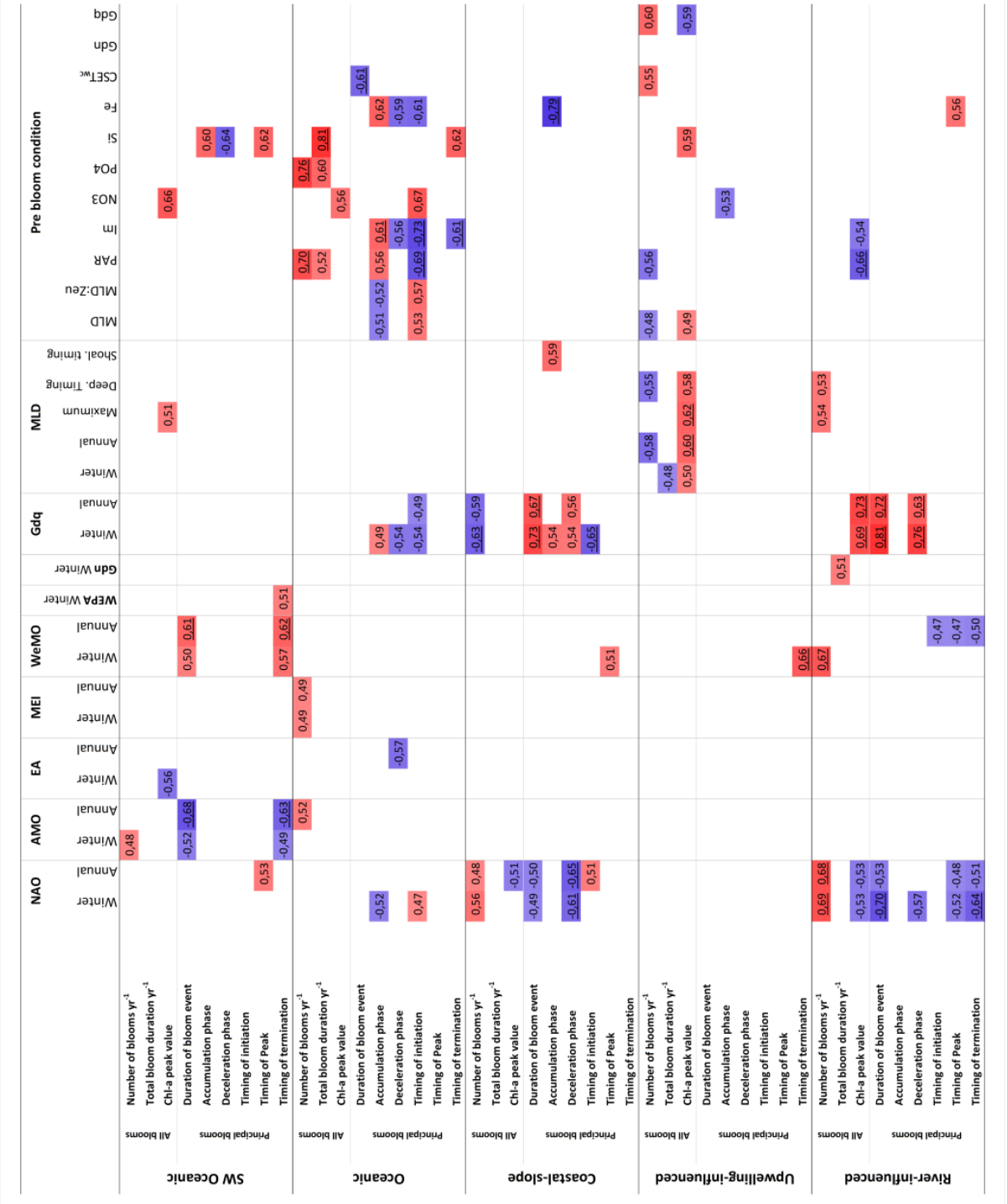
SW Oceanic
Oceanic
Coastal-slope
Upwelling-influenced
River-influenced
All blooms
Principal blooms
Number of blooms yr-1
Total bloom duration yr-1
Chl-a peak value
Duration of bloom event
Accumulation phase
Deceleration phase
Timing of initiation
Timing of Peak
Timing of termination
NAO
AMO
EA
MEI
WeMO
WEPA Winter
Gdn Winter
Gdq
MLD
Pre bloom condition
Winter
Annual
Winter
Annual
Winter
Annual
Winter
Annual
Winter
Annual
Winter
Annual
Winter
Annual
Winter
Annual
Maximum
Deep. Timing
Shoal. timing
MLD
MLD:Zeu
PAR
Im
NO3
PO4
Si
Fe
CSET_wc
Gdn
Gda

5.4 - Discussion

An 18-year time series of OCRS Chl-a was used to evaluate phytoplankton phenological patterns over the SWIP area, and subsequently used as the basis for an unsupervised, objective partition of the study area. In addition to the multiple benefits associated with the delineation of ecosystem partitions (e.g., biogeochemical modelling, marine spatial planning and ecosystem-based management strategies; see review by Krug et al., 2017), this SWIP partition was used as a framework for discriminating the environmental drivers of phytoplankton phenology over a complex marine domain (e.g., Sasaoka et al., 2011; Xu et al., 2013). Most phytoplankton global and regional phenology studies have addressed indices related to the principal annual bloom event (e.g., spring bloom), including bloom magnitude, timing and duration (e.g., Ueyama and Monger, 2005; Henson et al., 2006, 2010; Racault et al., 2012; Sapiano et al., 2012; Soppa et al., 2016; Kostadinov et al., 2017; see Friedland et al., 2016 and references therein). The number of studies evaluating multiple bloom events per year, usually two (e.g., spring and autumn blooms; Winder and Cloern, 2010; Martinez et al., 2011; Sapiano et al., 2012; Chiswell et al., 2013; Land et al., 2014; González Taboada and Anadón, 2014; Racault et al., 2015, 2017; Friedland et al., 2016) is, in fact, limited. Over complex coastal marine domains, such as upwelling-influenced areas with multiple bloom events per year (Foukal and Thomas, 2014), a more penetrating analysis of phytoplankton phenology is required. In the present study, in addition to the indices commonly associated to principal blooms, other indices were used, including the number of bloom events and the total duration of all events per year, and the duration of bloom accumulation and deceleration phases, as a way to enhance the comprehensive understanding of the processes shaping phytoplankton phenology, and their responses to environmental variability and change (Vargas et al., 2009). Our strategy delineated phenoregions over the heterogeneous SWIP domain, with distinct phenological indices and variable interannual trends and interactions with environmental variables (large scale climate indices, local scale hydrodynamic process indices, and ocean physical, optical and chemical conditions), enhancing the advantage of a partition-based strategy to investigate phytoplankton phenology features over heterogeneous regions (Zhao et al., 2013; Foukal and Thomas, 2014).

5.4.1 Phenology-based partition of the marine domain off SW Iberia

Our phenology-based static SWIP partition objectively delineated five regions over the SWIP area, including two over the oceanic domain and three phenoregions over the coastal and continental slope areas. This partition contrasts with global scale partitions, which subjectively imposed pre-defined rectilinear boundaries over the study region (e.g., Sherman, 1994; Longhurst, 2007; Spalding et al., 2007; 2012; see review by Krug et al., 2017). The phenology-based partition showed a remarkable spatial coherency, with clear coastal-offshore and latitudinal gradients. These gradients were also visible in previous unsupervised partitions, including the macroscale dynamic classification of the European seas (Hoepffner and Dowell, 2005), and the static (Krug et al., *in press*) and dynamic mesoscale SWIP partitions (chapter 3, also and hereafter Krug et al., *submitted*). The number of phenoregions was lower than the number of dynamic abiotic-based environmental provinces (up to 12; Krug et al., *submitted*), and static regions based on EOF dominant modes of Chl-a variability (9; Krug et al., *in press*), previously reported for the study area. Likewise, compared with the results of our study, a higher number of coastal regions (4) was identified in partition studies addressing the GoC (Navarro and Ruiz, 2006; Muñoz et al., 2015).

Our phenology-based partition clearly delimited the SWIP region with strongest upwelling intensity (Relvas et al., 2007), the Upwelling-influenced phenoregion, where upwelling patterns strongly modulate abiotic variables, phytoplankton biomass and annual cycles (Navarro and Ruiz, 2006; Goela et al., 2014; Krug et al., *in press, submitted*). The SWIP region with strongest influence of riverine discharges (Vargas et al., 2003; García-Lafuente et al., 2006; Caballero et al., 2014) was also differentiated, as the River-influenced phenoregion. Previous unsupervised partitions of the SWIP area also reflected the influence of coastal upwelling and riverine discharges (Navarro and Ruiz, 2006; Muñoz et al., 2015; Krug et al., *in press, submitted*). Over the open ocean, our unsupervised objective partition differentiated the southwesternmost area from the other oceanic domain, the SW Oceanic and Oceanic phenoregions (Fig. 5.4). These open ocean sectors were also differentiated in former SWIP partitions, based on Chl-a (Krug et al., *in press*) and abiotic variables (Krug et al., *submitted*). The former sector was previously associated with low to very low Chl-a (Hoepffner and Dowell, 2005), consistent with the oligotrophic nature of the eastern North Atlantic Subtropical Gyre province (Longhurst, 2007; Teira et al., 2005).

5.4.2 Phytoplankton phenological patterns off SW Iberia

During this 18-year study period, phytoplankton phenology patterns showed notorious differences between open ocean and coastal phenoregions (see Fig. 5.3), with increasing variability over the latter (Figs. 5.4 and 5.5). Despite the significant differences in the number of bloom events per year and bloom duration between open ocean and coastal phenoregions (Figs. 5.5A and 5.5D), the duration of all blooms events per year was similar across phenoregions (Fig. 5.5B). This similarity indicates that the environmental conditions that promote phytoplankton net growth rate (i.e., biomass accumulation) are more stable over the open ocean and more intermittent over coastal areas. Indeed, coastal areas are highly-heterogeneous transition zones (Cloern and Jassby, 2008; Winder and Cloern, 2010), with strong physical and chemical variability at short temporal scales, naturally imposed by the proximity with terrestrial sources and topographic irregularities, including riverine plumes, coastal upwelling events, and mesoscale circulation features, such as cyclonic and anticyclonic gyres (García-Lafuente and Ruiz, 2007; Relvas et al., 2007; Criado-Aldeanueva et al., 2009; Caballero et al., 2014).

Over the open ocean SWIP phenoregions, phytoplankton presented a unimodal annual cycle, and bloom events (*ca.* 1 year^{-1}) were prolonged (*ca.* 18-23 weeks), typically initiated around November, peaking in March and terminating in April. These phenological properties, including the absence of secondary autumn blooms, were consistent with those reported in global (Kahru et al., 2010; Cole et al., 2012; D'Ortenzio et al., 2012; Racault et al., 2012; Sapiano et al., 2012; Cabré et al., 2016) and basin-scale phenological studies which included the SWIP area (Siegel et al., 2002; Ueyema and Monger, 2005; Henson et al., 2009; Brody et al., 2013; Ferreira et al., 2014; Land et al., 2014; González Taboada and Anadón, 2014; Friedland et al., 2016). Over open ocean phenoregions, blooms mostly initiated during the MLD deepening stage (ca. one month after the timing of onset of MLD deepening), some blooms even terminated during this period, and mostly peaked during the MLD shoaling phase. I_m values at the time of bloom initiation (2.33±0.70 mol photons m^{-2} d^{-1}), usually interpreted as phytoplankton community compensation irradiance (*sensu* Sverdup, 1953), were consistent with published values of community compensation irradiance (ca. 1.0 - 3.6 mol photons m^{-2} d^{-1}; Siegel et al., 2002; Henson et al., 2006; Zhao et al., 2013). However, despite decreasing PAR, photoperiod and I_m values during the MLD deepening stage, light

conditions during this period were sufficient for phytoplankton exploitation of the new supply of nutrients entrained into the euphotic zone, leading to late winter-spring blooms. These events have been typically reported for subtropical regions, and interpreted as a sign of nutrient limitation (Follows and Dutkiewicz, 2002; Siegel et al., 2002; Longhurst, 2007). Conversely, over temperate and sub-polar regions (Henson et al., 2009; Lacour et al., 2015; Martinez et al., 2011; González Taboada and Anadón, 2014; Sallée et al., 2015), delayed spring blooms, usually initiated during the MLD shoaling phase, are interpreted as a sign of light limitation, in accordance with the critical depth hypothesis (Sverdrup, 1953).

Even if, from a bottom-up perspective, MLD deepening could effectively increase nutrient availability promoting bloom initiation, our data set does not allow the rejection of other alternative bloom initiation hypothesis (see reviews by Fischer et al., 2014; Franks, 2014; Chiswell et al., 2015; Cole et al., 2015 and references therein), including the critical turbulence hypothesis (Huisman et al., 1999), eddy-driven stratification hypothesis (Mahadevan et al., 2012) and the disturbance-recovery hypothesis (Behrenfeld, 2010; Boss and Behrenfeld; 2010; Behrenfeld et al., 2013). The latter predicts a net increase in Chl-a during the MLD deepening period, as observed over open ocean phenoregions, due to a decline in predator per capita ingestion rates of phytoplankton and grazing pressure induced by phytoplankton dilution. Thus, this (loss-driven) hypothesis could additionally support the initiation of phytoplankton blooms over these phenoregions (see Navarro et al., 2012; Krug et al., *in press*). Subsequent Chl-a increase and peak-values during the MLD shoaling phase probably reflect the effects of light-stimulation on phytoplankton growth rates (e.g., Sverdrup, 1953; Behrenfeld and Boss, 2014; Itoh et al., 2015). However, thoroughly testing the different hypotheses underlying bloom initiation, including the critical depth hypothesis (Sverdrup, 1953), would effectively require the measurement of short-term variability in vertical gradients of turbulence, which could allow the differentiation between the thoroughly mixed top layer (surface turbulent layer) and MLD derived from hydrographic data (see Franks, 2014), and *in situ* growth and mortality rates of phytoplankton.

Over the Coastal-slope phenoregion, Chl-a also presented a unimodal annual cycle but bloom duration (2-25 weeks), number of bloom events per year (*ca.* 3.5 events year^{-1}) and timing of bloom initiation were highly variable. Compared with open ocean phenoregions, bloom initiation was delayed over the Coastal-slope region, as also reported for other marine

domains (e.g., Liu et al., 2014), and a relatively large proportion of bloom events were initiated during the MLD shoaling phase (39% principal blooms and 60% all events), sometimes specifically during the upwelling-favourable period (May-September; Relvas et al., 2007; 14% principal blooms and 35% all events). These results are probably a reflection of reduced I_m values, due to higher turbidity (see Krug et al., *in press*, *submitted*) and increased nutrient availability due to the influence of continental sources (e.g., riverine sources: Caballero et al., 2014; Krug et al., *submitted*; submarine groundwater discharges: Hugman et al., 2015; Piló et al., *submitted*) and upwelling events (Krug et al., *in press*, *submitted*). Indeed, over this coastal phenoregion, high winter riverine discharge (Gdq) was significantly associated to earlier and longer bloom events ($p<0.01$; see Table 5.2). The beneficial influence of upwelling off the west Portuguese coast on the Coastal-Slope was particularly evident during Summer 2002, when four bloom events (2 - 8 weeks.event^{-1}) were detected during a period of strong upwelling intensity (see Fig. D.6). This influence is likely linked to the offshore advection of upwelling mesoscale filaments (Souza and Bricaud, 1992; Peliz et al., 2004; Sánchez et al., 2008), which can be extended beyond the 1000 m isobaths, at ca. 70 km from the west coast (Krug et al., *in press; submitted*).

In contrast to previous phenoregions, over the Upwelling-influenced region, Chl-a presented a bimodal annual cycle (Fig. 5.4E) and the region presented the highest number of bloom events per year (4.4 events year^{-1}). Frequent upwelling-driven phytoplankton blooms, associated with enhanced nutrient availability, have also been reported for western Iberia (e.g., Moita, 2001; Picado et al., 2014; Bode et al., 2015; Krug et al., *in press*) and other coastal upwelling systems (e.g., Carr and Kearns, 2003; Foukal and Thomas, 2014; Corredor-Acosta et al., 2015). In contrast to classic sustained phytoplankton blooms, in coastal upwelling systems, diatom blooms usually occur as a series of separate, recurrent short blooms, separated by upwelling-relaxation periods, when dinoflagellates often bloom (Pitcher et al., 2010; Smayda and Trainer, 2010). Over the Upwelling-influenced phenoregion, a large fraction of bloom events were initiated during the MLD shoaling phase (72% principal blooms and 80% all events), specifically during the upwelling-favourable period (33% principal blooms and 61% all events). Phenological studies addressing coastal upwelling systems have also reported a close linkage between phytoplankton phenology and upwelling intensity and patterns, with blooms mostly initiating during the upwelling active period (Henson and Thomas, 2007; Foukal and Thomas, 2014). Indeed, in our study, high upwelling

intensity (i.e., strong negative $CSET_{WC}$ values) preceding bloom initiation was significantly associated with a lower number of bloom events per year ($p<0.05$). This could be partially explained by the increased offshore horizontal advection of coastal phytoplankton, in upwelling filaments, eddies and meanders, during strong upwelling events (e.g., Pitcher et al., 2010; Foukal and Thomas, 2014; Palma et al., 2010), and/or longer blooms. Although no significant relationship was detected between upwelling intensity and bloom duration, the longest bloom event detected over this phenoregion, which initiated in May 2002, peaked in July and lasted a total of 18 weeks (see Fig. D.3), was associated to a period of persistently strong upwelling intensity over the west Portuguese coast (see Fig. D.6).

Over the River-influenced phenoregion, phytoplankton presented a unimodal annual cycle and, as for the other coastal phenoregions, multiple short bloom events along the year (*ca.* 3.4 blooms $year^{-1}$). This phenoregion receives multiple freshwater discharges, from the Guadiana and Guadalquivir rivers, coastal wetlands and lagoons (Ria Formosa and Doñana park), and small estuarine systems and rivers, including Piedras, Tinto-Odiel (northeastern GoC), Oued Loukkos and Sebou (southeastern GoC). Over this turbid Case-II water masses, satellite-derived Chl-a retrievals could represent an overestimate, especially during high discharge periods (IOCCG, 2000; Caballero et al., 2014; Picado et al., 2014). However a direct relationship between Chl-a and river discharge was previously reported for this area (coastal northeastern GoC) were derived using both OCRS (Navarro and Ruiz, 2006; Caballero et al., 2014; Krug et al., *in press*) and *in situ* collected data (Prieto et al., 2009; Huertas et al., 2006). Compared with the other coastal phenoregions, most bloom events initiated during the MLD deepening phase (as for open ocean regions), and a smaller fraction of the bloom events, were initiated during the MLD shoaling phase (33% principal blooms and 54% all events). Over this river-influenced phenoregion, phytoplankton phenological properties were strongly related to riverine discharge (Gdq), with prolonged and more intense bloom events, with longer deceleration phases ($p<0.01$), associated to higher discharges. Mechanisms underlying the positive effects of riverine discharge include its influence as a nutrient source (Cravo et al., 2006; Reul et al., 2006), probably more relevant for bloom duration and magnitude, and its role as a driver of water column stratification. Despite high turbidity (Caballero et al., 2014), due to salinity stratification, MLD shoaling could be anticipated within the area of influence of riverine plumes (Barbosa and Chícharo, 2011), thereby enabling earlier bloom initiation, compared with to the Coastal-Slope phenoregion.

5.4.3 Phytoplankton phenology off SW Iberia: interannual patterns and environmental drivers

During the 18-year study period, significant interannual trends in putative phytoplankton drivers were detected, namely a weak linear intensification of upwelling intensity over the Portuguese west coast, a complex non-linear pattern in riverine discharge and a (linear and/or monotonic) increase in MLD over the coastal phenoregions (for comparison, see Krug et al., *in press*). Furthermore, previously unreported trends over the SWIP area were also detected, including linearly-increasing delayed MLD deepening (over open ocean phenoregions) and shoaling onsets (except SW Oceanic), and a linear increasing pattern in NO_3 (except over Upwelling-influenced phenoregion). Taking into consideration the interannual variability in the environmental forcing over SWIP, the sea surface warming reported over the area (Baptista et al., *in press*), previous phenological studies (see section 4.2), as well the strong linkages between Chl-a and large-scale climate indices, upwelling intensity, riverine discharge and MLD over SWIP (see Krug et al., *in press*, and references therein), alterations in phytoplankton phenological indices during the study period are expected to occur, and vary among phenoregions.

Indeed, this study revealed across-region differences in interannual patterns of phenological indices and their linkages with large-scale climate indices, local-scale hydrological processes and ocean abiotic variables. A remarkable spatial variability in the environmental drivers of phytoplankton phenology over particular ocean basins (e.g., Henson et al., 2009; Kahru et al., 2010; Martinez et al., 2011; Sasaoka et al., 2011; González Taboada and Anadón, 2014; Lacour et al., 2015; Friedland et al., 2016), or even specific marine domains (e.g., Song et al., 2010; Lavigne et al., 2013; Zhao et al., 2013; Foukal and Thomas, 2014; Mayot et al., 2015), was also previously reported, thus stressing the relevance of our phenoregion-based analysis. The inclusion of other phytoplankton drivers frequently related to phenology, including abiotic environmental variables (e.g., sea surface temperature, heat fluxes, wind speed and direction, turbulence, eddy kinetic energy; Ueyama and Monger, 2005; Henson et al., 2006; Yamada and Ishizaka, 2006; Kahru et al., 2010; Martinez et al., 2011; Song et al., 2010, 2011; Racault et al., 2012; Zhao et al., 2013; Foukal and Thomas, 2014; González Taboada and Anadón, 2014; Shiozaki et al., 2014; Cole et al., 2015; Friedland et al., 2016), as well as top-down controls (e.g., grazing, viral lyses, sedimentation; e.g., Behrenfeld, 2014; Friedland et

al., 2016; Martinez et al., 2016; Zarubin et al., 2017) would likely promote a more robust understanding of phytoplankton phenology and controls over the SWIP region and should be explored according to data availability.

5.4.3.1 Open Ocean phenoregions

GAMM analysis identified complex non-linear interannual patterns in bloom peak timing and duration, more notable for the duration of the accumulation phase, over the SW Oceanic region, and no significant trends over the Oceanic region (Fig. D.4). Previous studies, based on linear analysis, a stiffer approach, reported no significant trends in spring bloom duration, magnitude and initiation timing over the SWIP region (Racault et al., 2012; Land et al., 2014). Yet, Kahru et al. (2010) detected a linearly increasing delay in bloom peak timing over this region. Further, González Taboada and Anadón (2014) and Zhang et al. (2017) also reported significant but spatially variable, in some cases contrasting, linear trends, for both bloom magnitude and timing over the SWIP area, thus supporting the relevance of a phenoregion-based analysis.

Phenological variability over the SW Oceanic region was mostly related to large-scale climate indices. Prolonged blooms, with delayed termination, were associated with low AMO and high WeMO periods, and delayed Chl-a peaks were related to high NAO conditions. The interpretation of these phenology-climate linkages is not easy since the effects of different climate indices can interact, and control different phytoplankton bottom-up and top-down controls (e.g., Friedland et al., 2016; Martinez et al., 2016). Low AMO periods are usually associated with a reduction in water column stratification and SST over the North Atlantic (Martinez et al., 2009), also off Iberia (Santos et al., 2011a), thereby enhancing the vertical advection of nutrients into the euphotic zone, and the duration of phytoplankton blooms. AMO was also negatively associated with Chl-a variability over the SWIP open ocean domains (see Krug et al., *in press*), and considered a relevant driver of phytoplankton biomass (Martinez et al., 2009) and phenology over the North Atlantic basin (D'Ortenzio et al., 2012; Martinez et al., 2016). For most of the eastern-central North Atlantic, previous studies have also reported shorter (Racault et al., 2012) and early bloom initiation (Ueyama and Monger, 2005; Friedland et al., 2016) during low NAO periods, usually associated with decreased (western) wind-induced vertical mixing and higher I_m. However, over the SW Oceanic region,

a nutrient limited domain, NAO was not associated to bloom initiation or duration. Instead, low NAO periods were associated to anticipated Chl-a peak timings, and other NAO-induced alterations over SWIP should be also considered (for a review on NAO impacts see Krug et al., *in press*). The lack of significant relationships between NAO and bloom initiation timing was also reported for the SWIP area and the subtropical North Atlantic (Henson et al., 2009).

Maximum MLD values and NO_3 conditions preceding bloom initiation were directly associated with bloom magnitude (Chl-a peak values), reinforcing the relevance of vertical mixing and nutrient limitation over the SW Oceanic phenoregion, where the light is likely less limiting. However, the interannual linear increasing delay in the initiation timing of MLD deepening was not associated to changes in bloom initiation timing. Previous studies have also found strong linkages between MLD or its timing metrics (e.g., initiation of mixed layer shoaling) and phytoplankton phenology over North Atlantic (e.g., Follows and Dutkiewicz, 2002; Siegel et al., 2002; Henson et al., 2009; Martinez et al., 2011; Zhai et al., 2011; Lavigne et al., 2013; Zhao et al., 2013; Ferreira et al., 2015; Lacour et al., 2015) and other marine domains (e.g., Yamada and Ishizaka, 2006; Yoo et al., 2008; Chiswell et al., 2013; Lavigne et al., 2013; Shiozaki et al., 2014), with usually opposing effects in subtropical (nutrient limited) *versus* temperate-polar (light limited) areas. Direct linkages between MLD, wind speed and phenological indices have been also reported (Ueyama and Monger, 2005; Yamada and Ishizaka, 2006; Henson et al., 2006; Martinez et al., 2011; González Taboada and Anadón, 2014).

Over the Oceanic phenoregion, NAO was apparently more relevant than AMO, and early bloom initiation was associated with low NAO periods, as reported for the temperate eastern-central North Atlantic (Ueyama and Monger, 2005; Henson et al., 2009; Friedland et al., 2016). NAO variability has been associated with changes in several coastal variables and processes over SWIP and adjacent areas, and is positively correlated with SST and upwelling intensity over the west Iberia (deCastro et al., 2006; Santos et al., 2011; Pardo et al., 2011), and negatively related to zonal westerly winds, wave height (Kumar et al., 2016), storminess (Plomaritis et al., 2015) and precipitation (Martin-Vide and Lopez-Bustins, 2006). Thus, during negative NAO periods, the intensification of wind-induced mixing could lead to increased availability of nutrients, triggering earlier blooms, with prolonged accumulation phases. Over the Oceanic region, higher MLD and lower PAR and I_m conditions preceding the

bloom initiation were associated to delayed bloom initiation and shorter accumulation phases, an expected condition as open ocean blooms generally started during the MLD deepening phase (see section 4.2). Delays in bloom initiation associated to enhanced vertical mixing have been also reported for subpolar North Atlantic (Ueyama and Monger, 2005; subpolar Henson et al., 2009). Yet, the strong positive association between NO_3 and bloom magnitude (see Song et al., 2010) and initiation timing probably reflected the signature of nutrient limitation over this phenoregion. Over this region, timing of bloom initiation was not related to bloom duration, as reported by other studies (e.g., Racault et al., 2012; González Taboada and Anadón; Friedland et al., 2016), but early blooms showed longer acceleration phases and shorter deceleration phases.

The Oceanic phenoregion was the only region depicting significant relationships between MEI and phytoplankton phenology. ENSO patterns and MEI have been reported as strong determinants of interannual variability in phytoplankton biomass and phenology over tropical regions, namely in the Pacific Ocean (Yoo et al., 2008; Boyce et al., 2010; D'Ortenzio et al., 2012; Racault et al., 2012; Foukal and Thomas, 2014; Corredor-Acosta et al., 2015). However, a recent study also reported significant MEI effects on phytoplankton phenology at a global scale, sometimes with opposing regional effects (Racault et al., 2017). For the non-tropical sectors of North Atlantic, positive MEI periods were associated with the enhancement of cyclonic wind and water column mixing that increase turbulence and reduce light availability, thereby reducing and delaying phytoplankton growth (Racault et al., 2017). Yet, over the SWIP area, this global study reported weaker and spatially variable linkages between MEI and phytoplankton phenology. In the present study, MEI was weakly positively correlated with the number of blooms per year over the Oceanic phenoregion, with a higher number of bloom events per year (two.year^{-1}) usually associated with high MEI, El Nino years (1997/1998, 2002/2003, and 2004/2005).

5.4.3.2 Coastal phenoregions

Interannual patterns in phenological indices were variable across the three coastal phenoregions, reflecting the higher complexity of environmental forces driving phytoplankton biomass and phenology over SWIP coastal areas (see Krug et al., *in press*, and references therein). GAMM analysis identified linear increases in bloom duration and its deceleration

phase, for the Coastal-slope and Upwelling-influenced regions, respectively, and a linear increasingly delay in the timings of bloom initiation and termination for River-influenced regions (see Fig. D.4). Previous phenological studies addressing the SWIP region generally used global or large scale spatial coverages (Kahru et al. 2010; Racault et al., 2012; González Taboada and Anadón, 2014; Land et al., 2014; Zhang et al., 2017), thus not allowing the inspection of trends in phenology over specific SWIP coastal domains.

Over the Coastal-slope phenoregion, negative NAO and high Gdq values were associated with a reduced number of bloom events per year, and earlier, longer and stronger principal blooms. As previously reported (see section 4.3.1), during negative NAO periods, the intensification of wind-induced mixing, precipitation and river discharge, could lead to increased availability of nutrients, triggering earlier principal blooms and sustaining stronger and prolonged blooms. The positive correlation between NAO and the number of bloom events per year probably reflected the effects of NAO on the intensity of coastal upwelling over this region. As previously discussed (see section 4.2), strong upwelling events over the west coast, occurring during high NAO periods, could transport Chl-a rich mesoscale filaments into the Coastal-slope region, supporting the development of multiple short-lived bloom events during the upwelling-favourable period (see Krug et al., *in press*).

Over the Coastal-slope region, interannual variability in river discharge (Gdq) was related to most phenological indices. High Gdq discharge periods were associated with persistent increases in turbidity and extended river plumes, affecting adjacent coastal areas (Caballero et al., 2014) within this phenoregion (Fig. 5.4A). These low-salinity nutrient-rich river plumes could promote an earlier stratification of the water column (Tweddle et al., 2010; Barbosa and Chícharo, 2011), thereby supporting an earlier initiation of phytoplankton blooms. Periods of high river discharge were also associated to prolonged bloom events over the Coastal-slope region, probably a result of increased nutrient availability associated to direct freshwater inputs (e.g., Guadiana and Guadalquivir rivers discharge; Caballero et al., 2014), submarine groundwater discharges (e.g., Hugman et al., 2015), or wet atmospheric deposition (Thompson et al., 2015; Zou et al., 2000). Interestingly, over this phenoregion, early bloom initiation was strongly associated to longer blooms, with prolonged accumulation phases and more intense events (higher Chl-a peak values). The association of timing and duration was previously observed in different ocean basins and associated to prolonged periods of nutrient

availability and reduced grazing pressure, under lower temperature (Racault et al., 2012; Friedland et al., 2016). However, the association between timing and magnitude was variable across marine systems (see Henson and Thomas, 2007; Henson et al., 2009; Song et al., 2011; Friedland et al., 2016).

Over the River-influenced region, negative NAO and high Gdq were also associated with longer and stronger principal blooms, with prolonged deceleration phases. In addition, negative NAO and WeMO periods were associated with a reduced number of blooms per year, with delayed peak and termination timings. Both NAO and WeMO indices have been described as strong modulators of precipitation and river discharge over Iberia, with NAO being more influential for southern rivers (Martin-Vide and Lopez-Bustins, 2006), and Chl-a variability in the study area (Krug et al., *in press*). Our dataset indeed showed higher river discharge during negative NAO periods (Figs. D.5 and D.6). River discharge is the most relevant source of inorganic nutrients (Cravo et al., 2006; Reul et al., 2006) and turbidity (Caballero et al., 2014). During negative NAO, high river discharge periods, increased nutrient availability probably supported prolonged and more intense blooms, with delayed peak and termination timings over the River-influenced phenoregion. Then, the linear increasing delay in the timing of bloom initiation and termination, and non-linear increasing delay in peak timing (Fig. D.4) detected over this region, during the study period, were probably related with river discharge patterns.

Over the Upwelling-influenced phenoregion, principal blooms occurred during multiple periods of the year, initiating both during the late winter-early spring period but also during upwelling-favourable period. This complexity probably constrained the analysis of interannual patterns in phytoplankton phenology, based predominantly on principal events for each year, also limiting the detection of linkages between phytoplankton phenology and environmental drivers. The highly significant linear increasing tendency in the duration of the bloom deceleration phase detected over this region (Fig. D.4) is difficult to interpret, and should be in-depth explored. Future evaluation of interannual trends in phytoplankton phenology over this region should discriminate different periods of the year (e.g., upwelling favourable and unfavourable periods).

Studies addressing other coastal upwelling systems have reported that interannual variability patterns in phytoplankton phenological indices and underlying environmental drivers vary across-regions. In the Southern California Bight, bloom timing and magnitude showed irregular interannual patterns, with no relationship to commonly-known environmental drivers (e.g., SST, wind, upwelling intensity; Kim et al., 2009). However, variable trends across regions, and significant linkages between bloom timings and upwelling intensity, onset timing of upwelling-favourable winds and ENSO were reported for the California Current System (Henson and Thomas, 2007; Foukal and Thomas, 2014). Off central-Southern Chile (Humboldt Upwelling System), ENSO was also a relevant driver of bloom duration, and upwelling season onset showed similarity with onset of bloom events (Corredor-Acosta et al., 2015).

In the present study, significant relationships between environmental drivers and phytoplankton phenology were only detected for phenological indices based on all blooms, including principal and secondary events (see Table 5.2). High mean annual and winter MLD values and delayed MLD deepening onset were associated with fewer and stronger blooms per year, probably reflecting the stimulatory effects of increased nutrient availability on late winter-early spring events, which represented ca. 67% of all events over this phenoregion. In contrast to previous studies (Henson and Thomas, 2007; Foukal and Thomas, 2014; Corredor-Acosta et al., 2015), no effects of upwelling intensity were detected on bloom timing or magnitude over this phenoregion. Conversely, stronger upwelling intensity preceding principal blooms (i.e., lower $CSET_{wc}$) was associated to fewer bloom events per year, but there was no association between the number of bloom events in an year and the proportion of these events initiating during upwelling-favourable or unfavourable periods (data not shown). The phenological alterations that could be anticipated considering the linear intensification in upwelling intensity over this region (see also Krug et al., *in press*), including a delay in principal bloom timings and an increase in the duration and intensity of bloom events during the upwelling-favourable season, were in fact not detected. Over this phenoregion, the stimulatory effects of intensified upwelling might be masked by concurrent environmental changes, negatively affecting phytoplankton (e.g., ocean warming; Baptista et al., *in press*). Moreover, phytoplankton in coastal upwelling systems are adapted to frequent disturbances, and considered inherently more resilient to environmental variability (see Bode et al., 2015; Krug et al., *in press*)

5.5 - Conclusions

An 18-year time series of satellite-derived Chl-a was used to explore phytoplankton phenological patterns, and phenological indices were directly used for objectively partitioning the heterogeneous SWIP area. Our analysis identified five spatially coeherent phenoregions, including two open ocean and three coastal regions, with similar phenological patterns.

Over the open ocean phenoregions, a single, low magnitude bloom per year typically initiated around November, lasting 18-23 weeks. Bloom initiation occurred during the MLD deepening phase, and significant associations between phenological indices and NO_3 and MLD probably reflected the relevance of nutrient limitation over these phenoregions. Changes in basin-scale climate indices, namely AMO and NAO, were also relevant drivers of bloom duration and timing over the SW Oceanic and Oceanic phenoregions, respectively. Coastal phenoregions presented multiple (average: 4 blooms $year^{-1}$), short (average: 8 weeks) bloom events throughout the year, higher intra-annual variability, and more complex linkages with environmental drivers. A significant proportion of the coastal blooms initiated during the MLD shoaling phase, indicating the increased relevance of light limitation for these nutrient rich regions. The River-influenced region showed an earlier bloom initiation (September-March), in respect to Coastal-Slope (November-March) and Upwelling-influenced phenoregions (November-June). Both NAO and Gdq were relevant environmental drivers of phenological patterns over the Coastal-Slope and River-influenced regions, affecting the number of blooms per year, bloom magnitude, duration and timing. Over the Upwelling-influenced region, linkages between environmental determinants and phenology were restricted to indices integrating all blooms per year, both principal and secondary events. No significant effects of basin-scale climate indices and upwelling intensity on principal bloom magnitude, timing or duration were detected over this complex phenoregion.

Interannual patterns in phenological indices and the underlying effects of climate-sensitive local variables (MLD, PAR, nutrients), river discharge, upwelling intensity, and regional and basin-scale climate indices (NAO, AMO, WeMO) varied across phenoregions. The occurrence of complex, non-linear interannual patterns, detected for some phenological indices, highlight the need of flexible statistical approaches, not limited to linear regression analyses, for exploring phenological trends. Globally, our phenology-based unsupervised

approach promoted a biologically-relevant SWIP partition, which enabled the exploration of processes driving phytoplankton phenology over a complex marine domain. Phenoregion-specific linkages between environmental forcing and phenology over the SWIP area reinforce the need to implement a proper geographic partition for the analysis of phytoplankton dynamics and phenology, namely over coastal areas.

CHAPTER 6

CONCLUDING REMARKS

6.1 General conclusions

The present study aimed to partition the SWIP ocean surface, and use it for assessing the variability patterns of phytoplankton and underlying environmental drivers, using their inherent spatial heterogeneity. The effectiveness of the partitioning strategies applied was increased by the use of two important elements. First, the use of satellite remote sensing as a data source, which provided a large set of relevant variables with long uninterrupted study periods (10 to 18 years) and relatively fine spatial and temporal resolutions (4 km, 8 to 16-day). Second, the use of objective partition methods (HAC, Chapters 3 and 5; EOF, Chapter 4), which provided a less-biased delineation of partition units (environmental provinces, Chla-regions and phenoregions) through the unsupervised exploration of the datasets. The resulting partitions showed consistency with previous work on the study area, therefore providing a plausible representation of SWIP ocean surface patterns.

The partition strategies employed in this thesis comprised two levels of temporal representation: dynamic (Chapter 3) and static (Chapters 4-5). The use of the dynamic approach showed additional advantages by allowing the evaluation of the temporal dynamism of abiotic property spatial patterns, as well as the assessment of the relative stability of areas and periods, highlighted by EP core maps. Nonetheless, all partition strategies offered valuable insights on environmental and phytoplankton spatial and temporal variability over SWIP. Chl-a regions (Chapter 4) and phenoregions (Chapter 5) resulted from partitions based on input datasets consisting of or including phytoplankton (biotic) information, whereas the EPs (Chapter 3) were the outcome of a partition based solely on the abiotic environment. The strategy applied on the EPs delineation relied on a common premise in plankton ecology, that physical-chemical forcing has strong control over phytoplankton. Indeed, further analyses of EPs phytoplankton variability and a quantitative comparison with Chl-a regions corroborated this assumption for SWIP, thus supporting the biological relevance of this abiotic-based partition.

The three different strategies produced a distinct number of partition units within SWIP, from five phenoregions up to twelve EPs. The spatial distribution of these partition units shared some general similarities. The spatial arrangement of the partition unit boundaries showed a distinction between coastal and open ocean SWIP areas and a latitudinal separation (*ca.*

36.5^{o}N) over the open ocean area. Over the coast and continental slope domains, the influence of coastal upwelling off the west Portuguese coast and Cape São Vicente areas, and river discharges along the northeastern Gulf of Cadiz were further discriminated. The variability of phytoplankton biomass (Chl-a) and phenology patterns also followed these spatial configurations, and presented the lowest variability over the southernmost open ocean partition units (south of 36.5^{o}N), increasing towards the coast, with highest variability near riverine discharge influenced areas. The increased variability of phytoplankton over the coast reflected the complexity aggregated by the proximity of terrestrial discharges and enhanced mesoscale circulation intensified by winds, topographic irregularities and upwelling filaments. Several environmental variables were evaluated as potential drivers of phytoplankton variability over SWIP. These included local physical, chemical and optical variables, hydrodynamic variables (riverine discharges and intensity of coastal upwelling), and large scale climate oscillation indices (MEI, AMO, NAO, EA, WEPA, WeMO).

All partition strategies detected strong intra-annual variability, with significant seasonal patterns for both environmental (Chapters 3-5) and phytoplankton variability (Chapters 4-5). Overall, the strong seasonality reflected the effects of large scale variability in atmospheric forcing, typical of temperate and subtropical zones, leading to changes in ocean surface circulation and coastal processes, affecting nutrient and light availability and, consequently, phytoplankton growth and biomass. In the open ocean SWIP, Chl-a increased systematically during late winter-early spring, with a single, low magnitude, long lasting bloom event every year. This uni-modal annual cycle, typically initiated around November, was propelled by changes in the water column stability, confirmed by the abiotic properties of cold period EPs (lower SST, deeper MLD, higher nutrient concentration). Over the coast, seasonal variability increased significantly with multiple bloom events throughout the year, with varying duration and timings. Seasonally, a notorious secondary Chl-a increase occurred during summer in regions under the influence of coastal upwelling, occasionally surpassing the late winter-early spring bloom in terms of magnitude. Warm period EPs over this sector presented strong V and W^{3} and lower SST, indicative of coastal upwelling, and the upwelling index CSET was significantly correlated with both phytoplankton and EPs area coverages over these SWIP domains. Over the coast, river discharge was another important driver, affecting significantly EPs area coverage and phytoplankton phenology (bloom frequency, magnitude, timing and duration). The highest Chl-a values were consistently presented by the partition units closer to

the Guadiana and Guadalquivir river mouths, where freshwater fluxes represented a significant source of inorganic nutrients during the cold period, also affecting turbidity and (haline) stratification.

Interannual variability patterns in EPs area coverage and phytoplankton were more complex, varying across SWIP regions, but significant trends were mostly detected within the Gulf of Cadiz. Over this domain, the area coverage of open ocean and coastal and slope EPs showed a non-linear shift (Chapter 3). During the first half of the study period (up to ca. 2006), the area covered by coastal and slope EPs decreased whereas two oceanic EPs displayed increasing area coverage, probably as a result of river discharge variability. Chl-a variability showed opposing interannual trends, with a declining trend over the coast and an increasing trend over open ocean Chl-a regions within the Gulf of Cadiz (Chapter 4). These were likely a consequence of between-region differences in the relative roles of nutrient and light limitation, corresponding to significant interannual increases in wind speed and mixed layer depth. With respect to trends in phytoplankton phenology, significant interannual patterns indicated increased duration of blooms and their deceleration phase over the Coastal-slope and Upwelling-influenced phenoregions, respectively, and a delay in bloom timings over the River-influenced region (Chapter 5). Environmental variability showed no clear relationships with these phenological patterns, although the observed decrease in riverine discharge could explain the delay on bloom timing within the Gulf of Cadiz coastal region, due to a reduction in nutrient availability. The interannual increase in upwelling intensity over the west coast, detected during the study period, was not associated to changes in Chl-a, or principal bloom magnitude and timing. Climate oscillations affected, directly and indirectly, multiple local scale phytoplankton drivers, usually presenting significant but minor effects on Chl-a and phenological indices. The climate indices most frequently associated to phytoplankton variability were AMO, NAO and WeMO, but their effects varied across partition units. In general, AMO showed significant effects over open ocean and continental slope areas, NAO was related to partition units south of 36.5^{o}N, and WeMO was significantly associated to phytoplankton patterns in regions under the influence of river discharge.

Considering the predictions of climate alteration over SWIP (e.g., reduction in rainfall, increase in heat waves, sea surface warming) and the relationships between phytoplankton and underlying environmental drivers presented in this thesis, climate-driven impacts over

phytoplankton variability are expected to vary across SWIP partition units. Their detection will be probably anticipated over less complex regions, such as the open ocean domains. However, the discrimination between climate-driven changes and natural variability requires longer time series, than those used in this thesis, thus supporting the requirement of a systematic and continuous observation of the SWIP ocean surface.

6.2 Recommendations and future perspectives

The partition strategies applied in this study were an efficient framework for interpreting SWIP phytoplankton variability patterns and underlying environmental forcing, representing inexpensive, objective and reproducible methodologies, which can be adapted to other marine ecosystems. Furthermore, the delineation of ocean surface partitions could be relevant for other research purposes, including data synthesis, definition of sampling design, prediction of species distribution, testing ecological hypotheses across environmental gradients, and as a support for ecosystem management and conservation policies.

The results of this thesis and the knowledge acquired during its development identified a set of additional elements (variables, data sources and methods) that could further improve the effectiveness of SWIP partitions and their use for assessing phytoplankton variability and its linkages with climate and environmental variability. The additional elements that should ideally be explored include:

- the incorporation of other relevant environmental determinants of phytoplankton including abiotic (e.g., currents, turbulence intensity, heat fluxes, vertical profiles of ocean properties) and biological variables (e.g., vertical profiles of phytoplankton functional types or species composition, phytoplankton primary production, zooplankton abundance, phytoplankton grazing rates);
- the calibration/validation of satellite remote sensing data with *in situ* sampling, and the use of remote sensing products derived from regional algorithms;
- the use of an integrated database derived from multiple ocean observation platforms (e.g., satellite, drifting and mooring platforms, ARGO floaters and gliders, etc.);
- the incorporation of input datasets comprising longer time series;
- the use of a fuzzy classification methods which enable smoother boundaries between partition units;

- the evaluation of other approaches to derive phytoplankton phenological indices;
- over the upwelling-influenced areas, the evaluation of phytoplankton phenological patterns for specific periods of the year, separating favourable and unfavourable upwelling periods ;
- the development of dedicated *in situ* experiments for testing specific hypothesis related to phytoplankton variability and driving forces.

Overall, the present study showed that phytoplankton was significantly related to SWIP ocean surface environmental variability, thus supporting the use of phytoplankton as an indicator of ecosystem status and as a key element to evaluate ecosystem responses to climate change.

CHAPTER 7

REFERENCES

Acevedo-Trejos, E., Brandt, G., Merico, A., Smith, S.L., 2013. Biogeographical patterns of phytoplankton community size structure in the oceans. Global Ecology and Biogeography, Volume 22, Issue 9, Pages 1060-1070, DOI 10.1111/geb.12071

Akoumianaki, I., Papaspyrou, S., Kormas, K.A., Nicolaidou, A., 2013. Environmental variation and macrofauna response in a coastal area influenced by land runoff. Estuarine, Coastal and Shelf Science, Volume 132, Pages 34-44, DOI 10.1016/j.ecss.2012.04.009.

Alpine, S.E., Cloern, J.E., 1988. Phytoplankton growth rates in a light-limited environment, San Francisco Bay. Marine Ecology Progress Series, Volume 44, Pages 167-173.

Alvarez, I., Gomez-Gesteira, M., deCastro, M., Dias, J.M., 2008. Spatiotemporal evolution of upwelling regime along the western coast of the Iberian Peninsula. Journal of Geophysical Research, Volume 113, C07020, DOI 10.1029/2008JC004744.

Alvarez, I., Gomez-Gesteira, M., deCastro, M., Lorenzo, M.N., Crespo, A.J.C., Dias, J.M., 2011. Comparative analysis of upwelling influence between the western and northern coast of the Iberian Peninsula. Continental Shelf Research, Volume 31, Issue 5, 2011, Pages 388-399, DOI 10.1016/j.csr.2010.07.009.

Amorim, P., Perán, A.D., Pham, C. K.; Juliano, M., Cardigos, F., Tempera, F., Morato, T., 2017. Overview of the ocean climatology and its variability in the Azores region of the North Atlantic including environmental characteristics at the seabed. Frontiers in Marine Science, Volume 4, Article 56, DOI 10.3389/fmars.2017.00056.

Anderson, C.R., Kudela, R.M., Kahru, M., Chao, Y., Rosenfeld, L.K., Bahr, F.L., Anderson, D.M., Norris, R.A., 2016. Initial skill assessment of the California Harmful Algae Risk Mapping (C-HARM) system. Harmful Algae, Volume 59, Pages 1-18, DOI 10.1016/j.hal.2016.08.006.

Aquarone, M.C., Adams, S., Valdés, L., 2008. XIII-40 Iberian Coastal LME. In: Sherman, K., Hempel, G. (Eds) The UNEP Large Marine Ecosystem Report: A perspective on changing conditions in LMEs of the world's Regional Seas. UNEP Regional Seas Report and Studies Number 182. United Nations Environment Programme. Nairobi, Kenya, pp. 553-561.

Ardyna, M., Babin, M., Gosselin, M., Devred, E., Rainville, L., Tremblay, J-É., 2014. Recent Artic Ocean sea ice loss triggers novel fall phytoplankton blooms. Geophysical Research Letters, Volume 41, Pages 6207-6212, DOI 10.1002/2014GL061047

Ardyna, M., Claustre, H., Sallée, J.-B., D'Ovidio, F., Gentili, B., van Dijken, G., D'Ortenzio, F., Arrigo, K. R., 2017. Delineating environmental control of phytoplankton biomass and phenology in the Southern Ocean, Geophysical Research Letters, Volume 44, DOI 10.1002/2016GL072428.

Arístegui., J., Barton, E.D., Álvarez-Salgado, X. A., Santos, A. M. P., Figueiras, F. G., Kifani, S., Hernández-León, S., Mason, E., Machú, E., Demarcq, H., 2009. Sub-regional ecosystem variability in the Canary Current upwelling. Progress in Oceanography, Volume 83, Issues 1-4, Pages 33-48, DOI 10.1016/j.pocean.2009.07.031.

Baker, M. R., Hollowed, A.B., 2014. Delineating ecological regions in marine systems: Integrating physical structure and community composition to inform spatial management in the eastern Bering Sea. Deep Sea Research Part II: Topical Studies in Oceanography, Volume 109, Pages 215-240, DOI 10.1016/j.dsr2.2014.03.001.

Bakun, A., 1973. Coastal upwelling indices, west coast of North America, 1946-1971. US Dept. Commerce NOAA Technical Report NMFS-SSRF 671, pp. 1-103.

Banse, K., 1995. Science and organization in open-sea research: the plankton. Helgoländer Meeresuntersuchungen , Volume 49, Issue 1-4, Pages 3-18, DOI 10.1007/BF02368329.

Baptista, V., Silva, P.L., Relvas, P., Teodósio, A., Leitão, F., *in press*. Sea surface temperature variability along the Portuguese coast since 1950. International Journal of Climatology, DOI 10.1002/joc.5231.

Barale, V., 2010. Toward an ecosystem approach to ICM: assessing ecological provinces at sea by remote sensing. Journal of Coastal Conservation, Volume 14, Issue 4, Pages 317-326, DOI 10.1007/s11852-009-0080-9.

Barbosa, A.B., Chícharo, M.A., 2011. Hydrology and Biota Interactions as Driving Forces for Ecosystem Functioning, in: Wolanski, E., McLusky, D.S. (Eds.) Treatise on Estuarine

and Coastal Science, Volume 10, Ecohydrology and Restoration, Elsevier, pp. 7-47, DOI 10.1016/B978-0-12-374711-2.01002-0.

Barbosa, A.B., Domingues, R.B., Galvão, H.M., 2009. Environmental forcing of phytoplankton in a Mediterranean estuary (Guadiana Estuary, southwestern Iberia): a decadal of anthropogenic and climatic influences. Estuaries and Coasts, Volume 33, Issue 2, Pages 324–341, DOI 10.1007/s12237-009-9200-x

Barth, J.A., Menge, B.A., Lubchenco, J., Chan, F., Bane, J.M., Kirincich, A.R., McManus, M.A., Nielsen, K.J., Pierce, S.D., Washburn, L., 2007. Delayed upwelling alters nearshore coastal ocean ecosystems in the northern California current. Proceedings of the National Academy of Sciences of the United States of America, Volume 104, Issue 10, Pages 3719-3724, DOI 10.1073/pnas.0700462104

Barton, E.D., Field, D.B., Roy, C., 2013. Canary current upwelling: More or less? Progress in Oceanography, Volume 116, Pages 167-178, DOI 10.1016/j.pocean.2013.07.007.

Behrenfeld, M.J., 2010. Abandoning Sverdrup's Critical Depth hypothesis on phytoplankton blooms. Ecology, Volume 91, Issue 4, Pages 977-989, DOI 10.1890/09-1207.1.

Behrenfeld, M.J., 2014. Climate-mediated dance of the plankton. Nature Climate Change, Volume 4, Pages 880-887, DOI 10.1038/nclimate2349.

Behrenfeld, M.J., O'Malley, R.T., Boss, E.S., Westberry, T.K., Graff, J.R., Halsey, K.H., Milligan, A.J., Siegel, D.A., Brown, M.B., 2016. Revaluating ocean warming impacts on global phytoplankton. Nature Climate Change, Volume 6, Pages 323–330, DOI 10.1038/nclimate2838.

Behrenfeld, M.J., Boss, E.S., 2014. Resurrecting the ecological underpinnings of ocean plankton blooms. Annual Review of Marine Science, Volume 6, Pages 167–194, DOI 10.1146/annurev-marine-052913-021325

Behrenfeld, M.J., Doney, S.C., Lima, I., Boss, E.S., Siegel, D.A., 2013. Annual cycles of ecological disturbance and recovery underlying the subarctic Atlantic spring plankton bloom. Global Biogeochemical Cycles, Volume 27, Pages 1-15, DOI 10.1002/gbc.20050

Behrenfeld, M.J., O'Malley, R.T., Siegel, D.A., McClain, C.R., Sarmiento, J.L., Feldman, G.C., Milligan, A.J., Falkowski, P.G., Letelier, R., Boss, E.S., 2006. Climate-driven trends in contemporary ocean productivity. Nature, Volume 444, Pages 752-755, DOI 10.1038/nature05317.

Belkin, I.M., Cornillon, P.C., Sherman, K., 2009. Fronts in Large Marine Ecosystems. Progress in Oceanography, Volume 81, Issues 1-4, Pages 223-236, DOI 10.1016/j.pocean.2009.04.015.

Bezdek, J.C., Ehrlich, R., Full, W., 1984. FCM: The fuzzy c-means clustering algorithm. Computer & Geosciences, Volume 10, Issues 2-3, Pages 191-203, DOI 10.1016/0098-3004(84)90020-7.

Blondeau-Patissier, D., Gower, J.F.R., Dekker, A.G., Phinn, S.R., Brando, V.E., 2014a. A review of ocean color remote sensing methods and statistical techniques for the detection, mapping and analysis of phytoplankton blooms in coastal and open oceans. Progress in Oceanography, Volume 123, Pages 123-144, DOI 10.1016/j.pocean.2013.12.008.

Blondeau-Patissier, D., Schroeder, T., Brando, V.E., Maier, S.W., Dekker, A.G., Phinn, S., 2014b. ESA-MERIS 10-year mission reveals contrasting phytoplankton bloom dynamics in two tropical regions of Northern Australia. Remote Sensing, Volume 6, Issue 4, Pages 2963-2988, DOI 10.3390/rs6042963.

Bode, A., Anadón, R., Morán X.A.G., Nogueira, E., Teira, E., Varela, M., 2011. Decadal variability in chlorophyll and primary -production off NW Spain. Climate Research, Volume 48, Issues 2-3, Pages 293-305, DOI 10.3354/cr00935.

Bode, A., Estévez, M.G., Varela, M., Vilar, J.A., 2015. Annual trend patterns of phytoplankton species abundance belie homogeneous taxonomical group responses to climate in the NE Atlantic upwelling. Marine Environmental Research, Volume 110, Pages 81-91, DOI 10.1016/j.marenvres.2015.07.017.

Bojinski, S., Vestraete, M., Peterson, T.C., Richter, C., Simmons, A., Zemp, M., 2014. The concept of Essential Climate Variables in support of climate research, applications, and

policy. American Meteorological Society, Volume 95, Pages 1431-1443, DOI 10.1175/BAMS-D-13-00047.1.

Boss, E., Behrenfeld, M.J., 2010. In situ evaluation of the initiation of the North Atlantic phytoplankton bloom. Geophysical Research Letters, Volume 37, L18603, DOI 10.1029/2010GL044174

Boss, E., Maritorena, S., 2006. Uncertainties in the products of Ocean-Colour Remote Sensing. In: Lee, Z.-P. (Ed) Remote sensing of inherent optical properties: Fundamentals, tests of algorithms, and applications. Reports and Monographs of the International Ocean-Colour Coordinating Group (IOCCG), Volume 5, Dartmouth, Canada, pp. 19-24.

Boyce, D.G., Lewis, M.R., Worm, B., 2010. Global phytoplankton decline over the past century. Nature, Volume 466, Pages 591-596, DOI 1 0.1038/nature09268.

Boyd, P.W., Cornwall, C.E., Davison, A., Doney, S.C., Fourquez, M., Hurd, C.L., Lima, I.D., McMinn, A., 2016. Biological responses to environmental heterogeneity under future ocean conditions. Global Change Biology, Volume 22, Issue 8, Pages 2633-2650, DOI 10.1111/gcb.13287.

Boyer, T.P., Antonov, J.I., Baranova, O.K., Coleman, C., Garcia, H.E., Grodsky, A., Johnson, D.R., Locarnini, R.A., Mishonov, A.V., O'Brien, T.D., Paver, C.R., Reagan, J.R., Seidov, D., Smolyar, I.V., Zweng, M.M., 2013. World Ocean Database 2013, NOAA Atlas NESDIS 72, S. Levitus, Ed., A. Mishonov, Technical Ed.; Silver Spring, MD, p. 209, DOI 10.7289/V5NZ85MT

Briceño, H.O., Boyer, J.N., 2010. Climatic controls on phytoplankton biomass in a sub-tropical estuary, Florida Bay, USA. Estuaries and Coasts, Volume 33, Issue 2, Pages 541-553, DOI 10.1007/s12237-009-9189-1.

Britten, G.L., Primeau, F.W., 2016. Biome-specific scaling of ocean productivity, temperature, and carbon export efficiency. Geophysical Research Letters, Volume 43, Issue 10, Pages 5210-5216, DOI 10.1002/2016GL068778.

Brock, J.C., Sathyendranath, S., Platt, T., 1998. Biohydro-optical classification of the northwestern Indian Ocean. Marine Ecology Progress Series, Volume 165, Pages 1-15, DOI 10.3354/meps165001.

Brody, S.R., Lozier, M.S., Dunne, J.P., 2013. A comparison of methods to determine phytoplankton bloom initiation. Journal of Geophysical Research Oceans, Volume 118, Pages 1-13, DOI 10.1002/jgrc.20167

Brown, C.W., Esaias, W.E., Thompson, A.M., 1995. Predicting phytoplankton composition from space-Using the ratio of euphotic depth to mixed-layer depth: An evaluation. Remote Sensing of Environment, Volume 53, Issue 3, Pages 172-176, DOI 10.1016/0034-4257(95)00099-M

Bruno, M., Chioua, J., Romero, J., Vázquez, A., Macías, D., Dastis, C., Ramírez-Romero, E., Echevarria, F., Reyes, J., García, C.M., 2013. The importance of sub-mesoscale processes for the exchange of properties through the Strait of Gibraltar. Progress in Oceanography, Volume 116, Pages 66-79, DOI 10.1016/j.pocean.2013.06.006.

Bruno, M., Vázquez, A., Gómez-Enri, J., Vargas, J.M., García-Lafuente, J., Ruiz-Cañavate, A., Mariscal, L., Vidal, J., 2006. Observations of internal waves and associated mixing phenomena in the Portimão Canyon area. Deep Sea Research Part II: Topical Studies in Oceanography, Volume 53, Issues 11-13, Pages 1219-1240, DOI 10.1016/j.dsr2.2006.04.015.

Caballero, I., Morris, E., Pietro, L., Navarro, G., 2014. The influence of the Guadalquivir river on spatio-temporal variability in the pelagic ecosystem of the eastern Gulf of Cádiz, Mediterranean Marine Science, Volume 15, Issue 4, Pages 721-738, DOI 10.12681/mms.844.

Cabral, H.N., Fonseca, V.F., Gamito, R., Gonçalves, C.I., Costa, J.L., Erzini, K., Gonçalves, J., Martins, J., Leite, L., Andrade, J.P., Ramos, S., Bordalo, A., Amorim, E., Neto, J.M., Marques, J.C., Rebelo, J.E., Silva, C., Castro, N., Almeida, P.R., Domingos, I., Gordo, L.S., Costa, M.J., 2012. Ecological quality assessment of transitional waters based on fish assemblages in Portuguese estuaries: The Estuarine Fish Assessment Index (EFAI). Ecological Indicators, Volume 19, Pages 144-153, DOI 10.1016/j.ecolind.2011.08.005.

Cabré, A., Shields, D., Marinov, I., Kostadinov, T.S., 2016. Phenology of size-partitioned phytoplankton carbon-biomass from Ocean Color Remote Sensing and CMIP5 models. Frontiers in Marine Science, Volume 3, Article 39, DOI 10.3389/fmars.2016.00039

Callejas-Jimenez, M., Santamaria-del-Angel, E., Gonzalez-Silvera, A., Millan-Nuñez, R., Cajal-Medrano, R., 2012. Dynamic Regionalization of the Gulf of Mexico based on normalized radiances (nLw) derived from MODIS-Aqua. Continental Shelf Research, Volume 37, Pages 8-14, DOI 10.1016/j.csr.2012.01.014.

Cardeira, S., Rita, F., Relvas, P., Cravo, A., 2013. Chlorophyll a and chemical signatures during an upwelling event off the South Portuguese coast (SW Iberia). Continental Shelf Research, Volume 52, Pages 133-149, DOI 10.1016/j.csr.2012.11.011.

Cardoso, I., Fonseca, L.C., Cabral, H.N., 2012. Ecological quality assessment of small estuaries from the Portuguese coast based on benthic macroinvertebrate assemblages indices. Marine Pollution Bulletin, Volume 64, Issue 6, Pages 1136-1142, DOI 10.1016/j.marpolbul.2012.03.030.

Carr, M-.E., Kearns, E.J., 2003. Production regimes in four Eastern Boundary Current systems. Deep-Sea Research II, Volume 50, Issues 22-26, Pages 3199-3221, DOI 10.1016/j.dsr2.2003.07.015.

Carstensen, J., Klais, R., Cloern, J.E., 2015. Phytoplankton blooms in estuarine and coastal waters: Seasonal patterns and key species. Estuarine, Coastal and Shelf Science. Volume 162, Pages 98-109, DOI 10.1016/j.ecss.2015.05.005

Castelle, B., Dodet, G. Masselink, G., Scott, T., 2017. A new climate index controlling winter wave activity along the Atlantic coast of Europe: The West Europe Pressure Anomaly. Geophysical Research Letters, Volume 44, DOI 10.1002/2016GL072379

Catalán, I.A., Rubín, J.P., Navarro, G., Prieto, L., 2006. Larval fish distribution in two different hydrographic situations in the Gulf of Cádiz. Deep-Sea Research, Volume 53, Issues 11-13, Pages 1377-1390, DOI 10.1016/j.dsr2.2006.04.010.

Cermeño, P., Dutkiewicz, S., Harris, R.P., Follows, M., Schofield, O., Falkowski, P.G., 2008. The role of nutricline depth in regulating the ocean carbon cycle. PNAS, Volume 105, Issue 51, Pages 20344-20349, DOI 10.1073/pnas.0811302106

Chassot, E., Mélin, F., Le Pape, O., Gascuel, D., 2007. Bottom-up control regulates fisheries production at the scale of eco-regions in European seas. Marine Ecology Progress Series, 343, 2007, 45-55, DOI 10.3354/meps06919.

Chavez, F.P., Messié, M., Pennington, J.T., 2011. Marine primary production in relation to climate variability and change. Annual Reviews Marine Science, Volume 3, Pages 227-260, DOI 10.1146/annurev.marine.010908.163917.

Chícharo, L., Chícharo, M.A., Ben-Hamadou, R., 2006. Use of a hydrotechnical infrastructure (Alqueva dam) to regulate planktonic assemblages in the Guadiana estuary: Basis for sustainable water and ecosystem services management. Estuarine, Coastal and Shelf Science, Volume 70, Issues 1-2, Pages 3-18, DOI 10.1016/j.ecss.2006.05.039.

Chiswell, S.M., Bradford-Grieve, J., Hadfield, M.G., Kennan, S.C., 2013. Climatology of surface chlorophylla, autumn-winter and spring blooms in the southwest Pacific Ocean. Journal of Geophysical Research Oceans, Volume 118, Pages 1003-1018, DOI 10.1002/jgrc.20088

Chiswell, S.M., Calil, P.H.R., Boyd, P.W., 2015. Spring blooms and annual cycles of phytoplankton: a unified perspective. Journal of Plankton Research, Volume 37, Issue 3, Pages 500-508, DOI 10.1093/plankt/fbv021

Clark, M.R., Watling, L., Rowden, A.A., Guinotte, J.M., Smith, C.R., 2011. A global seamount classification to aid the scientific design of marine protected area networks. Ocean & Coastal Management, Volume 54, Issue 1, Pages 19-36, DOI 10.1016/j.ocecoaman.2010.10.006.

Claus, S., De Hauwere, N., Vanhoorne, B., Souza Dias, F., Oset García, P., Hernandez, F., Mees, J., 2016. (Flanders Marine Institute) MarineRegions.org. Available at http://www.marineregions.org . Accessed on: 31 Mar 2016.

Cloern, J.E., Abreu, P.C., Carstensen, J., Chauvaud, L., Elmgren, R., Grall, J., Greening, H., Johansson, J.O.R., Kahru, M., Sherwood, E.T., Xu, J., Yin, K., 2016. Human activities and climate variability drive fast-paced change across the world's estuarine-coastal ecosystems. Global Change Biology, Volume 22, Issue 2, Pages 513-529, DOI 10.1111/gcb.13059.

Cloern, J.E., Dufford, R., 2005. Phytoplankton community ecology - Principles applied in San Francisco Bay. Marine Ecology Progress Series, Volume 285, Pages 11-28, DOI 10.3354/meps285011.

Cloern, J.E., Abreu, P.C., Carstensen, J., Chauvaud, L., Grall, J., Greening, H., Johansson, R.J.O., Kahru, M., Sherwood, E.T., Xu, J.I.E., Yin, K., 2016. Human activities and climate variability drive fast-paced change across the world's estuarine-coastal ecosystems. Global Change Biology, Volume 22, Issue 2, Pages 513-529, DOI 10.1111/gcb.13059.

Cloern, J.E., Jassby, A.D., 2008. Complex seasonal patterns of primary producers at the land-sea interface. Ecology Letters, Volume 11, Issue 12, Pages 1294-1303, DOI 10.1111/j.1461-0248.2008.01244.x.

Cloern, J.E., Jassby, A.D., 2010. Patterns and scales of phytoplankton variability in estuarine-coastal ecosystems. Estuaries and Coasts, Volume 33, Pages 230-241, DOI 10.1007/s12237-009-9195-3.

Cole, H., Henson, S., Martin, A., Yool, A., 2012. Mind the gap: the impact of missing data on the calculation of phytoplankton phenology metrics. Journal of Geophysical Research, Volume 117, C08030, DOI 10.1029/2012JC008249

Cole, H., Henson, S., Martin, A.P., Yool, A., 2015. Basin-wide mechanisms for spring bloom initiation: how typical is the North Atlantic? ICES Journal of Marine Science, Volume 72, Issue 6, Pages 2029-2040, DOI 10.1093/icesjms/fsu239

Corredor-Acosta, A., Morales, C.E., Hormazabal, S., Andrade, I., Correa-Ramirez, M.A., 2015. Phytoplankton phenology in the coastal upwelling region off central-southern Chile (35^{o}S–38^{o}S): Time-space variability, coupling to environmental factors, and sources of

uncertainty in the estimates. Journal of Geophysical Research Oceans, Volume 120, Issue 2, Pages 813-831, DOI 10.1002/2014JC010330

Couto, A.B., Brotas, V., Mélin, F., Groom, S., Sathyendranath, S., 2016. Inter-comparison of OC-CCI chlorophyll-a estimates with precursor data sets. International Journal of Remote Sensing, Volume 37, Issue 18, Pages 4337-4355, DOI 10.1080/01431161.2016.1209313.

Cravo, A., Madureira, M., Felícia, H., Rita, F., Bebianno, M.J., 2006. Impact of outflow from the Guadiana River on the distribution of suspended particulate matter and nutrients in the adjacent coastal zone. Estuarine, Coastal and Shelf Science, Volume 70, Issues 1-2, Pages 63-75, DOI 10.1016/j.ecss.2006.05.034.

Cravo, A., Relvas, P., Cardeira, S., Rita, F., 2013. Nutrient and chlorophyll a transports during an upwelling event in the NW margin of the Gulf of Cadiz. Journal of Marine Systems, Volume 128, Pages 208-221, DOI 10.1016/j.jmarsys.2013.05.001.

Cravo, A., Relvas, P., Cardeira, S., Rita, F., Madureira, M., Sánchez, R., 2010. An upwelling filament off southwest Iberia: Effect on the chlorophyll a and nutrient export. Continental Shelf Research, Volume 30, Issue 15, Pages 1601-1613, DOI 10.1016/j.csr.2010.06.007.

Criado-Aldeanueva, F., García-Lafuente, J, Vargas, J.M., Del Río, J., Vázquez, A., Reul, A., Sánchez, A., 2006. Distribution and circulation of water masses in the Gulf of Cadiz from in situ observations. Deep Sea Research Part II, Volume 53, Pages 1144-1160, DOI 10.1016/j.dsr2.2006.04.012.

Criado-Aldeanueva, F., García-Lafuente, J., Navarro, G., Ruiz, J., 2009. Seasonal and interannual variability of the surface circulation in the eastern Gulf of Cadiz (SW Iberia). Journal of Geophysical Research, Volume 114, C01011, DOI 10.1029/2008JC005069.

Cristina, S., Cordeiro, C., Lavender, S., Goela, P.C., Icely, J.D., Newton, A., 2016a. MERIS phytoplankton time series products from the SW Iberian Peninsula (Sagres) using seasonal-trend decomposition based on Loess. Remote Sensing, Volume 8, Issue 6, 449, DOI 10.3390/rs8060449.

Cristina, S., D'Alimonte, D., Goela, P. C., Kajiyama, T., Icely, J., Moore, G., Fragoso, B., Newton, A., 2016b. Standard and regional bio-optical algorithms for chlorophyll a

estimates in the Atlantic off the southwestern Iberian Peninsula. IEEE Geoscience and Remote Sensing Letters, Volume 13, Issue 6, Pages 757-761, DOI 10.1109/LGRS.2016.2529182.

Cristina, S., Icely, J., Goela, P.C., DelValls, T.A., Newton, A., 2015. Using remote sensing as a support to the implementation of the European Marine Strategy Framework Directive in SW Portugal. Continental Shelf Research, Volume 108, Pages 169-177, DOI 10.1016/j.csr.2015.03.011.

Cristina, S., Moore, G.F., Goela, P.R.F.C., Icely, J.D., Newton, A., 2014. In situ validation of MERIS marine reflectance off the southwest Iberian Peninsula: assessment of vicarious adjustment and corrections for near-land adjacency. International Journal of Remote Sensing, Volume 35, Issue 6, Pages 2347-2377, DOI 10.1080/01431161.2014.894657.

Cropper, T.E., Hanna, E., Bigg, G.R., 2014. Spatial and temporal seasonal trends in coastal upwelling off Northwest Africa, 1981-2012. Deep-Sea Research I, Volume 86, Pages 94-111, DOI 10.1016/j.dsr.2014.01.007.

Cusack, M., Alastuey, A., Pérez, N., Pey, J., Querol, X., 2012. Trends of particulate matter (PM2.5) and chemical composition at a regional background site in the Western Mediterranean over the last nine years (2002–2010). Atmospheric Chemistry and Physics, Volume 12, Pages 8341-8357, DOI 10.5194/acp-12-8341-2012.

D'Alimonte, D., Zibordi, G., Berthon, J.F., 2007. A Statistical Index of Bio-Optical Seawater Types. IEEE Transactions on Geoscience and Remote Sensing, Volume 45, Issue 8, Pages 2644-2651, DOI 10.1109/TGRS.2007.896561.

D'Ortenzio, F., d'Alcalà, M.R., 2009. On the trophic regimes of the Mediterranean Sea: a satellite analysis. Biogeosciences, Volume 6, Issue 2, Pages 139-148, DOI 10.5194/bg-6-139-2009.

deCastro, M., Gómez-Gesteira, M., Lorenzo, M.N., Alvarez, I., Crespo, A.J.C., 2008. Influence of atmospheric modes on coastal upwelling along the western coast of the Iberian Peninsula, 1985 to 2005. Climate Research, Volume 36, Issue 2, Pages 169-179, DOI 10.3354/cr00742.

deCastro, M., Lorenzo, N., Taboada, J.J., Sarmiento, M., Alvarez, I., Gomez-Gesteira, M., 2006. Influence of teleconnection patterns on precipitation variability and on river flow regimes in the Miño River basin (NW Iberian Peninsula). Climate Research, Volume 32, Issue 1, Pages 63-73, DOI 10.3354/cr032063.

Demarcq, H., 2009. Trends in primary production, sea surface temperature and wind in upwelling systems (1998-2007). Progress in Oceanography, Volume 83, Issues 1-4, Pages 376-385, DOI 10.1016/j.pocean.2009.07.022.

Demarcq, H., Reygondeau, G., Alvain, S., Vantrepotte, V., 2012. Monitoring marine phytoplankton seasonality from space. Remote Sensing of Environment, Volume 117, Pages 211-222, DOI 10.1016/j.rse.2011.09.019

Devred, E., Sathyendranath, S., Platt, T., 2007. Delineation of ecological provinces in the North West Atlantic using visible spectral radiometry (ocean colour). Marine Ecology Progress Series, Volume 346, Pages 1-13, DOI 10.3354/meps07149.

Devred, E., Sathyendranath, S., Platt, T., 2009. Decadal changes in ecological provinces of the Northwest Atlantic Ocean revealed by satellite observations. Geophysical Research Letters, Volume 36, Issue 19, L19607. DOI 10.1029/2009GL039896.

Dormann, C.F., Elith, J., Bacher, S., Buchmann, C., Carl, G., Carré, G., Marquéz, J.R.G., Grube, B., Lafourcade, B., Leitão, P.J., Münkemüller, T., McClean, C., Osborne, P.E., Reineking, B., Schröder, B., Skidmore, A.K., Zurell, D., Lautenbach, S., 2013. Collinearity: a review of methods to deal with it and a simulation study evaluating their performance. Ecography, Volume 36, Issue 1, Pages 27-46, DOI 10.1111/j.1600-0587.2012.07348.x.

D'Ortenzio, F., Antoine, D., Martinez, E., Ribera d'Alcalà, M., 2012. Phenological changes of oceanic phytoplankton in the 1980s and 2000s as revealed by remotely sensed ocean-color observations. Global Biogeochemical Cycles, Volume 26, GB4003, DOI 10.1029/2011GB004269.

Dowell, M., Moore, T., Platt, T., 2009. Retrieval of phytoplankton biomass, optical constituents and primary productivity. In: Dowell, M. Platt, T., Stuart, V. (Eds) Partition

of the ocean into ecological provinces: Role of ocean-colour radiometry. Reports and Monographs of the International Ocean-Colour Coordinating Group (IOCCG), Volume 9, Dartmouth, Canada, pp. 37-46.

Doyle, M.J., Picquelle, S.J., Mier, K.L., Spillane, M.C., Bond, N.A., 2009. Larval fish abundance and physical forcing in the Gulf of Alaska, 1981–2003. Progress in Oceanography, Volume 80, Issues 3-4, Pages 163-187, IDOI 10.1016/j.pocean.2009.03.002.

Drinkwater, K., Belgrano, A., Borja, A., Conversi, A., Edwards, M., Greene, C., Ottersen, G., Pershing, A., Walker, H., 2003. The response of marine ecosystems to climate variability associated with the North Atlantic Oscillation, in: Hurrell, J, Kushnir, Y., Ottersen, G., Visbeck, M. (Eds) The North Atlantic Oscillation: Climatic significance and environmental impact. Book Series: Geophysical Monograph Series, John Wiley & Sons, pp. 211-234, DOI 10.1029/GM134.

Ducklow, H.W., 2003. Biogeochemical provinces: Towards a JGOFS synthesis. In: Fasham, M. J.R. (Ed) Ocean Biogeochemistry: A New Paradigm, Springer, Berlin, pp. 3-18.

Dunn, D.C., Ardron, J., Bax, N., Bernal, P., Cleary, J., Cresswell, I., Donnelly, B., Dunstan, P., Gjerde, K., Johnson, D., Kaschner, K., Lascelles, B., Rice, J., von Nordheim, H., Wood, L., Halpin, P.N., 2014. The Convention on Biological Diversity's ecologically or biologically significant areas: origins, development, and current status. Marine Policy, Volume 49, Pages 137-145, DOI 10.1016/j.marpol.2013.12.002

Dutkiewicz, S., Beaugrand, G., Hoepffner, N., Kamykowski, D., Mélin, F., 2009. Applications to biogeochemical cycles and global climate change. In: Dowell, M., Platt, T., Stuart, V. (Eds) Partition of the ocean into ecological provinces: Role of ocean-colour radiometry. Reports and Monographs of the International Ocean-Colour Coordinating Group (IOCCG), Volume 9, Dartmouth, Canada, pp. 47-67.

Eakins, B.W., Sharman, G.F, 2010. Volumes of the World's Oceans from ETOPO1, NOAA National Geophysical Data Center, Boulder, CO. Available at https://www.ngdc.noaa.gov/mgg/global/etopo1_ocean_volumes.html (Accessed on: 22 July 2017).

Eastman, J.R., 1992. Time series map analysis using Standardized Principal Components. Proceedings, ASPRS/ACSM/RT 92 Convention on Monitoring and Mapping Global Change, Pages 195-204.

Echevarría, F., Zabala, L., Corzo, A., Navarro, G., Prieto, L., Macías, D., 2009. Spatial distribution of autotrophic picoplankton in relation to physical forcings: the Gulf of Cádiz, Strait of Gibraltar and Alborán Sea case study. Journal of Plankton Research, Volume 31, Issue 11, Pages 1339-1351, DOI 10.1093/plankt/fbp070.

Edwards, M., Richardson, A.J., 2004. Impact of climate change on marine pelagic phenology and trophic mismatch. Nature, Volume 430, Pages 881–884, DOI 10.1038/nature02808.

Eliasen, S.K., Hátún, H., Larsen, K.M.H., Hansen, B., Rasmussen, T.A.S., 2017. Phenologically distinct phytoplankton regions on the Faroe Shelf - identified by satellite data, observations and model. Journal of Marine Systems, Volume 169, Pages 99-110, DOI 10.1016/j.jmarsys.2017.01.015

Elsberry, R.L., Camp, N.T., 1978. Oceanic thermal response to strong atmospheric forcing. I. Characteristics of forcing events. Journal of Physical Oceanography, Volume 8, Issue 2, Pages 206-214, DOI 10.1175/1520-0485(1978)008<0206:OTRTSA>2.0.CO;2.

Encarnação, J., Leitão, F., Range, P., Piló, D., Chícharo, A., Chícharo, L., 2013. The influence of submarine groundwater discharges on subtidal meiofauna assemblages in south Portugal (Algarve). Estuarine, Coastal and Shelf Science, Volume 130, Pages 202-208, DOI 10.1016/j.ecss.2013.04.013.

Enfield, D.B., Mestas-Nunez, A.M., Trimble, P.J., 2001. The Atlantic multidecadal oscillation and it's relation to rainfall and river flows in the continental U.S.. Geophysical Research Letters, Volume 28, Issue 10, Pages 2077-2080, DOI 10.1029/2000GL012745.

Esaias, W.E., Iverson, R.L., Turpie, K., 2000. Ocean province classification using ocean colour data: observing biological signatures of variations in physical dynamics. Global Change Biology, Volume 6, Issue 1, Pages 39-55, DOI 10.1046/j.1365-2486.2000.00285.x.

Escudero, M., Castillo, S., Querol, X., Avila, A., Alarcón, M., Viana, M.M., Alastuey, A., Cuevas, E., Rodríguez, S., 2005. Wet and dry African dust episodes over Eastern Spain. Journal of Geophysical Research, Volume 110, D18S08, DOI 10.1029/2004JD004731.

Estrada, M., Delgado, M., Blasco, D., Latasa,M., Cabello, A.M., Benítez-Barrios, V., Fraile-Nuez, E., Mozetic, P., Vidal, M., 2016. Phytoplankton across Tropical and Subtropical Regions of the Atlantic, Indian and Pacific Oceans. PLoS ONE, Volume 11, Issue 3, e0151699, DOI 10.1371/journal.pone.0151699.

EU, 2008. Directive 2008/56/EC of 17 June 2008 on establishing a framework for community action in the field of marine environmental policy (Marine Strategy Framework Directive). Official Journal of the European Union, L 164, pp. 19-40.

Fay, A.R., McKinley, G.A., 2014. Global open-ocean biomes: mean and temporal variability. Earth System Science Data, Volume 6, Pages 273-284, DOI 10.5194/essd-6-273-2014.

Federal Geographic Data Committee (FGDC), 2012. Coastal and Marine Ecological Classification Standard, Volume 4.0, Doc XX, Standards Working Group, U.S. Geological Survey, p. 339.

Fendereski, F., Vogt, M., Payne, M.R., Lachkar, Z., Gruber, N., Salmanmahiny, A., Hosseini, S.A., 2014. Bio-geographic classification of the Caspian Sea. Biogeosciences, Volume 11, Issue 22, Pages 6451-6470, DOI 10.5194/bg-11-6451-2014.

Feng, H., Campbell, J.W., Dowell, M.D., Moore, T.S., 2005. Modeling spectral reflectance of optically complex waters using bio-optical measurements from Tokyo Bay. Remote Sensing of Environment, Volume 99, Issue 3, Pages 232-243, DOI 10.1016/j.rse.2005.08.015.

Ferreira, A.S., Visser, A.W., MacKenzie, B.R., Payne, M.R., 2014. Accuracy and precision in the calculation of phenology metrics. Journal of Geophysical Research Oceans, Volume 119, Pages 8438-8453, DOI 10.1002/2014JC010323.

Ferreira, A.S.A., Hátún, H., Counillon, F., Payne, M.R., Visser, A.W., 2015. Synoptic-scale analysis of mechanisms driving surface chlorophyll dynamics in the North Atlantic. Biogeosciences, Volume 12, Pages 3641-3653, DOI 10.5194/bg-12-3641-2015

Field, C.B., Behrenfeld, M.J., Randerson, J.T., Falkowski, P., 1998. Primary production of the biosphere: integrating terrestrial and oceanic components. Science, Volume 281, Pages 237-240, DOI 10.1126/science.281.5374.237.

Fischer, A.D., Moberg, E.A., Alexander, H., Brownlee, E.F., Hunter-Cevera, K.R., Pitz, K.J., Rosengard, S.Z., Sosik, H.M., 2014. Sixty years of Sverdrup: A retrospective of progress in the study of phytoplankton blooms. Oceanography, Volume 27, Issue 1, Pages 222-235, DOI 10..5670/oceanog.2014.26

Fiúza, A.F.deG., de Macedo, M.E., Guerreiro, M.R., 1982. Climatological space and time-variation of the portuguese coastal upwelling. Oceanologica Acta, Volume 5, Issue 1, Pages 31-40.

Follows, M., Dutkiewicz, S., 2002. Meteorological modulation of the North Atlantic spring bloom. Deep Sea Research Part II: Topical Studies in Oceanography, Volume 49, Issues 1-3, Pages 321-344, DOI 10.1016/S0967-0645(01)00105-9.

Foukal, N.P., Thomas, A.C., 2014. Biogeography and phenology of satellite-measured phytoplankton seasonality in the California current. Deep Sea Research Part I: Oceanographic Research Papers, Volume 92, Pages 11-25, DOI 10.1016/j.dsr.2014.06.008.

Franks, P.J.S., 2014. Has Sverdrup's critical depth hypothesis been tested? Mixed layers vs. turbulent layers. ICES Journal of Marine Science, Volume 72, Issue 6, Pages 1897-1907, DOI 10.1093/icesjms/fsu175

Friedland, K.D., Record, N.R., Asch, R.G., Kristiansen, T., Saba, V.S., Drinkwater, K.F., Henson, S., Leaf, R.T., Morse, R.E., Johns, D.G., Large, S.I., Hjøllo, S.S., Nye, J.A., Alexander, M.A., Ji, R., 2016. Seasonal phytoplankton blooms in the North Atlantic linked to the overwintering strategies of copepods. Elementa: Science of the Anthropocene, Volume 4, Pages 1-19, DOI 10.12952/journal.elementa.000099.

Fuentes-Yaco, C., Koeller, P.A., Sathyendranath, S., Platt, T., 2007. Shrimp (Pandalus borealis) growth and timing of the spring phytoplankton bloom on the Newfoundland–

Labrador Shelf. Fisheries Oceanography, Volume 16, Issue 2, Pages 116-129, DOI 10.1111/j.1365-2419.2006.00402.x

Gago, J., Cabanas, J.M., Casas, G., Miranda, A., 2011. Thermohaline measurements in the continental shelf zone of the NW Iberian Peninsula, 1994-2006. Climate Research, Volume 48, Pages 219-229, DOI 10.3354/cr00943.

Galí, M., Devred, E., Levasseur, M., Royer, S., Babin, M.A remote sensing algorithm for planktonic dimethylsulfoniopropionate (DMSP) and an analysis of global patterns. Remote Sensing of Environment, Volume 171, Pages 171-184, DOI 10.1016/j.rse.2015.10.012.

Gamito, R., Pita, C., Teixeira, C., Costa, M.J., Cabral, H.N., 2016. Trends in landings and vulnerability to climate change in different fleet components in the Portuguese coast. Fisheries Research, Volume 181, Pages 93-101, DOI 10.1016/j.fishres.2016.04.008.

García-Lafuente, J., Delgado, J., Criado-Aldeanueva, F., Bruno, M., del Río, J., Vargas, J.M., 2006. Water mass circulation on the continental shelf of the Gulf of Cádiz. Deep Sea Research II, Volume 53, Issue 11-13, Pages 1182-1197, DOI 10.1016/j.dsr2.2006.04.011.

García-Lafuente, J., Ruiz, J., 2007. The Gulf of Cádiz pelagic ecosystem: A review. Progress in Oceanography, Volume 74, Issues 2-3, Pages 228-251, DOI 10.1016/j.pocean.2007.04.001.

García-Reyes, M., Sydeman, W.J., Schoeman, D.S., Rykaczewski, R.R., Black, B.A., Smit, A.J., Bograd, S.J., 2015. Under Pressure: Climate Change, Upwelling, and Eastern Boundary Upwelling Ecosystems. Frontiers in Marine Science, Volume 2, Pages 1-10, DOI 10.3389/fmars.2015.00109.

Garel, E., Laiz, I., Drago, T., Relvas, P., 2016. Characterisation of coastal counter-currents on the inner shelf of the Gulf of Cadiz. Journal of Marine Systems, Volume 155, Pages 19-34, DOI 10.1016/j.jmarsys.2015.11.001.

Geider, R.J., 1987. Light and temperature dependence of the carbon to chlorophyll ratio in microalgae and cyanobacteria: Implications for physiology and growth of phytoplankton.

New Phytologist, Volume 106, Issue 1, Pages 1-34, DOI 10.1111/j.1469-8137.1987.tb04788.x.

Goela, P.C., Cordeiro, C., Danchenko, S., Icely, J., Cristina, S., Newton, A., 2016. Time series analysis of data for sea surface temperature and upwelling components from the southwest coast of Portugal. Journal of Marine Systems, Volume 163, Pages 12-22, DOI 10.1016/j.jmarsys.2016.06.002.

Goela, P.C., Icely, J., Cristina, S., Danchenko, S., DelValls, T.A., Newton, A., 2015. Using bio-optical parameters as a tool for detecting changes in the phytoplankton community (SW Portugal). Estuarine, Coastal and Shelf Science, Volume 167, Part A, Pages 125-137, DOI 10.1016/j.ecss.2015.07.037.

Goela, P.C., Danchenko, S., Icely, J.D., Lubian, L.M., Cristina, S., Newton, A., 2014. Using CHEMTAX to evaluate seasonal and interannual dynamics of the phytoplankton community off the South-west coast of Portugal. Estuarine, Coastal and Shelf Science, Volume 151, Pages 112-123, DOI 10.1016/j.ecss.2014.10.001.

Goela, P.C., Icely, J., Cristina, S., Danchenko, S., DelValls, T.A., Newton, A., 2015. Using bio-optical parameters as a tool for detecting changes in the phytoplankton community (SW Portugal). Estuarine, Coastal and Shelf Science, Volume 167, Pages 125-137, DOI 10.1016/j.ecss.2015.07.037.

Goela, P.C., Icely, J., Cristina, S., Newton, A., Moore, G., Cordeiro, C., 2013. Specific absorption coefficient of phytoplankton off the Southwest coast of the Iberian Peninsula: A contribution to algorithm development for ocean colour remote sensing. Continental Shelf Research, Volume 52, Issue 1, Pages 119-132, DOI 10.1016/j.csr.2012.11.009.

González Taboada, F.G., Anadón, R., 2014. Seasonality of North Atlantic phytoplankton from space: impact of environmental forcing on a changing phenology (1998–2012). Global Change biology, Volume 20, Issue 3, Pages 698-712, DOI 10.1111/gcb.12352

Grant, M., Jackson, T., Chuprin, A., Sathyendranath, S., Zühlke, M., Storm, T., Boettcher, M., Fomferra, N.,2016. Product User Guide Ocean Colour Climate Change Initiative

(OC_CCI) – Phase Two. Available at http://www.esa-oceancolour-cci.org/. Accessed on: 09 Mar 2016.

Gregg, W.W., Conkright, M.E., Ginoux, P., O'Reilly, J.E., Casey, N.W., 2003. Ocean primary production and climate: Global decadal changes. Geophysical Research Letters, Volume 30, Issue 15, 1809, DOI 10.1029/2003GL016889.

Gregg, W.W., Rousseaux, C.S., 2014. Decadal trends in global pelagic ocean chlorophyll: A new assessment integrating multiple satellites, in situ data, and models. Journal of Geophysical Research: Oceans, Volume 119, Issue 9, Pages 5921-5933, DOI 10.1002/2014JC010158.

Gregr, E.J., Ahrens, A.L., Perry, R.I., 2012. Reconciling classifications of ecologically and biologically significant areas in the world's oceans. Marine Policy, Volume 36, Issue 3, Pages 716-726, DOI 10.1016/j.marpol.2011.10.009.

Gregr, E.J., Bodtker, K.M., 2007. Adaptive classification of marine ecosystems: identifying biologically meaningful regions in the marine environment. Deep-Sea Research Part I: Oceanographic Research Papers, Volume 54, Pages 385-402, DOI 10.1016/j.dsr.2006.11.004.

Griffies, S.M., Treguier, A.M., 2013. Ocean Circulation Models and Modeling. In: Siedler, G., Griffies, S.M., Gould, J., Church, J.A. (Eds.). Ocean circulation and climate: a 21st century perspective. International Geophysics, Volume 103, Pages 521-551, DOI 10.1016/B978-0-12-391851-2.00020-9

Grilli, A.R., Schumchenia, E.J., 2015. Toward wind farm monitoring optimization: assessment of ecological zones from marine landscapes using machine learning algorithms. Hydrobiologia, Volume 756, Pages 117-137, DOI 10.1007/s10750-014-2139-3.

Grobbelaar, J.U., 1985. Phytoplankton productivity in turbid waters. Journal of Plankton Research, Volume 7, Issue 5, Pages 653-663, DOI 10.1093/plankt/7.5.653

Groetsch, P.M.M., Simis, S.G.H., Eleveld, M.A., Peters, S.W.M., 2016. Spring blooms in the Baltic Sea have weakened but lengthened from 2000 to 2014. Biogeosciences, Volume 13, Pages 4959-4973, DOI 10.5194/bg-13-4959-2016

Hao, H., Bin, C., Jinlan, L., 2015. The marine spatial classification and the identification of priority conservation areas (PCAs) for marine biodiversity conservation – A case study of the offshore China. Ocean & Coastal Management, Volume 116, Pages 224-236, DOI 10.1016/j.ocecoaman.2015.06.027.

Hardman-Mountford, N.J., Hirata, T., Richardson, K.A., Aiken, J., 2008. An objective methodology for the classification of ecological pattern into biomes and provinces for the pelagic ocean. Remote Sensing of Environment, Volume 112, Issue 8, Pages 3341-3352, DOI 10.1016/j.rse.2008.02.016.

Harrison, W.G., Børsheim, K.Y., Li, W.K.W., Maillet, G.L., Pepin, P., Sakshaug, E., Skogen, M.D., Yeats, P.A., 2013. Phytoplankton production and growth regulation in the Subarctic North Atlantic: A comparative study of the Labrador Sea-Labrador/Newfoundland shelves and Barents/Norwegian/Greenland seas and shelves. Progress in Oceanography, Volume 114, Pages 26-45, DOI 10.1016/j.pocean.2013.05.003

Hauke, J., Kossowski, T., 2011. Comparison of values of Pearson's and Spearman's correlation coefficient on the same sets of data. Quaestiones Geographicae, Volume 30, Issue 2, Pages 87-93, DOI 10.2478/v10117-011-0021-1.

Haynes, R., Barton, E.D., Pilling, I., 1993. Development, persistence, and variability of upwelling filaments off the Atlantic Coast of the Iberian Peninsula. Journal of Geophysical Research, Volume 98, Issue C12, Pages 22,681-22,692, DOI 10.1029/93JC02016.

Heileman, S., Tandstad, M., 2008. I -3 Canary Current LME. In: Sherman, K., Hempel, G. (Eds). The UNEP Large Marine Ecosystem Report: A perspective on changing conditions in LMEs of the world's Regional Seas. UNEP Regional Seas Report and Studies Number 182. United Nations Environment Programme. Nairobi, Kenya., pp. 131-141.

Hemmings, J.C.P., Srokosz, M.A., Challenor, P., Fasham, M.J.R., 2004. Split-domain calibration of an ecosystem model using satellite ocean colour data. Journal of Marine Systems, Volume 50, Issues 3-4, Pages 141-179, DOI 10.1016/j.jmarsys.2004.02.003.

Henson, S.A., Beaulieu, C., Ilyina, T., John, J.G., Long, M., Séférian, R., Tjiputra, J., Sarmiento, J.L., 2017. Rapid emergence of climate change in environmental drivers of marine ecosystems. Nature Communications, Volume 8, 14682, Pages 1-9, DOI 10.1038/ncomms14682.

Henson, S.A., Beaulieu, C., Lampitt, R., 2016. Observing climate change trends in ocean biogeochemistry: when and where. Global Change Biology, Volume 22, Issue 4, Pages 1561-1571, DOI 10.1111/gcb.13152.

Henson, S.A., Beaulieu, C., Ilyina, T., John, J.G., Long, M., Séférian, R., Tjiputra, J., Sarmiento, J.L., 2017. Rapid emergence of climate change in environmental drivers of marine ecosystems. Nature Communications, Volume 8, Article 14682:1–9, DOI 10.1038/ncomms14682

Henson, S.A., Dunne, J.P., Sarmiento, J.L., 2009. Decadal variability in North Atlantic phytoplankton blooms. Journal of Geophysical Research, Volume 114, C04013, DOI 10.1029/2008JC005139

Henson, S.A., Sarmiento, J.L., Dunne, J.P., Bopp, L., Lima, I., Doney, S.C., John, J., Beaulieu, C., 2010. Detection of anthropogenic climate change in satellite records of ocean chlorophyll and productivity. Biogeosciences, Volume 7, Pages 621-640, DOI 10.5194/bg-7-621-2010

Henson, S.A., Thomas, A.C., 2007. Interannual variability in timing of bloom initiation in the California Current System. Journal of Geophysical Research, Volume 112, C08007, DOI 10.1029/2006JC003960

Henson, S.A.,Robinson,I., Allen, J.T., Waniek, J.J., 2006. Effect of meteorological conditions on interannual variability in timing and magnitude of the spring bloom in the Irminger Basin, North Atlantic. Deep Research Part I Oceanographic Research Papers, Volume 53, Issue 10, Pages 1601-1615, DOI 10.1016/j.dsr.2006.07.009

Hertig, E., Beck, C., Wanner, H., Jacobeit, J., 2015. A review of non-stationarities in climate variability of the last century with focus on the North Atlantic–European sector. Earth-Science Reviews, Volume 147, Pages 1-17, DOI 10.1016/j.earscirev.2015.04.009.

Hidalgo-Muñoz, J.M., Argüeso, D., Gámiz-Fortis, S.R., Esteban-Parra, M.J., Castro-Díez, Y., 2011. Trends of extreme precipitation and associated synoptic patterns over the southern Iberian Peninsula. Journal of Hidrology, Volume 409, Pages 497-511, DOI 10.1016/j.jhydrol.2011.08.049.

Hoepffner, N., Dowell, M.D., 2005. Assessing the dynamics of ecological provinces in European Seas, European Commission, EUR 21514 EN, Ispra, pp. 1-43.

Hooker, S.B., Rees, N.W., Aiken, J., 2000. An objective methodology for identifying oceanic provinces. Progress in Oceanography, Volume 45, Issue 3, Pages 313-338, DOI 10.1016/S0079-6611(00)00006-9.

Horta e Costa, B., Assis, J., Franco, G., Erzini, K., Henriques, M., Gonçalves, E.J., Caselle, J.E., 2014. Tropicalization of fish assemblages in temperate biogeographic transition zones. Marine Ecology Progress Series, Volume 504, Pages 241-252, DOI 10.3354/meps10749.

Huertas, I. E., Navarro, G., Rodríguez-Gálvez, S., Lubián, L. M., 2006. Temporal patterns of carbon dioxide in relation to hydrological conditions and primary production in the northeastern shelf of the Gulf of Cadiz (SW Spain). Deep Sea Research Part II: Topical Studies in Oceanography, Volume 53, Issues 11-13, Pages 1344-1362, DOI 0.1016/j.dsr2.2006.03.010.

Huertas, I.E., Navarro, G., Rodríguez-Gálvez, S., Prieto, L.M., 2005. The influence of phytoplankton biomass on the spatial distribution of carbon dioxide in surface seawater of a coastal area of the Gulf of Cádiz (SW Spain). Canadian Journal of Botany, Volume 83, Pages 929-940, DOI 10.1139/B05-082.

Hugman, R., Stigter, T.Y., Monteiro, J.P., Costa, L., Nunes, L.M., 2015. Modeling the spatial and temporal distribution of coastal groundwater discharge for different water use

scenarios under epistemic uncertainty: case study in South Portugal. Environmental Earth Sciences, Volume 73, Issue 6, Pages 2657-2669, DOI 10.1007/s12665-014-3709-4.

Huisman, J., van Oostveen, P., Weissing, F.J., 1999. Critical depth and critical turbulence: Two different mechanisms for the development of phytoplankton blooms. Limnology and Oceanography, Volume 44, Pages 1781-1787, DOI 10.4319/lo.1999.44.7.1781

Hurrell, J.W., Kushnir, Y., Ottersen, G., Visbeck, M., 2003. The North Atlantic Oscillation: Climatic significance and environmental impact. Book Series: Geophysical Monograph Series, John Wiley & Sons, DOI 10.1029/GM134.

Hurrell, J.W., 1995. Decadal Trends in the North Atlantic Oscillation: Regional Temperatures and Precipitation. Science, Volume 269, Issue 5224, Pages 676-679, DOI 10.1126/science.269.5224.676.

Hurrell, J.W., Dickson, R.R., 2004. Climate variability over the North Altantic. In: Stenseth, N.G., Otternsen, G., Hurrel, J.W., Belgrano, A. (Eds.) Marine Ecosystems and Climate Variation – the North Atlantic. Oxford University Press.

Iglesias, I., Lorenzo, M.N., Taboada, J.J., 2014. Seasonal Predictability of the East Atlantic Pattern from Sea Surface Temperatures. PLoS ONE, Volume 9, Issue 1, Pages e86439, DOI 10.1371/journal.pone.0086439.

International Council for the Exploration of the Sea (ICES), 2004. Report of the ICES Advisory Committee on Fishery Management and Advisory Committee on Ecosystems, Volume 1, Number 2, p. 290.

International Maritime Organization (IMO), 2005. Revised Guidelines for the Identification and Designation of Particularly Sensitive Sea Areas. IMO A 24/Res. 982. Available at http://www.imo.org/en/OurWork/Environment/PSSAs/Documents/A24-Res.982.pdf. (Accessed on 16 August 2017).

International Ocean Colour Coordinating Group (IOCCG), 2000. Remote Sensing of Ocean Colour in Coastal, and Other Optically-Complex, Waters. Sathyendranath, S. (Ed.), Reports and Monographs of the International Ocean-Colour Coordinating Group (IOCCG), Volume 3, IOCCG, Dartmouth, p. 140.

International Ocean Colour Coordinating Group (IOCCG), 2009. Partition of the ocean into ecological provinces: Role of ocean-colour radiometry. Dowell, M. Platt, T., Stuart, V. (Eds) Reports and Monographs of the International Ocean-Colour Coordinating Group (IOCCG), Volume 9, Dartmouth, p. 98.

International Ocean Colour Coordinating Group (IOCCG), 2011. Bio-Optical Sensors on Argo Floats. Claustre, H. (Ed), Reports and Monographs of the International Ocean-Colour Coordinating Group (IOCCG), Volume 11, Dartmouth, p. 96.

International Ocean Colour Coordinating Group (IOCCG), 2012. Ocean-Colour Observations from a Geostationary Orbit. Antoine, D. (Ed) Reports and Monographs of the International Ocean-Colour Coordinating Group (IOCCG), Volume 12, Dartmouth, p. 110.

International Ocean Colour Coordinating Group (IOCCG), 2014. Phytoplankton Functional Types from Space. Sathyendranath, S. (Ed) Reports and Monographs of the International Ocean-Colour Coordinating Group (IOCCG), Volume 15, Darthmouth, p. 164.

IOC, IHO and BODC, 2003. Centenary Edition of the GEBCO Digital Atlas, published on CD-ROM on behalf of the Intergovernmental Oceanographic Commission and the International Hydrographic Organization as part of the General Bathymetric Chart of the Oceans, British Oceanographic Data Centre, Liverpool.

Irwin, A.J., Oliver, M.J., 2009. Are ocean deserts getting larger? Geophysical Research Letters, Volume 36, L18609, DOI 10.1029/2009GL039883

Itoh, S., Yasuda, I., Saito, H., Tsuda, A., Komatsu, K., 2015. Mixed layer depth and chlorophyll a: Profiling float observations in the Kuroshio–Oyashio Extension region. Journal of Marine Systems, Volume 151, Pages 1-14, DOI 10.1016/j.jmarsys.2015.06.004

Jackson, T., Sathyendranath, S., Mélin, F., *in press*. An improved optical classification scheme for the Ocean Colour Essential Climate Variable and its applications. Remote Sensing of Environment, DOI 10.1016/j.rse.2017.03.036.

Jacox, M.G., Edwards, C.A., Kahru, M., Rudnick, D.L., Kudela, R.M., 2015. The potential for improving remote primary productivity estimates through subsurface chlorophyll and irradiance measurement. Deep Sea Research Part II: Topical Studies in Oceanography, Volume 112, Pages 107-116, DOI 10.1016/j.dsr2.2013.12.008.

Ji, R., Edwards, M., Mackas, D.L., Runge, J.A., Thomas, A.C., 2010. Marine plankton phenology and life history in a changing climate: current research and future directions. Journal of Plankton Research. Volume 32, Pages 1355–1368, DOI 10.1093/plankt/fbq062

Jickells, T.D., An, Z.S., Andersen, K.K., Baker, A.R., Bergametti, G., Brooks, N., Cao, J.J., Boyd, P.W., Duce, R.A., Hunter, K.A., Kawahata, H., Kubilay, N., laRoche, J., Liss, P.S., Mahowald, N., Prospero, J.M., Ridgwell, A.J., Tegen, I., Torres, R., 2005. Global iron connections between desert dust, ocean biogeochemistry, and climate. Science, Volume 308, Issue 5718, Pages 67-71, DOI 10.1126/science.1105959.

Kahru, M., Brotas, V., Manzano-Sarabia, M., Mitchell, B.G., 2010. Are phytoplankton blooms occurring earlier in the Arctic? Global Change Biology, Volume 17, Issue 4, Pages 1733-1739, DOI 10.1111/j.1365-2486.2010.02312.x

Kahru, M., Elmgren, R., Savchuk, O.P., 2015. Changing seasonality of the Baltic Sea. Biogeosciences Discussions, Volume 12, Pages 18855-18882, DOI 10.5194/bgd-12-18855-2015

Kahru, M., Gille, S.T., Murtugudde, R., Strutton, P., Mitchell, B.G., 2010. Mapping of ocean bio- geochemical provinces using correlations between satellite-derived winds and chlorophyll. In: Barale, V., Gower, J.F.R., Alberotanza, L. (Eds) Proceedings of Oceans from Space, Venice, European Commission, EUR 24324 EN, pp. 123-124.

Kaplan, A., Cane, M.A., Kushnir, Y., Clement, A.C., Blumenthal, M.B., Rajagopalan, B., 1998. Analyses of global sea surface temperature 1856-1991. Journal of Geophysical Research, Volume 103, Issue C9, Pages 18567-18589, DOI 10.1029/97JC01736

Karabashev, G., Evdoshenko, M., Sheberstov, S., 2002. Penetration of coastal waters into the Eastern Mediterranean Sea using the SeaWiFS data. Oceanologica Acta, Volume 25, Pages 31-38, DOI 10.1016/S0399-1784(02)01180-5.

Kim, H.-J., Miller, A.J., McGowan, J., Carter, M.L., 2009. Coastal phytoplankton blooms in the Southern California Bight. Progress in Oceanography, Volume 82, Pages 137-147, DOI 10.1016/j.pocean.2009.05.002

Kirk, J.T.O., 1986. Light and photosynthesis in aquatic ecosystems, Cambridge University Press, Cambridge.

Koeller, P., Fuentes-Yaco, C., Platt, T., Sathyendranath, S., Richards, A., Ouellet, P., Orr, D., Skúladóttir, U., Wieland, K., Savard, L., Aschan, M., 2009. Basin-scale coherence in phenology of shrimps and phytoplankton in the North Atlantic Ocean. Science, Volume 324, Issue 5928, Pages 791-793, DOI 10.1126/science.1170987

Kohonen, T., 2001. Self-Organizing Maps, Springer Science & Business Media, p. 501.

Kostadinov, T.S., Cabré, A., Vedantham, H., Marinov, I., Bracher, A., Brewin, R.J.W., Bricaud, A., Hirata, T., Hirawake, T., Hardman-Mountford, N.J., Mouw, C., Roy, S., Uitz, J., 2017. Inter-comparison of phytoplankton functional type phenology metrics derived from ocean color algorithms and Earth System Models. Remote Sensing of Environment, Volume 190, Pages 162-177, DOI 10.1016/j.rse.2016.11.014

Kovats, R.S., Valentini, R., Bouwer, L.M., Georgopoulou, E., Jacob, D., Martin, E., Rounsevell, M., Soussana, J.-F., 2014. Europe. In: Barros, V.R., Field, C.B., Dokken, D.J., Mastrandrea, M.D., Mach, K.J., Bilir, T.E., Chatterjee, M., Ebi, K.L., Estrada, Y.O., Genova, R.C., Girma, B., Kissel, E.S., Levy, A.N., MacCracken, S., Mastrandrea, P.R., White, L.L. (Eds). Climate Change 2014: Impacts, Adaptation, and Vulnerability. Part B: Regional Aspects. Contribution of Working Group II to the Fifth Assessment Report of the Intergovernmental Panel on Climate Change. Cambridge University Press, Cambridge, United Kingdom and New York, NY, USA, pp. 1267-1326.

Kromkamp, J.C, van Engeland, T., 2010. Changes in Phytoplankton Biomass in the Western Scheldt Estuary During the Period 1978–2006. Estuaries and Coasts, Volume 33, Pages 270-285, DOI 10.1007/s12237-009-9215-3

Krug, L. A., Platt, T., Sathyendranath, S., Barbosa, A. B., 2017. Ocean surface partitioning strategies using Ocean Colour Remote Sensing: a review. Progress in Oceanography , Volume 155, Pages 41-53, DOI 10.1016/j.pocean.2017.05.013.

Krug, L. A., Platt, T., Sathyendranath, S., Barbosa, A. B., *in press*. Unravelling region-specific environmental drivers of phytoplankton across a complex marine domain (off SW Iberia). Remote Sensing of Environment, DOI 10.1016/j.rse.2017.05.029.

Krug, L.A., Platt,T., Barbosa, A.B., *submitted*. Delineation of ocean surface provinces over a complex marine domain (off SW Iberia): an objective abiotic-based approach. Regional Studies in Marine Science.

Kumar, P., Min, S., Weller, E., Lee, H., Wang, X., 2016. Influence of climate variability on extreme ocean surface wave heights assessed from ERA-Interim and ERA-20C. Journal of Climate, Volume 29, Issue 11, Pages 4031-4046, DOI 10.1175/JCLI-D-15-0580.1.

Lachkar, Z., Gruber, N., 2011. What controls biological productivity in coastal upwelling systems? Insights from a comparative modeling study. Biogeosciences, Volume 8, Pages 2961-2976, DOI 10.5194/bg-8-2961-2011.

Lachkar, Z., Gruber, N., 2012. A comparative study of biological production in eastern boundary upwelling systems using an artificial neural network. Biogeosciences, Volume 9, Pages 293-308, DOI 10.5194/bg-9-293-2012.

Lacour, L., Claustre, H., Prieur, L., D'Ortenzio, F., 2015. Phytoplankton biomass cycles in the North Atlantic subpolar gyre: A similar mechanism for two different blooms in the Labrador Sea. Geophysical Research Letters, Volume 42, Pages 5403–5410,DOI 10.1002/2015GL064540.

Land, P.E., Shutler, J.D., Platt, T., Racault, M.F., 2014. A novel method to retrieve oceanic phytoplankton phenology fromsatellite data in the presence of data gaps. Ecological Indicators, Volume 37, Pages 67-80, DOI 10.1016/j.ecolind.2013.10.008

Lavigne, H., D'Ortenzio, F., Migon, C., Claustre, H., Testor, P., d'Alcalá, M.R., Lavezza, R., Houpert, L., Prieur, L., 2013. Enhancing the comprehension of mixed layer depth control on the Mediterranean phytoplankton phenology. Journal of Geophysical Research Oceans, Volume 118, Pages 1-15, DOI 10.1002/jgrc.20251

Le Quéré, C., Saltzman, E.S. (Eds.), 2009. Surface Ocean-Lower Atmosphere Processes, Geophysical Monograph Series. American Geophysical Union, Washington, p. 329, DOI 10.1029/gm187.

Lecher, A.L., Mackey, K., Kudela, R., Ryan, J., Fisher, A., Murray, J., Paytan, A., 2015. Nutrient Loading through Submarine Groundwater Discharge and Phytoplankton Growth in Monterey Bay, CA. Environmental Science and Technology, Volume 49, Issue 11, Pages 6665-6673, DOI 10.1021/acs.est.5b00909.

Leitão, F., Encarnação, J., Range, P., Schmelz, R.M., Teodósio, M.A., Chícharo, L., 2015. Submarine groundwater discharges create unique benthic communities in a coastal sandy marine environment. Estuarine, Coastal and Shelf Science, Volume 163, Part B, Pages 93-98, DOI 10.1016/j.ecss.2015.06.007.

Lemos, R.T., Pires, H. O., 2004. The upwelling regime off the west Portuguese coast, 1941-2000. International Journal of Climatology, Volume 24, Issue 4, Pages 511-524, DOI 10.1002/joc.1009.

Lemos, R.T., Sansó, B., 2006. Spatio-temporal variability of ocean temperature in the Portugal Current System. Journal of Geophysical Research, Volume 111, C04010, DOI 10.1029/2005JC003051.

Lévy, M., 2008. The modulation of biological production by oceanic mesoscale turbulence, in: Weiss, J. B., Provenzale, A. (Eds.) Transport and mixing in geophysical flows. Lectures Notes of Physics Volume 744, Springer Berlin Heidelberg, pp. 219-261, DOI 10.1007/978-3-540-75215-8_9.

Lima, F.P., Wethey, D.S., 2012. Three decades of high-resolution coastal sea surface temperatures reveal more than warming. Nature Communications, Volume 3, Pages 1-13, DOI 10.1038/ncomms1713.

Liu, F., Su, J., Moll, A., Krasemann, H., Chen, X., Pohlmann, T., Wirtz, K., 2014. Assessment of the summer–autumn bloom in the Bohai Sea using satellite images to identify the roles of wind mixing and light conditions. Journal of Marine Systems, Volume 129, Pages 303-317, DOI 10.1016/j.jmarsys.2013.07.007

Liu, Y., Weisberg, R. W., 2011. A review of Self-Organizing Map applications in meteorology and oceanography. In: Mwasiagi, J.I. (Ed.) Self-Organizing Maps - applications and novel algorithm design, InTech, 253-272.

Llope, M., Chan, K.-S., Ciannelli, L., Reid, P.C., Stige, L.C., Stenseth, N.C., 2009. Effects of environmental conditions on the seasonal distribution of phytoplankton biomass in the North Sea. Limnology and Oceanography, Volume 54, Issue 2, Pages 512-524, DOI 10.4319/lo.2009.54.2.0512.

Longhurst, A., 1995. Seasonal cycles of pelagic production and consumption. Progress in Oceanography, Volume 36, Issue 2, Pages 77-167, DOI 10.1016/0079-6611(95)00015-1.

Longhurst, A., 1998. Ecological Geography of the Sea. Academic Press, London, p. 398.

Longhurst, A., 2007. Ecological geography of the sea. Academic Press, Burlington, p. 560.

Longhurst, A., Sathyendranath, S., Platt, T., Caverhill, C., 1995. An estimate of global primary production in the ocean from satellite radiometer data. Journal of Plankton Research, Volume 17, Issue 6, Pages 1245-1271, DOI 10.1093/plankt/17.6.1245.

Loureiro, S., Icely, J., Newton, A., 2008. Enrichment experiments and primary production at Sagres (SW Portugal). Journal of Experimental Marine Biology and Ecology, Volume 359, Issue 2, Pages 118-125, DOI 10.1016/j.jembe.2008.03.001.

Loureiro, S., Newton, A., Icely, J.D., 2005. Microplankton composition, production and upwelling dynamics in Sagres (SW Portugal) during the summer of 2001. Scientia Marina, Volume 69, Issue 3, pages 323-341, DOI 10.3989/scimar.2005.69n3.

Loureiro, S., Reñé, A., Garcés, E., Camp, J., Vaqué, D., 2011. Harmful algal blooms (HABs), dissolved organic matter (DOM), and planktonic microbial community dynamics at a

near-shore and a harbour station influenced by upwelling (SW Iberian Peninsula). Journal of Sea Research, Volume 65, Issue 4, Pages 401-413, DOI 10.1016/j.seares.2011.03.004.

Lourenço, C.R., Nicastro, K.R., Serrão, E.A., Zardi, G.I., 2012. First record of the brown mussel (Perna perna) from the European Atlantic coast. Marine Biodiversity Records, Volume 5, e39, DOI 10.1017/S1755267212000280.

Lubac, B., Loisel, H., 2007. Variability and classification of remote sensing reflectance spectra in the eastern English Channel and southern North Sea. Remote Sensing of Environment, Volume 110, Issue 1, Pages 45-58, DOI 10.1016/j.rse.2007.02.012.

Lucieer, V., Lucieer, A., 2009. Fuzzy clustering for seafloor classification. Marine Geology, Volume 264, Issues 3-4, Pages 230-241, DOI 10.1016/j.margeo.2009.06.006.

Lutz, M.J., Caldeira, K., Dunbar, R.B., Behrenfeld, M.J., 2007. Seasonal rhythms of net primary production and particulate organic carbon flux to depth describe the efficiency of biological pump in the global ocean. Journal of Geohysical Research, Volume 112, C10011, DOI 10.1029/2006JC003706

Macías, D.M., Guerreiro, C.T., Prieto, L., Peliz, A., Ruiz, J., 2014. A high-resolution hydrodynamic-biogeochemical coupled model of the Gulf of Cadiz - Alboran Sea region. Mediterranean Marine Science, Volume 15, Issue 4, Pages 739-752, DOI 10.12681/mms.841.

Macías, D., Lubián, L.M., Echevarría, F., Huertas, I.E., García, C.M., 2008. Chlorophyll maxima and water mass interfaces: Tidally induced dynamics in the Strait of Gibraltar. Deep Sea Research Part I: Oceanographic Research Papers, Volume 55, Issue 7, Pages 832-846, DOI 10.1016/j.dsr.2008.03.008.

Macías, D., Navarro, G., Echevarría, F., García, C.M., Cueto, J.L., 2007. Phytoplankton pigment distribution in the north-western Alboran Sea and meteorological forcing: a remote sensing study, Journal of Marine Research, Volume 65, Issue 4, Pages 523-543, DOI 10.1357/002224007782689085.

Mahadevan, A., 2016. The impact of submesoscale physics on primary productivity of plankton. Annual Review of Marine Science, Volume 8, Pages 161-184, DOI 10.1146/annurev-marine-010814-015912.

Mahadevan, A., D'asaro, E., Lee, C., Perry, M.J., 2012. Eddy-driven stratification initiates North Atlantic spring phytoplankton blooms. Science, Volume 337, Pages 54-58, DOI 10.1126/science.1218740

Malick, M.J., Cox, S.P., Mueter, F.J., Peterman, R.M., 2015. Linking phytoplankton phenology to salmon productivity along a north/south gradient in the Northeast Pacific Ocean. Canadian Journal of Fisheries and Aquatic Sciences, Volume 72, Issue 5, Pages 697-708, DOI 10.1139/cjfas-2014-0298

Malta, T., Santos, P.T., Santos, A.M.P., Rufino, M., Silva, A., 2016. Long-term variations in Ibero-Atlantic sardine (Sardina pilchardus) population dynamics: Relation to environmental conditions and exploitation history. Fisheries Research, Volume 179, Pages 47-56, DOI 10.1016/j.fishres.2016.02.009.

Margalef, R., 1978. Life-forms of phytoplankton as survival alternatives in an unstable environment. Oceanologica Acta, Volume 1, Issue 4, Pages 493-509.

Marshall, J., Kushnir, Y., Battisti, D., Chang, P., Czaja, A., Dickson, R., Hurrell, J., McCartney, M., Saravanan, R., Visbeck, M., 2001. North Atlantic climate variability: phenomena, impacts and mechanisms. International Journal of Climatology, Volume 21, Pages 1863-1898, DOI 10.1002/joc.693.

Marta-Almeida, M., Reboreda, R., Rocha, C., Dubert, J., Nolasco, R., Cordeiro, N., Luna, T., Rocha, A., Lencart e Silva, J.D., Queiroga, H., Peliz, A., Ruiz-Villarreal, M., 2012. Towards Operational Modeling and Forecasting of the Iberian Shelves Ecosystem. PLoS ONE, Volume 7, Issue 5, e37343, DOI 10.1371/journal.pone.0037343.

Martinez, E., Antoine, D., D'Ortenzio, F., Gentili, B., 2009. Climate-driven basin-scale decadal oscillations of oceanic phytoplankton. Science, Volume 326, Pages 1253-1256, DOI: 10.1126/science.1177012.

Martinez, E., Antoine, D., D'Ortenzio, F., Montégut, C.B., 2011. Phytoplankton spring and fall blooms in the North Atlantic in the 1980s and 2000s. Journal of Geophysical Research, Volume 116, C11029, DOI 10.1029/2010JC006836.

Martinez, E., Raitson, D.E., Antoine, D., 2016. Warmer, deeper, and greener mixed layers in the North Atlantic subpolar gyre over the last 50 years. Global Change Biology, Volume 22, Issue 2, Pages 604-612, DOI 10.1111/gcb.13100.

Martin-Vide J., Lopez-Bustins, J.A., 2006. The Western Mediterranean Oscillation and Iberian Peninsula Rainfall. International Journal of Climatology, Volume 26, Issue 11, Pages 1455-1475, DOI 10.1002/joc.1388.

Mayot, N., D'Ortenzio, F., d'Alcalá, M.R., Lavigne, H., Claustre, H., 2015. Interannual variability of the Mediterranean trophic regimes from ocean color satellites. Biogeosciences Discussions, Volume 12, Pages 14941-14980, DOI 10.5194/bgd-12-14941-2015.

McGillicuddy Jr., D.J., 2016. Mechanisms of physical-biological-biogeochemical interaction at the oceanic mesoscale. Annual Review of Marine Science, 8, 125-159, DOI 10.1146/annurev-marine-010814-015606.

Mélin, F., Sclep, G., Jackson, T., Sathyendranath, S., 2016. Uncertainty estimates of remote sensing reflectance derived from comparison of ocean color satellite data sets. Remote Sensing of Environment, Volume 177, Pages 107-124, DOI 10.1016/j.rse.2016.02.014.

Mélin, F., Vantrepotte, V., 2015. How optically diverse is the coastal ocean? Remote Sensing of Environment, Volume 160, Pages 235-251, DOI 10.1016/j.rse.2015.01.023.

Merchant, C.J., Paul, F., Popp, T., Ablain, M., Bontemps, S., Defourny, P., Hollmann, R., Lavergne, T., Laeng, A., de Leeuw, G., Mittaz, J., Poulsen, C., Povey, A.C., Reuter, M., Sathyendranath, S., Sandven, S., Sofieva, V.F., Wagner, W, 2017. Uncertainty information in climate data records from Earth observation. Earth System Science Data, Volume 9, Pages 511-527, DOI 10.5194/essd-9-511-2017

Moita, M.T., 2001. Estrutura, variabilidade e dinâmica do fitoplâncton na costa de Portugal continental [Structure, variability and dynamics of phytoplankton off the coast of

Continental Portugal]. PhD dissertation (In Portuguese), University of Lisbon, Lisbon. https://www.ipma.pt/resources.www/docs/publicacoes.site/teses/Teresa_Moitathesis.pdf (accessed 09.08.16).

Monahan, A.H., Fyfe, J.C., Ambaum, M.H.P., Stephenson, D.B., North, G.R., 2009. Empirical orthogonal functions: the medium is the message. Journal of Climate, Volume 22, Pages 6501-6514, DOI 10.1175/2009JCLI3062.1.

Moore, T.S., Campbell, J.W., Dowell, M.D., 2009. A class-based approach to characterizing and mapping the uncertainty of the MODIS ocean chlorophyll product. Remote Sensing of Environment, Volume 113, Issue 11, Pages 2424-2430, DOI 10.1016/j.rse.2009.07.016.

Moore, T.S., Campbell, J.W., Feng, H., 1998. Fuzzy classification of ocean color satellite data for bio-optical algorithm constituent retrievals. NASA contractor report, Washington, National Technical Information Service, NASA CR-207771.

Moore, T.S., Campbell, J.W., Feng, H., 2001. A fuzzy logic classification scheme for selecting and blending satellite ocean color algorithms. IEEE Transactions on Geoscience and Remote Sensing, Volume 39, Issue 8, Pages 1764-1776, DOI 10.1109/36.942555

Morales, J., Sathyendranath, S., Beaugrand, G., Hoepffner, N., Mata, A., 2009. Applications to marine resources and biodiversity. In: Dowell, M. Platt, T., Stuart, V. (Eds) Partition of the ocean into ecological provinces: Role of ocean-colour radiometry. Reports and Monographs of the International Ocean-Colour Coordinating Group (IOCCG), Volume 9, Dartmouth, pp. 69-81.

Morel, A., 1988. Optical modeling of the upper ocean in relation to its biogenous matter content (case 1 water). Journal of Geophysical Research, Volume 93, Issue C9, Pages 10749-10768, DOI 10.1029/JC093iC09p10749.

Morel, A., Prieur, L., 1977. Analysis of variations in ocean color. Limnology and Oceanography, Volume 22, Issue 4, Pages 709-722, DOI 10.4319/lo.1977.22.4.0709.

Muacho, S., da Silva, J.C.B., Brotas, V., Oliveira, P.B., 2013. Effect of internal waves on near-surface chlorophyll concentration and primary production in the Nazaré Canyon

(west of the Iberian Peninsula). Deep Sea Research I, Volume 81, Pages 89-96, DOI 10.1016/j.dsr.2013.07.012.

Mueller, J.L., Lange, R.E., 1989. Bio-optical provinces of the Northeast Pacific Ocean: A provisional analysis. Limnology and Oceanography, Volume 34, Issue 8, Pages 1572-1586, DOI 10.4319/lo.1989.34.8.1572.

Muñoz, M., Reul, A., Plaza, F., Gómez-Moreno, M.-L., Vargas-Yañez, M., Rodríguez, V., Rodríguez, J., 2015. Implication of regionalization and connectivity analysis for marine spatial planning and coastal management in the Gulf of Cadiz and Alboran Sea. Ocean & Coastal Management, Volume 118, Part A, Pages 60-74, DOI 10.1016/j.ocecoaman.2015.04.011.

Nagai, T., Gruber, N., Frenzel, H., Lachkar, Z., McWilliams, J.C., Plattner, G.-K., 2015. Dominant role of eddies and filaments in the offshore transport of carbon and nutrients in the California Current System. Journal of Geophysical Research Oceans, Volume 120, Pages 5318–5341, DOI 10.1002/2015JC010889.

Navarro, G., Caballero, I., Prieto, L., Vázquez, A., Flecha, S., Huertas, I.E., Ruiz, J., 2012. Seasonal-to-interannual variability of chlorophyll-a bloom timing associated with physical forcing in the Gulf of Cádiz. Advances in Space Research, Volume 50, Issue 8, Pages 1164-1172, DOI 10.1016/j.asr.2011.11.034.

Navarro, G., Escudier, R., Gómez-Enri, J., Pascual, A., Caballero, I., Vázquez, A., 2013. Singular value decomposition of ocean surface chlorophyll and sea level anomalies in the Gulf of Cádiz (South-Western Iberian Peninsula), in: European Space Agency Publications. 20 years of progress in radar altimetry Conference.

Navarro, G., Prieto, L., Huertas, I.E., Ruiz, J., Gomez-Enri, J., 2007. Seasonal and interannual patterns of chlorophyll bloom timing in the Gulf of Cádiz. IEEE International Geoscience and Remote Sensing Symposium, Pages 50-53, DOI 10.1109/IGARSS.2007.4422727.

Navarro, G., Ruiz, J., 2006. Spatial and temporal variability of phytoplankton in the Gulf of Cádiz through remote sensing images, Deep Sea Research Part II: Topical Studies in

Oceanography, Volume 53, Issues 11-13, Pages 1241-1260, DOI 10.1016/j.dsr2.2006.04.014.

Navarro, G., Ruiz, J., Huertas, I.E., García, C.M., Criado-Aldeanueva, F., Echevarría,F., 2006. Basin-scale structures governing the position of the deep fluorescence maximum in the Gulf of Cádiz. Deep Sea Research Part II: Topical Studies in Oceanography, Volume 53, Issues 11-13, Pages 1261-1281, DOI 10.1016/j.dsr2.2006.04.013.

Navarro, G., Vazquez, A., Macias, D., Bruno, M., Ruiz, J., 2011. Understanding the patterns of biological response to physical forcing in the Alboran Sea (western Mediterranean). Geophysical Research Letters, Volume 38, L23606, DOI 10.1029/2011GL049708.

Nechad, B., Ruddick, K., Schroeder, T., Oubelkheir, K., Blondeau-Patissier, D., Cherukuru, N., Brando, V., Dekker, A., Clementson, L., Banks, A.C., Maritorena, S., Werdell, J., Sá, C., Brotas, V., Caballero de Frutos, I., Ahn, Y.-H., Salama, S., Tilstone, G., Martinez-Vicente, V., Foley, D., McKibben, M., Nahorniak, J., Peterson, T., Siliò-Calzada, A., Röttgers, R., Lee, Z., Peters, M., Brockmann, C., 2015. CoastColour Round Robin datasets: a database to evaluate the performance of algorithms for the retrieval of water quality parameters in coastal waters. Earth System Science Data, Volume 7, Pages 173-258, DOI 10.5194/essd-7-319-2015

Newton, A., Icely, J., Cristina, S., Brito, A., Cardoso, A.C., Colijn, F., Riva, S.D., Gertz, F., Hansen, J.W., Holmer, M., Ivanova, K., Leppäkoski, E., Canu, D.M., Mocenni, C., Mudge, S., Murray, N., Pejrup, M., Razinkovas, A., Reizopoulou, S., Pérez-Ruzafa, A., Schernewski, G., Schubert, H., Carr, L., Solidoro, C., PierluigiViaroli, Zaldívar, J., 2014. An overview of ecological status, vulnerability and future perspectives of European large shallow, semi-enclosed coastal systems, lagoons and transitional waters. Estuarine, Coastal and Shelf Science, Volume 140, Pages 95-122, DOI 10.1016/j.ecss.2013.05.023.

Nicastro, K.R., Zardi, G.I., Teixeira, S., Neiva, J., Serrão, E.A., Pearson, G.A., 2013. Shift happens: trailing edge contraction associated with recent warming trends threatens a distinct genetic lineage in the marine macroalga Fucus vesiculosus. BMC Biology, Volume 11, 6, DOI 10.1186/1741-7007-11-6.

Nieblas, A-E., Drushka, K., Reygondeau, G., Rossi, V., Demarcq, H., Dubroca, L., Bonhommeau, S., 2014. Defining Mediterranean and Black Sea biogeochemical subprovinces and synthetic ocean indicators using mesoscale oceanographic features. PLoS ONE, Volume 9, Issue 10, e111251, DOI 10.1371/journal.pone.0111251

Nixon, S.W., Fulweiler, R.W., Buckley, B.A., Granger, S.L., Nowicki, B.L., Henry, K.M., 2009. The impact of changing climate on phenology, productivity, and benthic–pelagic coupling in Narragansett Bay. Estuarine, Coastal and Shelf Science, Volume 82, Pages 1-18, DOI 10.1016/j.ecss.2008.12.016

North, G.R., Bell, T.L., Cahalan, R.F., Moeng, F.J., 1982. Sampling errors in the estimation of empirical orthogonal functions. Monthly Weather Review, Volume 110, Issue 7, Pages 699-706, DOI 10.1175/1520-0493(1982)110<0699:SEITEO>2.0.CO,2.

Oliver, M.J., Glenn, S., Kohut, J.T., Irwin, A.J., Schofield, O.M., Moline, M.A., Bissett, W.P., 2004. Bioinformatic approaches for objective detection of water masses on continental shelves. Journal of Geophysical Research, Volume 109, Issue C7, C07S04, DOI 10.1029/2003JC002072

Oliver, M.J., Irwin, A.J., 2008. Objective global ocean biogeographic provinces. Geophysical Research Letters, Volume 35, L15601, DOI 10.1029/2008GL034238.

O'Reilly, J.E., Maritorena, S., Siegel, D., O'Brien, M., Toole, D., Mitchell, B.G., Kahru, M., Chavez, F., Strutton, P., Cota, G., Hooker, S., McClain, C., Carder, K., Muller-Karger, F., Harding, L., Magnuson, A., Phinney, D., Moore, G., Aiken, J., Arrigo, K., Letelier, R., Culver, M., 2000. Ocean color chlorophyll a algorithms for SeaWiFS, OC2, and OC4: Version 4, in: Hooker, E.R., Firestone, S.B. (Eds.): SeaWiFS Postlaunch Calibration and Validation Analyses, Part 3. NASA Tech. Memo. 2000-206892, Volume 11, NASA Goddard Space Flight Center, Greenbelt.

Otto, S.A., Diekmann, R., Flinkman, J., Kornilovs, G., Möllmann, C., 2014. Habitat heterogeneity determines climate impact on zooplankton community structure and dynamics. PLoS ONE, Volume 9, Issue 3, e90875, DOI 10.1371/journal.pone.0090875.

Oziel, L., Neukermans, G., Ardyna, M., Lancelot, C., Tison, J-L., Wassmann, P., Sirven, J., Ruiz-Pino, D., Gascard, J-C., 2017. Role for Atlantic inflows and sea ice loss on shifting phytoplankton blooms in the Barents Sea. Journal of Geophysical Research Oceans, Volume 122, Pages 5121–5139, DOI 10.1002/2016JC012582

Painter, S.C., Finlay, M., Hemsley, V.S., Martin, A.P., 2016. Seasonality, phytoplankton succession and the biogeochemical impacts of an autumn storm in the northeast Atlantic Ocean. Progress in Oceanography, Volume 142, Pages 72-104, DOI 10.1016/j.pocean.2016.02.001.

Palma, S., Mouriño, H., Silva, A., Barão, M.I., Moita, M.T., 2010. Can *Pseudo-nitzschia* blooms be modeled by coastal upwelling in Lisbon Bay? Harmful Algae, Volume 9, Issue 3, Pages 294-303, DOI 10.1016/j.hal.2009.11.006.

Pardo, P.C., Padín, X.A., Gilcoto, M., Farina-Busto, L., Pérez, F.F., 2011. Evolution of upwelling systems coupled to the long-term variability in sea surface temperature and Ekman transport. Climate Research, Volume 48, Pages 231-246, DOI 10.3354/cr00989.

Patti, B., Guisande, C., Vergara, A.R., Riveiro, I., Maneiro, I., Barreiro, A., Bonanno, A., Buscaino, G., Cuttitta, A., Basilone, G., Mazzola, S., 2008. Factors responsible for the differences in satellite-based chlorophyll a concentration between the major global upwelling areas. Estuarine, Coastal and Shelf Science, Volume 76, Issue 4, Pages 775-786, DOI 10.1016/j.ecss.2007.08.005.

Peliz, Á., Boutov, D., Aguiar, A. B., Carton, X., 2014. The Gulf of Cadiz Gap wind anticyclones. Continental Shelf Research, Volume 91, Pages 171-191, DOI 10.1016/j.csr.2014.09.004.

Peliz, Á., Fiúza, A., 1999. Temporal and spatial variability of CZCS-derived phytoplankton pigment concentrations off the Western Iberian Peninsula. International Journal of Remote Sensing, Volume 20, Issue 7, Pages 1363-1403, DOI 10.1080/014311699212786.

Peliz, Á., Santos, A. M. P., Oliveira, P. B., Dubert, J., 2004. Extreme cross-shelf transport induced by eddy interactions southwest of Iberia in winter 2001. Geophysical Research Letters, Volume 31, L08301, DOI 10.1029/2004GL019618.

Peliz, Á., Teles-Machado, A., Marchesiello, P., Dubert, J., García-Lafuente, J., 2009. Filament generation off the Strait of Gibraltar in response to Gap winds. Dynamics of Atmospheres and Oceans, Volume 46, Issues 1-4, Pages 36-45, DOI 10.1016/j.dynatmoce.2008.08.002.

Pérez, F.F., Padín, X. A., Pazos, Y., Gilcoto, M., Cabanas, M., Pardo, P.C., Doval, M.D., Farina-Bustos, L., 2010. Plankton response to weakening of the Iberian coastal upwelling. Global Change Biology, Volume 16, Pages 1258-1267, DOI 10.1111/j.1365-2486.2009.02125.x.

Picado, A., Alvarez, I., Vaz, N., Varela, R., Gomez-Gesteira, M., Dias, J. M., 2014. Assessment of chlorophyll variability along the northwestern coast of Iberian Peninsula. Journal of Sea Research, Volume 93, Pages 2-11, DOI 10.1016/j.seares.2014.01.008.

Picado, A., Lorenzo, M.N., Alvarez, I., deCastro, M., Vaz, N., Dias, J.M., 2015. Upwelling and Chl-a spatiotemporal variability along the Galician coast: dependence on circulation weather types. International Journal of Climatology, Volume 36, Issue 9, Pages 3280-3296, DOI 10.1002/joc.4555.

Piló, D., Barbosa, A., Teodósio, M., Encarnação, J., Leitão, F., Range, P., Krug, L.A., Cruz, J., Chicharo, L., *submitted*. Are submarine groundwater discharges affecting the structure and physiological status of rocky intertidal communities? Estuarine, Coastal and Shelf Science.

Pitcher, G.C., Figueiras, F.G., Hickey, B.M., Moita, M.T., 2010. The physical oceanography of upwelling systems and the development of harmful algal blooms. Progress in Oceanography, Volume 85, Pages 5-32, DOI 10.1016/j.pocean.2010.02.002

Platt, T., Bird, D.F., Sathyendranath, S.,1991. Critical depth and marine primary production. Proceedings of the Royal Society B, Volume 246, Pages 205-217, DOI 10.1098/rspb.1991.0146.

Platt, T., Bouman, H., Devred, E., Fuentes-Yaco, C., Sathyendranath, S., 2005. Physical forcing and phytoplankton distributions. Scientia Marina, Volume 69, Issue S1, Pages 55-73, DOI 10.3989/scimar.2005.69s155.

Platt, T., Dowell, M., 2009. Introduction. In: Dowell, M. Platt, T., Stuart, V. (Eds) Partition of the ocean into ecological provinces: Role of ocean-colour radiometry. Reports and Monographs of the International Ocean-Colour Coordinating Group (IOCCG), Volume 9, Dartmouth, pp. 1-8.

Platt, T., Fuentes-Yaco, C., Frank, K.T., 2003. Spring algal bloom and larval fish survival. Nature, Volume 423, Pages 398-399, DOI 10.1038/423398b.

Platt, T., Sathyendranath, S., 1988. Oceanic primary production: Estimation by remote sensing at local and regional scales. Science, Volume 241, Issue 4873, Pages 1613-1620, DOI 10.1126/science.241.4873.1613.

Platt, T., Sathyendranath, S., 1999. Spatial structure of pelagic ecosystem processes in the global Ocean. Ecosystems, Volume 2, Issue 5, Pages 384-394, DOI 10.1007/s100219900088.

Platt, T., Sathyendranath, S., 2008. Ecological indicators for the pelagic zone of the ocean from remote sensing. Remote Sensing of Environment, Volume 112, Issue 8, Pages 3426–3436, DOI 10.1016/j.rse.2007.10.016.

Platt, T., Sathyendranath, S., White III, G.N., Fuentes-Yaco, C., Zhai, L., Devred, E., Tang, C., 2010. Diagnostic properties of phytoplankton time series from remote sensing. Estuaries and Coasts, Volume 33, Pages 428-439, DOI 10.1007/s12237-009-9161-0.

Platt, T., White III, G.N., Zhai, L., Sathyendranath, S., Roy, S., 2009. The phenology of phytoplankton blooms: Ecosystem indicators from remote sensing. Ecological Modelling, Volume 220, Issue 21, Pages 3057-3069, DOI 10.1016/j.ecolmodel.2008.11.022

Plomaritis, T.A., Benavente, J., Laiz, I., Del Río, L., 2015. Variability in storm climate along the Gulf of Cadiz: the role of large scale atmospheric forcing and implications to coastal hazards. Climate Dynamics, Volume 45, Issue 9-10, Pages 2499-2514, DOI 10.1007/s00382-015-2486-4.

Priede, I.G., 2014. Biogeography of the Oceans: a Review of Development of Knowledge of Currents, Fronts and Regional Boundaries from Sailing Ships in the Sixteenth Century to Satellite Remote Sensing. Pure and Applied Geophysics, Volume 171, Pages 1013-1027, DOI 10.1007/s00024-013-0708-4.

Prieto, L., Navarro, G., Rodríguez-Gálvez, S., Huertas, I.E., Naranjo, J.M., Ruiz, J., 2009. Oceanographic and meteorological forcing of the pelagic ecosystem on the Gulf of Cadiz shelf (SW Iberian Peninsula). Continental Shelf Research, Volume 29, Issue 17, Pages 2122-2137, DOI 10.1016/j.csr.2009.08.007

R Core Team, 2016. R: A language and environment for statistical computing. R Foundation for Statistical Computing, Vienna, Austria. http://www.R-project.org/ (accessed 24.03.17).

Racault, M., Platt, T., Sathyendranath, S., Ağirbaş, E., Vicente, V.M., Brewin, R., 2014a. Plankton indicators and ocean observing systems: support to the marine ecosystem state assessment. Journal of Plankton Research, Volume 36, Issue 3, Pages 621-629, DOI 10.1093/plankt/fbu016

Racault, M., Sathyendranath, S. Platt, T., 2014b. Impact of missing data on the estimation of ecological indicators from satellite ocean-colour time-series. Remote Sensing of Environment, Volume 152, Pages 15-28, DOI 10.1016/j.rse.2014.05.016.

Racault, M.F., Le Quéré, C., Buitenhuis, E., Sathyendranath, S., Platt, T., 2012. Phytoplankton phenology in the global ocean. Ecological Indicators, Volume 14, Pages 152-163, DOI 10.1016/j.ecolind.2011.07.010

Racault, M.F., Raitsos, D.E., Berumen, M.L., Brewin, R.J.W., Platt, T., Sathyendranath, S., Hoteit, I., 2015. Phytoplankton phenology indices in coral reef ecosystems: Application to ocean-color observations in the Red Sea. Remote Sensing of Environment, Volume 160, Pages 222-234, DOI 10.1016/j.rse.2015.01.019.

Racault, M.F., Sathyendranath, S., Menon, N., Platt, T., 2017. Phenological responses to ENSO in the global oceans. Surveys in Geophysics, Volume 38, Issue 1, Pages 277-293, DOI 10.1007/s10712-016-9391-1

Ramírez-Romero, E., Macías, D., Bruno, M., Reyes, E., Navarro, G., García, C.M., 2012. Submesoscale, tidally-induced biogeochemical patterns in the Strait of Gibraltar. Estuarine, Coastal and Shelf Science, Volume 101, Pages 24-32, DOI 10.1016/j.ecss.2012.02.010.

Reboreda, R., Cordeiro, N.G.F., Nolasco, R., Castro, C.G., Álvarez-Salgado, X.A., Queiroga, H., Dubert, J., 2014a. Modeling the seasonal and interannual variability (2001-2010) of chlorophyll-a in the Iberian margin. Journal of Sea Research, Volume 93, Pages 133-149, DOI 10.1016/j.seares.2014.04.003.

Reboreda, R., Nolasco, R., Castro, C. G., Álvarez-Salgado, X.A., Cordeiro, N.G.F., Queiroga, H., Dubert, J., 2014b. Seasonal cycle of plankton production in the Iberian margin based on a high resolution ocean model. Journal of Marine Systems, Volume 139, Pages 396-408, DOI 10.1016/j.jmarsys.2014.08.004.

Relvas, P., Barton, D., 2002. Mesoscale patterns in the Cape São Vicente (Iberian Peninsula) upwelling region. Journal of Geophysical Research, Volume 107, Issue C10, Pages 3164, DOI 10.1029/2000JC000456.

Relvas, P., Barton, E.D., Dubert, J., Oliveira, P.B., Peliz, A., da Silva, J.C.B., Santos, A.M.P., 2007. Physical oceanography of the western Iberia ecosystem: Latest views and challenges. Progress in Oceanography, Volume 74, Issue 2-3, Pages 149-173, DOI 10.1016/j.pocean.2007.04.021.

Relvas, P., Luís, J., Santos, A.M.P., 2009. Importance of the mesoscale in the decadal changes observed in the northern Canary upwelling system. Geophysical Research Letters, Volume 36, L22601, DOI 10.1029/2009GL040504.

Reul A., Muñoz, M., Criado-Aldeanueva, F., Rodríguez, V., 2006. Spatial distribution of phytoplankton <13 μm in the Gulf of Cádiz in relation to water masses and circulation pattern under westerly and easterly wind regimes. Deep Sea Research Part II: Topical Studies in Oceanography, Volume 53, Issues 11-13, Pages 1294-1313, DOI 10.1016/j.dsr2.2006.04.008.

Reygondeau, G., Longhurst, A., Martinez, E., Beaugrand, G., Antoine, D., Maury, O., 2013. Dynamic biogeochemical provinces in the global ocean. Global Biogeochemical Cycles, Volume 27, Issue 1, Pages 1046-1058, DOI 10.1002/gbc.20089.

Robinson, I.S., 2010. Discovering the Ocean From Space: The Unique Applications of Satellite Oceanography. Springer-Praxis Books, Great Britain, p. 685.

Rochford, P.A., Kara, A.B., Wallcraft, A.J., Arnone, R.A., 2001. Importance of solar subsurface heating in ocean general circulation models. Journal of Geophysical Research - Oceans, Volume 106, Issue C12, Pages 30923-30938, DOI 10.1029/2000JC000355.

Rossi, V., Garçon, V., Tassel, J., Romagnan, J., Stemmann, L., Jourdin, F., Morin, P., Morel, Y., 2013. Cross-shelf variability in the Iberian Peninsula Upwelling System: Impact of a mesoscale filament. Continental Shelf Research, Volume 59, Pages 97-114, DOI 10.1016/j.csr.2013.04.008.

Rousseaux, C.S., Gregg, W.W., 2015. Recent decadal trends in global phytoplankton composition. Global Biogeochemical Cycles, Volume 29, Issue 10, Pages 1674-1688, DOI 10.1002/2015GB005139.

Ruiz, J., González-Quirós, R., Prieto, L., Navarro, G., 2009. A Bayesian model for anchovy (Engraulis encrasicolus): the combined forcing of man and environment. Fisheries Oceanography, Volume 18, Issue 1, Pages 62-6, DOI 10.1111/j.1365-2419.2008.00497.x.

Ruiz, J., Polo, M.J., Díez-Minguito, M., Navarro, G., Morris, E.P., Huertas, E., Caballero, I., Contreras, E., Losada, M.A., 2014. The Guadalquivir Estuary: A hot spot for environmental and human conflicts. In: Finkl, C.W., Makowski, C. (Eds) Environmental management and governance: Advances in coastal and marine resources. Coastal Research Library, Volume 8, Pages 199-232, DOI 10.1007/978-3-319-06305-8_8.

Sá, C., D'Alimonte, D., Brito, A.C., Kajiyama, T., Mendes, C.R., Vitorino, J., Oliveira, P.B., da Silva, J.C.B., Brotas, V., 2015. Validation of standard and alternative satellite ocean-color chlorophyll products off Western Iberia. Remote Sensing of Environment, Volume 168, Pages 403-419, DOI 10.1016/j.rse.2015.07.018.

Saba, V.S., Friedrichs, M.A.M., Antoine, D., Armstrong, R.A., Asanuma, I., Behrenfeld, M.J., Ciotti, A.M., Dowell, M., Hoepffner, N., Hyde, K.J.W., Ishizaka, J., Kameda, T., Marra, J., Méli, F., Morel, A., O'Reilly, J., Scardi, M., Smith Jr., W.O., Smyth, T.J., Tang, S., Uitz, J., Waters, K., Westberry, T.K., 2011. An evaluation of ocean color model estimates of marine primary productivity in coastal and pelagic regions across the globe. Biogeosciences, Volume 8, Pages 489-503, DOI 10.5194/bg-8-489-2011.

Sallée, J-B., Llort, J., Tagliabue, A., Lévy, M., 2015. Characterization of distinct bloom phenology regimes in the Southern Ocean. ICES Journal of Marine Science, Volume 72, Issue 6, Pages 1985-1998, DOI 10.1093/icesjms/fsv069

Sánchez, R.F., Relvas, P., 2003. Spring-summer climatological circulation in the upper layer in the region of Cape St. Vincent, Southwest Portugal. ICES Journal of Marine Science, Volume 60, Pages 1232-1250, DOI 10.1016/S1054–3139(03)00137-1.

Sánchez, R.F., Relvas, P., Martinho, A., Miller, P., 2008. Physical description of an upwelling filament west of Cape St. Vincent in late October 2004. Journal of Geophysical Research, Volume 113, C07044, DOI 10.1029/2007JC004430.

Sánchez, R.F., Relvas, P., Pires, H.O., 2007. Comparisons of ocean scatterometer and anemometer winds off the southwestern Iberian Peninsula. Continental Shelf Research, Volume 27, Issue 2, Pages 155-175, DOI 10.1016/j.csr.2006.09.007.

Santamaría-del-Ángel, E., González-Silvera, A., Millán-Nuñez, R., Callejas-Jiménez, M.E., Cajal-Medrano, R., 2011. Determining Dynamic Biogeographic Regions using Remote Sensing Data, in: Morales, J., Stuart, V., Platt, T., Sathyendranath, S. (Eds.) Handbook of Satellite Remote Sensing Image Interpretation: Applications for Marine Living Resources Conservation and Management, EU PRESPO and IOCCG, Dartmouth, pp 241-260.

Santos, A.M.P., Borges, M.F., Groom, S., 2001. Sardine and horse mackerel recruitment and upwelling off Portugal. ICES Journal of Marine Science, Volume 58, Issue 3, Pages 589-596, DOI 10.1006/jmsc.2001.1060.

Santos, A.M.P., Chícharo, A., Santos, A., Moita, T., Oliveira, P.B., Peliz, A., Ré, P., 2007. Physical–biological interactions in the life history of small pelagic fish in the Western

Iberia Upwelling Ecosystem. Progress in Oceanography, Volume 74, Issue 2-3, Pages 192-209, DOI 10.1016/j.pocean.2007.04.008.

Santos, F., Gesteira, M.G., deCastro, M., 2011a. Coastal and oceanic SST variability along the western Iberian Peninsula. Continental Shelf Research, Volume 31, Pages 2012-2017, DOI 10.1016/j.csr.2011.10.005.

Santos, F., Gómez-Gesteira, M., deCastro, M., Álvarez, I., 2011b. Upwelling along the western coast of the Iberian Peninsula: dependence of trends on fitting strategy. Climate Research, Volume 48, Pages 213-218, DOI 10.3354/cr00972.

Sapiano, M.R.P., Brown, C.W., Uz, S.S.,Vargas, M., 2012. Establishing a global climatology of marine phytoplankton phenological characteristics. Journal of Geophysical Research, Volume 117, C08026, DOI 10.1029/2012JC007958

Saraceno, M., Provost, C., Lebbah, M., 2006. Biophysical regions identification using an artificial neuronal network: A case study in the South Western Atlantic. Advances in Space Research, Volume 37, Issue 4, Pages 793-805, DOI 10.1016/j.asr.2005.11.005.

Sarmiento, J., Slater, R., Barber, R., Bopp, L., Doney, S.C., Hirst, A.C., Kleypas, J., Matear, R., Mikolajewicz, U., Monfray, P., Soldatov, V., Spall, S., Slater, R., Stouffer, R., 2004. Response of ocean ecosystems to climate warming. Global Biogeochemical Cycles, Volume 18, GB3003, DOI 10.1029/2003GB002134

Sasaoka, K., Chiba, S., Saino, T., 2011. Climatic forcing and phytoplankton phenology over the subarctic North Pacific from 1998 to 2006, as observed from ocean color data. Geophysical Research Letters, Volume 38, L15609, 10.1029/2011GL048299

Sathyendranath, S., 2000. General Introduction. In: Sathyendranath, S. (Ed) Remote Sensing of Ocean Colour in Coastal, and Other Optically-Complex, Waters. Reports and Monographs of the International Ocean-Colour Coordinating Group (IOCCG), Volume 3, Darthmouth, pp. 5-21.

Sathyendranath, S., Brewin, R.J.W., Jackson, T., Mélin, F., Platt, T., *in press*. Ocean-colour products for climate-change studies: what are their ideal characteristics? Remote Sensing of Environment. DOI 10.1016/j.rse.2017.04.017

Sathyendranath, S., Groom, S., Grant, M., Brewin, R.J.W., Thompson, A., Chuprin, A., Horseman, A., Jackson, T., Martinez Vicente , V., Platt, T., Brockmann, C., Zühlke, M., Doerffer, R., Valente, A., Brotas, V., Krasemann, H., Müller, D., Dowell, M., Mélin, F., Swinton, J., Farman, A., Lavender, S., Moore, T.S., Regner, P., Roy, S., Steinmetz, F., Mazeran, C., Brando, V.E., Taberner, M., Antoine, D., Arnone, R., Balch, W.M., Barker, K., Barlow, R., Bélanger, S., Berthon, J., Beşiktepe, Ş., Canuti, E., Chavez, F., Claustre, H., Crout, R., Frouin, R., García-Soto, C., Gibb, S.W., Gould, R., Hooker, S., Kahru, M., Klein, H., Kratzer, S., Loisel, H., McKee, D., Mitchell, B.G., Moisan, T., Feldman, G., Franz, B., Muller-Karger, F., O'Dowd, L., Ondrusek, M., Poulton, A.J., Repecaud, M., Smyth, T., Sosik, H.M., Twardowski, M., Voss, K., Werdell, J., Wernand, M., Zibordi, G., 2016. ESA Ocean Colour Climate Change Initiative (Ocean_Colour_cci): Version 2.0 Data. Centre for Environmental Data Analysis. DOI 10.5285/b0d6b9c5-14ba-499f-87c9-66416cd9a1dc

Sathyendranath, S., Longhurst, A., Caverhill, C.M., Platt, T., 1995. Regionally and seasonally differentiated primary production in the North Atlantic. Deep Sea Research Part I: Oceanographic Research Papers, Volume 42, Issue 10, Pages 1773-1802, DOI 10.1016/0967-0637(95)00059-F.

Sathyendranath, S., Platt, T., Horne, E.P.W., Harrison, W.G., Ulloa, O., Outerbridge, R., Hoepffner, N., 1991. Estimation of new production in the ocean by compound remote sensing, Nature, Volume 353, Pages 129-133, DOI 10.1038/353129a0.

Sayre, R., J. Dangermond, D. Wright, S. Breyer, K. Butler, K. Van Graafeiland, M.J. Costello, P. Harris, K. Goodin, M. Kavanaugh, N. Cressie, J. Guinotte, Z. Basher, P. Halpin, M. Monaco, P. Aniello, C. Frye, D. Stephens, P. Valentine, J. Smith, R. Smith, D.P. VanSistine, J. Cress, H. Warner, C. Brown, J. Steffenson, D. Cribbs, B. Van Esch, D. Hopkins, G. Noll, S. Kopp, and C. Convis. 2017. A New Map of Global Ecological Marine Units – An Environmental Stratification Approach. Washington, DC: American Association of Geographers, 36 p.

Scheffers, B.R., Meester, L.D., Bridge, T.C.L., Hoffmann, A.A., Pandolfi, J.M., Corlett, R.T., Butchart, S.H.M., Pearce-Kelly, P., Kovacs, K.M., Dudgeon, D., Pacifici, M., Rondinini, C., Foden, W.B., Martin, T.G., Mora, C., Bickford, D., Watson, J.E.M., 2016. The broad

footprint of climate change from genes to biomes to people. Science, Volume 354, Issue 6313, Pages 1-11, DOI 10.1126/science.aaf7671.

Schwartz, M.D., 2003. Chapter 1.1 Introduction. In: Phenology: an integrative environmental science, Ed.: M.D.Schartw, Springer, Netherlands. 3-7 pp.

Sherman, K., 1991. The large marine ecosystem concept: Research and management strategy for living marine resources. Ecological Applications, Volume 1, Issue 4, Pages 349-360, DOI 10.2307/1941896.

Sherman, K., 1994. Sustainability, biomass yields, and health of coastal ecosystems: an ecological perspective. Marine Ecology Progress Series, Volume 112, Pages 277-301.

Shi, K., Li, Y., Li, L., Lu, H., Song, K., Liu, Z., Xu, Y., Li, Z., 2013. Remote chlorophyll-a estimates for inland waters based on a cluster-based classification. Science of the Total Environment, Volume 444, Pages 1-15, DOI 10.1016/j.scitotenv.2012.11.058.

Shiozaki, T., Ito, S-I., Takahashi, K., Saito, H., Nagata, T., Furuya, K., 2014. Regional variability of factors controlling the onset timing and magnitude of spring algal blooms in the northwestern North Pacific. Journal of Geophysical Research Oceans, Volume 119, Pages 253-265, 10.1002/2013JC009187

Siedler, G., Griffies, S.M., Gould, J., Church, J.A. (Eds.), 2013. Ocean Circulation and Climate: A 21st Century Perspective. International Geophysics, Volume 103, Academic Press, San Diego.

Siegel, D.A., Buesseler, K.O., Behrenfeld, M.J., Benitez-Nelson, C.R., Boss, E., Brzezinski, M.A., Burd, A., Carlson, C.A., D'Asaro, E.A., Doney, S.C., Perry, M.J., Stanley, R.H.R., Steinberg, D.K., 2016. Prediction of the Export and Fate of Global Ocean Net Primary Production: The EXPORTS Science Plan. Frontiers in Marine Science, Volume 3, Issue 22, Pages 1-10, DOI 10.3389/fmars.2016.00022

Siegel, D.A., Buesseler, K.O., Doney, S.C., Sailley, S.F., Behrenfeld, M.J., Boyd, P.W., 2014. Global assessment of ocean carbon export by combining satellite observations and food-web models. Global Biogeochemical Cycles, Volume 28, Issue 3, Pages 181-196, DOI 10.1002/2013GB004743.

Siegel, D.A., Doney, S.C., Yoder, J.A., 2002. The North Atlantic spring phytoplankton bloom and Sverdrup's critical depth hypothesis. Science, Volume 296, Pages 730-733, DOI 10.1126/science.1069174

Silva, A., Palma, S., Oliveria, P.B., Moita, M.T., 2009. Composition and interannual variability of phytoplankton in a coastal upwelling region (Lisbon Bay, Portugal). Journal of Sea Research, Volume 62, Pages 238-249, DOI 10.1016/j.seares.2009.05.001.

Silva, D., Bento, A.R., Martinho, P., Soares, C.G., 2015. High resolution local wave energy modelling in the Iberian Peninsula. Energy,Volume 91, Pages 1099-1112, DOI 10.1016/j.energy.2015.08.067.

Smayda, T.J., Trainer, V.L., 2010. Dinoflagellate blooms in upwelling systems: Seeding, variability, and contrasts with diatom bloom behaviour. Progress in Oceanography, Volume 85, Issues 1-2, Pages 92-107, DOI 10.1016/j.pocean.2010.02.006

Smetacek, V., Cloern, J.E., 2008. On phytoplankton trends. Science, Volume 319, Issue 5868, Pages 1346-1348, DOI 10.1126/science.1151330.

Sokal, R.R., Rohlf, F.J. Biometry. 3rd edition. W.H. Freeman, 880 p.

Song, H., Ji, R., Stock, C., Kearney, K., Wang, Z., 2011. Interannual variability in phytoplankton blooms and plankton productivity over the Nova Scotian Shelf and in the Gulf of Maine. Marine Ecology Progress Series, Volume 426, Pages 105-118, DOI 10.3354/meps09002

Song, H., Ji, R., Stock, C., Wang, Z., 2010. Phenology of phytoplankton blooms in the Nova Scotian Shelf–Gulf of Maine region: remote sensing and modeling analysis. Journal of Plankton Research, Volume 32, Issue 11, Pages 1485-1499, DOI 10.1093/plankt/fbq086

Soppa, M.A., Völker C., Bracher, A., 2016. Diatom phenology in the Southern Ocean: mean patterns, trends and the role of climate oscillations. Remote Sensing, Volume 8, 420, DOI 10.3390/rs8050420

Sotillo, M.G., Cailleau, S., Lorente, P., Levier, B., Aznar, R., Reffray, G., AmoBaladrón, A., Chanut, J., Benkiran, M., Alvarez-Fanjul, E., 2015. The MyOcean IBI Ocean Forecast

and Reanalysis Systems: operational products and roadmap to the future Copernicus Service. Journal of Operational Oceanography, Volume 8, Issue 1, Pages 63-79, DOI 10.1080/1755876X.2015.1014663.

Sousa, M.C., deCastro, M., Alvarez, I., Gomez-Gesteira, M., Dias, J.M., 2017. Why coastal upwelling is expected to increase along the western Iberian Peninsula over the next century? Science of the Total Environment, Volume 592, Pages 243-251, DOI 10.1016/j.scitotenv.2017.03.046

Souza, F.M., Bricaud, A., 1992. Satellite-derived phytoplankton pigment structures in the Portuguese upwelling area. Journal of Geophysical Research - Oceans, Volume 97, Issue C7, Pages 22343-11356, DOI 10.1029/92JC00786.

Spalding, M.D., Agostini, V.N., Rice, J., Grant, S.M., 2012. Pelagic provinces of the world: A biogeographic classification of the world's surface pelagic waters. Ocean & Coastal Management, Volume 60, Pages 19-30, DOI 10.1016/j.ocecoaman.2011.12.016.

Spalding, M.D., Fox, H.E., Allen, G.R., Davidson, N., Ferdaña, Z.A., Finlayson, M., Halpern, B.S., Jorge, M.A., Lombana, A., Lourie, S.A., Martin, K.D., McManus, E., Molnar, J., Recchia, C.A., Robertson, J., 2007. Marine Ecoregions of the World: A Bioregionalization of Coastal and Shelf Areas. BioScience, Volume 57, Issue 7, Pages 573-583, DOI 10.1641/B570707.

Steele, J., Carpenter, S., Cohen, J., Dayton, P. ; Ricklefs, R., 1989. Comparison of terrestrial and marine ecological systems. Mimeograph report of a workshop held in Santa Fe, USA (Nat. Sci. Found., grant No. OCE 8814769).

Stenseth, N.C., Ottersen, G., Hurrell, J.W., Mysterud, A., Lima, M., Chan, K.S., Yoccoz, N.G., Ådlandsvik, B., 2003. Studying climate effects on ecology through the use of climate indices: the North Atlantic Oscillation, El Niño Southern Oscillation and beyond. Proceedings of the Royal Society B- Biological Sciences, Volume 270, Pages 2087-2096, DOI 10.1098/rspb.2003.2415.

Storm, T., Boettcher, M., Grant, M., Zühlke, M., Fomferra, N., Jackson, T., Sathyendranath, S., 2013. Product User Guide, Ocean Colour Climate Change Initiative. http://www.esa-oceancolour-cci.org/?q=webfm_send/317 (accessed 02.06.16).

Stratoudakis, Y., Bernal, M., Borchers, D.L., Borges, M.F., 2003. Changes in the distribution of sardine eggs and larvae off Portugal, 1985-2000. Fisheries Oceanography, Volume 12, Issue 1, Pages 49-60, DOI 10.1046/j.1365-2419.2003.00222.x.

Sutton, R.T., Dong, B., 2012. Atlantic Ocean influence on a shift in European climate in the 1990s. Nature Geoscience, Volume 5, Pages 788-792, DOI 10.1038/ngeo1595.

Sverdrup, H.U., 1953. On conditions for the vernal blooming of phytoplankton. Journal du Conseil International pour l'Exploration de la Mer, Volume 18, Issue 3, Pages 287-295, DOI 10.1093/icesjms/18.3.287.

Taylor, B.B., Torrecilla, E., Bernhardt, A., Taylor, M.H., Peeken, I., Röttgers, R., Piera, J., Bracher, A., 2011. Bio-optical provinces in the eastern Atlantic Ocean and their biogeographical relevance. Biogeosciences, Volume 8, Issue 12, Pages 3609-3629, DOI 10.5194/bg-8-3609-2011.

Teira, E., Mouriño, B., Marañón, E., Pérez, V., Pazó, M.J., Serret, P., de Armas, D., Escánez, J., Woodward, E.M.S., Fernández, E., 2005. Variability of chlorophyll and primary production in the Eastern North Atlantic Subtropical Gyre: potential factors affecting phytoplankton activity. Deep Sea Research Part I: Oceanographic Research Papers, Volume 52, Issue 4, Pages 569-588, DOI 10.1016/j.dsr.2004.11.007.

Thackeray, S.J., Jones, I.D., Maberly, S.C., 2008. Long-term change in the phenology of spring phytoplankton: species-specific responses to nutrient enrichment and climatic change. Journal of Ecology, Volume 96, Issue 3, Pages 523-535, DOI 10.1111/j.1365-2745.2008.01355.x.

The Nature Conservancy, 2012. Marine Ecoregions and Pelagic Provinces of the World. GIS layers developed by The Nature Conservancy with multiple partners, combined from Spalding et al. (2007) and Spalding et al. (2012). Cambridge (UK): The Nature

Conservancy. Available at http://data.unep-wcmc.org/datasets/38. Accessed on: 31 Mar 2016.

Thomas, A.C., Strub, P.T., Weatherbee, R.A., James, C., 2012. Satellite views of Pacific chlorophyll variability: Comparisons to physical variability, local versus nonlocal influences and links to climate indices. Deep Sea Research Part II: Topical Studies in Oceanography, Volumes 77-80, Pages 99-116, DOI 10.1016/j.dsr2.2012.04.008.

Thompson, P.A., O'Brien, T.D., Paerl, H.W., Peierls, B.L., Harrison, P.J., Robb, M., 2015. Precipitation as a driver of phytoplankton ecology in coastal waters: A climatic perspective, Estuarine, Coastal and Shelf Science, Volume 162, Pages 119-129, DOI 10.1016/j.ecss.2015.04.004.

Tilstone, G.H., Xie, Y., Robinson, C., Serret, P., Raitsos, D.E., Powell, T., Aranguren-Gassis, M., Garcia-Martin, E.E., Kitidis, V., 2015. Satellite estimates of net community production indicate predominance of net autotrophy in the Atlantic Ocean. Remote Sensing of Environment, Volume 164, Pages 254-269, DOI 10.1016/j.rse.2015.03.017.

Traykovski, L.V.M., Sosik, H.M., 2003. Feature-based classification of optical water types in the Northwest Atlantic based on satellite ocean color data. Journal of Geophysical Research - Oceans, Volume 108, Issue C5, 3150, DOI 10.1029/2001JC001172.

Trigo, I.F., 2006. Climatology and interannual variability of storm-tracks in the Euro-Atlantic sector: a comparison between ERA-40 and NCEP/NCAR reanalyses. Climate Dynamics, Volume 26, Issue 2, Pages 127-143, DOI 10.1007/s00382-005-0065-9.

Turner, J.T., 2015. Zooplankton fecal pellets, marine snow, phytodetritus and the ocean's biological pump. Progress in Oceanography, Volume 130, Pages 205-248, DOI 10.1016/j.pocean.2014.08.005

Tweddle, J.F., Strutton, P.G., Foley, D.G., O'Higgins, L., Wood, A.M., Scott, B., Everroad, R.C., Peterson, W.T., Cannon, D., Hunter, M., Forster, Z., 2010. Relationships among upwelling, phytoplankton blooms, and phycotoxins in coastal Oregon shellfish. Marine Ecology Progress Series, Volume 405, Pages 131-145, DOI 10.3354/meps08497

Ueyama, R., Monger, B.C., 2005. Wind-induced modulation of seasonal phytoplankton blooms in the North Atlantic derived from satellite observations. Limnology and Oceanography, Volume 50, Issue 6, Pages 1820-1829, DOI 10.4319/lo.2005.50.6.1820.

Uitz, J., Claustre, H., Gentili, B., Stramski, D., 2010. Phytoplankton class-specific primary production in the world's oceans: Seasonal and interannual variability from satellite observations. Global Biogeochemical Cycles, Volume 24, Issue 3, GB3016, DOI 10.1029/2009GB003680.

UNESCO, 2009. Global Open Oceans and Deep Seabed (GOODS) – Biogeographic Classification. IOC Technical Series, Paris, 84, 95 p.

Vantrepotte, V., Loisel, H., Dessailly, D., Mériaux, X., 2012. Optical classification of contrasted coastal waters. Remote Sensing of Environment, Volume 123, Pages 306-323, DOI 10.1016/j.rse.2012.03.004.

Varela, R., Álvarez, I., Santos, F., deCastro, M., Gómez-Gesteira, M., 2015. Has upwelling strengthened along worldwide coasts over 1982-2010? Scientific Reports, Volume 5, 10016, DOI 10.1038/srep10016.

Vargas, J.M., García-Lafuente, J., Delgado, J., Criado, F., 2003. Seasonal and wind-induced variability of Sea Surface Temperature patterns in the Gulf of Cádiz. Journal of Marine Systems, Volume 38, Issues 3-4, Pages 205-219, DOI 10.1016/S0924-7963(02)00240-3.

Vargas, M., Brown, C.W., Sapiano, M.R.P., 2009. Phenology of marine phytoplankton from satellite ocean color measurements. Geophysical Research Letters, Volume 36, L01608, DOI 10.1029/2008GL036006

Vázquez, A., Flecha, S., Bruno, M., Macías, D., Navarro, G., 2009. Internal waves and short-scale distribution patterns of chlorophyll in the Strait of Gibraltar and Alborán Sea. Geophysical Research Letters Oceans, Volume 36, L23601, DOI 10.1029/2009GL040959.

Verfaille, E., Degraer, S., Schelfaut, K., Willems, W., Van Lancker, V., 2009. A protocol for classifying ecologically relevant marine zones, a statistical approach. Estuarine, Coastal and Shelf Science, Volume 83, Issue 2, Pages 175-185, DOI 10.1016/j.ecss.2009.03.003.

Vesanto, J., Himberg, J., Alhoniemi, E., Parhankangas, J., 2000. SOM Toolbox for Matlab 5. Helsinki University of Technology Rep. A57, p. 59.

Vichi, M., Allen, J.I., Masina, S., Hardman-Mountford, N.J., 2011. The emergence of ocean biogeochemical provinces: A quantitative assessment and a diagnostic for model evaluation. Global Biogeochemical Cycles, Volume 25, Issue 2, GB2005, DOI 10.1029/2010GB003867.

Waite, J.N., Mueter, F.J., 2013. Spatial and temporal variability of chlorophyll-a concentrations in the coastal Gulf of Alaska, 1998-2011, using cloud-free reconstructions of SeaWiFS and MODIS-Aqua data. Progress in Oceanography, Volume 116, Pages 179-192, DOI 10.1016/j.pocean.2013.07.006.

Ward, J.H., 1963. Hierarchical grouping to optimize an objective function. Journal of the American Statistical Association, Volume 58, Issue 301, Pages 236-244, DOI 10.1080/01621459.1963.10500845.

Watling, L., Guinotte, J., Clark, M.R., Smith, C.R., 2013. A proposed biogeography of the deep ocean floor. Progress in Oceanography, Volume 111, Pages 91-112, DOI 10.1016/j.pocean.2012.11.003.

Watts, L.J., Sathyendranath, S., Caverhill, C., Maass, H., Platt, T., Owens, N.J.P., 1999. Modelling new production in the north west Indian Ocean region. Marine Ecology Progress Series, Volume 183, Pages 1-12, DOI 10.3354/meps183001.

Weber, T.S., Deutsch, C., 2010. Ocean nutrient ratios governed by plankton geography. Nature, Volume 467, Pages 550-554, DOI 10.1038/nature09403.

Weissbach, A., Rudström, M., Olofsson, M., Béchemin, C., Icely, J., Newton, A., Tillmann, U., Legranda, C., 2011. Phytoplankton allelochemical interactions change microbial food web dynamics. Limnology and Oceanography, Volume 56, Issue 3, DOI 10.4319/lo.2011.56.3.0899.

Wilks, D.S., 2006. Statistical Methods in the Atmospheric Sciences. London, Academic Press, p. 627.

Wiltshire, K.H., Malzahn, A.M., Wirtz, K., Greve, W., Janisch, S., Mangelsdorf, P., Manly, B.F.J., Boersma, M., 2008. Resilience of North Sea phytoplankton spring bloom dynamics: An analysis of long-term data at Helgoland Roads. Limnology and Oceanography, Volume 53, Issue, 4, Pages 1294-1302, DOI 10.4319/lo.2008.53.4.1294

Winder, M., Cloern, J.E., 2010. The annual cycles of phytoplankton biomass. Philosophical Transactions of the Royal Society B-Biological Sciences, Volume 365, Pages 3215-3226, DOI 10.1098/rstb.2010.0125.

Wolter, K., Timlin, M.S., 2011. El Niño/Southern Oscillation behaviour since 1871 as diagnosed in an extended multivariate ENSO index (MEI.ext). International Journal of Climatology, Volume 31, Issue 7, Pages 1074-1087, DOI 10.1002/joc.2336.

Wood, S.N., 2006. Generalized additive models: an introduction with R. Boca Raton, Chapman & Hall/CRC, p. 410.

Xu, Y., Chant, R., Gong, D., Castelao, R., Glenn, S., Schofield, O., 2011. Seasonal variability of chlorophyll a in the Mid-Atlantic Bight. Continental Shelf Research, Volume 31, Issue 16, Pages 1640-1650, DOI 10.1016/j.csr.2011.05.019.

Xu, Y., Ishizaka, J., Yamaguchi, H., Siswanto, E., Wang, S., 2013. Relationships of interannual variability in SST and phytoplankton blooms with giantjellyfish (Nemopilema nomurai) outbreaks in the Yellow Sea and East China Sea. Journal of Oceanography, Volume 69, Issue 5, Pages 511-526, DOI 10.1007/s10872-013-0189-1

Yamada, K., Ishizaka, J., 2006. Estimation of interdecadal change of spring bloom timing, in the case of the Japan Sea. Geophysical Research Letters, Volume 33, L02608, DOI 10.1029/2005GL024792

Yoder, J.A., Kennelly, M.A., 2003. Seasonal and ENSO variability in global ocean phytoplankton chlorophyll derived from 4 years of SeaWiFS measurements. Global Biogeochemical Cycles, Volume 17, Issue 4, 1112, DOI 10.1029/2002GB001942.

Yoder, J.A., Schollaert, S.E., O'Reilly, J.E., 2002. Climatological phytoplankton chlorophyll and sea surface temperature patterns in continental shelf and slope waters off the

northeast U. S. coast. Limnology and Oceanography, Volume 47, Pages 672-682, DOI 10.4319/lo.2002.47.3.0672.

Yoo, S., Batchelder, H.P., Peterson, W.T., Sydeman, W.J., 2008. Seasonal, interannual and event scale variation in North Pacific ecosystems. Progress in Oceanography, Volume 77, Pages 155-181, DOI 10.1016/j.pocean.2008.03.013

Zarauz, L., Irigoien, X., Fernandes, J.A., 2008. Modelling the influence of abiotic and biotic factors on plankton distribution in the Bay of Biscay, during three consecutive years (2004–06). Journal of Plankton Research, Volume 30, Issue 8, Pages 857-872, DOI 10.1093/plankt/fbn049.

Zarauz, L., Irigoien, X., Urtizberea, A., Gonzalez, M., 2007. Mapping plankton distribution in the Bay of Biscay during three consecutive spring surveys. Marine Ecology Progress Series, Volume 345, Pages 27-39, DOI 10.3354/meps06970.

Zarubin, M., Lindermann, Y., Genin, A., 2017. The dispersion-confinement mechanism: Phytoplankton dynamics and the spring bloom in a deeply-mixing subtropical sea. Progress in Oceanography, Volume 155, Pages 13-27, DOI 10.1016/j.pocean.2017.05.005

Zhai, L., Platt, T., Tang, C., Sathyendranath, S., Walls, R.H., 2011. Phytoplankton phenology on the Scotian Shelf. ICES Journal of Marine Science, Volume 68, Issue 4, Pages 781-791, DOI 10.1093/icesjms/fsq175

Zhai, L., Platt, T., Tang, C., Sathyendranath, S., Walne, A., 2013. The response of phytoplankton to climate variability associated with the North Atlantic Oscillation. Deep-Sea Research II, Volume 93, Pages 159-168, DOI 10.1016/j.dsr2.2013.04.009

Zhang, H.-M., Bates, J.J., Reynolds, R.W., 2006. Assessment of composite global sampling: Sea surface wind speed. Geophysical Research Letters, Volume 33, L17714, DOI 10.1029/2006GL027086.

Zhang, M., Zhang, Y., Qiao, F., Deng, J., Wang, G., 2017. Shifting trends in bimodal phytoplankton blooms in the North Pacific and North Atlantic Oceans from space with the Holo-Hilbert spectral analysis. Journal of Selected Topics in Applied Earth

Observations and Remote Sensing, Volume 10, Issue 1, Pages 57-64, DOI 10.1109/JSTARS.2016.2625813

Zhao, H., Han, G., Wang, D., 2013. Timing and magnitude of spring bloom and effects of physical environments over the Grand Banks of Newfoundland. Journal of Geophysical Research Biogeosciences, Volume 118, Pages 1385-1396, DOI 10.1002/jgrg.20102

Zou, L., Chen, H.T., Zhang, J., 2000. Experimental examination of the effects of atmospheric wet deposition on primary production in the Yellow Sea. Journal of Experimental Marine Biology and Ecology, Volume 249, Issue 1, Pages 111-121, DOI 10.1016/S0022-0981(00)00186-6.

APPENDIX A

Table A.1 – List of orbital sensors dedicated to ocean colour radiometry and references of ocean colour partitioning applying their data. Adapted from http://ioccg.org/

Sensor	Satellite	Agencies (Countries)	Operating period	Orbit*	References
Coastal Zone Colour Scanner (CZCS)	Nimbus-7	NASA (USA)	Oct 1978 - Jun 1986	P	Platt and Sathyendranath, 1988; Longhurst, 1995; Longhurst et al., 1995; Longhurst, 1998; Brock et al., 1998; Watts et al., 1999; Esaias et al., 2000; Traykovski and Sosik, 2003
Modular Optoelectronic Scanner (MOS)	IRS P3	DLR (Germany and India)	Mar 1996 - May 2004	P	
POLarization and Directionality of the Earth's Reflectance (POLDER)	ADEOS	CNES (France and Japan)	Aug 1996 - Jun 1997	P	
Ocean Color and Temperature Scanner (OCTS)	ADEOS	NASDA (Japan)	Sep 1996 - Jun 1997	P	
Sea-Viewing Wide Field-of-View Sensor (SeaWiFS)	OrbView-2	NASA (USA)	Aug 1997 - Feb 2011	P	Moore et al, 1998; Moore et al., 2001; Karabashev et al., 2002; Traykovski and Sosik, 2003; Hemmings et al., 2004; Oliver et al., 2004; Hoepffner and Dowell, 2005; Platt et al., 2005; Navarro and Ruiz, 2006; Saraceno et al., 2006; Devred et al., 2007; Gregr and Botker, 2007; Macías et al., 2007; Hardman-Mountford et al., 2008; Devred et al., 2009; D'Ortenzio and d'Alcalà, 2009; Barale, 2010; Henson et al., 2010; Kahru et al., 2010; Santamaría-Del-Ángel et al., 2011; Vantrepotte et al., 2012; Acevedo-Trejos et al., 2013; Waite and Mueter, 2013; Reygondeau et al, 2013; Fay and McKinley, 2014; Fendereski et al., 2014; Foukal and Thomas, 2014; Mayot et al., 2015; Mélin and Vantrepotte, 2015; Muñoz et al., 2015
Ocean Color Imager (OCI)	ROCSAT-1	NEC (Japan and Taiwan)	Jan 1999 - Jun 2004	P	
Ocean Colour Monitor (OCM)	IRS-P4	ISRO (India)	May 1999 - Aut 2010	P	
Ocean Scanning Multi-spectral Imager (OSMI)	KOMPSAT-1 / Arirang-1	KARI (Korea)	Dec 1999 - Jan 2008	P	
Moderate Resolution Imaging Spectroradiometer (MODIS-Terra)	Terra (EOS-AM1)	NASA (USA)	Feb 2000 - present	P	
Medium Resolution Imaging Spectrometer (MERIS)	ENVISAT	ESA (Europe)	Feb 2002 - May 2012	P	Kahru et al., 2010; Shi et al., 2013; Fendereski et al., 2014; Blondeau-Patissier et al., 2014b
Chinese Moderate Resolution Imaging Spectroradiometer (CMODIS)	SZ-3	CNSA (China)	Mar 2002 - Sep 2002	P	
Chinese Ocean Color and Temperature Scanner (COCTS)	HY-1A	SOA (China)	May 2002 - Apr 2004	P	
Coastal Zone Imager (CZI)	HY-1A	SOA (China)	May 2002 - Apr 2004	P	

Moderate Resolution Imaging Spectroradiometer (MODIS-Aqua)	Aqua (EOS-PM1)	NASA (USA)	May 2002 - present	P	Oliver and Irwin, 2008; Irwin and Oliver, 2009; Moore et al., 2009; Kahru et al., 2010; Callejas-Jimenez et al., 2012; Waite and Mueter, 2013; Caballero et al., 2014; Fendereski et al., 2014; Nieblas et al., 2014; Mayot et al., 2015
Global Imager (GLI)	ADEOS-II	NASDA (Japan)	Dec 2002 - Oct 2003	P	
POLarization and Directionality of the Earth's Reflectance-2 (POLDER-2)	ADEOS-II	CNES (France and Japan)	Dec 2002 - Oct 2003	P	
POLarization and Directionality of the Earth's Reflectance-3 (POLDER-3)	Parasol	CNES (France)	Dec 2004 - Dec 2013	P	
Chinese Ocean Colour and Temperature Scanner (COCTS)	HY-1B	SOA (China)	Apr 2007 - present	P	
Coastal Zone Imager (CZI)	HY-1B	SOA (China)	Apr 2007 - present	P	
Hyperspectral Imager for the Coastal Ocean (HICO)	International Space Station	ONR, DOD and NASA (USA)	Sep 2009 - Dec 2014	LE	
Ocean Colour Monitor-2 (COM-2)	Oceansat-2	ISRO (India)	Sep 2009 - present	P	
Geostationary Ocean Color Imager (GOCI)	COMS	KARI/KIOST (South Korea)	Jun 2010 - present	G	
Visible and Infrared Imager/Radiometer Suite (VIIRS)	Suomi NPP	NOAA (USA)	Oct 2011 - present	P	
Ocean and Land Colour Instrument (OLCI)	Sentinel 3A	ESA/EUMETSAT (Europe)	Feb 2016 - present	P	
Coastal Zone Imager (CZI)	HY-1E/F	CNSA (China)	2017	P	
Hyperspectral Imager (HSI)	EnMAP	DLR (Germany)	2017	P	
Second-Generation Global Imager (SGLI)	GCOM-C	JAXA (Japan)	2017	P	
Visible Infrared Imaging Radiometer Suite (VIIRS)	JPSS-1	NOAA /NASA (USA)	2017	P	
Chinese Ocean Color and Temperature Scanner (COCTS)	HY-1C/D	CNSA (China)	2018	P	
Coastal Zone Imager (CZI)	HY-1C/D	CNSA (China)	2018	P	
Ocean Color Monitor (COM)	OCEANSAT-3	ISRO (India)	2018	P	
Ocean and Land Colour Instrument (OLCI)	Sentinel-3B	ESA/EUMETSAT (Europe)	2018	P	
Geostationary Ocean Color Imager-II (GOCI-II)	GeoKompsat 2B	KARI/KIOST (South Korea)	2019	G	
Multi-spectral Optical Camera - NIR/SWIR (MUS- NIR/SWIR)	SABIA-MAR	CONAE (Argentina and	2019	P	

		Brazil)		
Ocean Ecology Sensor (OES)	ACE	NASA (USA)	>2020	P
Coastal Ocean Color Imaging	GEO-CAPE	NASA (USA)	>2022	G
Visible Short Wave InfraRed (VSWIR)	HyspIRI	NASA (USA)	>2022	LE
Ocean Color Instrument (OCI)	PACE	NASA (USA)	2022/2023	P
Hyper-spectral VNIR imager (YSI-VNIR)	GISAT-1	ISRO (India)	TBD	G

* Orbit are usually classified in Polar (P), also known as sun-synchronous, or Geostationery (G). Sensors onboard the International Space Station have a Low-Earth orbit (LE).

APPENDIX B

Table B.1 - Summary results of generalized additive mixed models (GAMM) used to model area coverage variability for the Environmental Provinces (EP) off South West Iberia Peninsula, using fortnight-of-the-year (expressed as month) and time (2002 - 2011) as covariates. Information includes model adjusted coefficient of determination (R^2_a), equivalent to total explained deviance, parametric coefficients (intercept ± 1 Standard Error), estimated degrees of freedom (edf) and approximate significance level (p-value) for the model covariates. Smoothing functions are referred to as s(Month/Time). Values of edf equal to 1 imply a linear effect and values higher than 1 indicate progressively stronger nonlinear effects. Symbols *, **, *** indicate p-value <0.05, <0.01 and <0.001, respectively.

EP1		
Intercept	**SE**	**p-value**
11.452	1.249	$<2e^{-16}$ ***
Smooth terms	**edf**	**p-value**
s (Month)	6.566	$<2e^{-16}$ ***
s (Time)	1.000	0.0791
		$R^2_{adj.}$ = 0.57; n = 228

EP2		
Intercept	**SE**	**p-value**
9.187	1.197	$5.23e^{-13}$ ***
Smooth terms	**edf**	**p-value**
s (Month)	4.443	$7.2e^{-15}$ ***
s (Time)	1.890	0.535
		$R^2_{adj.}$ = 0.29; n = 228

EP3		
Intercept	**SE**	**p-value**
1.7337	0.3387	$6.69e^{-7}$ ***
Smooth terms	**edf**	**p-value**
s (Month)	6.495	$4.99e^{-15}$ ***
s (Time)	1.000	0.296
		$R^2_{adj.}$ = 0.52; n = 228

EP4		
Intercept	**SE**	**p-value**
6.447	2.699	0.0177 *
Smooth terms	**edf**	**p-value**
s (Month)	5.745	$9.78e^{-6}$ ***
s (Time)	1.000	0.647
		$R^2_{adj.}$ = 0.27; n = 228

EP5		
Intercept	**SE**	**p-value**
8.939	1.227	$5.84e^{-12}$ ***
Smooth terms	**edf**	**p-value**
s (Month)	6.773	$4e^{-14}$ ***
s (Time)	1.322	0.709
		$R^2_{adj.}$ = 0.33; n = 228

EP6		
Intercept	**SE**	**p-value**
4.814	0.447	$<2e^{-16}$ ***
Smooth terms	**edf**	**p-value**
s (Month)	7.664	$<2e^{-16}$ ***
s (Time)	2.681	$4.48e^{-4}$ ***
		$R^2_{adj.}$ = 0.58; n = 228

EP7		
Intercept	**SE**	**p-value**
12.2561	0.7473	$<2e^{-16}$ ***
Smooth terms	**edf**	**p-value**
s (Month)	7.532	$<2e^{-16}$ ***
s (Time)	1.000	0.944
		$R^2_{adj.}$ = 0.60; n = 228

EP8		
Intercept	**SE**	**p-value**
10.8647	0.6335	$<2e^{-16}$ ***
Smooth terms	**edf**	**p-value**
s (Month)	7.161	$<2e^{-16}$ ***
s (Time)	1.293	0.813
		$R^2_{adj.}$ = 0.57; n = 228

EP9		
Intercept	**SE**	**p-value**
3.2847	0.2143	$<2e^{-16}$ ***
Smooth terms	**edf**	**p-value**
s (Month)	7.488	$<2e^{-16}$ ***
s (Time)	1.973	$2.75e^{-5}$ ***
		$R^2_{adj.}$ = 0.63; n = 228

EP10		
Intercept	**SE**	**p-value**
10.9103	0.8895	$<2e^{-16}$ ***
Smooth terms	**edf**	**p-value**
s (Month)	6.253	$<2e^{-16}$ ***
s (Time)	2.054	0.0275 *
		$R^2_{adj.}$ = 0.77; n = 228

EP11		
Intercept	**SE**	**p-value**
7.3229	0.6582	$<2e^{-16}$ ***
Smooth terms	**edf**	**p-value**
s (Month)	6.135	$<2e^{-16}$ ***
s (Time)	2.639	$3.61e^{-3}$ ***
		$R^2_{adj.}$ = 0.73; n = 228

EP12		
Intercept	**SE**	**p-value**
12.9850	0.3991	$<2e^{-16}$ ***
Smooth terms	**edf**	**p-value**
s (Month)	7.534	$<2e^{-16}$ ***
s (Time)	3.528	0.0153 *
		$R^2_{adj.}$ = 0.881; n = 228

Table B.2 – Environmental provinces median and standard deviation (SD) values for variables representative of the physical, optical and chemical environments and phytoplankton properties for the period between February 2002 and December 2011. MLD= mixed layer depth (m), SST = sea surface temperature (^{o}C), W^3= turbulent mixing index (m s^{-1}); U= zonal and V= meridional wind components (m s^{-1}), PAR= photosynthetically available radiation (mol phot m^{-2} day^{-1}), Z_{eu} = euphotic zone depth (m) and I_m = mean PAR intensity in the mixed layer (µmol phot m^{-2} s^{-1}) Fe= iron (nM), PO_4 = phosphate (µM), DO = dissolved oxygen (µM) and NO_3 = nitrate (µM) subsurface concentrations. Phytoplankton data was based on Chl-a = chlorophyll-a concentration (µg L^{-1}) and PP = net primary productivity (mg C m^{-3} day^{-1}).

Median ±SD	I				II		III			IV		
	EP1	**EP2**	**EP3**	**EP4**	**EP5**	**EP6**	**EP7**	**EP8**	**EP9**	**EP10**	**EP11**	**EP12**
						Physical environment						
MLD	113.3	110.0	45.7	106.0	41.0	60.7	26.1	27.0	23.3	18.4	19.2	21.4
	±31.1	±31.0	±50.5	±44.5	±24.1	±33.5	±13.0	±15.9	±28.6	±7.5	±7.4	±26.0
SST	16.5	16.5	16.1	15.5	20.1	16.7	20.6	19.7	18.1	21.3	19.6	21.4
	±0.6	±0.8	±1.9	±0.7	±1.4	±1.7	±1.8	±1.9	±2.0	±1.7	±1.7	±2.1
U	0.3	-1.0	0.6	-0.2	0.9	-0.1	0.7	1.2	1.4	1.4	2.2	0.9
	±2.6	±1.7	±2.9	±2.4	±2.1	±2.7	±1.4	±1.5	±2.7	±1.3	±1.3	±2.1
V	-1.9	-3.6	-2.2	-2.7	-1.0	-0.6	-5.0	-4.5	-2.8	-5.1	-5.2	-2.6
	±2.0	±1.9	±3.0	±2.7	±2.6	±2.1	±2.4	±2.9	±2.6	±1.8	±1.9	±1.8
W^3	260.7	348.3	353.7	346.0	273.4	290.1	332.2	350.3	295.6	273.3	345.6	174.9
	±157.6	±184.9	±274.2	±169.7	±203.4	±188.3	±148.7	±170.8	±215.5	±143.1	±174.7	±102.2
						Optical environment						
I_m	17.0	19.6	17.9	20.5	49.7	27.7	157.5	136.0	85.4	219.9	184.0	195.9
	±9.3	±10.1	±43.3	±11.6	±40.0	±32.6	±70.1	±75.2	±60.9	±56.3	±49.0	±80.0
PAR	30.9	34.7	33.0	34.1	28.1	29.1	54.2	52.6	47.8	57.6	57.6	53.9
	±8.2	±8.7	±12.7	±8.5	±5.5	±8.2	±12.0	±13.2	±13.9	±5.6	±6.0	±12.0
Z_{eu}	24.9	25.9	14.8	24.0	28.3	20.8	30.6	29.0	16.9	31.4	27.0	29.1
	±1.7	±1.2	±3.8	±2.6	±1.4	±3.2	±1.2	±2.1	±2.7	±0.7	±1.7	±1.9
						Chemical environment						
Fer	0.41	0.30	1.61	0.28	0.62	0.83	0.54	0.50	1.61	0.64	0.92	1.10
	±0.08	±0.04	±0.42	±0.09	±0.11	±0.17	±0.11	±0.14	±0.42	±0.08	±0.14	±0.48
PO_4	0.025	0.033	0.162	0.091	0.009	0.027	0.014	0.007	0.034	0.013	0.009	0.017
	±0.021	±0.023	±0.090	±0.046	±0.007	±0.016	±0.008	±0.008	±0.014	±0.007	±0.008	±0.019
DO	246.2	246.8	254.3	251.5	233.6	246.0	231.2	234.8	251.8	228.9	235.8	232.8
	±2.8	±2.7	±5.9	±4.7	±5.1	±7.4	±7.5	±8.1	±6.3	±7.3	±7.4	±11.8
NO_3	0.077	0.242	2.136	1.168	0.007	0.215	0.008	0.017	0.302	0.001	0.020	0.024
	±0.285	±0.306	±1.437	±0.761	±0.023	±0.204	±0.030	±0.048	±0.237	±0.010	±0.036	±0.248
						Phytoplankton data						
Chl-a	0.31	0.26	1.05	0.38	0.15	0.57	0.11	0.17	1.11	0.10	0.27	0.19
	±0.12	±0.07	±0.71	±0.24	±0.04	±0.33	±0.03	±0.07	±0.36	±0.02	±0.16	±0.07
PP	377	327	1198	434	246	614	284	340	1283	296	549	478
	±137	±82	±555	±284	±56	±307	±55	±76	±410	±36	±174	±229

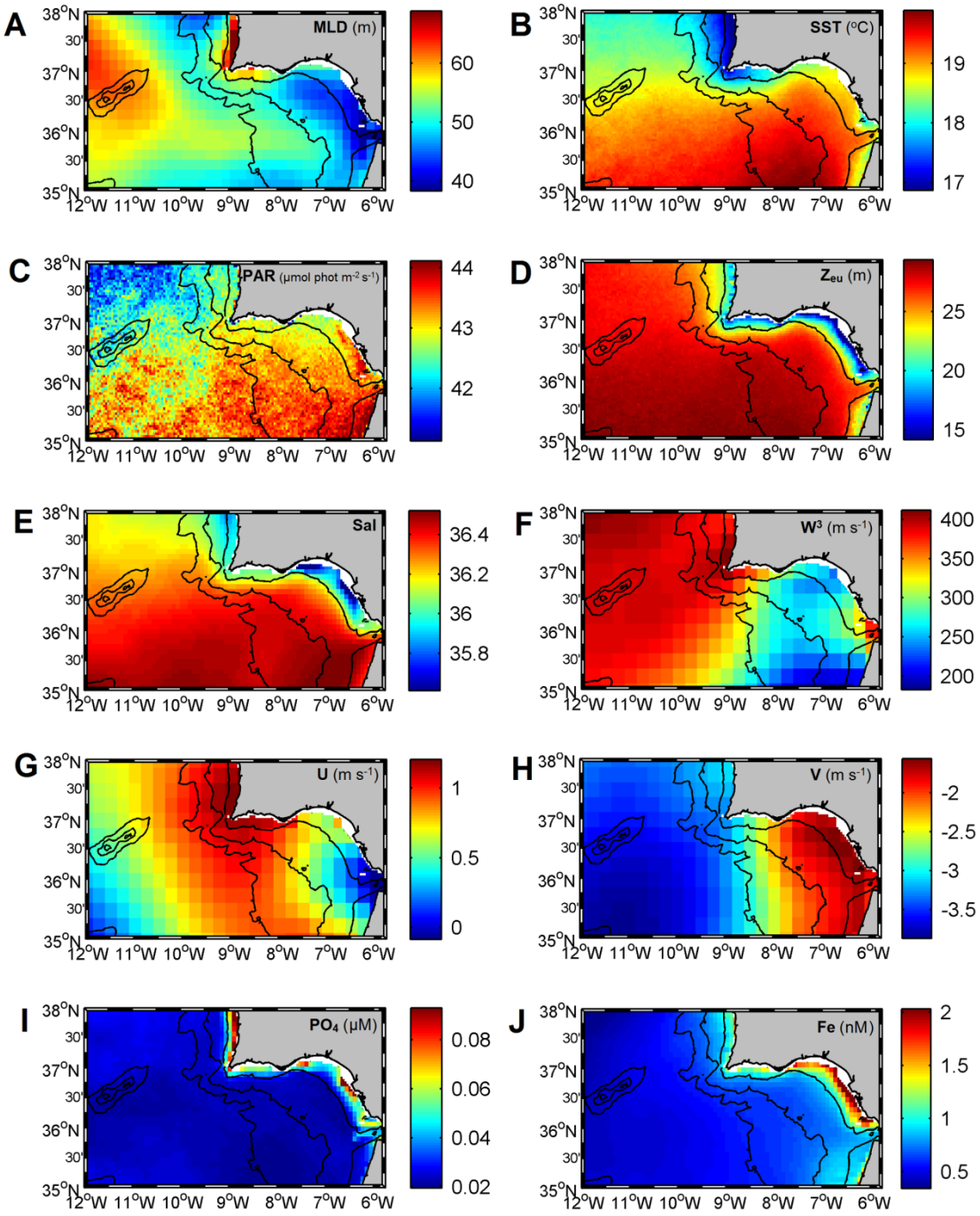

Figure B.1 - Distribution of mean values of selected abiotic variables used for the delineation of environmental provinces off SW Iberia, during the period between February 2002 and December 2011. (A) mixed layer depth (MLD), (B) sea surface temperature (SST), (C) surface photosynthetically active radiation (PAR), (D) euphotic depth (Z_{eu}), (E) subsurface salinity (Sal), (F) turbulence index (W^3), (G) zonal (U) and (H) meridional (V) wind speed, (I) subsurface phosphate (PO_4) and (J) iron (Fe) concentration. Black lines represent the 20m, 200m, 1000m and 2500m isobathimetric contours.

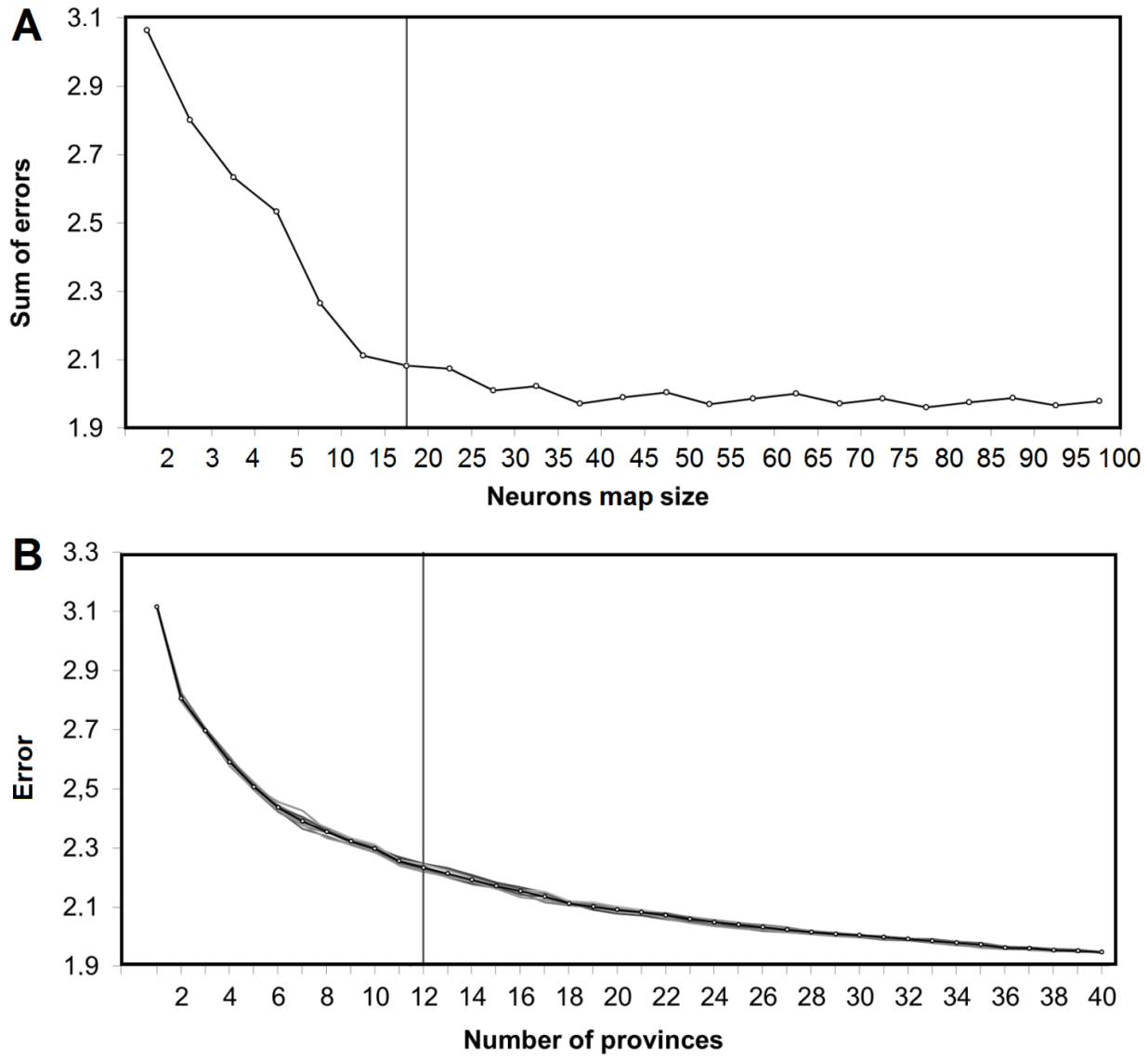

Figure B.2 – A) Sum of normalized quantization and topological errors as a function of number of neurons (i.e., neuron map size; see section 3.2.3.2) and B) Average error of cross-validations as a function of number of clusters (i.e., number of abiotic environmental provinces; see section 3.2.3.3). Gray vertical lines indicate the threshold defining the optimal neuron map size in A and number of provinces in B.

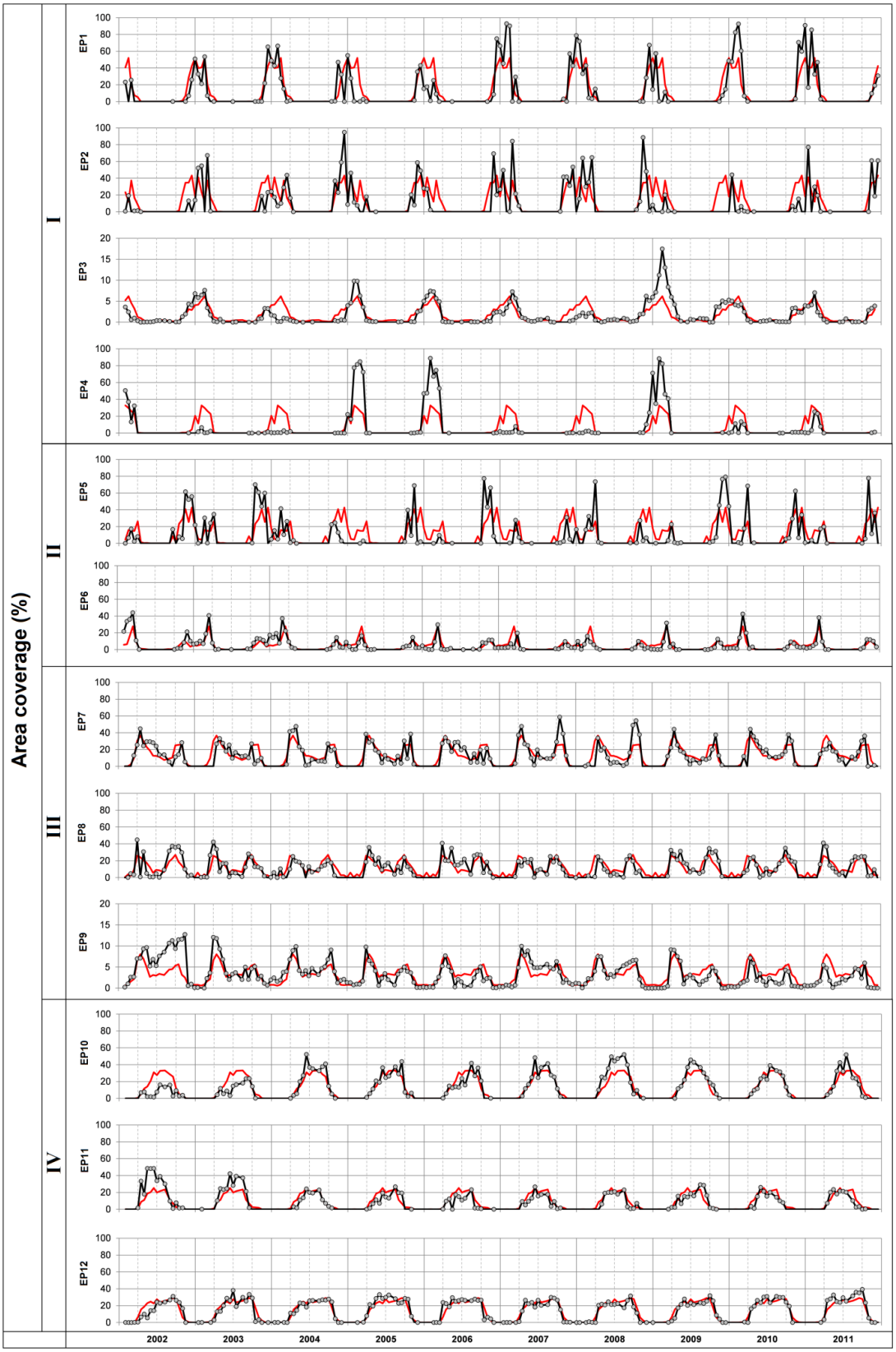

Figure B.3 – Time series (gray circles) and climatological (red line) percentage of South West Iberian Peninsula area coverage for each environmental province for the period between February 2002 and December 2011.

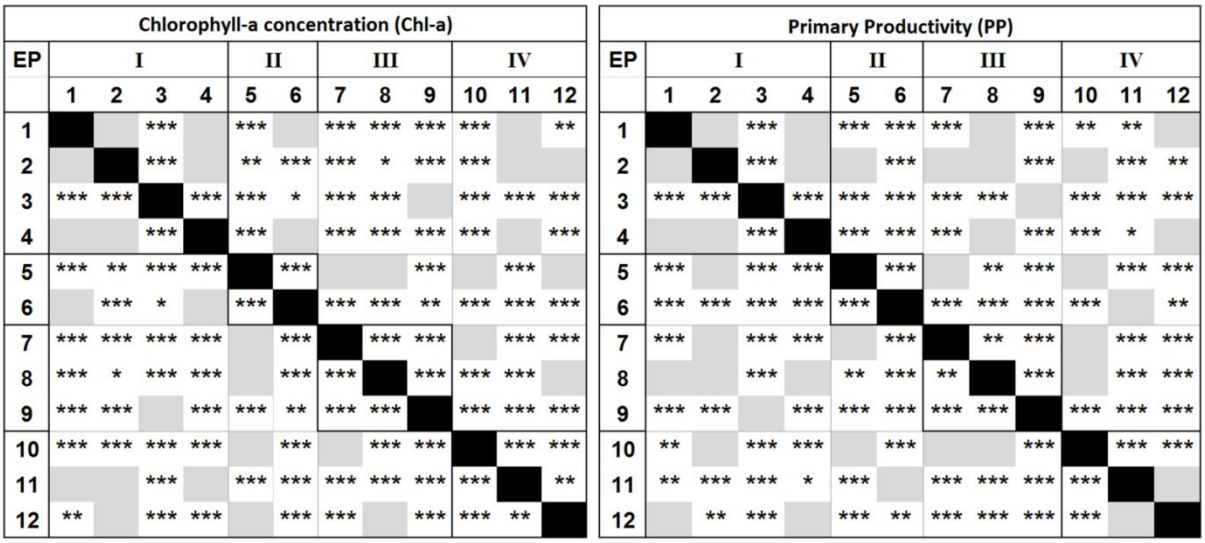

Chlorophyll-a concentration (Chl-a)												
EP	I				II		III			IV		
	1	2	3	4	5	6	7	8	9	10	11	12
1			***		***		***	***	***	***		**
2			***		**	***	***	*	***	***		
3	***	***		***	***	*	***	***		***	***	***
4			***		***		***	***	***	***		***
5	***	**	***	***		***			***		***	
6		***	*		***		***	***	**	***	***	***
7	***	***	***	***		***		***	***		***	***
8	***	*	***	***		***	***		***	***	***	
9	***	***		***	***	**	***	***		***	***	***
10	***	***	***	***		***		***	***		***	***
11			***		***	***	***	***	***	***		**
12	**		***	***		***	***		***	***	**	

Primary Productivity (PP)												
EP	I				II		III			IV		
	1	2	3	4	5	6	7	8	9	10	11	12
1			***		***	***	***		***	**	**	
2			***			***			***		***	**
3	***	***		***	***	***	***	***		***	***	***
4			***		***	***	***		***	***	*	
5	***		***	***		***		**	***		***	***
6	***	***	***	***	***		***	***	***	***		**
7	***		***	***		***		**	***		***	***
8			***		**	***	**		***		***	***
9	***	***		***	***	***	***	***		***	***	***
10	**		***	***		***			***		***	***
11	**	***	***	*	***		***	***	***	***		
12		**	***		***	**	***	***	***	***		

Figure B.4 – Kruskal-Wallis test and Dunn's test Pair-wise test of significance between environmental provinces average chlorophyll-a concentration (left) and phytoplankton net primary production (right) values for the period between February 2002 and December 2011. Symbols *, **, *** indicate p-value <0.05, <0.01 and <0.001, respectively.

Video B.1 – Spatial and temporal dynamics of the 12 environmental provinces (EPs) delineated off the South West Iberian Peninsula, during the period February 2002 - December 2011. Black lines are isobathymetric contours (200m, 500m, 1000m and 2500m). (See digital support)

APPENDIX C

Table C.1 – Summary results of generalized additive mixed models (GAMM) used to model dominant modes of chlorophyll-a variability off SW Iberia, derived from empirical orthogonal function analyses (EOF1, EOF2 and EOF3), using fortnight-of-the-year (expressed as month) and time (1997 - 2012) as covariates. Information includes model adjusted coefficient of determination (R^2_{adj}), equivalent to total explained deviance, Akaike's Information Criteria (AIC), parametric coefficients (intercept ± *1* Standard Error), estimated degrees of freedom (edf) and approximate significance level (p-value) for the model covariates. Smoothing functions are referred to as s(i), where i indicates the covariate. Values of edf equal to 1 imply a linear effect and values higher than 1 indicate progressively stronger non-linear effects. Symbols *, **, *** indicate p-value <0.05, <0.01 and <0.001, respectively.

Log(EOF1+1)		
Intercept	**SE**	**p-value**
0.0081	0.0002	$4.3e^{-5}$***
Smooth terms	**edf**	**p-value**
s (Month)	5.120	$4.33e^{-7}$ ***
s (Time)	1.765	0.134
	$R^2_{adj.}$ = 0.23; AIC = -1813.9; n = *342*	
Log(EOF2+1)		
Intercept	**SE**	**p-value**
-0.0013	0.0011	0.268
Smooth terms	**edf**	**p-value**
s (Month)	5.461	$<2e^{-16}$ ***
s (Time)	1.000	0.129
	$R^2_{adj.}$ = 0.571; AIC = -1891.1; n = 3*42*	
Log(EOF3+1)		
Intercept	**SE**	**p-value**
0.0027	0.0014	0.05
Smooth terms	**edf**	**p-value**
s (Month)	5.472	$4.13e^{-5}$ ***
s (Time)	5.122	$1.14e^{-5}$ ***
	$R^2_{adj.}$ = 0.216; AIC = -1681.6; n = 342	

Table C.2 – Summary results of the best-performing generalized additive mixed models (GAMM) used to model dominant modes of chlorophyll-a variability off SW Iberia (period: 1997 - 2012), derived from empirical orthogonal function analyses (EOF1, EOF2 and EOF3), as a function of multiple environmental predictors. Note that only statistically significant covariates were retained in the models. Information includes: model adjusted coefficient of determination (R^2_{adj}), equivalent to total explained deviance; Akaike's Information Criteria

(AIC); parametric coefficients (intercept ± 1 Standard Error); and estimated degrees of freedom (edf) and approximate significance level (p-value) for the model covariates. Smoothing functions are referred to as s(i), where i indicates the covariate: Atlantic Multidecadal Oscillation index (AMO*);* Eastern Atlantic index (EA); Guadalquivir river discharge (Gdq); Mixed layer depth (MLD); North Atlantic Oscillation index (NAO); Surface photosynthetically available radiation (PAR); Sea surface temperature (SST); Zonal (U), meridional (V) and resultant (Win) wind speed and Western Mediterranean Oscillation index (WeMO). Climate indices with 1 month lag are denoted with -1. Values of edf equal to 1 imply a linear effect and values higher than 1 indicate progressively stronger non-linear effects. Symbols *, **, *** indicate p-value <0.05, <0.01 and <0.001, respectively.

Log(EOF1+1)		
Intercept	**SE**	**p-value**
0.009	0.0012	$1.28e^{-12}$ ***
Smooth terms	**Edf**	**p-value**
s (MLD)	6.684	$5.12e^{-13}$ ***
s (Gdq)	3.794	$2.07e^{-9}$ ***
s (WeMO)	1.000	$5.64e^{-5}$ ***
s (U)	1.000	$7.39e^{-5}$ ***
s (PAR)	1.480	$5.05e^{-4}$ ***
s (Win)	1.000	0.013 *
s (AMO)	3.366	0.017 *
s (NAO-1)	3.312	0.024 *
$R^2_{adj.}$ = 0.62; AIC = -1653.8; n = *296*		
Log(EOF2+1)		
Intercept	**SE**	**p-value**
-0.0012	0.0012	0.289
Smooth terms	**Edf**	**p-value**
s (PAR)	1.000	$<2e^{-16}$ ***
s (SST)	1.000	$1.96e^{-8}$ ***
s (V)	2.881	0.005 **
s (WeMO-1)	1.000	0.006 **
s (NAO-1)	1.000	0.019 *
$R^2_{adj.}$ = 0.56; AIC = -1883.6; n = *341*		
Log(EOF3+1)		
Intercept	**SE**	**p-value**
0.0043	0.0017	0.013 *
Smooth terms	**Edf**	**p-value**
s (V)	1.807	$2.79e^{-6}$ ***
s (NAO)	2.169	0.0028 **
s (EA)	1.000	0.0033 **
s (MLD)	4.050	0.0041 **
s (Gdq)	1.000	0.0070 **
s (U)	1.000	0.0132 *
s (AMO)	1.000	0.0417 *
$R^2_{adj.}$ = 0.20; AIC = -1453.3; n = *296*		

Table C.3 – Summary results of generalized additive mixed models (GAMM) used to model of wind speed (WIN) and mixed layer depth (MLD) variability over the Gulf of Cadiz (GoC) and South Coast (SC) regions (period: 1997 – 2012), using fortnight-of-the-year (expressed as month) and time (1997 - 2012) as covariates. Information includes model adjusted coefficient of determination (R^2_{adj}), equivalent to total explained deviance, Akaike's Information Criteria (AIC), parametric coefficients (intercept ± 1 Standard Error), estimated degrees of freedom (edf) and approximate significance level (p-value) for the model covariates. Smoothing functions are referred to as s(i), where i indicates the covariate. Values of edf equal to 1 imply a linear effect and values higher than 1 indicate progressively stronger non-linear effects. Symbols *, **, *** indicate p-value <0.05, <0.01 and <0.001, respectively.

Gulf of Cadiz (GoC)		
	WIN	
Intercept	**SE**	**p-value**
6.3109	0.0589	$<2e^{-16}$ ***
Smooth terms	**edf**	**p-value**
s (Month)	4.131	$3.87e^{-6}$ ***
s (Time)	3.826	0.0007 ***
	$R^2_{adj.}$ = 0.13 ; AIC = 1039.6; n = *342*	
	MLD	
Intercept	**SE**	**p-value**
52.464	1.957	$<2e^{-16}$ ***
Smooth terms	**edf**	**p-value**
s (Month)	7.615	$<2e^{-16}$ ***
s (Time)	1.000	0.0093**
	$R^2_{adj.}$ = 0.85; AIC = 2645.9; n = *342*	
South Coast (SC)		
	WIN	
Intercept	**SE**	**p-value**
6.1431	0.0584	$<2e^{-16}$ ***
Smooth terms	**edf**	**p-value**
s (Month)	4.259	$<2e^{-16}$ ***
s (Time)	4.862	$7.88e^{-9}$ ***
	$R^2_{adj.}$ = 0.30; AIC = 1058.0; n = 3*42*	
	MLD	
Intercept	**SE**	**p-value**
38.026	1.539	$<2e^{-16}$ ***
Smooth terms	**edf**	**p-value**
s (Month)	7.253	$<2e^{-16}$ ***
s (Time)	1.000	$1.43e^{-8}$ ***
	$R^2_{adj.}$ = 0.83; AIC = 2304.4; n = 3*42*	

Table C.4 – Summary results of generalized additive mixed models (GAMM) used to model region-specific chlorophyll-a variability off SW Iberia (period: 1997 – 2012), using fortnight-of-the-year (expressed as month) and time (1997 - 2012) as covariates. Information includes

model adjusted coefficient of determination (R^2_{adj}), equivalent to total explained deviance, Akaike's Information Criteria (AIC), parametric coefficients (intercept ± *1* Standard Error), estimated degrees of freedom (edf) and approximate significance level (p-value) for the model covariates. Smoothing functions are referred to as s(i), where i indicates the covariate. Values of edf equal to 1 imply a linear effect and values higher than 1 indicate progressively stronger non-linear effects. Symbols *, **, *** indicate p-value <0.05, <0.01 and <0.001, respectively.

Offshore (Off)

Intercept	SE	p-value
0.2096	0.0158	$<2e^{-16}$ ***
Smooth terms	**edf**	**p-value**
s (Month)	6.692	$<2e^{-16}$ ***
s (Time)	1.000	0.167

$R^2_{adj.}$ = 0.59 ; AIC = -802.5; n = 3*42*

North Offshore (NOff)

Intercept	SE	p-value
0.2976	0.0094	$<2e^{-16}$ ***
Smooth terms	**edf**	**p-value**
s (Month)	5.997	$<2e^{-16}$ ***
s (Time)	1.000	0.0734

$R^2_{adj.}$ = 0.39; AIC = -513.0; n = *342*

Gulf of Cadiz (GoC)

Intercept	SE	p-value
0.1837	0.0043	$<2e^{-16}$ ***
Smooth terms	**edf**	**p-value**
s (Month)	6.597	$<2e^{-16}$ ***
s (Time)	1.000	0.0037 **

$R^2_{adj.}$ = 0.67; AIC = -972.8; n = 3*42*

West Coast (WC)

Intercept	SE	p-value
0.8090	0.0247	$<2e^{-16}$ ***
Smooth terms	**edf**	**p-value**
s (Month)	4.142	$5.43e^{-10}$ ***
s (Time)	1.000	0.393

$R^2_{adj.}$ = 0.18; AIC = 218.2; n = 3*42*

West Slope (WSlp)

Intercept	SE	p-value
0.4502	0.0150	$<2e^{-16}$ ***
Smooth terms	**edf**	**p-value**
s (Month)	5.941	$3.94e^{-9}$ ***
s (Time)	1.000	0.423

$R^2_{adj.}$ = 0.22; AIC = -260.0; n = 3*42*

South Slope (SSlp)

Intercept	SE	p-value
0.4051	0.0218	$<2e^{-16}$ ***
Smooth terms	**edf**	**p-value**
s (Month)	4.188	$1.52e^{-6}$ ***
s (Time)	1.140	0.175

$R^2_{adj.}$ = 0.16; AIC = 44.4; n = 3*42*

South Coast (SC)

Intercept	SE	p-value
0.8440	0.0446	$<2e^{-16}$ ***
Smooth terms	**edf**	**p-value**
s (Month)	2.907	0.0011 **
s (Time)	2.151	0.0352 *

$R^2_{adj.}$ = 0.15; AIC = 383.3; n = 3*42*

Guadiana (Gdn)

Intercept	SE	p-value
1.4697	0.0814	$<2e^{-16}$ ***
Smooth terms	**edf**	**p-value**
s (Month)	3.645	$5.43e^{-10}$ ***
s (Time)	2.538	0.0122 *

$R^2_{adj.}$ = 0.28; AIC = 870.8; n = 3*42*

Guadalquivir (Gdq)

Intercept	SE	p-value
1.1357	0.0471	$<2e^{-16}$ ***
Smooth terms	**edf**	**p-value**
s (Month)	4.315	$4.83e^{-13}$ ***
s (Time)	1.000	0.0811 ‘

$R^2_{adj.}$ = 0.30; AIC = 502.0; n = 3*42*

Table C.5 – Summary results of the best-performing generalized additive mixed models (GAMM) including sea surface temperature used to model region-specific chlorophyll-a variability (log Chl-a) off SW Iberia (period: 1997 - 2012) as a function of multiple environmental covariates (predictors). Note that only statistically significant covariates were

retained in the models. Information includes: model adjusted coefficient of determination (R^2_{adj}), equivalent to total explained deviance; Akaike's Information Criteria (AIC)*;* parametric coefficients (intercept ± *1* Standard Error); and estimated degrees of freedom (edf) and approximate significance level (p-value) *for* the model covariates. Smoothing functions are referred to as s(i), where i indicates the covariate: Atlantic Multidecadal Oscillation index (AMO); Eastern Atlantic index (EA)*;* Guadiana river discharge (Gdn); Guadalquivir river discharge (Gdq); Multivariate ENSO Index (MEI); Mixed layer depth (MLD); North Atlantic Oscillation index (NAO); Surface photosynthetically available radiation (PAR); Sea surface temperature (SST); Zonal (U), meridional (V) and resultant (Win) wind speed and Western Mediterranean Oscillation index (WeMO). Climate indices with 1 month lag are denoted with -1. Values of edf equal to 1 imply a linear effect and values higher than 1 indicate progressively stronger non-linear effects. Symbols *, **, *** indicate p-value <0.05, <0.01 and <0.001, respectively.

Offshore

Intercept	**Intercept**	**Intercept**
-1.6777	-1.6777	-1.6777
Smooth terms	**edf**	**p-value**
s (SST)	1.000	$< 2e^{-16}$ ***
s (PAR)	5.606	$3.13e^{-6}$ ***
s (AMO-1)	3.819	0.006 **
s (U)	1.000	0.015 *

$R^2_{adj.}$ = 0.76; AIC = -138.9; n = *341*

North Offshore

Intercept	**Intercept**	**Intercept**
-1.3039	-1.3039	-1.3039
Smooth terms	**edf**	**p-value**
s (SST)	2.204	$<2e^{-16}$ ***
s (PAR)	4.600	$2.7e^{-4}$ ***
s (AMO)	1.000	0.0089 **
s (U)	1.000	0.0136 *
s (EA)	1.000	0.0140 *
s (MEI)	1.000	0.0395 *

$R^2_{adj.}$ = 0.55; AIC = 26.4; n = *341*

Gulf of Cadiz

Intercept	**Intercept**	**Intercept**
-1.8193	-1.8193	-1.8193
Smooth terms	**edf**	**p-value**
s (SST)	5.996	$< 2e^{-16}$ ***
s (PAR)	5.773	$4.06e^{-5}$ ***
s (U)	1.000	0.0015 **
s (NAO)	3.908	0.0019 **

$R^2_{adj.}$ = 0.82; AIC = -263.5; n = *341*

West Slope

Intercept	**Intercept**	**Intercept**
-0.8726	-0.8726	-0.8726
Smooth terms	**edf**	**p-value**
s (SST)	3.565	$9.54e^{-9}$ ***
s (PAR)	4.820	$2.16e^{-7}$ ***
s (EA)	1.000	0.004 **
s (AMO)	1.000	0.026 *
s (V)	1.000	0.030 *

$R^2_{adj.}$ = 0.32; AIC = 93.9; n = *304*

West Coast

Intercept	**Intercept**	**Intercept**
-0.3079	-0.3079	-0.3079
Smooth terms	**edf**	**p-value**
s (PAR)	2.942	$1.49e^{-8}$ ***
s (V)	2.858	$1.22e^{-4}$ ***
s (SST)	3.523	$6.17e^{-4}$ ***
s (EA)	1.000	0.0183 *
s (MEI-1)	1.000	0.0474 *

$R^2_{adj.}$ = 0.33; AIC = 246.6; n = *339*

South Coast

Intercept	**Intercept**	**Intercept**
-0.3266	-0.3266	-0.3266
Smooth terms	**edf**	**p-value**
s (SST)	3.315	$4.82e^{-15}$ ***
s (Gdq)	2.898	$3.13e^{-8}$ ***
s (NAO-1)	1.000	0.0014 **
s (PAR)	2.362	0.0021 **
s (EA-1)	1.000	0.0119 *
s (MEI-1)	1.000	0.0324 *
s (U)	1.846	0.0506

$R^2_{adj.}$ = 0.51; AIC = 175.4; n = 296

South Slope		
Intercept	**Intercept**	**Intercept**
-1.0481	-1.0481	-1.0481
Smooth terms	**edf**	**p-value**
s (SST)	1.000	$1.63e^{-10}$ ***
s (Gdq)	4.009	$2.44e^{-10}$ ***
s (PAR)	3.435	$2.12e^{-6}$ ***
s (MEI-1)	1.000	$3.06e^{-4}$ ***
s (AMO)	1.000	0.0047 **
s (NAO)	4.838	0.0115 *
s (Gdn)	1.000	0.0200 *
s (Win)	1.000	0.0303 *
$R^2_{adj.}$ = 0.55; AIC = 81.6; n = 265		

Guadiana		
Intercept	**Intercept**	**Intercept**
0.1739	0.1739	0.1739
Smooth terms	**edf**	**p-value**
s (SST)	3.037	$< 2e^{-16}$ ***
s (Gdq)	3.671	$1.24e^{-11}$ ***
s (U)	1.000	0.0014 **
s (WeMO)	1.000	0.0029 **
s (EA-1)	1.000	0.0042 **
s (AMO-1)	3.527	0.0052 **
s (NAO-1)	2.840	0.0060 **
s (PAR)	2.600	0.0087 **
$R^2_{adj.}$ = 0.70; AIC = 209.2; n = *296*		

Guadalquivir		
Intercept	**Intercept**	**Intercept**
-0.0046	-0.0046	-0.0046
Smooth terms	**edf**	**p-value**
s (SST)	2.742	$< 2e^{-16}$ ***
s (U)	1.000	$3.21e^{-9}$ ***
s (Gdq)	3.218	$1.43e^{-6}$ ***
s (Win)	1.000	$7.45e^{-4}$ ***
s (V)	1.000	$9.94e^{-4}$ **
s (WeMO)	1.000	0.0325 *
$R^2_{adj.}$ = 0.61; AIC = 121.2; n = *296*		

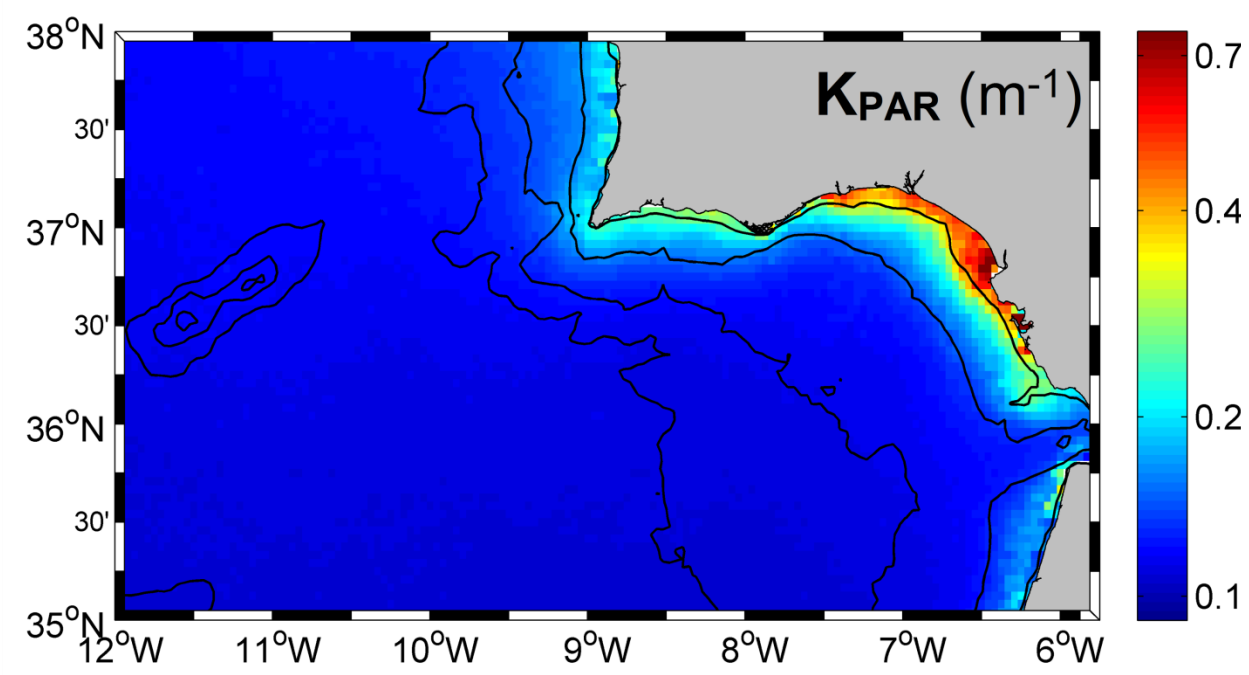

Figure C.1 - Distribution of mean values of PAR light attenuation coefficient (K_{PAR}) in the southwest area off the Iberian Peninsula, during the period between September 1997 and July 2012. Black lines represent 20m, 200m, 1000m and 2500m isobathimetric contours.

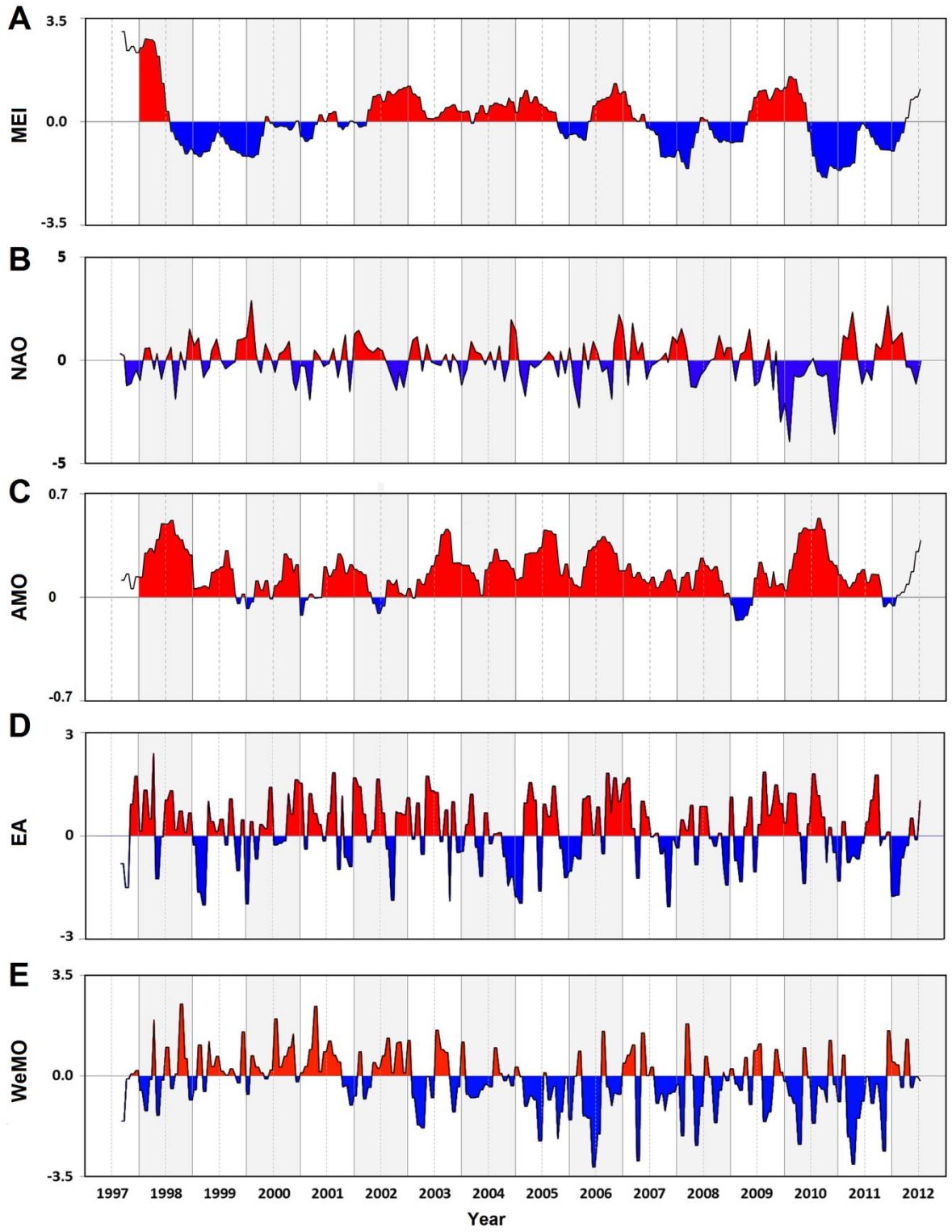

Figure C.2 - Temporal variability of climate indices during the period 1997 to 2012. (A) Multivariate ENSO Index (MEI); (B) North Atlantic Oscillation index (NAO); (C) Atlantic Multidecadal Oscillation index (AMO); (D) East Atlantic pattern index (EA); and (E) Western Mediterranean Oscillation index (WeMO).

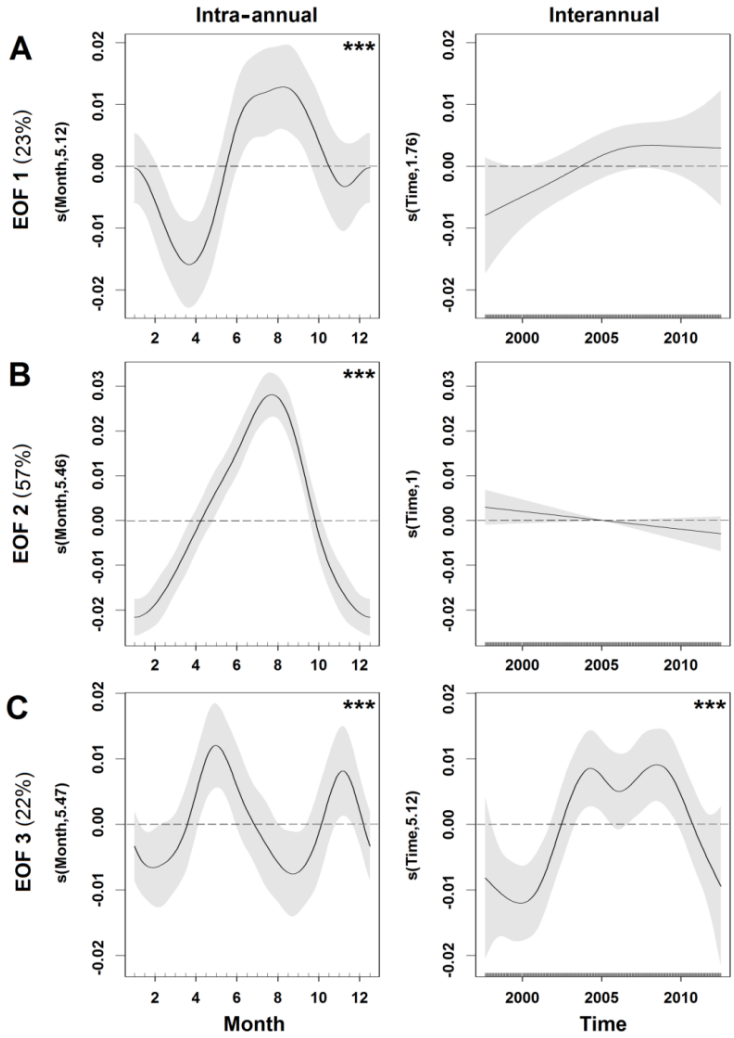

Figure C.3 - Generalized additive mixed models (GAMM) of the dominant modes of chlorophyll-a variability off Southwest Iberia Peninsula, derived from temporal components of the A) first, B) second, and C) third modes of an Empirical Orthogonal Function, using fortnight-of-the-year (expressed as month) and time (1997 - 2012) as covariates. For each EOF model, the model explanatory power (as % of temporal component variance explained) is shown in brackets, the significance level (p-value) of each predictor is denoted by asterisk symbols (top right), where *, **, *** indicate p-value <0.05, <0.01 and <0.001, respectively. For each plot, predictor values are represented on the x-axis, where short vertical lines indicate the exact predictor observations. Values on the y-axis represent the partial effects of the specific predictor, holding the other predictor constant. On y-axis, numbers in parentheses represent the effective degrees of freedom (edf), indicative of the smoothness of each function. Values of edf equal to 1 represent a linear effect of the predictor on Chl-a anomaly, and values higher than 1 indicate progressively stronger non-linear effects. Solid lines indicate the smoothed non-parametric trends, and gray shaded areas designate the point-wise 95% confidence intervals. Regions where the 95% CI bands enclose the x-axis line indicate no significant effects of the predictor. At each stage, the value of the EOF temporal component is given by the sum of the partial effects of both predictors plus a constant. (See Fig. 4.5 for temporal components time series and Table C.1 for detailed statistics).

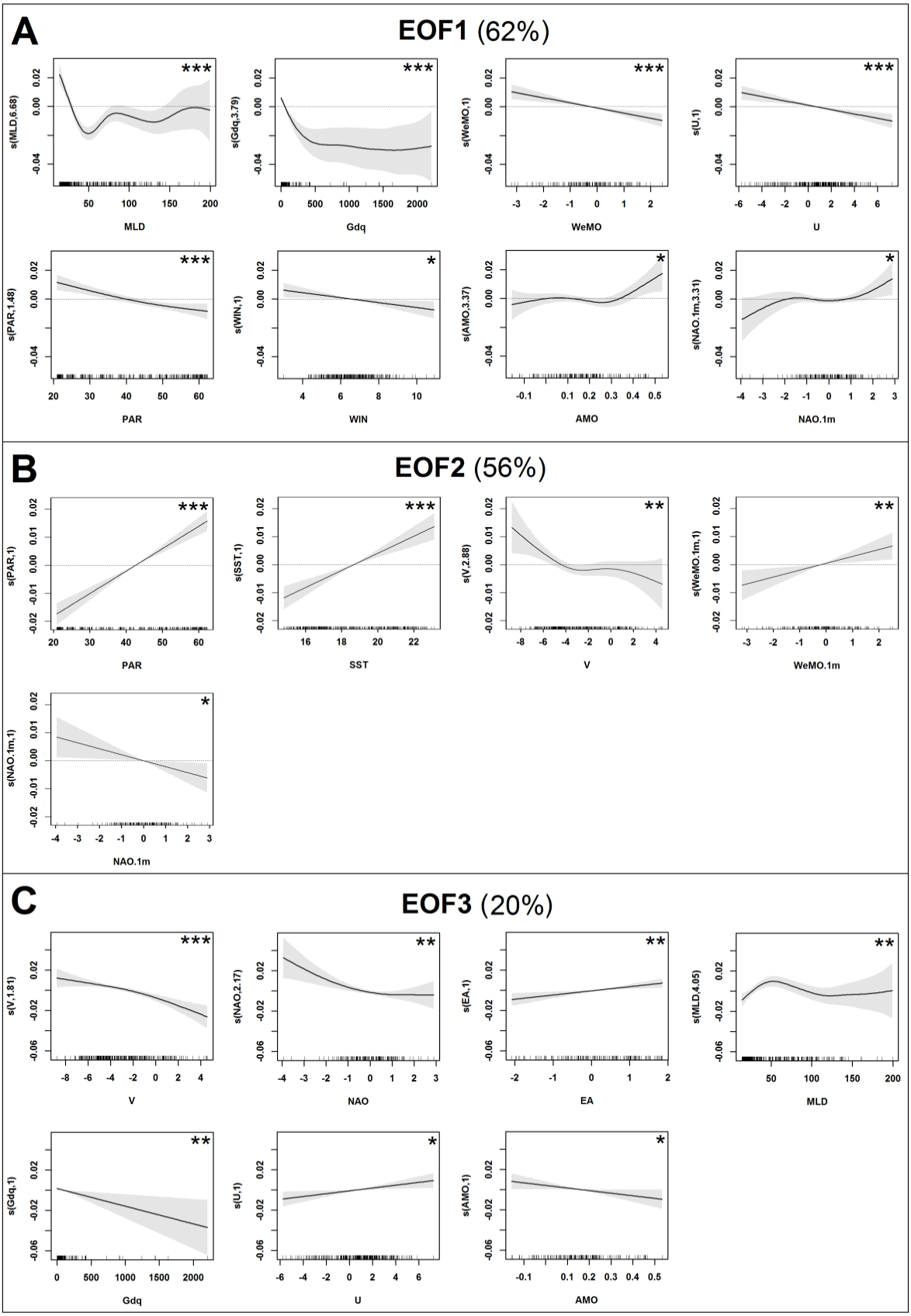

Figure C.4 – Partial effects of individual environmental covariates on global chlorophyll-a

variability concentrated on the A) first, B) second, and C) third modes of an Empirical Orthogonal Function, derived from the best performing generalized additive mixed models (GAMMs). For each EOF model, the model explanatory power (as % of temporal component variance explained) is shown in brackets, the significance level (p-value) of each predictor is denoted by asterisk symbols (top right), where *, **, *** indicate p-value <0.05, <0.01 and <0.001, respectively. For each plot, predictor values are represented on the x-axis, where short vertical lines indicate the exact predictor observations. Values on the y-axis represent the partial effects of the specific predictor, holding the other predictor constant. On y-axis, numbers in parentheses represent the effective degrees of freedom (edf), indicative of the smoothness of each function. Values of edf equal to 1 represent a linear effect of the predictor on Chl-a anomaly, and values higher than 1 indicate progressively stronger non-linear effects. Solid lines indicate the smoothed non-parametric trends, and gray shaded areas designate the point-wise 95% confidence intervals. Regions where the 95% CI bands enclose the x-axis line indicate no significant effects of the predictor. At each stage, the value of the EOF temporal component is given by the sum of the partial effects of all predictors plus a constant. (See Fig. 4.5 for temporal components time series, Figs. 4.2, 4.3 and C.2 for predictor abbreviations and Table C.2 for detailed statistics).

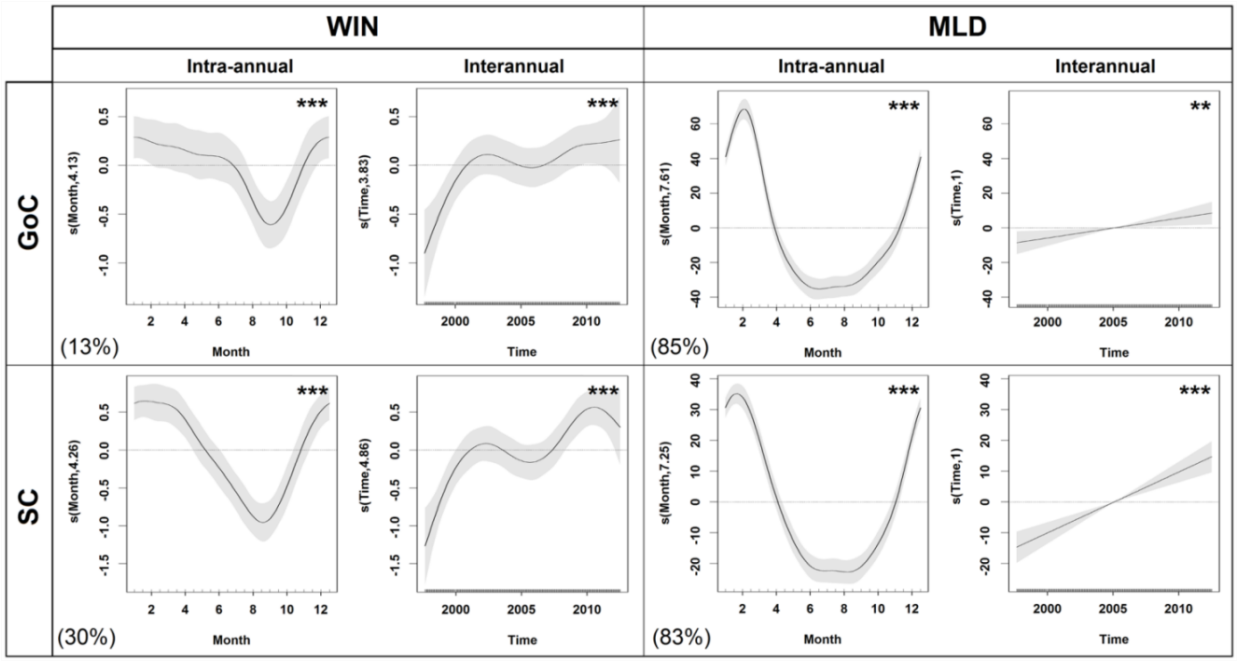

Figure C.5 – Generalized additive mixed models (GAMM) of wind speed (WIN) and mixed layer depth (MLD) temporal variability for the Gulf of Cadiz (GoC) and South Coast (SC) regions, using fortnight-of-the-year (expressed as month) and time (1997 - 2012) as covariates. For each region model, the model explanatory power (as % of MLD or WIN variance explained) is shown in brackets, the significance level (p-value) of each predictor is denoted by asterisk symbols (top right), where *, **, *** indicate p-value <0.05, <0.01 and <0.001, respectively. For each plot, predictor values are represented on the x-axis, where short vertical lines indicate the exact predictor observations. Values on the y-axis represent the partial effects of the specific predictor, holding the other predictor constant. On y-axis, numbers in parentheses represent the effective degrees of freedom (edf), indicative of the smoothness of each function. Values of edf equal to 1 represent a linear effect of the predictor on the environmental variable, and values higher than 1 indicate progressively stronger non-linear effects. Solid lines indicate the smoothed non-parametric trends, and gray shaded areas designate the point-

wise 95% confidence intervals. Regions where the 95% CI bands enclose the x-axis line indicate no significant effects of the predictor. At each stage, the value of the variable is given by the sum of the partial effects of both predictors plus a constant. (See Fig. 4.6 for region location and Table C.3 for detailed statistics).

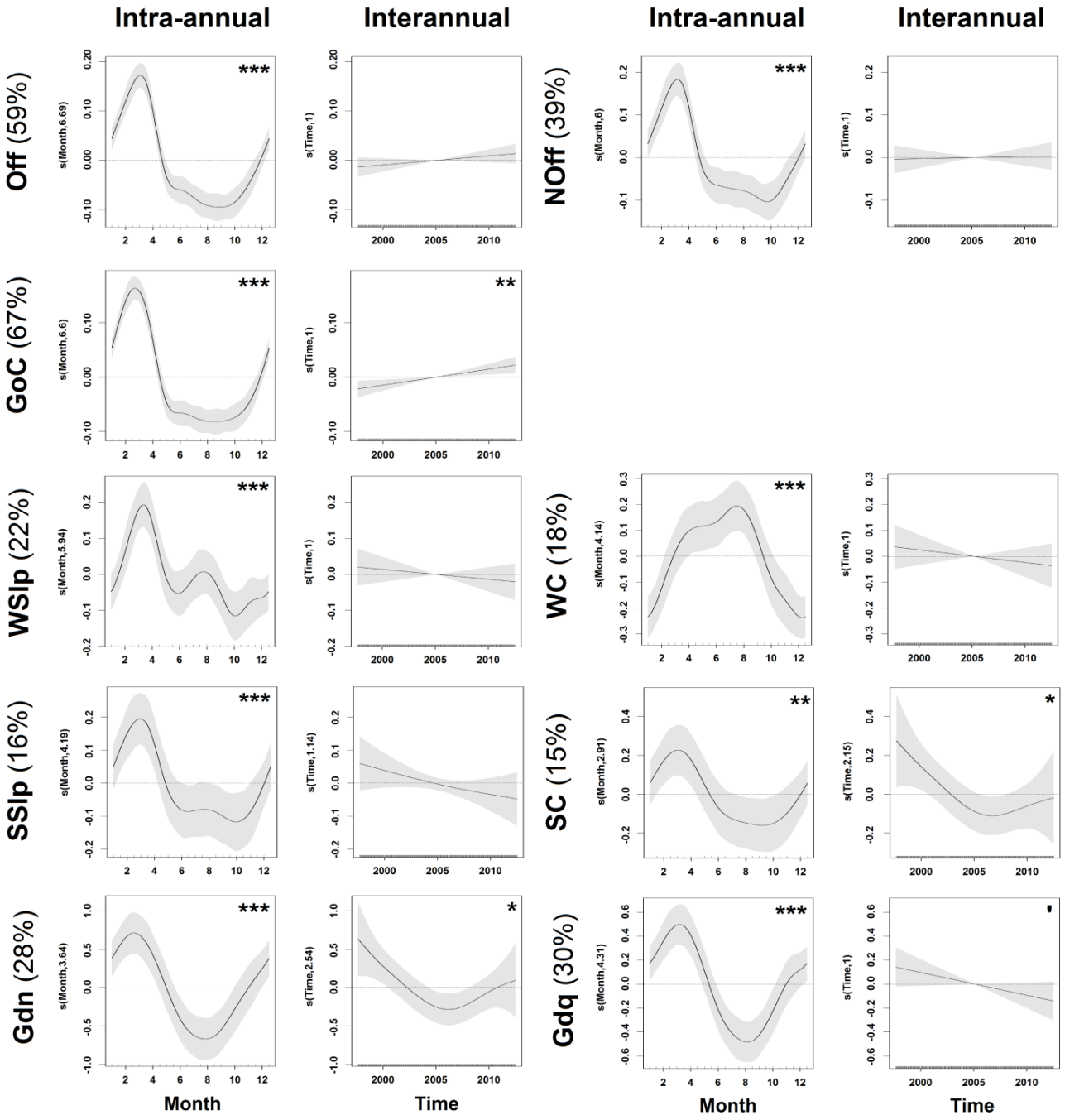

Figure C.6 - Generalized additive mixed models (GAMM) of region-specific chlorophyll-a concentration temporal variability, using fortnight-of-the-year (expressed as month) and time (1997 - 2012) as covariates. For each region model, the model explanatory power (as % of Chl-a variance explained) is shown in brackets, the significance level (p-value) of each predictor is denoted by asterisk symbols (top right), where *, **, *** indicate p-value <0.05, <0.01 and <0.001, respectively. For each plot, predictor values are represented on the x-axis, where short vertical lines indicate the exact predictor observations. Values on the y-axis represent the partial effects of the specific predictor, holding the other predictor constant. On y-axis, numbers in parentheses represent the effective degrees of freedom (edf), indicative of the smoothness of each function. Values of edf equal to 1 represent a linear effect of the predictor on Chl-a anomaly, and values higher than 1 indicate progressively stronger non-linear effects. Solid lines indicate the smoothed non-parametric trends, and gray shaded areas designate the point-wise 95% confidence intervals. Regions where the 95% CI bands enclose the x-axis line indicate no significant effects of the predictor. At each stage, the value of Chl-a is given by the sum of the partial effects of both predictors plus a constant. (See Fig. 4.8 for region specific Chl-a time series and Table C.4 for detailed statistics).

APPENDIX D

Table D.1 – Significant Spearman rank correlation (r_S) matrices of phytoplankton phenological indices for the five phenoregions delineated off SW Iberia, during the period 1997 to 2015 (See Fig. 5.4 for region location). Underlined r_S are significant at $p<0.01$.

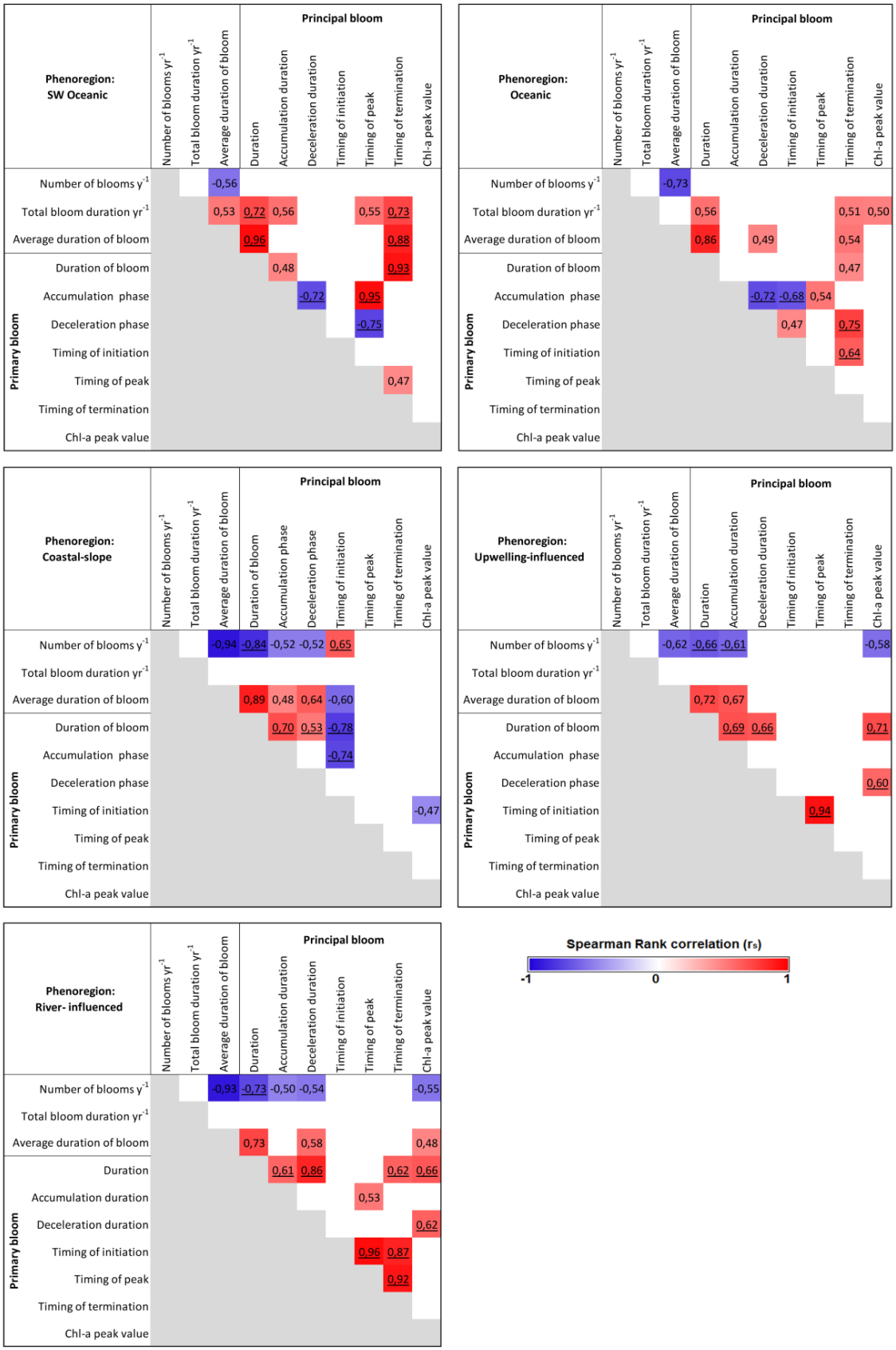

Table D.2 - Summary of results from the generalized additive mixed models (GAMM) used to model interannual variability for SW Oceanic, Oceanic, Coastal-Slope and River-influenced phenoregions off South West Iberia Peninsula (1997 - 2015). Information includes model adjusted coefficient of determination (R^2_a), equivalent to total explained deviance, parametric coefficients (intercept ± 1 Standard Error), estimated degrees of freedom (edf) and approximate significance level (p-value) for the model covariates. Smoothing functions are referred to as s(Month/Time). Values of edf equal to 1 imply a linear effect and values higher than 1 indicate progressively stronger nonlinear effects. Symbols *, **, *** indicate p-value <0.10, ≤0.05 and <0.001, respectively.

Total duration of bloom events per year

Coastal-slope phenoregion

Intercept	**SE**	**p-value**
23.160	0.7017	$3.8e^{-16***}$
Smooth terms	**edf**	**p-value**
s (Year)	1.000	0.09^{*}

$R^2_{adj.}$ = 0.12; n = 18

River-influenced phenoregion

Intercept	**SE**	**p-value**
21.8910	0.5499	$2.27e^{-16***}$
Smooth terms	**edf**	**p-value**
s (Year)	2.317	0.07^{*}

$R^2_{adj.}$ = 0.32; n =18

Duration of the principal bloom event

SW Oceanic phenoregion

Intercept	**SE**	**p-value**
20.944	0.2167	$<2e^{-16***}$
Smooth terms	**edf**	**p-value**
s (Year)	6.710	0.06^{*}

$R^2_{adj.}$ = 0.54; n = 18

Coastal-slope phenoregion

Intercept	**SE**	**p-value**
13.708	1.021	$3.95e^{-10***}$
Smooth terms	**edf**	**p-value**
s (Year)	1.000	0.06^{*}

$R^2_{adj.}$ = 0.10; n = 18

Duration of principal bloom accumulation phase

SW Oceanic phenoregion

Intercept	**SE**	**p-value**
14.678	0.2018	$3.4e^{-16***}$
Smooth terms	**edf**	**p-value**
s (Year)	5.927	$9.34e^{-5***}$

$R^2_{adj.}$ = 0.42; n = 18

Duration of principal bloom deceleration phase

Upwelling-influenced phenoregion

Intercept	**SE**	**p-value**
3.993	0.350	$4.26e^{-9***}$
Smooth terms	**edf**	**p-value**
s (Year)	1.000	$9.02e^{-4***}$

$R^2_{adj.}$ = 0.22; n = 18

Principal bloom timing of initiation

River-influenced phenoregion

Intercept	**SE**	**p-value**
12.048	1.583	$1.05e^{-6***}$
Smooth terms	**edf**	**p-value**
s (Year)	1.000	0.09^{*}

$R^2_{adj.}$ = 0.12; n = 18

Principal bloom timing of peak

SW Oceanic phenoregion

Intercept	**SE**	**p-value**
24.731	0.2477	$<2e^{-16***}$
Smooth terms	**edf**	**p-value**
s (Year)	5.091	$7.75e^{-4***}$

$R^2_{adj.}$ = 0.41; n = 18

River-influenced phenoregion

Intercept	**SE**	**p-value**
16.798	1.355	$2.5e^{-9***}$
Smooth terms	**edf**	**p-value**
s (Year)	1.872	0.03^{**}

$R^2_{adj.}$ = 0.26; n = 18

Principal bloom timing of termination

River-influenced phenoregion

Intercept	**SE**	**p-value**
23.445	1.705	$2.78e^{-10***}$
Smooth terms	**edf**	**p-value**
s (Year)	1.00	0.06^{**}

$R^2_{adj.}$ = 0.04; n = 18

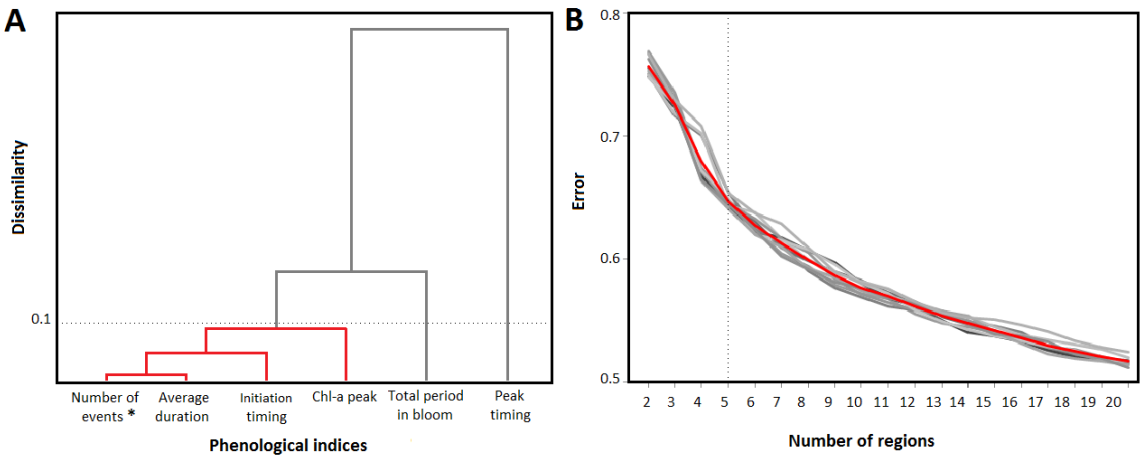

Figure D.1 – A) Dissimilarity analysis based on phenological indices averages off SW Iberia, during the 1997-2015 period. Red nodes indicate the group with dissimilarity values below the defined threshold (0.1), and the asterisk symbol denotes the index selected to represent it. B) Average error (red line) of cross-validations (gray lines) as a function of number of regions and the vertical dashed line indicate the threshold defining the optimal number of regions.

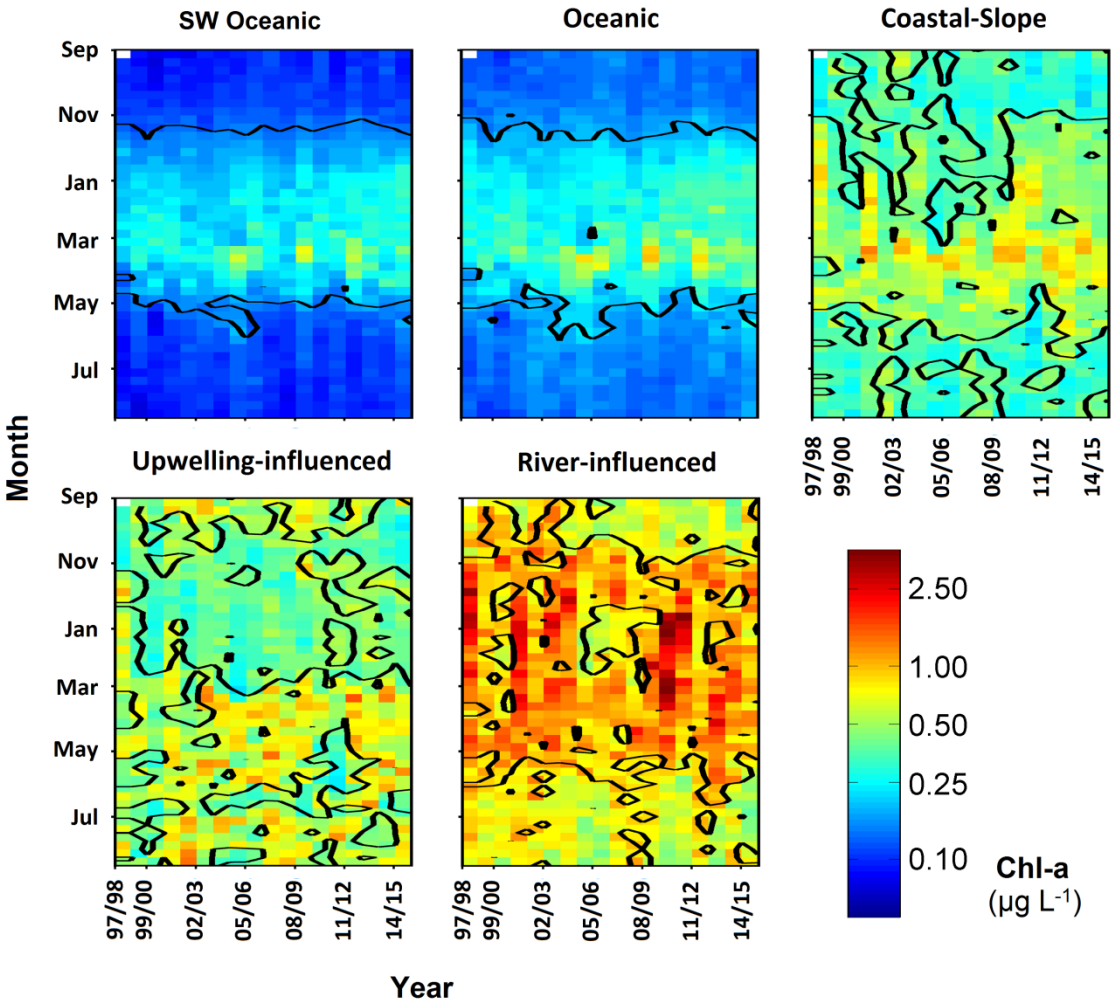

Figure D.2 – Weekly Chl-a values for each phenological region between 1997 and 2015.

Black lines represent the annual threshold limit and periods delimited represent a bloom situation (see Fig. 5.4 for region location).

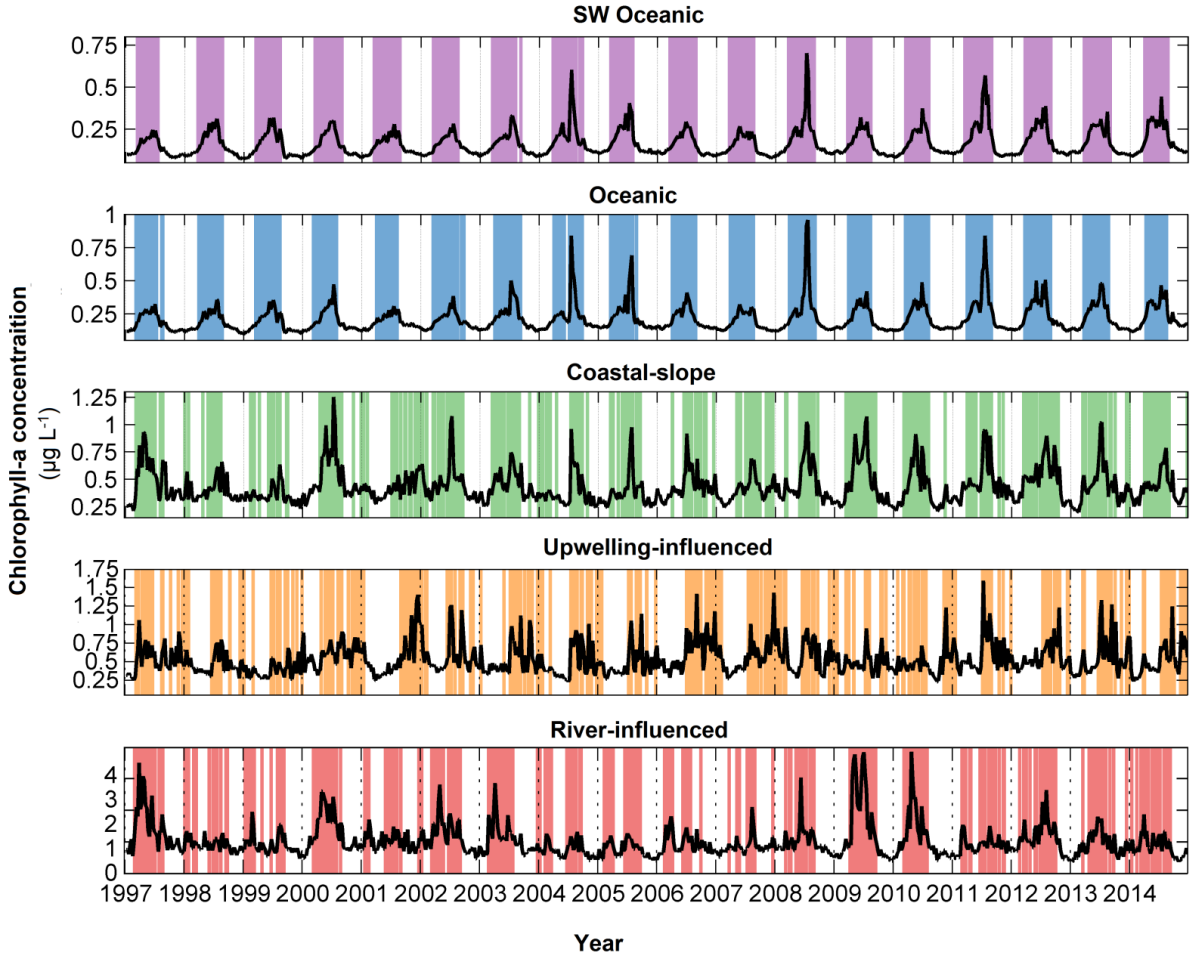

Figure D.3 - Time series of chlorophyll-a (Chl-a; black lines; note different y-scales) and bloom periods (coloured-shaded columns) for each phenoregion off SW Iberian Peninsula (see Fig. 5.4 for region location and colour code). Vertical dashed lines indicate the first week of September of the respective year.

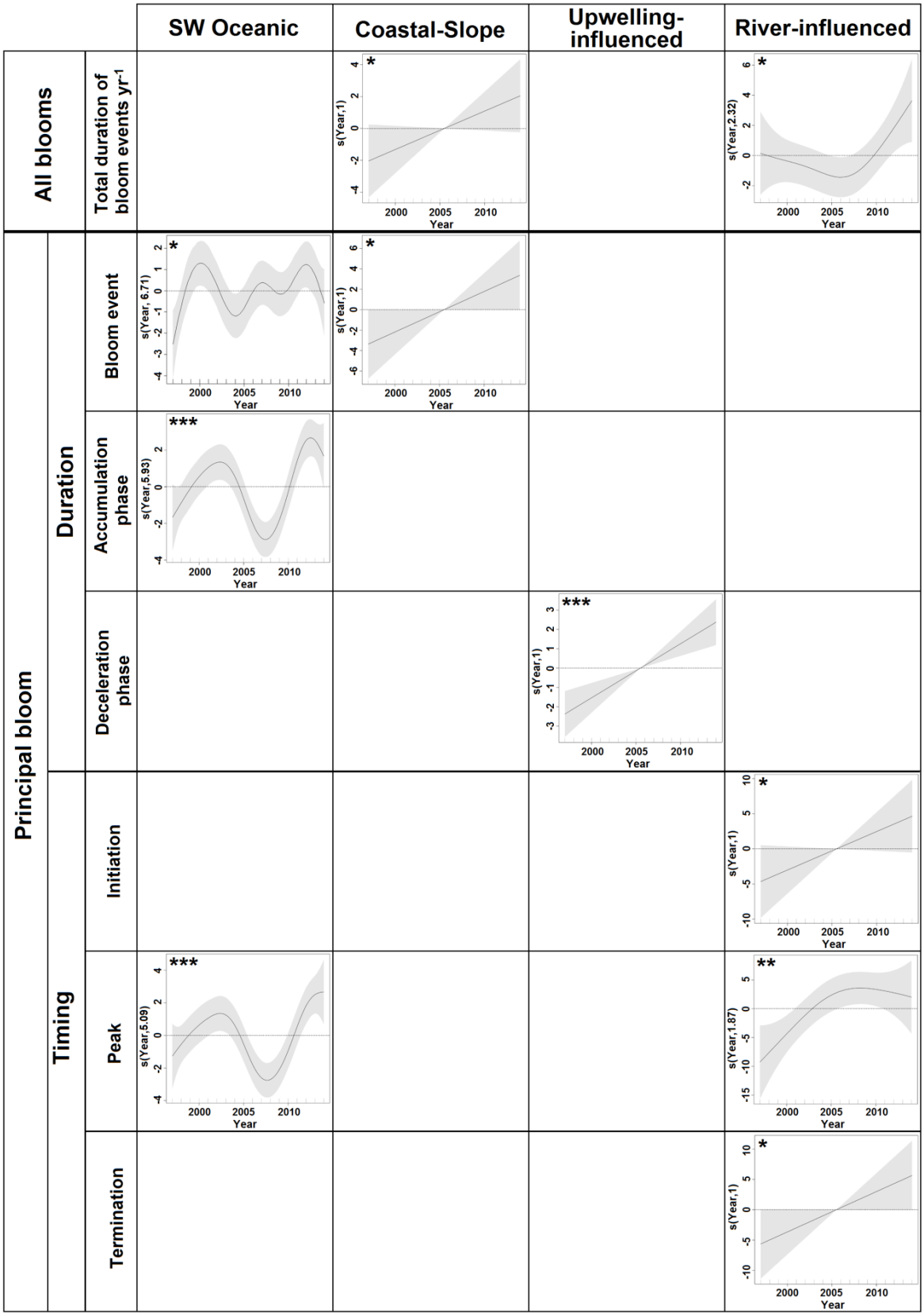

Figure D.4 - Partial effects of significant interannual variability (expressed as year) of the SW Oceanic, Coastal-Slope, Upwelling and River-influenced phenoregions off Southwest Iberia

Peninsula (period: 1997-2015; see Fig. 5.4 for region location), derived from generalized additive mixed models (GAMMs). Model explanatory power (as % explained variance) is shown on the top left with the significance level (p-value; in parenthesis) of the predictor (year), denoted by asterisk symbols, where *, **, *** indicate p-value <0.10, ≤0.05 and <0.001, respectively. For each plot, years are represented on the x-axis, while values on the y-axis represent the partial effects of the specific predictor. Numbers in parentheses on the y-axis represent the effective degrees of freedom (edf), indicative of the smoothness of each function; values of edf equal to 1 represent a linear effect of the predictor, and values higher than 1 indicate progressively stronger non-linear effects. Solid lines indicate the smoothed non-parametric trends, and gray shaded areas designate the point-wise 95% confidence intervals. Regions where the 95% CI bands enclose the x-axis line indicate no significant effects of the prediction (see Table D.2 for detailed statistics).

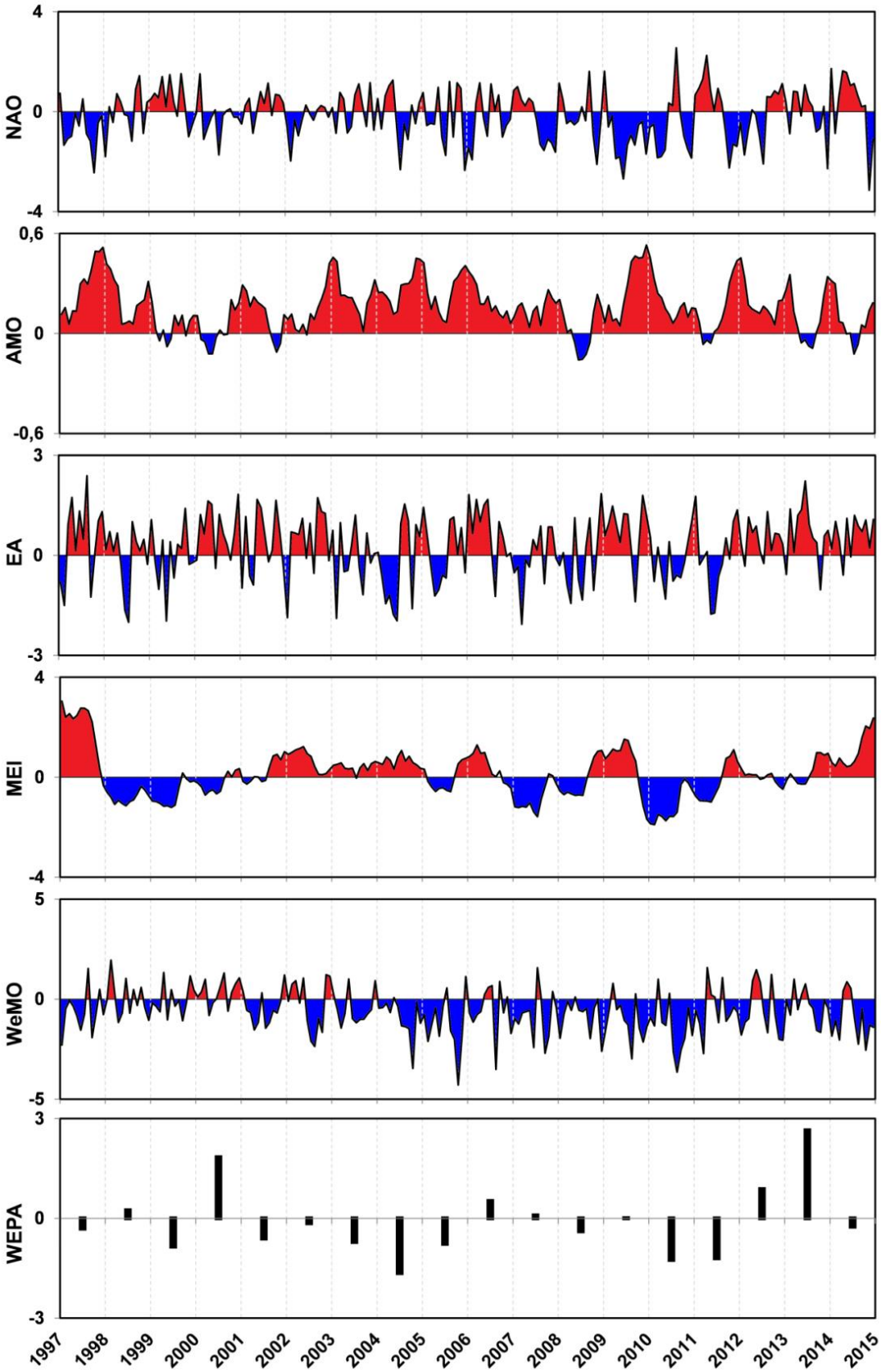

Figure D.5– Temporal variability of climate indices during the period 1997 to 2015 based on monthly values of North Atlantic Oscillation index (NAO); Atlantic Multidecadal Oscillation

index (AMO); East Atlantic pattern index (EA); Multivariate ENSO Index (MEI); Western Mediterranean Oscillation index (WeMO) and winter-averaged (December-March) West Europe Pressure Anomaly (WEPA). Vertical dashed lines signalize the month of September of the respective year.

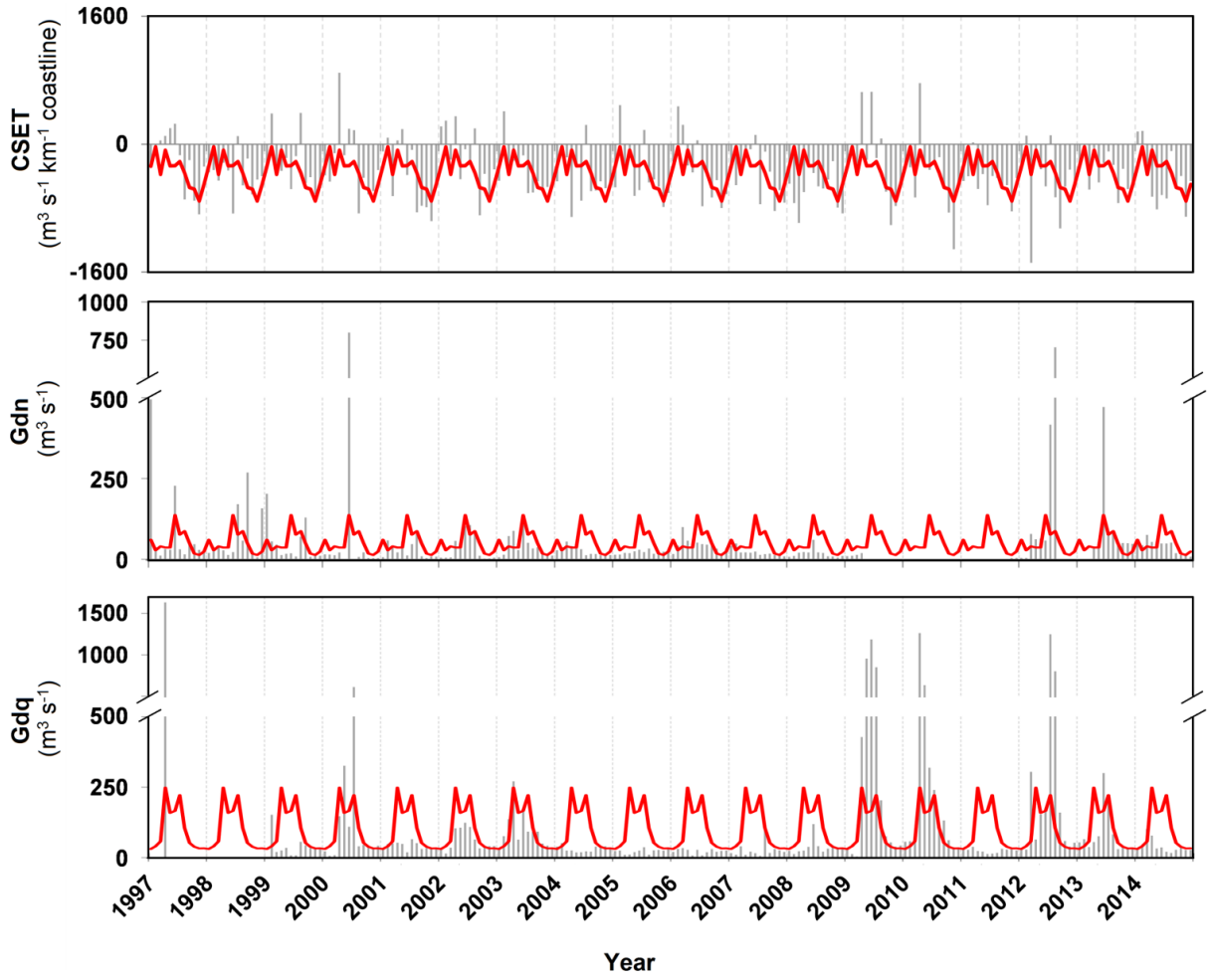

Figure D.6 - Temporal variability of upwelling intensity and river discharge over the southwest area off the Iberian Peninsula (SWIP), during the period 1997 to 2015. Cross-shore Ekman transport, a wind-based upwelling index, for the west Portuguese coast ($CSET_{WC}$); negative (positive) values indicate upwelling-favourable (upwelling-unfavorable) conditions. Guadiana (Gdn) and Guadalquivir (Gdq) river discharge. Red lines represent monthly climatologies for the study period and gray vertical dashed lines signalize the month of September of the respective year